British Geological Survey

Expert | Impartial | Innovative

# Environmental Monitoring - Phase 5 Final Report (April 2019 - March 2020)

Groundwater Science Programme

Open Report OR/20/035

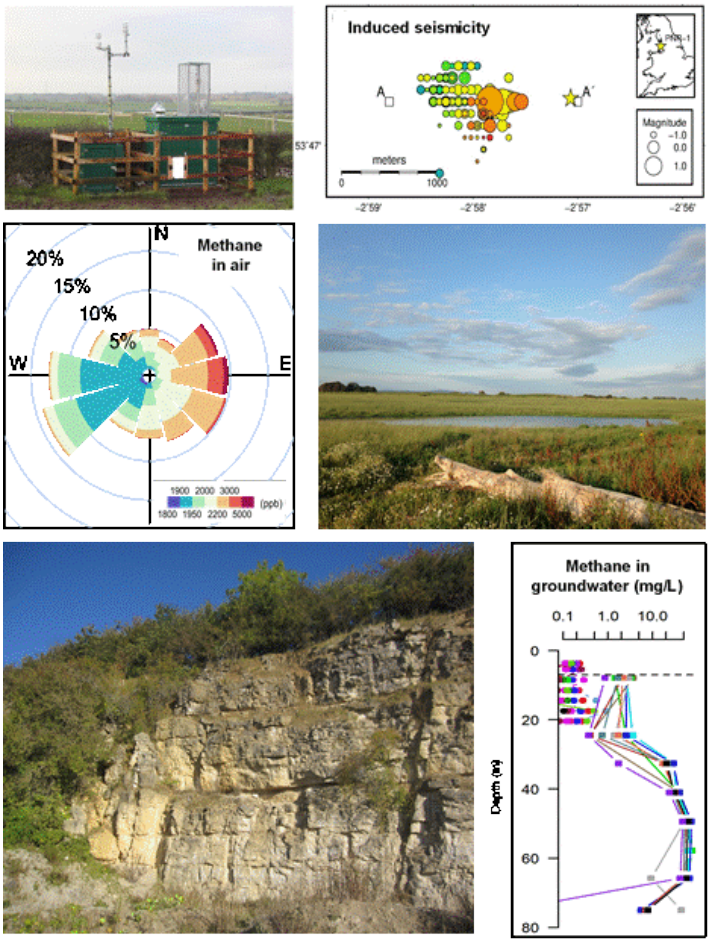

BRITISH GEOLOGICAL SURVEY

GROUNDWATER SCIENCE PROGRAMME

OPEN REPORT OR/20/035

# Environmental Monitoring - Phase 5 Final Report (April 2019 - March 2020)

R.S. Ward (1), P.L. Smedley (1), G. Allen (2), B.J. Baptie (1), P Barker (2), A.K.A.P. Barkwith (1), P. Bates (2), L. Bateson (1), R.A. Bell (1), M. Coleman (5), G. Cremen (6), E. Crewdson (1), Z. Daraktchieva (3), M Gong, Mengyi (1), C.H. Howarth (3), J. France (5), D. Hawthorn (1), D.G. Jones (1), C. Jordan (1), M. Lanoisellé (5), A.C. Lewis (4), T.R. Lister (1), D. Lowry (5), R. Luckett (1), D. Mallin-Martin (1), B.P. Marchant (1), C.A. Miller (3), C.J. Milne (1), A. Novellino (1), J. Pitt (2), R.M. Purvis (4), M.O. Rivett (7), J. Shaw (2), H. Taylor-Curran (1), J.M. Wasikiewicz (3), M. Werner (6) and S Wilde (4)

(1): British Geological Survey
(2): University of Manchester
(3): Public Health England
(4): University of York (National Centres for Atmospheric Science)
(5): Royal Holloway University of London
(6): University of Bristol
(7): GroundH20 plus Ltd



*Keywords*

Monitoring, groundwater, seismicity, ground motion, greenhouse gases, atmospheric composition, air quality, radon, soil gas, water quality, shale gas.

*Bibliographical reference*

WARD, R.S., SMEDLEY, P.L., ALLEN, G., BAPTIE, B.J., BARKER, P., BARKWITH, A.K.A.P., BATES, P., BATESON, L., BELL, R.A., BOWES, M., COLEMAN, M., CREMEN,G., DARAKTCHIEVA, Z., GONG, M., HOWARTH, C.H., ET AL.2020. Environmental Monitoring - Phase 5 Final Report (April 2019 - March 2020). *British Geological Survey Open Report*, OR/20/035. 137 pp.



Keyworth, Nottingham British Geological Survey 2020

## BRITISH GEOLOGICAL SURVEY

The full range of our publications is available from BGS shops at Nottingham, Edinburgh, London and Cardiff (Welsh publications only) see contact details below or shop online at www.geologyshop.com

The London Information Office also maintains a reference collection of BGS publications, including maps, for consultation.

We publish an annual catalogue of our maps and other publications; this catalogue is available online or from any of the BGS shops.

*The British Geological Survey carries out the geological survey of Great Britain and Northern Ireland (the latter as an agency service for the government of Northern Ireland), and of the surrounding continental shelf, as well as basic research projects. It also undertakes programmes of technical aid in geology in developing countries.*

*The British Geological Survey is a component body of UK Research and Innovation.*

*British Geological Survey offices*


**Environmental Science Centre, Keyworth, Nottingham NG12 5GG**

Tel 0115 936 3100

**BGS Central Enquiries Desk**

Tel 0115 936 3143
email enquiries@bgs.ac.uk

**BGS Sales**

Tel 0115 936 3241
email sales@bgs.ac.uk

**The Lyell Centre, Research Avenue South, Edinburgh EH14 4AP**

Tel 0131 667 1000
email scotsales@bgs.ac.uk

**Natural History Museum, Cromwell Road, London SW7 5BD**

Tel 020 7589 4090
Tel 020 7942 5344/45 email bgslondon@bgs.ac.uk

**Cardiff University, Main Building, Park Place, Cardiff CF10 3AT**

Tel 029 2167 4280

**Maclean Building, Crowmarsh Gifford, Wallingford OX10 8BB**

Tel 01491 838800

**Geological Survey of Northern Ireland, Department of Enterprise, Trade & Investment, Dundonald House, Upper Newtownards Road, Ballymiscaw, Belfast, BT4 3SB**

Tel 01232 666595
www.bgs.ac.uk/gsni/

**Natural Environment Research Council, Polaris House, North Star Avenue, Swindon SN2 1EU**

Tel 01793 411500 Fax 01793 411501
www.nerc.ac.uk

**UK Research and Innovation, Polaris House, Swindon SN2 1FL**

Tel 01793 444000
www.ukri.org

Website www.bgs.ac.uk
Shop online at www.geologyshop.com

# Foreword

This report presents the results and interpretation for Phase 5 of an integrated environmental monitoring programme that is being undertaken around two proposed shale gas sites in England – Preston New Road, Lancashire and Kirby Misperton, North Yorkshire. The report should be read in conjunction with previous reports freely available through the project website[1]. These provide additional background to the project, presentation of earlier results and the rationale for establishment of the different elements of the monitoring programme.

# Acknowledgements

The work reported here has been enabled through a combination of BGS National Capability funding and a grant awarded by the UK Government's Department for Business, Energy & Industrial Strategy (BEIS). Additional benefit-in-kind contributions have also been provided by the project partners.

The authors would like to acknowledge the support provided by a wide range of organisations, community groups and individuals that have allowed the sampling teams to continue to undertake their work in The Fylde and the Vale of Pickering.

[1] www.bgs.ac.uk/research/groundwater/shaleGas/monitoring/home.html

# Contents

## FIGURES

**TABLES**

# Technical summary

This report describes the results of activities carried out as part of the Environmental Monitoring Project (EMP) led by the British Geological Survey (BGS) in areas around two shale gas sites in England – Kirby Misperton (Vale of Pickering, North Yorkshire) and Preston New Road (The Fylde, Lancashire). It focuses on the monitoring undertaken during the period April 2019 – March 2020 (Phase 5) but also considers this in the context of earlier monitoring results that have been covered in reports for earlier phases of the project[2].

The EMP is a multi-partner project involving BGS together with Public Health England (PHE), University of Birmingham, University of Bristol, University of Manchester, Royal Holloway University of London (RHUL) and University of York. The work has been enabled by funding from a combination of the BGS National Capability programme, a grant awarded by the UK Government's Department for Business Energy & Industrial Strategy (BEIS) and additional benefit-in-kind contributions from all partners.

The project comprises the comprehensive monitoring of different environment compartments and properties at and around the two shale-gas sites. The component parts of the EMP are all of significance when considering environmental and human health risks associated with shale gas development. Included are seismicity, ground motion, water (groundwater and surface water), soil gas, greenhouse gases, air quality, and radon in air.

The monitoring started in both areas before hydraulic fracturing operations were planned to take place, so a robust assessment of baseline conditions could be made. It is important to characterise adequately the baseline so that any future changes caused by shale gas operations can subsequently be identified. This is also the case for any other new activities that may impact those compartments of the environment being monitored as part of the project. The timeline for activities at/around the two shale gas sites is summarised in Figure 1.

Whilst some impacts from shale gas operations are expected, e.g. induced seismicity and emissions to air, others should not occur, e.g. groundwater pollution, if effective risk mitigation and management measures are put in place. The timescales for detection of impacts are also different. Induced seismicity is normally observed during and shortly after the period of hydraulic fracturing operations. Pollutant emissions to air are expected during periods of significant vehicle movement and when pumps are operating on site, although emissions could continue during periods of flow testing when gas is flared, and methane emissions throughout the lifetime of the well. Slow movement of groundwater means that any pollutant impacts might take a long time to become evident and the pollution risk continues throughout the lifetime of well operations and after de-commissioning has taken place. As a result of these characteristics, different approaches to monitoring are required and for some elements, such as groundwater and greenhouse gases,

[2] Ward, R.S., Allen, G.; Baptie, B.J., Daraktchieva, Z., Jones, D.G., Jordan, C.J., Purvis, R.M., Smedley, P.L. 2016. *Environmental baseline monitoring - Vale of Pickering: Phase I - Final Report (2015/16).* BGS Report, OR/16/002.

Ward, R.S., Smedley, P.L., Allen, G., Baptie, B.J., Daraktchieva, Z., Horleston, A., Jones, D.G., Jordan, C.J., Lewis, A., Lowry, D., Purvis, R.M., Rivett, M.O. 2017. *Environmental Baseline Monitoring Project. Phase II, Final Report*. BGS Report, OR/17/049.

Ward, R.S., Smedley, P.L., Allen, G., Baptie, B.J., Cave, M.R., Daraktchieva, Z., Fisher, R., Hawthorn, D., Jones, D.G., Lewis, A., Lowry, C., Luckett, R., Marchant, B.P., Miller, C.A., Purvis, R. and Wilde, S. 2018. *Environmental Baseline Monitoring: Phase III Final Report (2017-2018).* BGS Report, OR/18/026.

Ward, R.S.; Smedley, P.L.; Allen, G.; Baptie, B.J.; Barkwith, A.K.A.P.; Bateson, L.; Bell, R.A.; Bowes, M.; Coleman, M.; Cremen, G.; Daraktchieva, Z.; Gong, M.; Howarth, C.H.; Fisher, R.; Hawthorn, D.; Jones, D.G.; Jordan, C.; Lanoiselle, M.; Lewis, A.C.; Lister, T.R.; Lowry, D.; Luckett, R.; Mallin-Martin, D.; Marchant, B.P.; Miller, C.A.; Milne, C.J.; Novellino, A.; Pitt, J.; Purvis, R.M.; Rivett, M.O.; Shaw, J.; Taylor-Curran, H.; Wasikiewicz, J.M.; Werner, M.; Wilde, S.. 2019 *Environmental monitoring: P*hase 4 final report (April 2018 - March 2019). BGS Report, OR/19/044.

monitoring needs to continue after site operations have ceased. The project has published guidance on environmental monitoring for shale gas operations[3].

During August 2019 the shale gas well known as PNR-2 located at the Preston New Road (PNR) shale-gas site in Lancashire was hydraulically fractured. This followed hydraulic fracturing of the PNR-1z well at the same site in 2018 (October – December). As for PNR-1z, the hydraulic fracturing was followed by a period of well cleaning and flow testing during October and November 2019. The proposed hydraulic fracturing programme for well PNR-2 was not completed because a magnitude 2.9ML induced seismicity event was detected on 26th August, using the seismometer array installed as part of this project, and this led to the suspension of operations by the Oil and Gas Authority (OGA).

The project team continued monitoring during the period before hydraulic fracturing of PNR-2, during hydraulic fracturing and flow testing and then subsequently during the period whilst that site has been suspended. This has provided a unique environmental dataset that builds on that acquired during 2018 and the hydraulic fracturing operations on PNR-1z. As in that case, several environmental impacts were observed during the different stages of activity at PNR-2. These are summarised below and described in more detail within this report. In contrast to the PNR site, no shale gas operations have taken place at the Kirby Misperton (KMA) site during the reporting period. Approval for hydraulic fracturing of the shale gas well (KM8) has not been forthcoming, and the operator has now turned its attention to conventional hydrocarbon development elsewhere in the Vale of Pickering. Therefore the monitoring at the KMA site over the reporting year reflects the on-going baseline at a conventional gas well site, although production from all the Vale of Pickering gas fields has been suspended since November 2019.

***Atmospheric composition*** (greenhouse gas and air-quality composition) has continued to be monitored near the PNR and KMA shale gas sites. The use of both fixed site and mobile monitoring for emission detection have been characterised, and a series of case studies now completed for key points in the shale gas site's life cycle (especially during flowback testing and flaring). Well cleaning and flow testing at the PNR site (PNR-2) was accompanied by flaring of vented gases. Emissions were detected both at the project's monitoring station and visually through smoke emitted from the flare stacks. Although perturbations in methane ($CH_4$) were detected during the flow-testing/flaring operations in October/November 2019, there were no exceedances of the threshold criteria developed during Phase 4 of the project. A similar perturbation in carbon dioxide ($CO_2$) was observed and this provided evidence for the successful flaring of methane emissions. Small enhancements in air quality pollutant concentrations, especially nitrogen oxides ($NO_x$) and non-methane hydrocarbons were also observed at this time. However, there were no observed exceedances of any statutory air quality limit. During the periods of flaring a series of mobile surveys was carried out to supplement the fixed site monitoring data. These surveys were unable to detect emissions from the shale gas site, or at least unable to differentiate them from other pre-existing local sources as there are a number of significant point sources in the area. These include dairy farms, manure piles, landfills and leaking pipelines, all of which have been detected throughout the lifetime of the project.

Measurement of ***radon in air*** has been undertaken at over 100 homes in the Vale of Pickering with results continuing to indicate that indoor radon concentrations are consistent with the usual log-normal distribution for indoor radon in the UK. The results for Kirby Misperton and Little Barugh area are consistent with their status as not being radon Affected Areas. In Yedingham, also an area with low radon potential, all measurements are below the Action Level (200 Bq $m^{-3}$ as an annual average) with the exception of one house which has consistently shown results that are above the Action Level.

[3] R.S. Ward, M.O. Rivett, P.L. Smedley, G. Allen, A. Lewis, R.M. Purvis, C.J. Jordan, Z. Daraktchieva, B.J. Baptie, H. Taylor-Curran, L. Bateson, A. Novellino, D. Lowry And R. E. Fisher. 2019. *Recommendations for Environmental Baseline Monitoring in areas of shale gas development*. British Geological Survey Open Report, OR/18/043.

The results for Pickering and Malton confirmed their status as a radon Affected Areas with radon concentrations up to 650 Bq $m^{-3}$ measured in Pickering. Several homes were found to have results exceeding the Action Level, and in these cases, householders were given standard advice on any action required; those with high radon levels were given additional information on reducing their radon concentrations. All areas follow the normal seasonal pattern in the UK with the highest radon concentrations in winter and lowest radon concentrations in summer.

For outdoor radon, measurements indicate that radon concentrations in the Vale of Pickering have varied over time. The latest year of data shows concentrations that are twice as high as the previous two years but similar to the year before that. There is no indication of elevated outdoor radon concentrations in the Pickering or Malton radon Affected Areas, relative to those that are not radon affected. Results from an active monitor and passive detectors, placed at the KMA site are in good agreement with the average outdoor radon concentrations within the area of Kirby Misperton village.

Over the baseline monitoring period, a range of techniques has been used to measure ***soil gas*** and characterise baseline conditions around the PNR and KMA sites. Gas composition analysis indicates that baseline $CO_2$ primarily originates from biological processes in the shallow subsurface, with a smaller contribution from the oxidation of $CH_4$, depending on the time of year. An initial estimate of the baseline $CO_2$ flux and soil gas has been developed. Monitoring and soil gas surveys carried out after hydraulic fracturing indicate similar concentration patterns to the baseline period indicating that to date there has been no impact from shale gas operations.

The challenge with soil gas measurement in survey mode is weather dependency. The pragmatic optimum season for UK soil gas surveys has been found from the long-term monitoring to be autumn; winter campaigns in the UK typically yield limited useful data because moisture conditions mean that soil gas becomes trapped and flux to atmosphere is impeded. Statistical analysis of Vale of Pickering data suggests autumn campaigns are least sensitive to changes in grid spacing. Early summer is also a favourable season, based on weather statistics, although variations in parameter values are higher overall (because of the growing season).

***Water-quality*** monitoring under baseline conditions has continued during the Phase 5 period in The Fylde area and Vale of Pickering. Spatial variability in chemical composition continues to be large and temporal variability is large for streamwater. The patterns observed are consistent with previous years, with the variability reflecting aquifer lithology, hydrogeology, land use and anthropogenic activity. The data acquired to date do not show evidence for contamination of groundwater or surface water from shale-gas exploration activities (hydraulic fracturing and/or flow-testing etc) or subsequently. A user-friendly version of the change-detection algorithm developed in Phase 4 has been developed as an app.

In both The Fylde and the Vale of Pickering, the shallow (Superficial) aquifers closest to the proposed or actual shale-gas exploration sites are strongly influenced by reactions with aquifer minerals and, due to the prevalence of clay deposits and organic matter, are naturally reducing to strongly reducing. In the Fylde, concentrations of $CH_4$ are seen up to around 7 mg/L in a small number of boreholes but concentrations are otherwise low (µg/L range). In the Vale of Pickering, high concentrations of $CH_4$ (>10–80 mg/L) are a feature of some shallow groundwaters from the Superficial (Kimmeridge ± Quaternary) aquifer, and $C_2H_6$ (ethane) is detected at some sites.

The networks of sensors measuring ***seismicity*** in both the Vale of Pickering and The Fylde have continued to operate with levels of data completeness of over 95%. Event detection capability is 0.5 ML or less.

A number of small local (≤ 100 km away) seismic events have been detected in the Vale of Pickering which relate to quarry blasting. All of these events are in the daytime and have ranged from 1.0 ML to 2.0 ML. These observations are similar to those previously reported.

The detected seismicity during hydraulic fracturing operations on PNR-2 was strongly clustered at the start of operations and closely associated with periods of injection, with only small numbers

of events outside these times. However, after 21st August, more scattered behaviour was observed with a number of larger trailing events occurring outside the periods of operation during the evening or night. The largest of these trailing events had a magnitude of 2.9 ML (26th August), almost 72 hours after a hydraulic fracture stage on 23rd August. This is the largest fracking related earthquake recorded in the UK to date and BGS received over 2000 reports from members of the public who felt the earthquake.

Previous reports have presented an analysis of baseline ***ground motion*** across The Fylde and the Vale of Pickering. This report focusses on The Fylde and the periods of hydraulic fracturing at the PNR shale gas site. The assessment indicates that the majority of the full region covered by the satellite image stack was stable, although discrete zones a considerable distance from, and unrelated to, the shale gas site were affected by ground motion. Examination of the Sentinel-1 satellite time series data for the area close to the PNR site and the locations of the induced seismic events, showed no evidence of change in ground motion at the time of the events and afterwards. In line with the results reported previously, the 2019 to 2020 period did not significantly deviate from the variability and patterns observed in the baselines.

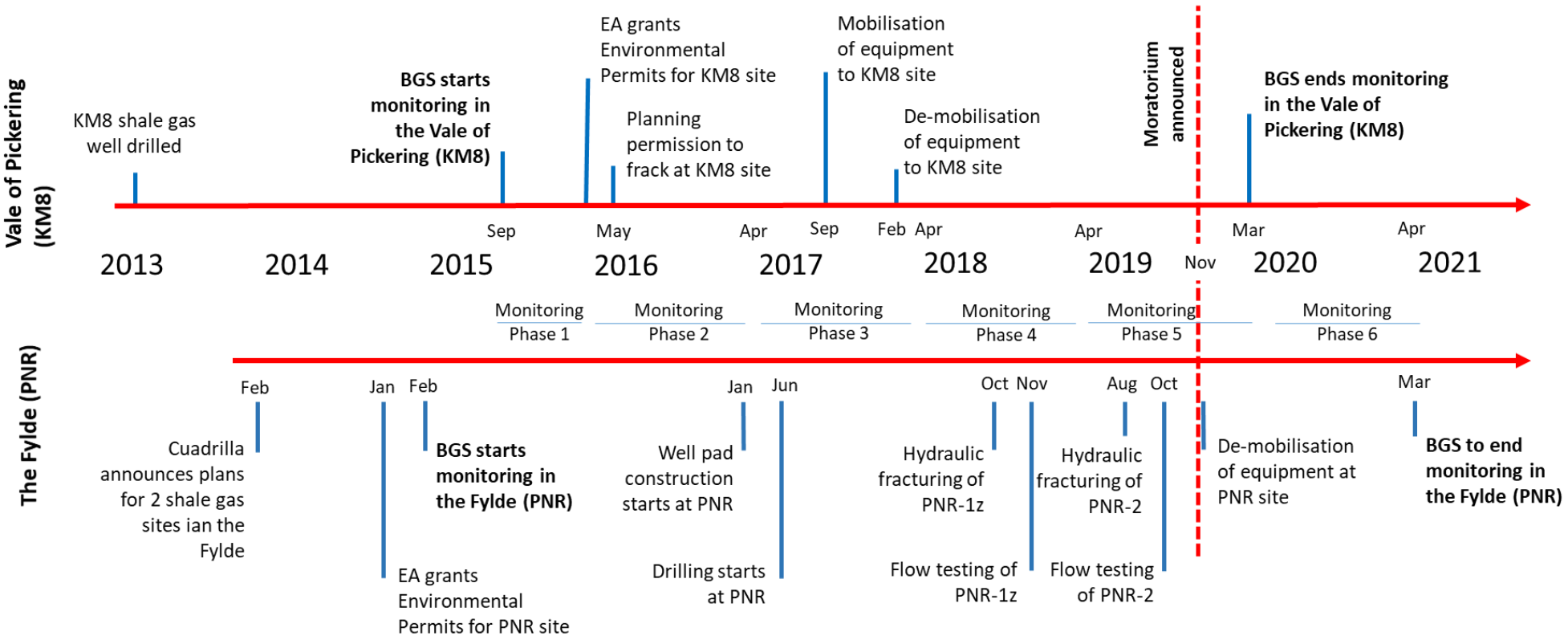


**Figure 1. Summary timeline of key activities and events at/around the Preston New Road (PNR) shale gas site and the Kirby Misperton (KM8) shale gas site.**

# 1 Greenhouse gases

## 1.1 INTRODUCTION

This section discusses measurements of greenhouse gases (GHG) sampled near the Preston New Road (PNR) and Kirby Misperton (KMA) shale gas sites (Figure 1-1 and Figure 1-2).

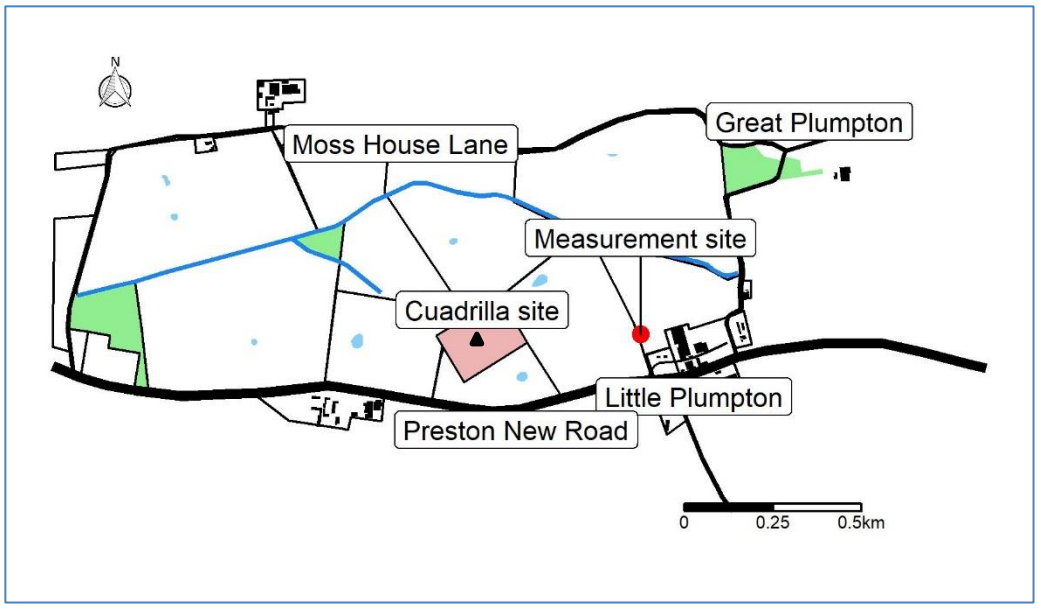


**Figure 1-1. Map showing the location of the measurement station at PNR relative to the Cuadrilla operated unconventional shale gas extraction facility. The black triangle indicates the position of the shale gas well(s).**

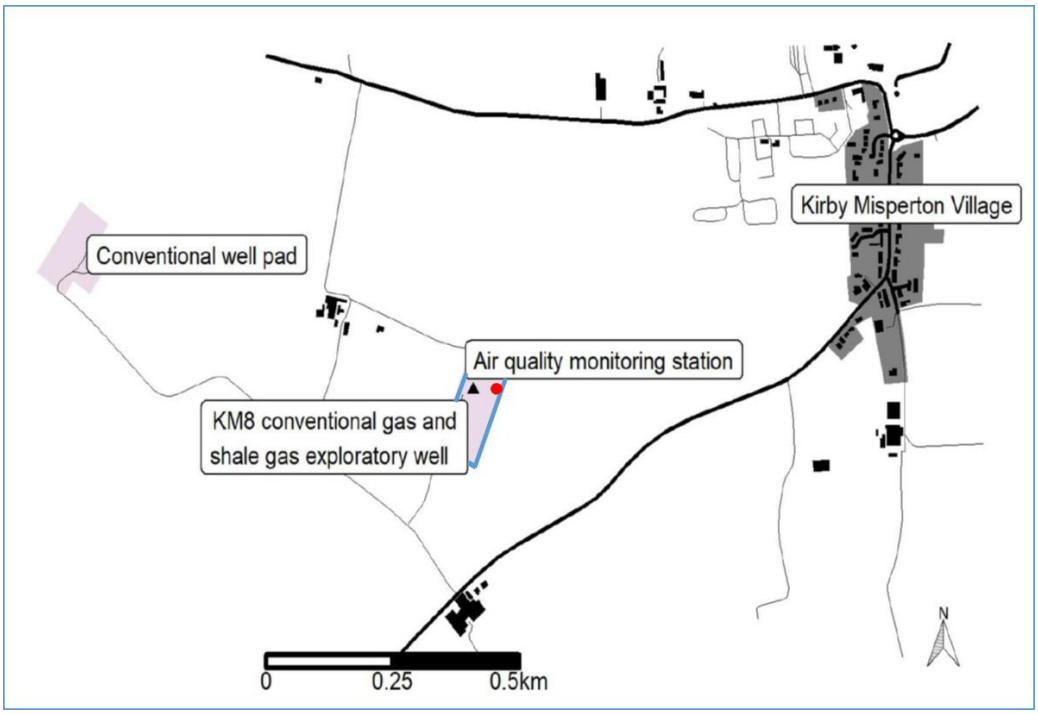


**Figure 1-2. Map showing the location of the measurement station on the KM8 shale gas site relative to the locality and other gas production infrastructure. The black triangle indicates the position of the shale gas well(s).**

The data presented and interpreted in this report includes data collected during the period 1st April 2019 – 31st January 2020 (Phase 5) and compares and contrasts the four full years of atmospheric

sampling conducted between February 1st 2016 and January 31st 2020. The four-years of continuous monitoring are split into four 12-month periods, consistent with reporting for the previous phases of the Environmental Baseline Project (Ward et al. (2017), Ward et al. (2018) and Ward et al. (2019)). The previous reports discuss the analysis of measurements during the first three annual phases of monitoring. It is assumed that the reader is familiar with these reports; the reader is directed to them for details on instrumentation and sampling, and prior conclusions regarding the earlier phases of work.

The fourth year of measurements (Phase 5 - February 2019 to January 2020) has seen further industrial activity at the PNR site. Hydraulic fracturing was carried in well PNR-2 in August 2019. This was followed by a period of flow testing in October and November 2019, which involved the flaring of vented emissions. This flaring was accompanied by the visible emission of particulate (smoke) from one of the flare stacks during the flaring period.

Several peer-reviewed journal articles discussing various aspects of the atmospheric monitoring data have now been published, or are currently under review. Purvis et al. (2019) discussed a baseline and pre-operational analysis of concentrations of $NO_x$ and other air quality indicators at the KM site. Shaw et al. (2019) described a baseline of greenhouse gas measurements at both sites, and presented an algorithmic method for the identification of periods of elevated $CH_4$ above the typical range of baseline conditions. This algorithm was used by Shaw et al. (*in review*) to detect a period of enhanced $CH_4$ at PNR during flowback operations involving a nitrogen lift at the shale gas site, which took place in January 2019. An initial report on this event can also be found via a BGS web publication (Allen et al., 2019). Further, Shaw et al. (*in review*) used three independent flux quantification methods to derive a $CH_4$ flux from the detected $CH_4$ enhancements resulting from the nitrogen lift. The results of that study are discussed in more detail later in this report. A fourth paper describes monitoring of shale gas developments using mobile monitoring methods, along with the identification and characterisation of local $CH_4$ sources in the vicinity of PNR and KM (Lowry et al., 2020). Finally, a series of additional peer-reviewed papers linked to this monitoring project have also been published, which describe the use of unmanned aerial vehicles (UAVs) for the detection and quantification of $CH_4$ emissions from shale gas infrastructure (Shah et al., 2019; Shah et al., 2020). Shah et al. (2020) derived a $CH_4$ flux from the same nitrogen lift emission as that described in Shaw et al. (*in review*), which provided a direct comparison between mobile and fixed-site monitoring, and various flux quantification modelling methods. It is recommended that these articles are read alongside this project report for further detail.

## 1.2 MONITORING ACTIVITIES

Data continued to be collected at the fixed-site monitoring stations located at KM and PNR over the 12 months reporting period. The KM site was decommissioned for both AQ and GHG measurements (after the end of the Phase 5 reporting period), on the 26th February 2020. This decision was taken as it was determined that no further shale gas exploration at the site was likely following public statements made by the site operator, Third Energy.

### 1.2.1 Data calibration and quality assurance

The calibration and quality assurance procedures outlined in the Phase 2 report (Ward et al., 2017) have continued to be upheld to ensure consistency and continuity in the dataset. Data from both sites employ quality assurance (QA) and quality control (QC) for air quality and greenhouse gas concentration data covering all aspects of network operation, including equipment evaluation, site operation, site maintenance and calibration, data review, and ratification. All instrumental calibrations are traceable through an unbroken chain to international reference standards to ensure high accuracy, comparability with similarly calibrated high-precision instrumentation, and quantified uncertainties in the dataset. Metadata concerning the precision and guidance on use of the data is prepared for each measurement reported and made available to view publicly on the

Centre for Environmental Data Analysis (CEDA) archive (www.CEDA.ac.uk) after final QC approval.

Site visits occurred at 3-weekly intervals to check the condition of the instruments and to perform checks on analyser accuracy, precision and response times, as well as calibration. A full list of instrument technical specifications and precision is available in the Phase 2 project report (Ward et al., 2017).

**Table 1-1. Details of the four 12-month measurement periods at both the PNR and KMA sites.**

| Period start | Period end | Year number | Reporting phase | Report reference |
|---|---|---|---|---|
| 1st February 2016 | 31st January 2017 | 1 | 2 | Ward et al. (2017) |
| 1st February 2017 | 31st January 2018 | 2 | 3 | Ward et al. (2018) |
| 1st February 2018 | 31st January 2019 | 3 | 4 | Ward et al. (2019) |
| 1st February 2019 | 31st January 2020 | 4 | 5 | This work |

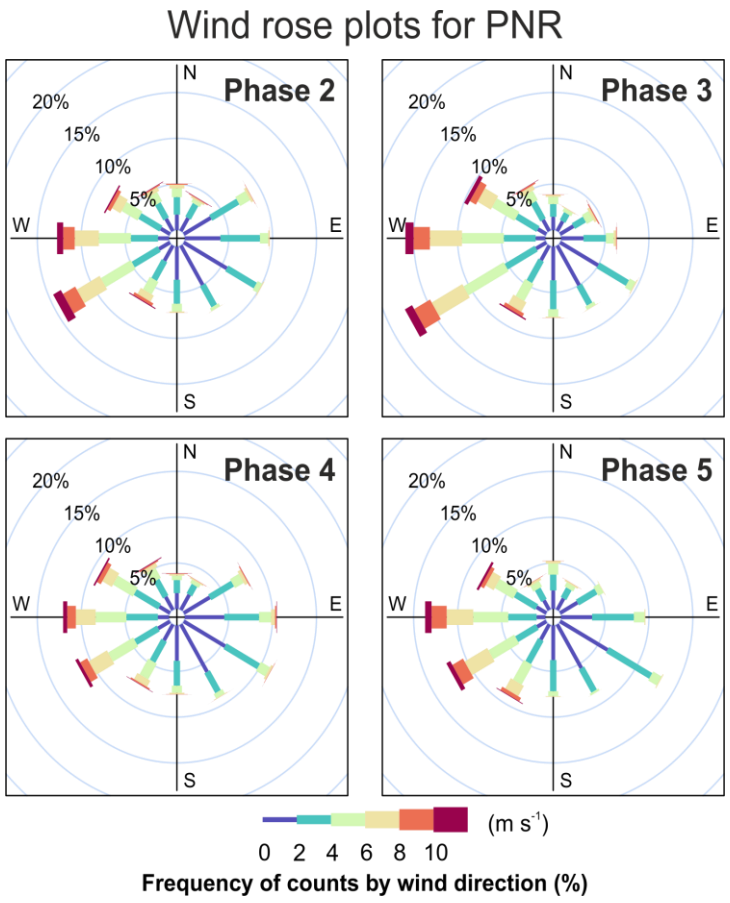


**Figure 1-3. Wind rose plots for the Preston New Road site showing wind speed and direction statistics. Data from four 12-month periods defined in Table 1 are shown. The radii of the paddles illustrate the percentage of total sampling time in each of the 12 wind**

**direction cones (30 degree increments relative to true North) and the colour of the paddle shows the wind speed (see colour legend). © Manchester University, 2020**

## 1.3 ANALYSIS AND DISCUSSION

The following sections discuss the greenhouse gas measurements from the previous four years. The data were analysed in four separate 12-month periods which are related to the different annual phases of the Environmental Monitoring Project. These 12-month periods begin in February and end in January of the following year. The four periods were analysed to examine inter-year consistency, the variance in baseline conditions, and any changes due to operational industrial activity at either site.

Table 1-1 provides an overview of the four measurement periods, their start and end dates, and the "phase number", as referred to hereafter in many of the figures below. The visualisation style and analytical rationale of these figures is consistent with the methods established in previous project reports and it is assumed here that the reader is familiar with the approach. For further explanations of the types of figures presented here, and how to interpret them, please consult the Phase 2 and Phase 3 reports (Ward et al., 2017; Ward et al., 2018).

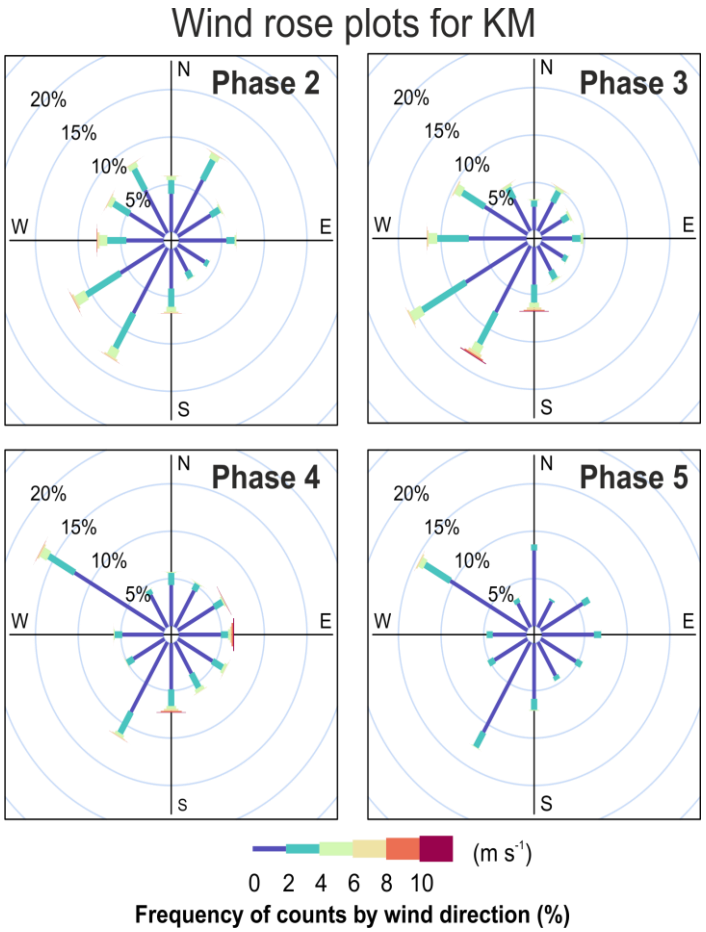


**Figure 1-4. Wind rose plots for the Kirby Misperton site showing wind speed and direction statistics. Data from four 12-month periods defined in Table 1 are shown. The radii of the paddles illustrate the percentage of total sampling time in each of the 12 wind direction cones (30 degree increments relative to true North) and the colour of the paddle shows the wind speed (see colour legend). © Manchester University, 2020**

## 1.4 PNR WIND CLIMATOLOGY

The dominant wind direction at PNR continued to be from the west in the Phase 5 period (Figure 1-3), particularly for higher wind speed periods (i.e. those greater than 4 m $s^{-1}$). The wind rose has been relatively consistent at PNR over the four years of measured data.

## 1.5 KM WIND CLIMATOLOGY

The climatology of wind directions at the KMA site changed in Phase 4, with a more frequent north-westerly component rather than the typical wind directions between 225° and 285° (Figure 1-4). This effect was consistent throughout the year and has been attributed to a change in on-site infrastructure, e.g. construction of a sound barrier around the perimeter, leading to wind shadowing rather than a real change in prevailing local meteorology or a change instrumentation location. This regime of wind direction statistics was continued through into Phase 5 of monitoring.

It is not possible to post-correct for the influences of changes in surrounding infrastructure on localised wind measurements, but these influences must be considered when interpreting atmospheric data from the KMA site, in particular when comparisons are being made between different data from different years. For example, they could create apparent changes in air pollutant concentrations for particular 30-degree sectors.

## 1.6 PNR GREENHOUSE GASES

Figure 1-5 shows the time series of one-hour averaged $CH_4$ mixing ratios measured at PNR across the four year period. There has been little significant change in the mean $CH_4$ mixing ratio across the four years, especially when considering the scale of natural variability (large standard deviations). Such variance in the yearly averaged $CH_4$ mixing ratio is significantly smaller than the corresponding intra-year variance especially considering the global rise in annual mean $CH_4$ concentrations in the northern hemisphere, which is ~0.01 ppm per year. The mean $CH_4$ mixing ratio in Year 4 (Phase 5) was the lowest recorded over the four monitoring phases. This appears to be largely due to the frequency of one-hour average mixing ratios greater than 6 ppm decreasing year-on-year, as have the frequency of measurements greater than 4 ppm. There are transient but large variations in the mixing ratio on very short (less than 3 hour) temporal scales (visible as "spikes" in Figure 1-5); many of these transient changes were consistent with rapidly changing meteorological conditions, particularly when winds were from an easterly direction, consistent with previously reported local methane emissions associated with a nearby dairy farm ~200 m to the east of the measurement site. The impact of operational activities on the shale gas extraction facility cannot be easily discerned from Figure 1-5, though we deconvolve this signal more meaningfully when considering the simultaneous wind direction (see Figure 1-7 and later discussion on site event-based analysis).

As is the case for $CH_4$ in Figure 1-5, there were no statistically significant inter-annual changes in the $CO_2$ mixing ratio time series presented in Figure 1-6. The time series for each year show the expected distinct seasonal variation in $CO_2$ mixing ratios, with a decrease in background $CO_2$ concentrations in summer months due to northern hemisphere biospheric respiration. The mean $CO_2$ mixing ratio is noted to increase between years 2, 3 and 4, broadly consistent with the rate of global increase in background average $CO_2$ concentrations.

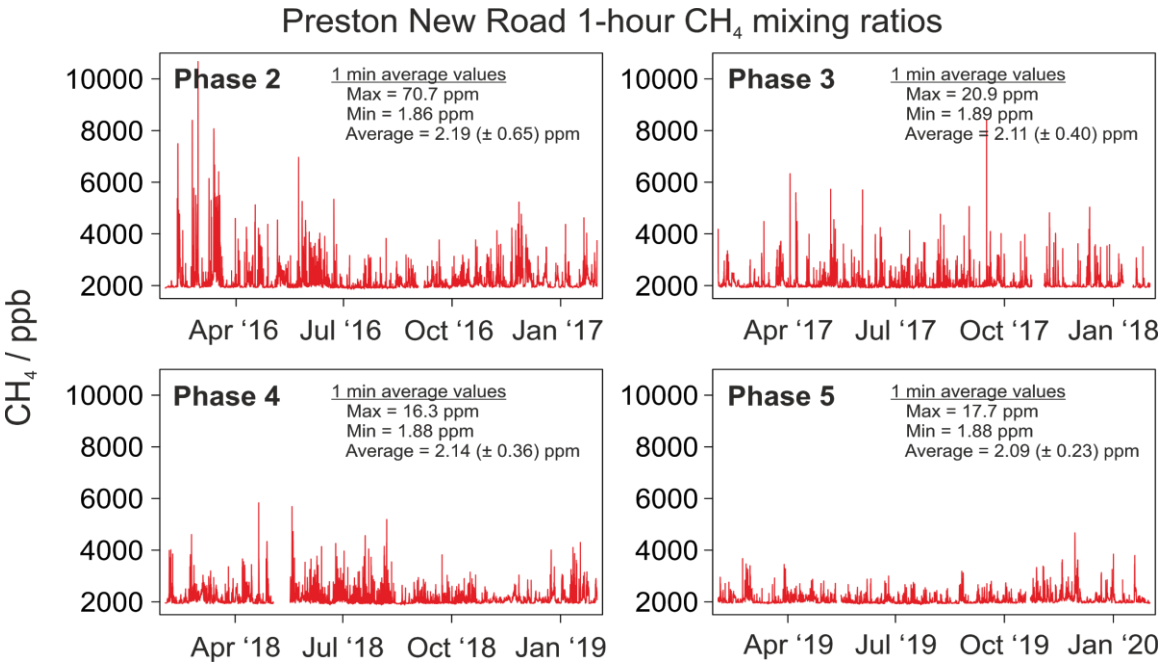


**Figure 1-5. Time series of one-hour averaged $CH_4$ mixing ratios measured at PNR for the four 12-month periods between 1st February 2016 and 31st January 2020. © Manchester University, 2020.**

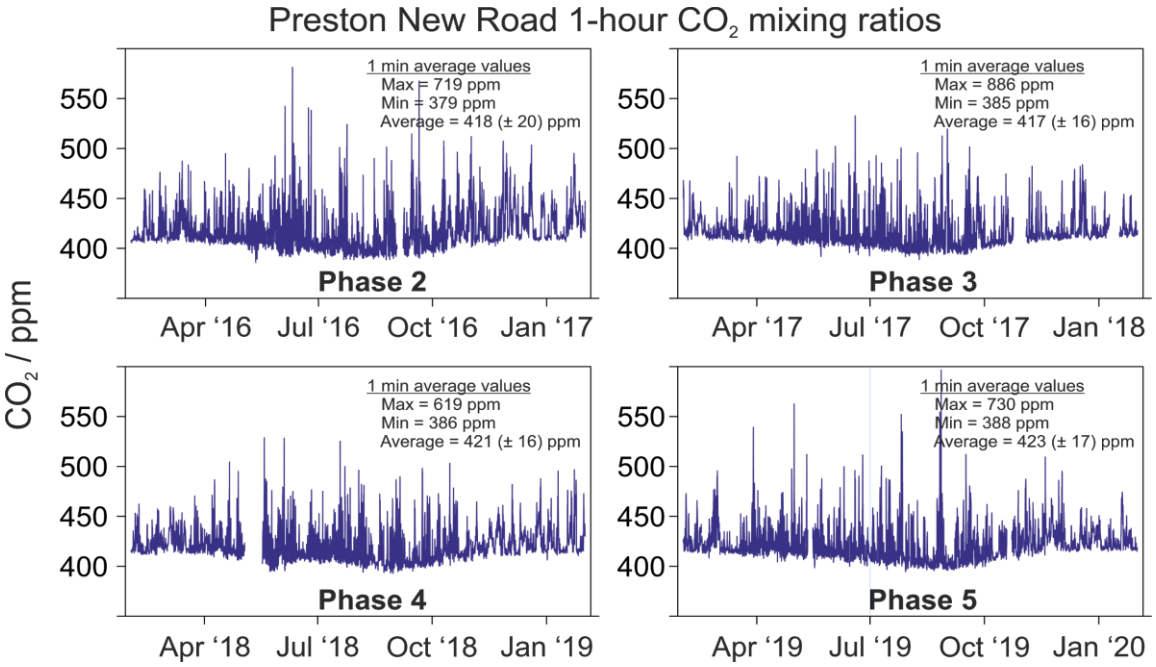


**Figure 1-6. Time series plots of one-hour averaged $CO_2$ mixing ratios measured at PNR for four 12-month periods between 1st February 2016 and 31st January 2020. © Manchester University, 2020.**

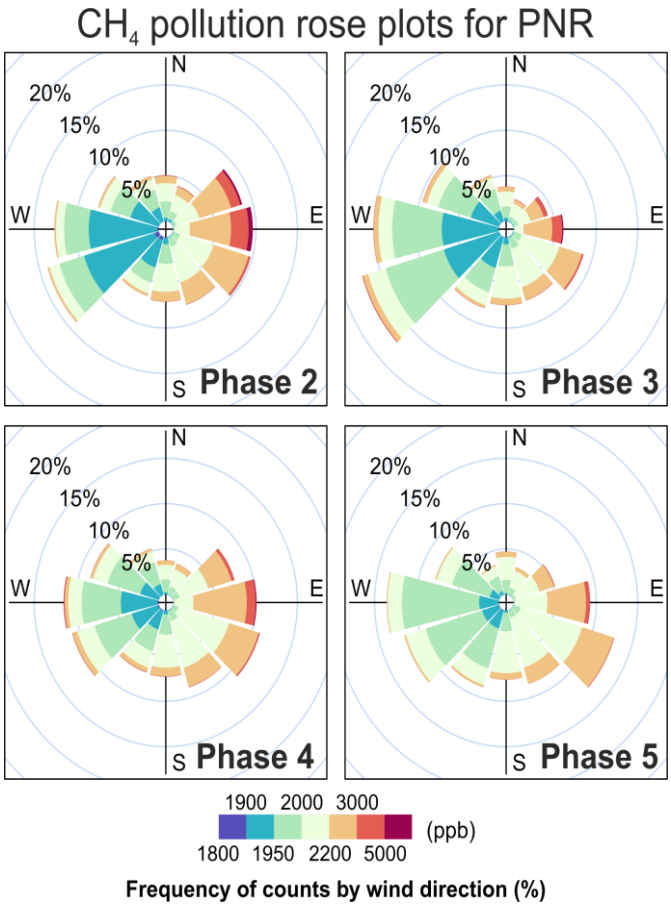


**Figure 1-7. $CH_4$ concentration-frequency and wind rose plots showing CH4 mixing ratios as a function of wind direction for the four 12-month periods. The radii of the paddles illustrates the percentage of total time in each of the 12 wind direction cones (30 degree sections relative to true North) and the colour of the paddle shows the CH4 mixing ratio (see colour legend). The shale gas well pad is to the west of the monitoring site.**


Figure 1-7 illustrates the frequency of $CH_4$ mixing ratios associated with different wind directions. The four years are observed to be broadly consistent. Wind directions from the west generally resulted in $CH_4$ mixing ratios below 2200 ppb for >90% of the total sampling time whilst wind directions from the east resulted in a much greater proportion (>50%) of $CH_4$ mixing ratios above 2200 ppb. This is consistent with conclusions made for earlier phases, which identify the local dairy farm to the east as being responsible for the highest (transient) $CH_4$ enhancements at PNR, and longer-range (longer temporal and more chemically and dynamically mixed) urban and industrial pollution sources to the south east (including cities such as Manchester, Birmingham and London).

Figure 1-8 shows the frequency of $CO_2$ mixing ratios associated with 12 wind direction sectors. As for $CH_4$, the dominant frequency (>50%) of mixing ratios greater than 425 ppm is associated with easterly winds throughout the four year period. Most mixing ratios below 425 ppm are associated with westerly wind directions. There was no appreciable change in this general wind-correlated regime over the four years.

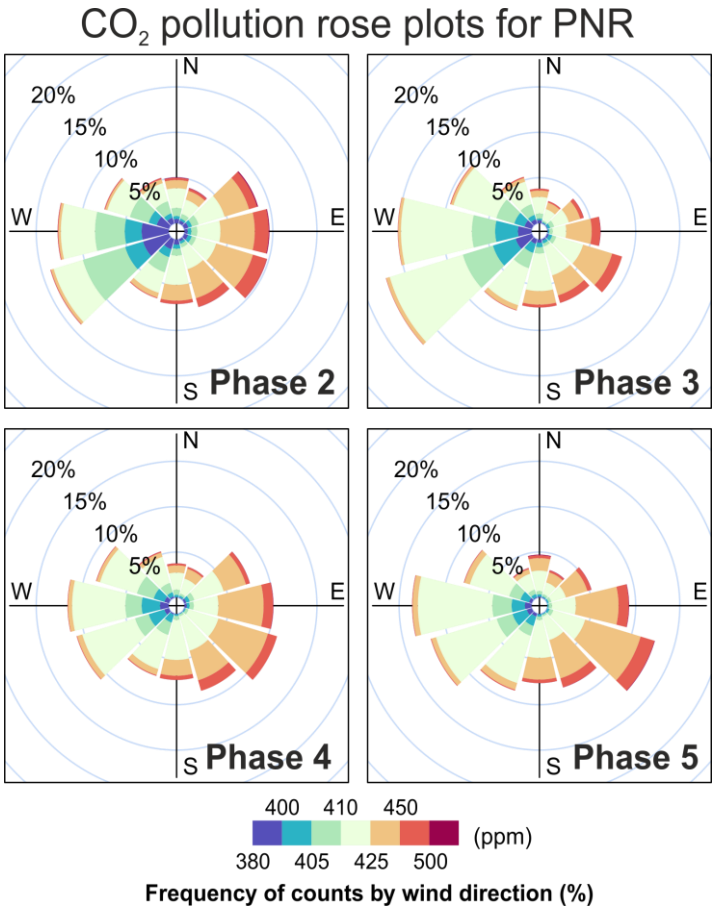


**Figure 1-8. $CO_2$ pollution rose plots showing $CO_2$ mixing ratios as a function of wind direction for four 12-month periods. The radii of the paddles illustrates the percentage of total time in each of the 12 wind direction cones (30 degree sections relative to true North) and the colour of the paddle shows the $CO_2$ mixing ratio (see colour legend). The shale gas well pad is to the west of the monitoring site. © Manchester University, 2020.**

## 1.7 IMPACT OF INDUSTRIAL ACTIVITIES ON SAMPLED GREENHOUSE GASES AT PNR

Operational activity related to shale gas extraction via hydraulic fracturing occurred intermittently throughout Phase 4 and Phase 5. Operational activity at the shale gas site began with hydraulic fracturing of the PNR-1z exploration well in October and November 2018. The operator reportedly began flow testing immediately afterwards and used a nitrogen lift to unload the well in January 2019 (see Figure 1-10 and discussion). Hydraulic fracturing of the second horizontal shale gas well (PNR-2) began in August 2019 with flow testing commencing on 30th September 2019. Through a combination of visual monitoring via a camera at the PNR monitoring station, as well as during mobile monitoring campaigns and site visits, flaring was first observed on 11th October 2019. This continued until at least 8th November 2019. Flaring appeared to be intermittent and varied in intensity. For some of this time period, only a heat haze was visible from one of the flare stacks. However, flames were observed occasionally, accompanied by the observed emission of particulates (smoke). Table 1-2 summarises this information.

The impact of these operational activities on greenhouse gas concentrations was evaluated using data recorded at the fixed-site monitoring station at PNR. The baseline statistics recorded during Phase 2 and Phase 3 of this project were used to derive a set of threshold criteria which, if exceeded, indicated a high likelihood of cold-vented $CH_4$ emissions from the shale gas extraction facility. These threshold criteria were presented in Shaw et al. (2019) and Ward et al (2019), alongside a flow diagram for an algorithmic approach to detecting baseline exceedances (Figure 1-9).

**Table 1-2. Summary of activities at the PNR shale gas site.**

| Activity | Start date | End date | Project Phase |
|---|---|---|---|
| Hydraulic fracturing (PNR-1z) | October 2018 | December 2018 | 4 |
| Flow testing (no flaring) | November 2018 | January 2019 | 4 |
| Hydraulic fracturing (PNR-2) | August 2019 | August 2019 | 5 |
| Flow testing (including flaring) | October 2019 | November 2019 | 5 |

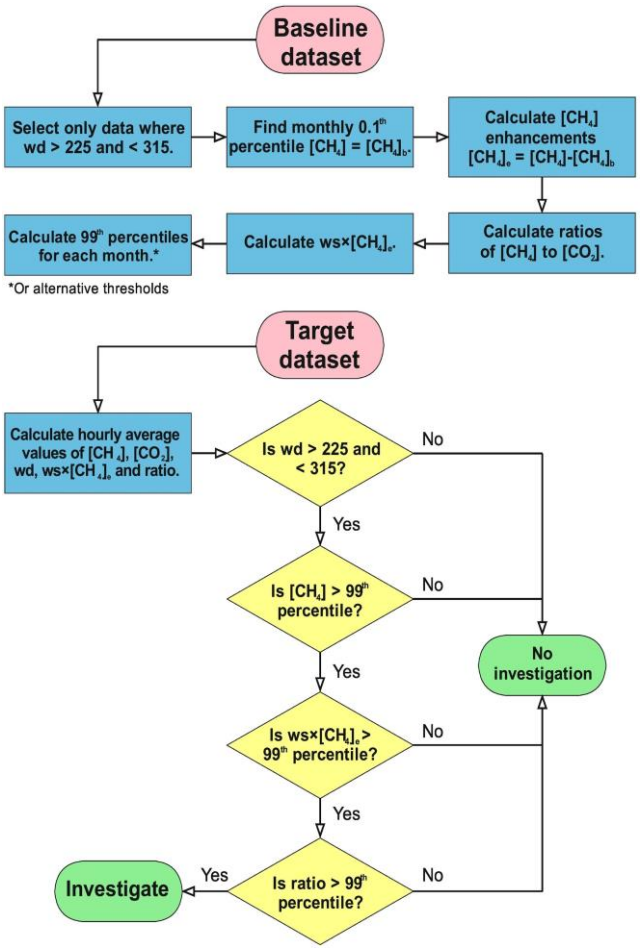


**Figure 1-9. Algorithm application of the threshold criteria for detecting exceedances of the baseline conditions at PNR. Data which exceed these criteria indicate a high likelihood of cold-vented emissions of CH4 from the shale gas extraction facility. For more information on these criteria, readers are asked to refer to Shaw et al. (2019). © Manchester University, 2020.**

Exceedances of the threshold criteria at PNR were first detected in December 2018 for a short period of westerly winds (Figure 1-10). However, the meteorology (wind direction) was generally unfavourable for detection of emissions from the shale gas site for the majority of December. More favourable meteorology returned in January, and the threshold criteria were exceeded multiple times during a one week period between 10 and 16 January 2019 (see periods highlighted in red

in Figure 1-10). This event is discussed in brief in Allen et al. (2019) and in further detail in Shaw et al. (*in review*). Additional plots illustrating the impact of this event on monthly $CH_4$ statistics were also presented as part of the Phase 4 report (Ward et al., 2019).

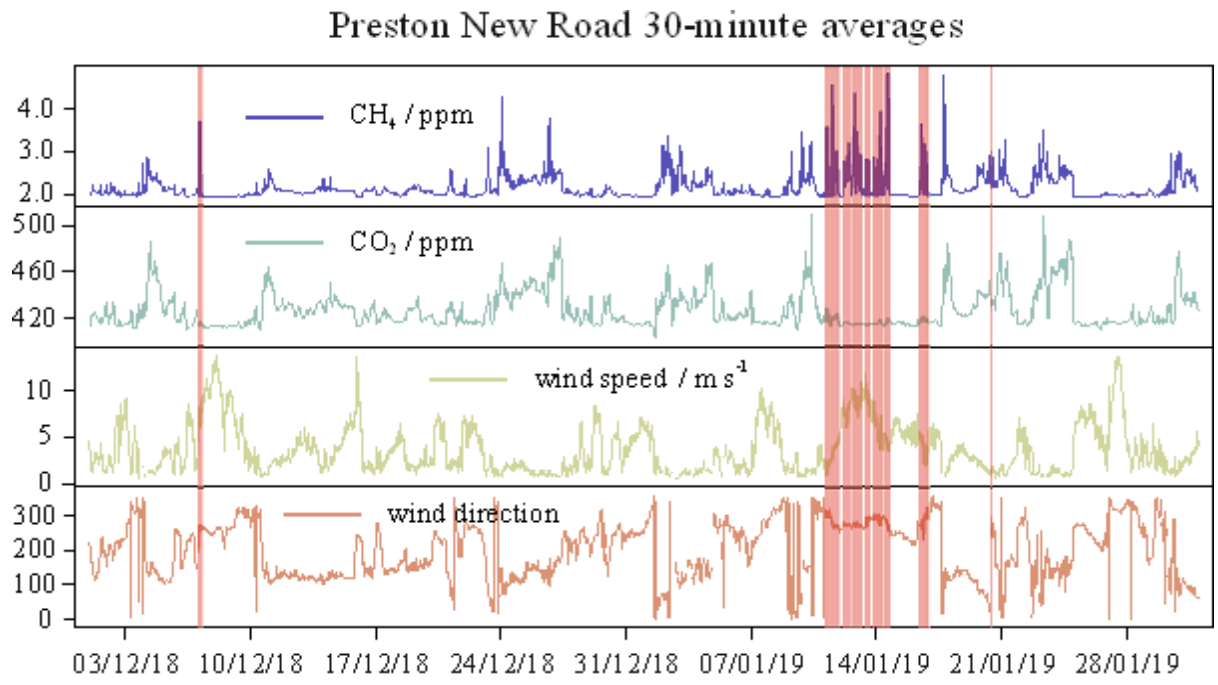


**Figure 1-10. 30-minute averaged $CH_4$ and $CO_2$ mixing ratios, wind speeds, and wind direction at PNR between 1 December 2018 and 31 January 2019. The red highlighted areas represent hourly periods in which the threshold criteria were exceeded.**


The measured $CH_4$ enhancements in January 2019 were caused by a process known as a nitrogen lift (Cuadrilla Resources Ltd., 2019a). This process is one of a number of standard techniques used to artificially unload, or clear, a well, to stimulate the flow of gas (for more information on nitrogen lifts see e.g. Gu, 1995; EPA, 2014). Importantly, the measured $CH_4$ enhancements were used to derive a $CH_4$ flux for the nitrogen lift. Flux quantification was performed using three independent methods; two involving a Gaussian plume simulation, and a third using WindTrax, a stochastic Lagrangian particle transport model. Whilst the use of these three simulations is discussed in detail in Shaw et al. (*in review*), an outline of the flux results is presented in Table 1-3, alongside values reported from UAV (Unmanned Aerial Vehicle) monitoring (Shah et al. 2020) and operator and regulator reported values (Cuadrilla Resources Ltd, 2019b; Environment Agency, 2019). Values for total $CH_4$ mass emitted during the event were also calculated using each of the three flux quantification methods (Table 1-3).

The values estimated using WindTrax were determined to be the most confident assessment of $CH_4$ emissions from the nitrogen lift, largely due to the more rigorous treatment of meteorology within the WindTrax framework in comparison to the other two much simpler models. The best estimate of peak $CH_4$ flux during this event is therefore 81 (± 68) g $s^{-1}$, with a much lower mean flux of approximately 16.3 g $s^{-1}$. The best estimate of total $CH_4$ mass emitted during the event is 4.2 (± 1.4) tonnes. As mentioned above, for a more comprehensive discussion of flux quantification using each of these methods, please refer to Shaw et al. (*in review*).

**Table 1-3. Summary of peak and mean CH4 fluxes, and total CH4 mass emitted, during the January 2019 event, as calculated by three different flux quantification methods. Fluxes are quoted as a mass emission rate (g s-1), while the total mass emitted represents the sum of emissions (in tonnes) integrated over the sampling time for the duration of the event (see text for detail).**

| Flux estimation method | Maximum calculated $CH_4$ flux / g $s^{-1}$ | Mean $CH_4$ flux / g $s^{-1}$ | Cumulative $CH_4$ mass emitted / tonnes |
|---|---|---|---|
| Simple Gaussian simulation* | 72 | 5.6 | 2.9 |
| OTM-33A | 64 ± 19 | N/A | 7.1 ± 2.1 |
| WindTrax | 81 ± 68 | 16.3 | 4.2 ± 1.4 |
| UAV | 9 - 156† | | N/A |
| Operator/regulator reported | 44 | 22 | 2.7 or 6.8 |

* Using Pasquill stability class C (Pasquill, 1961) and time-averaged to 15-mins (to match the WindTrax time step).

† Instantaneous emission flux

Figure 1-11 shows a series of monthly boxplots of $CH_4$ mixing ratios measured at PNR under westerly wind conditions (i.e. 270° ± 45°), up until December 2019, with boxes representing the interquartile range and whiskers representing the range between the 10th and 90th percentile values. Baseline months in this plot directly relate to those evaluated as part of the greenhouse gas baseline assessment (see Shaw et al., 2019). An indication of the confirmed activities at the shale gas extraction facility, for each month and year, is provided by the coloured rectangles below the boxplots. The January 2019 nitrogen lift is clearly visible when compared with analogous statistics during January baseline months, particularly in the extent of the whiskers (10th and 90th percentile values).

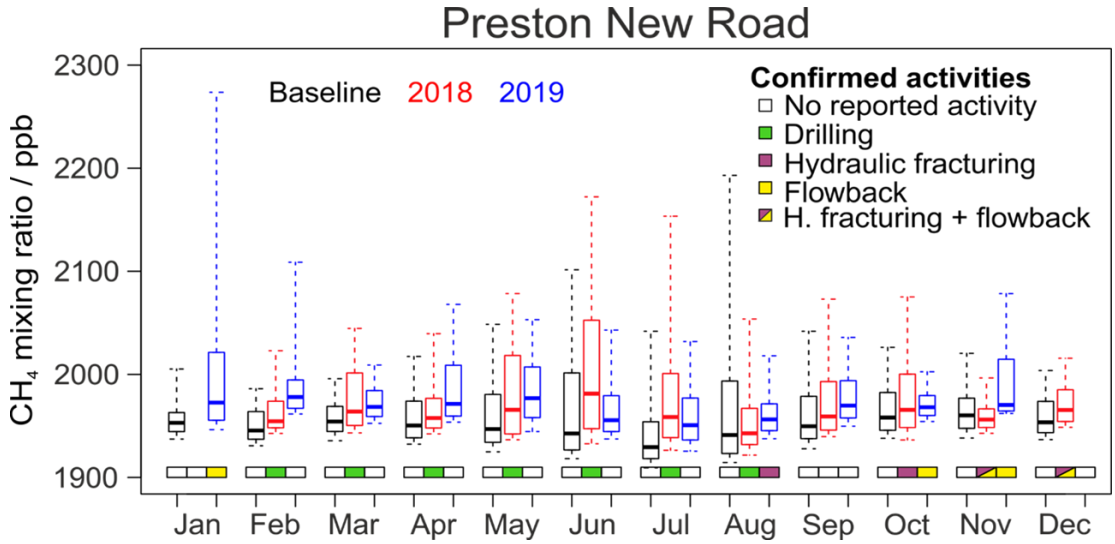


**Figure 1-11. Boxplots for monthly CH4 mixing ratios measured at PNR under westerly winds (270° ± 45°). Baseline months (i.e. months which were evaluated as part of the baseline assessment, between February 2016 and January 2018 (see Shaw et al., 2019)) are shown in black, the rest of 2018 in red and 2019 in blue. The extent of the boxes represents the interquartile range and the whiskers extend to the 10th and 90th percentile values. The coloured rectangles at the bottom of the plots indicate reported activities occurring at the shale gas extraction facility during that month and year. © Manchester University, 2020.**

A second period of flow testing occurred during Phase 5, in October and November 2019. It is currently unknown whether a nitrogen lift was used during this period but the produced gas was successfully flared. This directly contrasts to the January 2019 flow testing, in which the produced gas was not successfully flared. Although no periods exceeded the threshold criteria during October and November 2019, some perturbation (relative to November 2018 and November baseline boxplots) in the $CH_4$ boxplot for November 2019 is clearly visible in Figure 1-11.

A similar perturbation in the $CO_2$ statistics for November 2019 is also clearly visible in similar boxplots for $CO_2$ mixing ratios Figure 1-12. This is evidence for the successful flaring of emissions that occurred in October and November 2019 as $CO_2$ is produced as a direct consequence of the combustion of hydrocarbons, including $CH_4$.

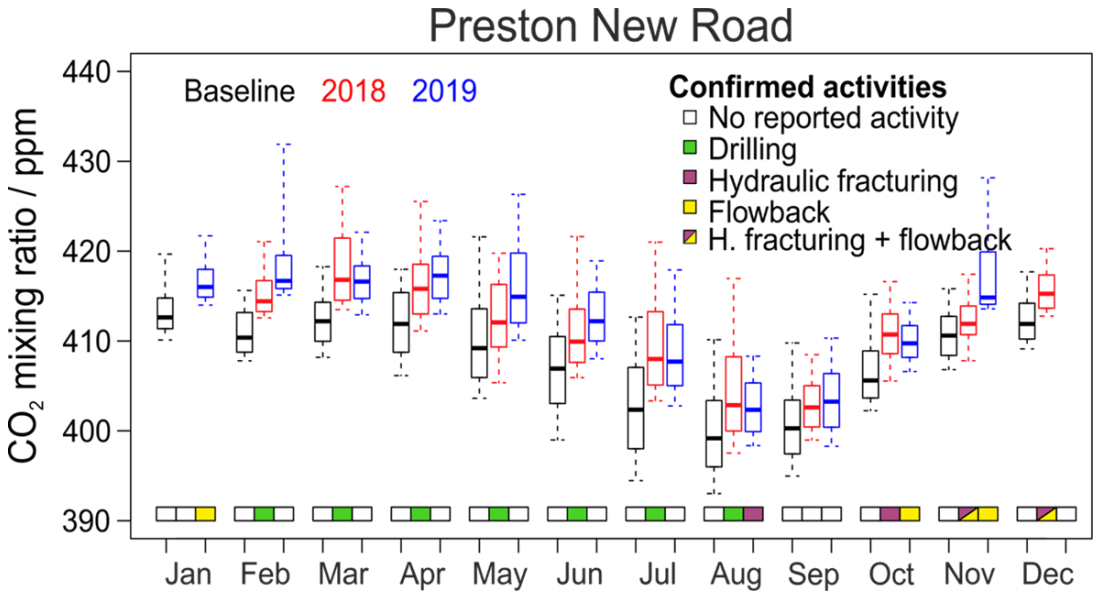


**Figure 1-12. Boxplots for monthly $CO_2$ mixing ratios measured at PNR under westerly winds (270° ± 45°). Baseline months (i.e. months which were evaluated as part of the baseline assessment, between February 2016 and January 2018 (see Shaw et al., 2019)) are shown in black, the rest of 2018 in red and 2019 in blue. The extent of the boxes represents the interquartile range and the whiskers extend to the 10th and 90th percentile values. The coloured rectangles at the bottom of the plots indicate reported activities occurring at the shale gas extraction facility during that month and year. © Manchester University, 2020.**

## 1.8 KM GREENHOUSE GASES

Figure 1-13 shows a time series of hourly $CH_4$ mixing ratios measured at KMA for the four year period. The data are comparable year-to-year. The large (but transient) enhancements, where $CH_4$ mixing ratios reached hourly values greater than 4 ppm, have been confirmed to be due to emissions from controlled venting of a nearby conventional wellhead on the KMA site (see Ward et al., 2019).

Figure 1-14 shows time series for $CO_2$ at KM. Measurements during Phase 5 were comparable to the previous phases of measurement. The data is also directly comparable to $CO_2$ measurements recorded at the same time at PNR (Figure 1-6).

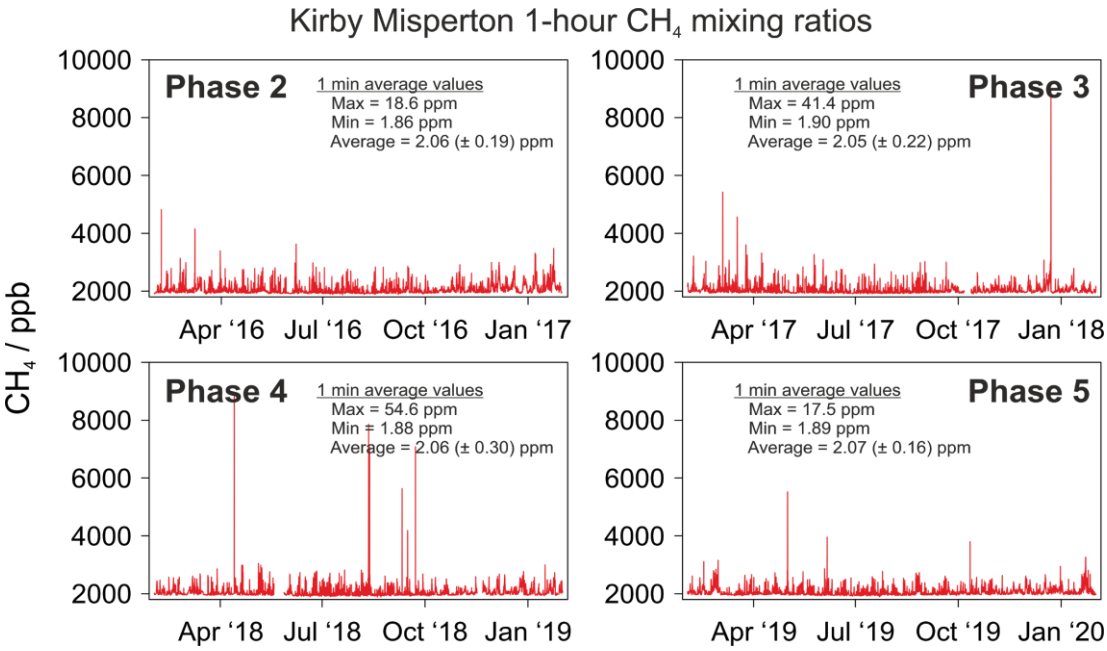


**Figure 1-13. Time series of one-hour averaged $CH_4$ mixing ratios measured at KM for the four 12-month periods between 1st February 2016 and 31st January 2020. © Manchester University, 2020.**

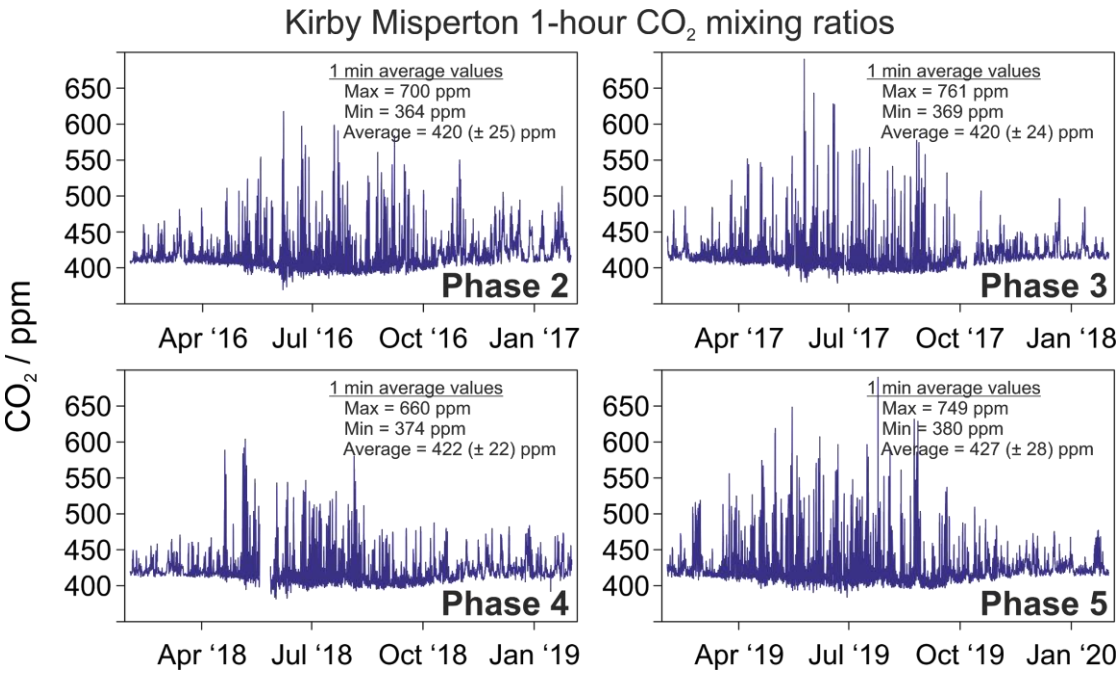


**Figure 1-14. Time series plots of one-hour averaged $CO_2$ mixing ratios measured at KM for four 12-month periods between 1st February 2016 and 31st January 2020. © Manchester University, 2020.**

## 1.9 MOBILE METHANE MEASUREMENT SURVEYS

### 1.9.1 Introduction

Mobile methane baseline surveys during Phase 5 were carried out by Royal Holloway University of London (RHUL), and samples collected for isotopic analysis on the following dates:

- Fylde, Lancashire: 13th and 14th November 2019 (FY14 - 28 samples), 22nd and 23rd January 2020 (FY15 - 28 samples) and 26th and 27th February 2020 (FY16 - 18 samples)

- Vale of Pickering (Ryedale), North Yorkshire: 4th December 2019 (KM10 - 16 samples) and 4th and 5th February 2020 (KM11 - 26 samples).

These surveys build on the baseline work already completed (see Lowry et al., 2020, and Ward et al, 2019 for further details) and show the continued activity of the predominant prevailing methane sources in these regions. Additional rapid-response surveys, were carried out on the 14th and 24th October 2019, during the period of flow testing and flaring at the PNR site to assess activity-related emissions.

Real-time measurements of methane mole fraction were made by cavity ringdown spectroscopy using a Picarro 2301 instrument, and of ethane mole fraction by off-axis optical spectroscopy using a Los Gatos Research Inc (LGR) ultraportable methane-ethane analyser (uMEA) instrument. Samples of air from the located methane plumes were collected in Flexfoil bags (SKC Ltd.) so that sources could be isotopically characterised, as well as at locations where a stable background mole fraction was measured so that baseline $\delta^{13}C$ could be identified. The instrumentation and technique are based on that described by Zazzeri et al. (2015).

One major change to the methodology has been the addition of a LiCOR 7810 (cavity enhanced absorption spectroscopy) trace gas analysis instrument to the mobile survey suite in January 2020 giving extra $CH_4$ and $CO_2$ measurements for two of the Fylde campaigns and one Vale of Pickering campaign. This instrument can be used with a backpack harness for closer measurement of sources plus field and footpath walking, but for these campaigns was used for data inter-comparison with older mobile instruments.

### 1.9.2 Comparison of methane instruments during 2020 field campaigns

The instruments installed for Phase 5 measurements of $CH_4$ are a Picarro 2301-m, Los Gatos uMEA and since 20 January 2020, a LiCOR 7810. The instrument sampling rates are 0.3 Hz, 1 Hz and 1 Hz respectively. However, the cell volume of the uMEA is considerably larger than the other instruments, leading to a 10 second response time compared to an expected 1.5 second response time for the LiCOR.

The three instruments each have different cell size, flow rates and measurement frequency. These combine to give a different response when driving through a series of emissions peaks. Small aircraft measurements of methane demonstrate that the faster response instruments are critical for determining the emission plume structure (France et al., *submitted*). Here, despite only travelling at 10's of km/h compared to 100's of km/h in an aircraft, the principles are the same. The overall structure of the emissions is generally captured by all three instruments (Figure 1-15, top panel). However the uMEA fails to capture the dual peak structure seen in both the Picarro and the LiCOR data over a 15 second period (Figure 1-15, bottom panel). There is a similar contrast in the detection of a cow barn peak, where the vehicle stopped in the narrow plume for filling of a Flexfoil bag sample in the village of Wilton, approximately 12km ENE of the KMA site (Figure 1-16 and Figure 1-17). Where large plumes are encountered they are normally transected a second time for the purposes of sample collection, or the same route might be surveyed on both days of a survey, in which case the figures show the highest measurements (in red) on the top layer, with those closer to background (blue) as the underlayer.

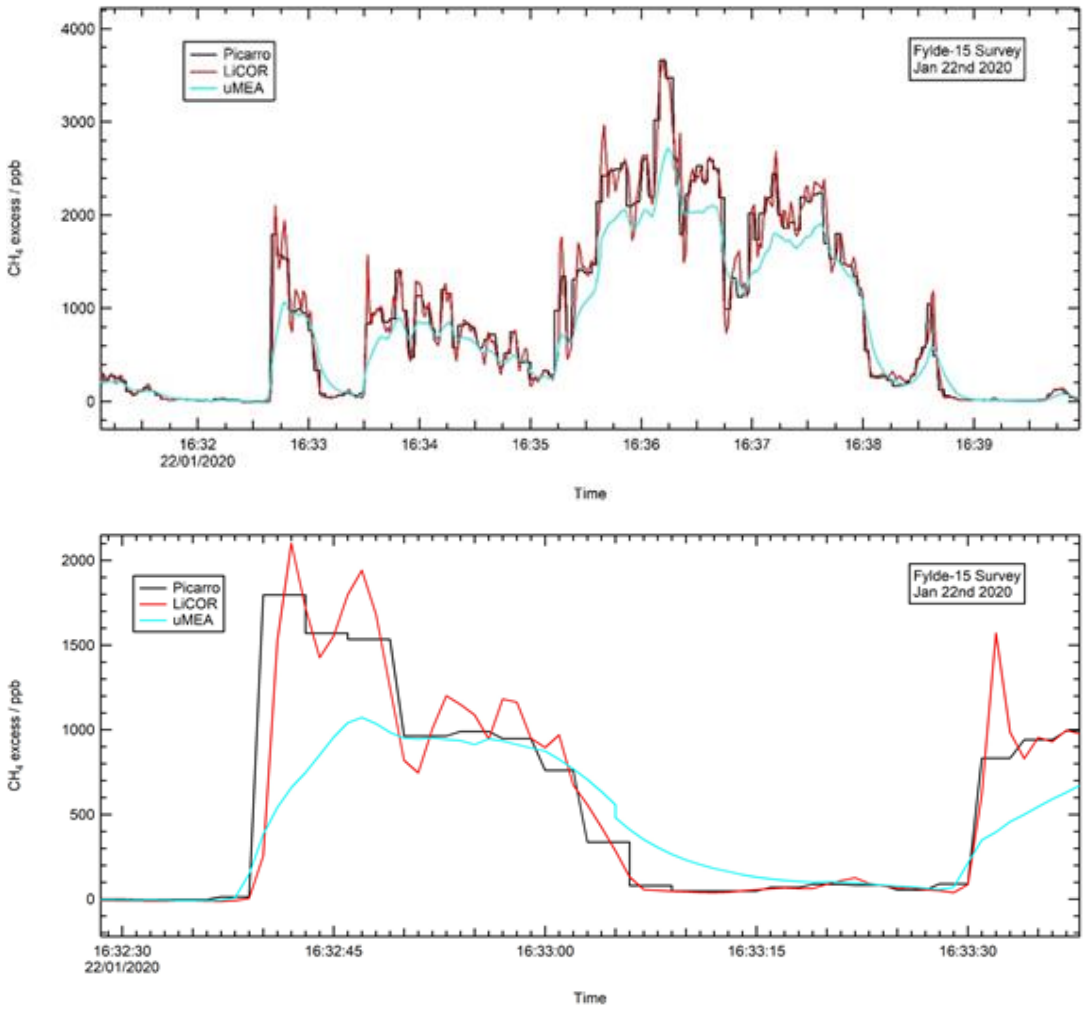


**Figure 1-15. Top, detailed transit through a series of methane plumes, all sampled simultaneously by three instruments using inlets mounted alongside each other. Bottom, detailed view of one minute of data clearly show lags and sampling rate variation between instruments. © RHUL, 2020.**

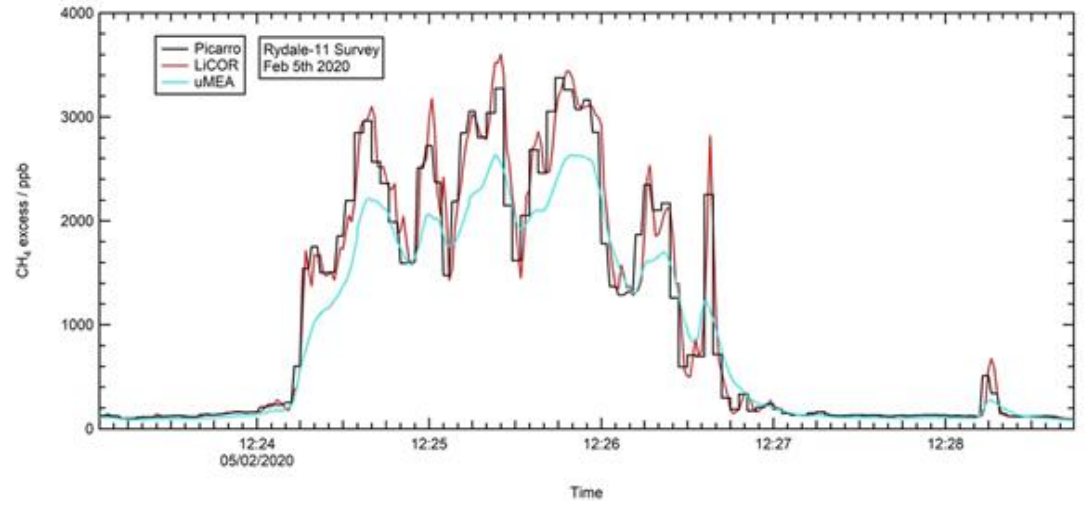


**Figure 1-16. A similar three instrument comparison when the vehicle was stopped for air sampling in a plume from a cow barn in the village of Wilton during the KM11 survey. © RHUL, 2020.**

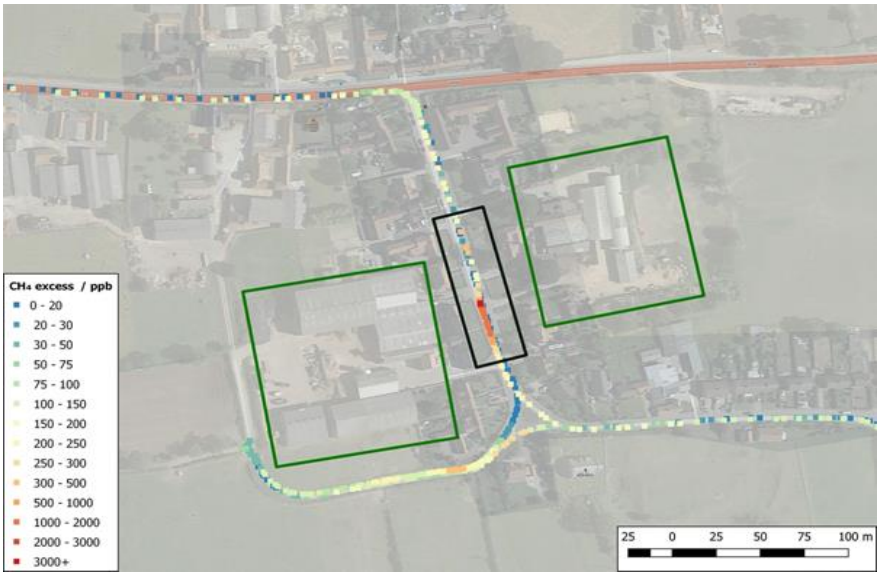


**Figure 1-17. Cow barns in the village of Wilton during the RY11 survey highlighted by the green boxes. The one to the west is normally the source of a significant $CH_4$ plume, the one to the east is not. The plume in Figure 1-16 is highlighted by the black box. This route was surveyed on both days of the KM11 survey. © RHUL, 2020.**

The route identified in Figure 1-17 was surveyed on both days of the KM11 survey. Each coloured circle represents one measurement. On the first day the wind direction was from the north so the survey does not encounter the plume (blue underlayer). On the second day the wind was from the western sector (SW-NW) so the plume was encountered (red points). The Picarro instrument measures GPS and concentrations every 1 second so the spacing of points reflects the distance driven in 1 second as can be seen by the wider spacing of dots on the main road toward the top of Fig 1-15. From 12:24:30 to 12:26:00 the vehicle was stationary in the emission plume during collection of an air sample, but overall direction of travel through the black box shown was south to north at this time.

Although the uMEA has a fast sampling rate, the larger measurement cell volume leads to a relatively slow cell overturn, allowing the air to become mixed internally, the sharp features being smoothed out over a period of ~10 seconds. It can also be seen that the peak response is much slower, rendering the uMEA a poor instrument choice for using as a guide to spot sampling in the field. On average it appears that the peak areas are underestimated by the uMEA by ~15%, whereas the Picarro and LiCOR peak area estimates match within a few percent. This discrepancy has implications in using the uMEA data for flux quantification and also demonstrates that only the $CH_4$ measurements made with the uMEA are suitable for C2:C1 ratio calculations; this is because the $C_2H_6$ measurements will also suffer from the same inherent underestimation problems.

The value of a faster sampling rate with comparable flow and measurement cell size can be seen in a comparison of data from the FY16 survey with three sharp peaks sampled in rapid succession (Figure 1-18). The LiCOR instrument is able to show that the middle peak comprises two separate peaks which is not shown by the other instruments. The 0.3 Hz response rate of the Picarro (compared to 1 Hz of the LiCOR) means that this is missed during the sampling and would require slower transit of the plume to capture. The addition of the LiCOR to the mobile laboratory may make post field interpretation simpler, especially where there are overlapping plumes.

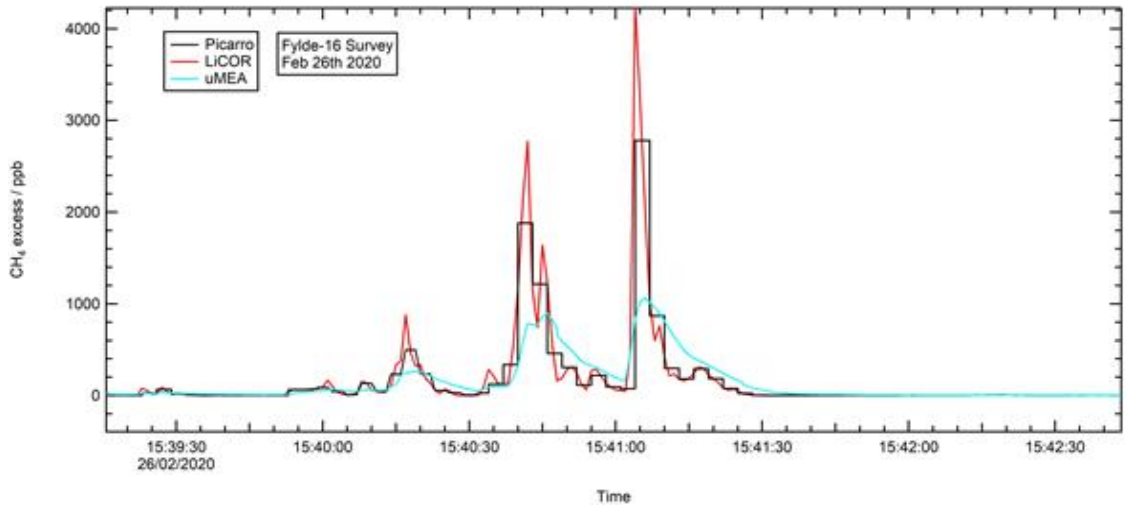


**Figure 1-18. Three sharp peaks of methane sampled during the FY16 campaign. © RHUL, 2020.**

### 1.9.3 Fylde region surveys: FY14-16

The three surveys conducted in the Fylde region (see Section 1.9.1 for details) each consisted of two survey days. Data from FY14, FY15 and FY16 are shown in Figure 1-19, Figure 1-20 and Figure 1-21 respectively. Each survey is compared to the baseline emissions study of excess $CH_4$ over background conducted prior to hydraulic fracturing (Lowry et al., 2020) to allow easy determination of new sources or discounting of previously identified sources. A moving background is calculated as the lowest 2nd percentile of values over 1200 seconds of measurement, which consisted of 600 seconds before and 600 seconds after each point. This gives a background $CH_4$ value at 1 second intervals and allows the calculation of the "excess $_{CH4}$" in ppb above the moving averaged background at a particular point in time. The background is calculated using this method to account for variation in background methane spatially and temporally during the surveying.

The maps shown in Figures Figure 1-17 - Figure 1-25 allow comparison of more recent Phase 5 surveys with the average enhancements measured during BEIS Phases 2-4 (surveys FY1-FY 9 and KM1-KM9) that are shown as the 1 $km^2$ coloured grid. Full details of the methodology can be found in Lowry et al, 2020, but in summary the methane above baseline measurements for all 1km grid squares visited at least twice were binned into 10x10m grids, which were then binned into 100x100m grids and finally into 1x1km grids to produce the 1$km^2$ methane above baseline map layer. Scaling is done in this way so that small features may only influence one or two 10x10m bins, and do not overly influence a larger than realistic area. In general it is seen that the high excess squares have not changed since Phase 2, although some new sources encountered during Phase 5 are discussed below.

FY14 (Figure 1-19) and FY16 (Figure 1-21) show new gas leak emissions in the central west of the map compared to the background (red squares, related to gas pipe replacement) as well as emissions from a former landfill which was not surveyed prior to Jan 2019 (black square) but has been recorded under prevailing wind conditions since. The red square on both FY15 (Figure 1-20) and FY16 (Figure 1-21) surveys represent narrow gas leak plumes on the dual carriageway close to Squires Gate, where it has not been possible to stop and successfully sample the emission.

Some changes have been observed during Phase 5 compared to previous surveys. Recent circuits around the PNR shale gas site have shown reduced emissions from the farm, starting with the withdrawal of cows, and by FY16 in February 2020 the introduction of sheep in the fields previously occupied by cows. This removes much of the barn source, much of the waste emission and gives a very dispersed emission plume from normally widely spread sheep. Many dairy farm barns continue to be significant $CH_4$ emitters and at least 20 have been surveyed regularly during

Phases 2-5. The increase of sheep in the whole survey region has been widespread during Phase 5 to the extent where ewes and new-born lambs were put to graze on the emitting pastures of Clifton restored landfill during Feb 2020. This landfill and the Midgeland restored landfill on the eastern periphery of Blackpool were consistently regular emitters during recent surveys. Fugitive gas leaks on Peg's Lane, 3 km S, and Peel Road, 2 km SW of the PNR site are persistent emitters under appropriate wind directions to catch plumes. The high spatial resolution provided by the new LiCOR instrument has been particularly useful on Peg's Lane where at least 7 different pipeline leaks over a 1 km length of road were isolated in the data record.

During FY15 and FY16 the new emissions are again captured with two extra emission spikes in the west of the region (red squares, Figure 1-20 and Figure 1-21). All other emissions seen during FY16 are consistent with baseline work (Lowry et al., 2020).

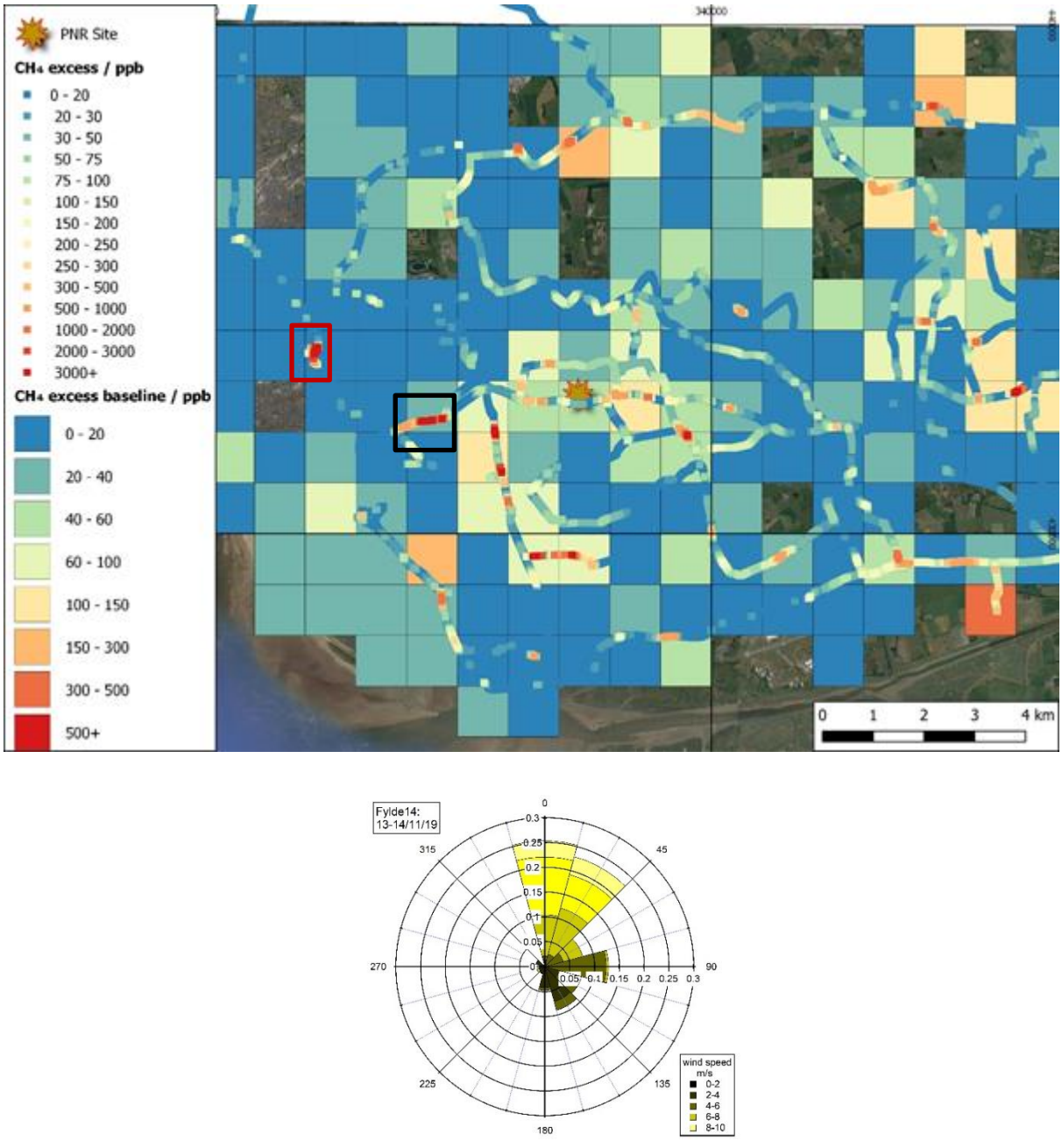


**Figure 1-19. Mapping of methane excess over background levels for the FY14 survey compared to baseline excess over background averages in 1km$^2$ for FY1-9 surveys (Lowry et al., 2020) with Wind Rose for the two survey days for FY14. Northerly winds dominate the meteorology. Red box – gas pipe replacement. Black box – Midgeland restored landfill sampled during the survey period with SE winds. © RHUL, 2020.**

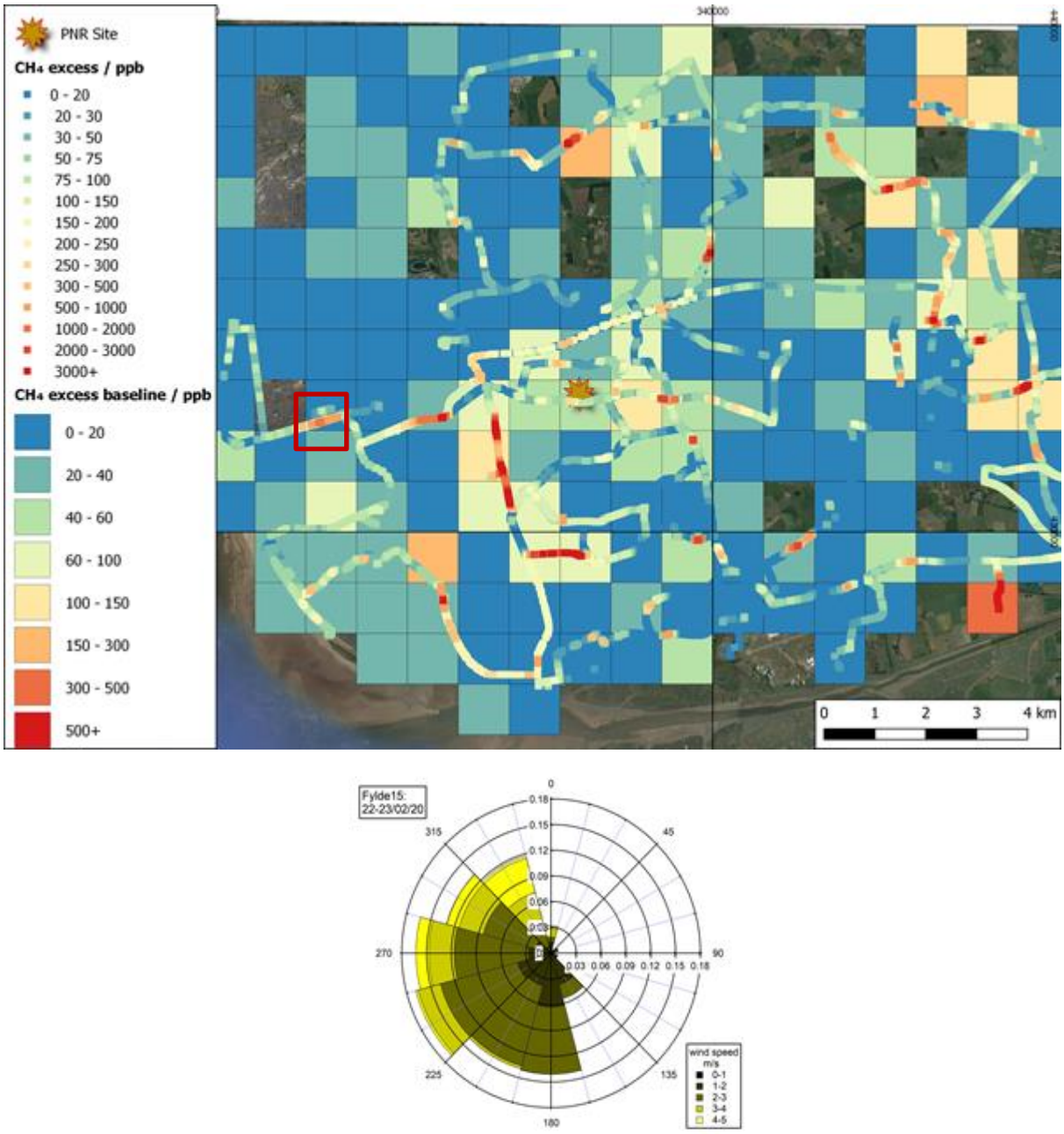


**Figure 1-20. Mapping of methane excess over background levels on the FY15 survey compared to baseline excess over background averages in 1km$^2$ for FY1-9 surveys (Lowry et al., 2020) with Wind Rose for the two survey days for FY16. South-Westerly winds are most common, but the wind fields are very variable ranging from Southerly to Northerly. Note the wind speeds are considerably lower than for the FY14 or FY16 surveys.**

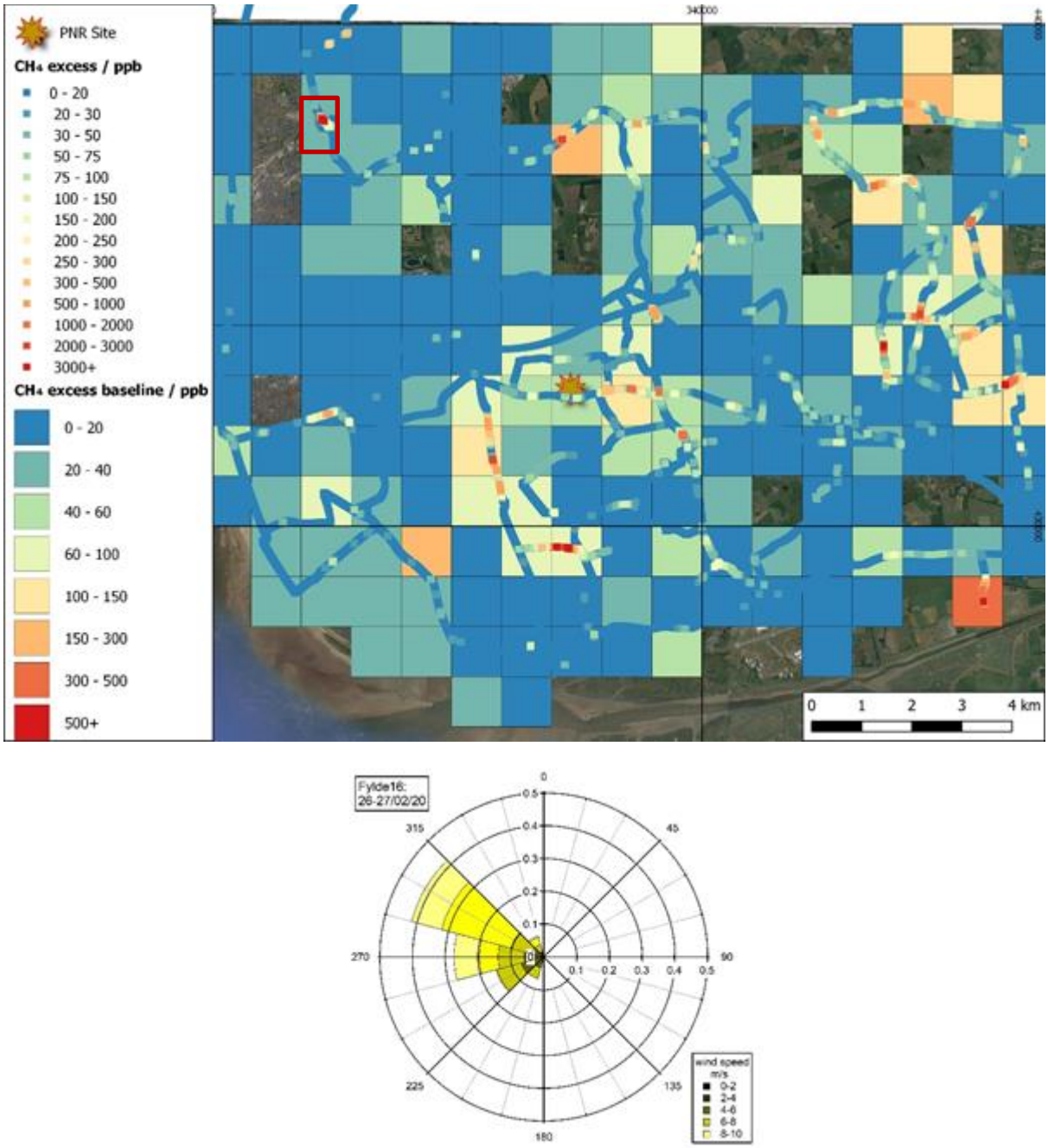


**Figure 1-21. Mapping of methane excess over background levels on the FY16 survey compared to baseline excess over background averages in 1km$^2$ (Lowry et al., 2020) with Wind Rose for the two survey says for FY16. Westerly winds dominate the meteorology. © RHUL, 2020.**

### 1.9.4 **FY14-16 C2:C1 data**

In order to identify sources of $CH_4$ plumes, when the emission source is not obvious, the C2:C1 (ethane:methane) ratio has been calculated for each 10-second period where the mean methane signal is 500 ppb or more above background. The C2:C1 is determined through a regression of ethane v methane for that 10 second period, and if the correlation coefficient (r) is greater than the critical r then the data is plotted as shown in Figure 1-22. This figure is a composite of data from FY15 and FY16 (the ethane:methane instrument was not functional for FY14). It clearly separates fugitive gas leaks (thermogenic) from biogenic $CH_4$ sources (and in some previous surveys combustion sources), but to distinguish between biogenic sources (e.g. cattle, sheep and landfills), the stable isotopic proxies are required.

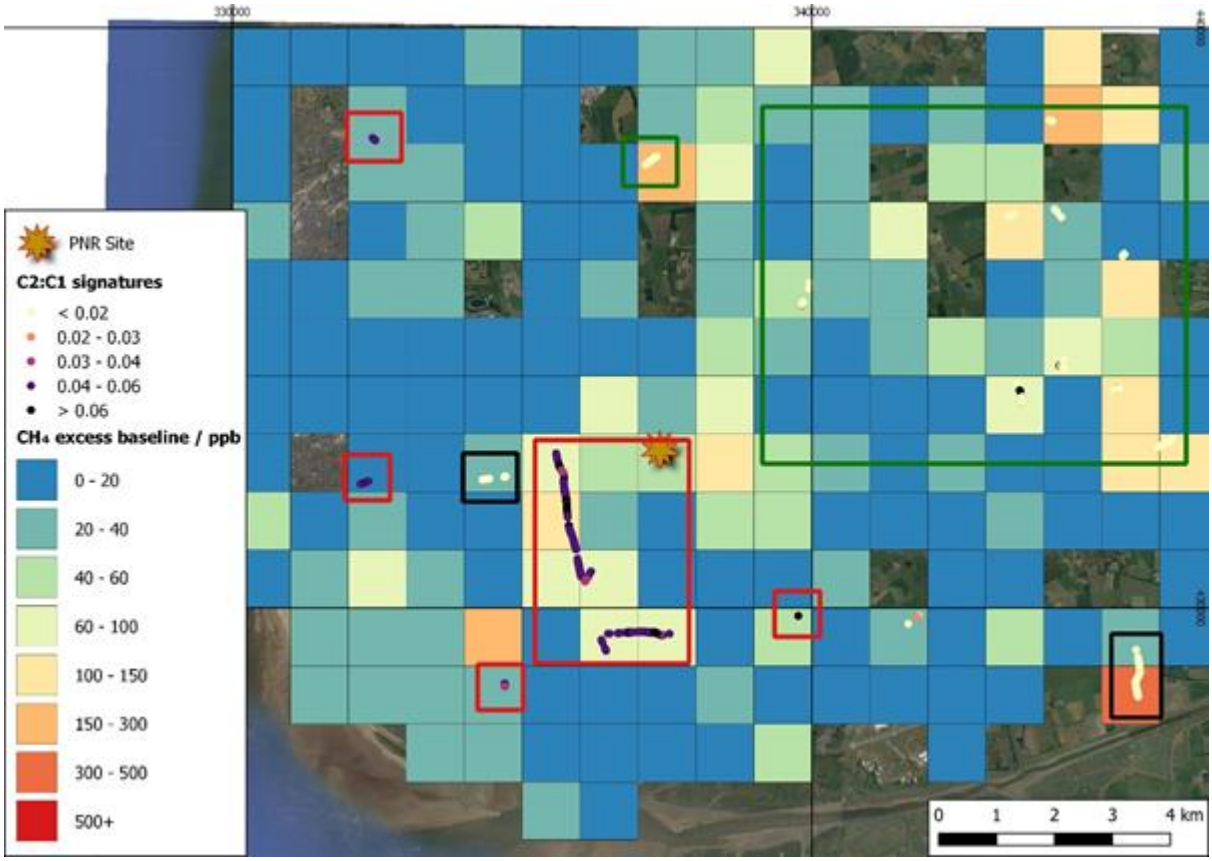


**Figure 1-22. FY15 and FY16 C2:C1 data. Highlighted emissions are coloured as follows: Red to Black - Gas leaks, Pale Yellow - Biogenic emissions from manure piles, landfill sites, dairy farms and sheep. Red boxes – gas leak areas, black boxes – restored landfills, green boxes – farm areas. The new for Phase 5 source in the NW of the region appears to have a source signature in line with previously identified gas leak emissions in the area.**


### 1.9.5 **FY14-16 isotopic source signatures**

Where it was possible to stop the vehicle in a plume with >200 ppb excess $CH_4$ over background the opportunity was taken to fill a Flexfoil bag with air over a time interval of approximately 30 seconds. This integrated plume sample was used for $\delta^{13}C$ analysis in the laboratory, to allow calculation of a $\delta^{13}C$ signature for each source plume. The source signature for each point, determined using a two-point keeling plot (Keeling, 1961) is shown in Figure 1-23 for the 59 analysed samples. More negative values (lighter coloured circles) indicate a biogenic source and less negative values (darker colours) indicate a thermogenic source. They are overlain on the $1km^2$ grids of averaged excess for surveys FY1-9 (Lowry et al., 2020) for ease of referencing with other map figures.

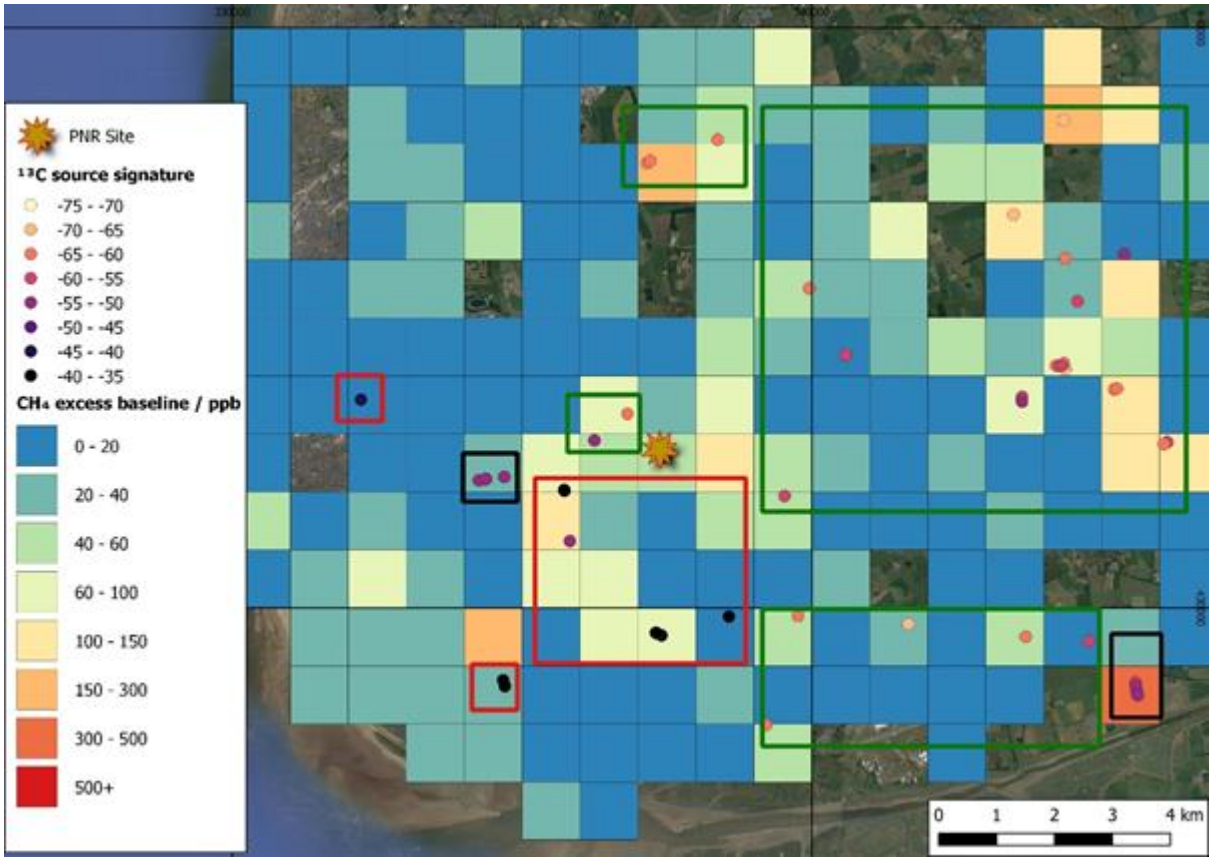


**Figure 1-23. δ13C source signatures for samples taken during FY14-16 surveys. δ13C determined from spot sampling and analysis through GC-IRMS at Royal Holloway university (Fisher et al., 2006). Coloured boxes are as for the C2:C1 analysis in Figure 1-22. © RHUL, 2020.**

Most of the $CH_4$ sources (both individual sources and grouped source types) have consistent $\delta^{13}C$ signatures across multiple surveys over 4 years (Phases 2-5, Table 1-4 ), particularly fugitive gas emissions at -41 to -40 ‰, closed landfills at -56 to -55 ‰ and an active landfill at -59 to -58 ‰. Dairy farms vary greatly depending on the proportions of eructation (-70 ‰) to excreted waste (- 50 ‰).

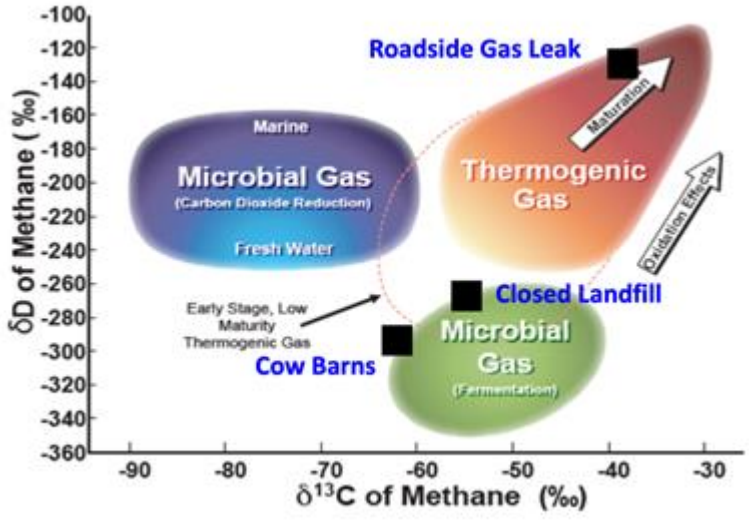


**Figure 1-24. Cross-plot of δD vs δ13C source signatures for 3 source categories identified during the FY14 campaign in November 2019. After Whiticar & Schaefer (2007). © RHUL, 2020.**

In November 2019 the RHUL greenhouse gas laboratory installed a prototype mass spectrometer for the measurement of the δD ($^2H/^1H$) ratio of $CH_4$. The instrument is still under test but was used to make preliminary measurements of FY14 campaign samples for 3 identified source categories (gas leaks, closed landfill, cow barns). These are shown plotted in δD vs $\delta^{13}C$ space in Figure 1-24. With enough measurements of both isotopes it is hoped that this technique will provide further discrimination between different biological pathways and gas reservoirs.

**Table 1-4. δ13C signatures of the main methane sources seen on each campaign in the Fylde identified from Keeling plot analysis. On some campaigns two different signatures were identified for cows, the top one when they were in barns and the bottom one when they were in fields.**

| Source | Location (Lat, Long) | $\delta^{13}C$ signatures (‰) | | | | | | | | | | | | | | |
|---|---|---|---|---|---|---|---|---|---|---|---|---|---|---|---|---|
| | | Mar 2016 | Jul 2016 | Jun 2017 | Oct 2017 | Jan 2018 | Feb 2018 | July 2018 | Aug 2018 | Oct 2018 | Jan 2019 | Mar 2019 | Oct 2019 | Nov 2019 | Jan 2020 | Feb 2020 |
| Gas leaks | Many | -41.2 | | -40.9 | -42.8 | -42.6 | -40.6 | -40.8 | -40.5 | -39.4 | -40.8 | -39.6 | -40.9 | -39.9 | -39.1 | -39.9 |
| Clifton landfill (closed) | 53.75°N 2.82°W | -55.1 | | | | -55.5 | | -55.8 | | | | -52.0 | | | -55.2 | -54.6 |
| Anna's Rd Landfill (closed) | 53.78°N 2.98°W | | | | | | -59.8 | | | | -57.2 | -57.5 | | | | |
| Midgeland Landfill (closed) | 53.78°N 2.99°W | | | | | | | | | | -55.3 | -55.0 | -55.1 | -53.9 | -53.5 | |
| Fleetwood Landfill (active, closed) | 53.91°N 3.03°W | -57.8 | -58.4 | -58.3 | | | | -58.7 | | -54.3 | | | | | | |
| Manure piles | Many | -51.6 | | -53.1 | | -58.6 | | -55.9 | -51.6 | | | | | | | -50.8 |
| Dairy farms | Many | -60.2, -64.4 | -58.4 | -59.1 | -60.9 | -66.2 | -61.0 | -62.7 | -59.1, -67.9 | -62.9 | -62.2 | -62.6 | -58.5 | -61.9 | -62.0 | -60.5 |

Comparison of Figure 1-22 and Figure 1-23 clearly highlights the use of the C2:C1 and isotopic proxies, with both giving clear separation of gas from biogenic sources. $\delta^{13}C$ analysis allows for further careful subdivision between ruminant emissions and waste sources compared to the C2:C1 data, but ethane measurements are instantaneous in the field and will immediately separate gas leaks and combustion sources from biogenic sources. Furthermore most combustion sources encountered are very small (bonfires, old car exhausts) and can only very rarely be collected in sample bags, but which can be separated from gas leaks by C2:C1 analysis (Lowry et al., 2020).

### 1.9.6 **Vale of Pickering (Ryedale) surveys: RY10-11**

Two surveys were carried out in the Vale of Pickering (Ryedale) region, the first (RY10) had some focus on the Pickering gas offtake station, following discussions with National Grid, during which the location area of 1 of 2 significant plumes was narrowed down to the NW corner of the installation. The other significant source in the region, the East Knapton quarry landfill, which was inactive and partially landscaped at the end of Phase 4, was undergoing landscaping and related

cap disturbance had released significant emissions again with a signature more typical of unoxidised $CH_4$ from an open landfill.

Other gas leaks persisted to the east of Kirby Misperton, on Edenhouse Road and on the A170. Eight or nine regularly sampled cow barns and some manure piles also persisted, the one that forms the deep orange square on the excess baseline layer of Figure 9 being The Grange farm near Malton.

The second day of RY11 campaign saw a major temperature inversion in the morning, which persisted until 13:30, resulting in a mix of trapped emissions between the southern chalk escarpment and the North Yorks Moors to the north. This resulted in a variable and elevated background, giving rise to the anomalous excesses recorded for the S-N transect seen along the right-hand edge of Figure 1-25, and which would cause anomalous average excesses if included in a baseline excess compilation.

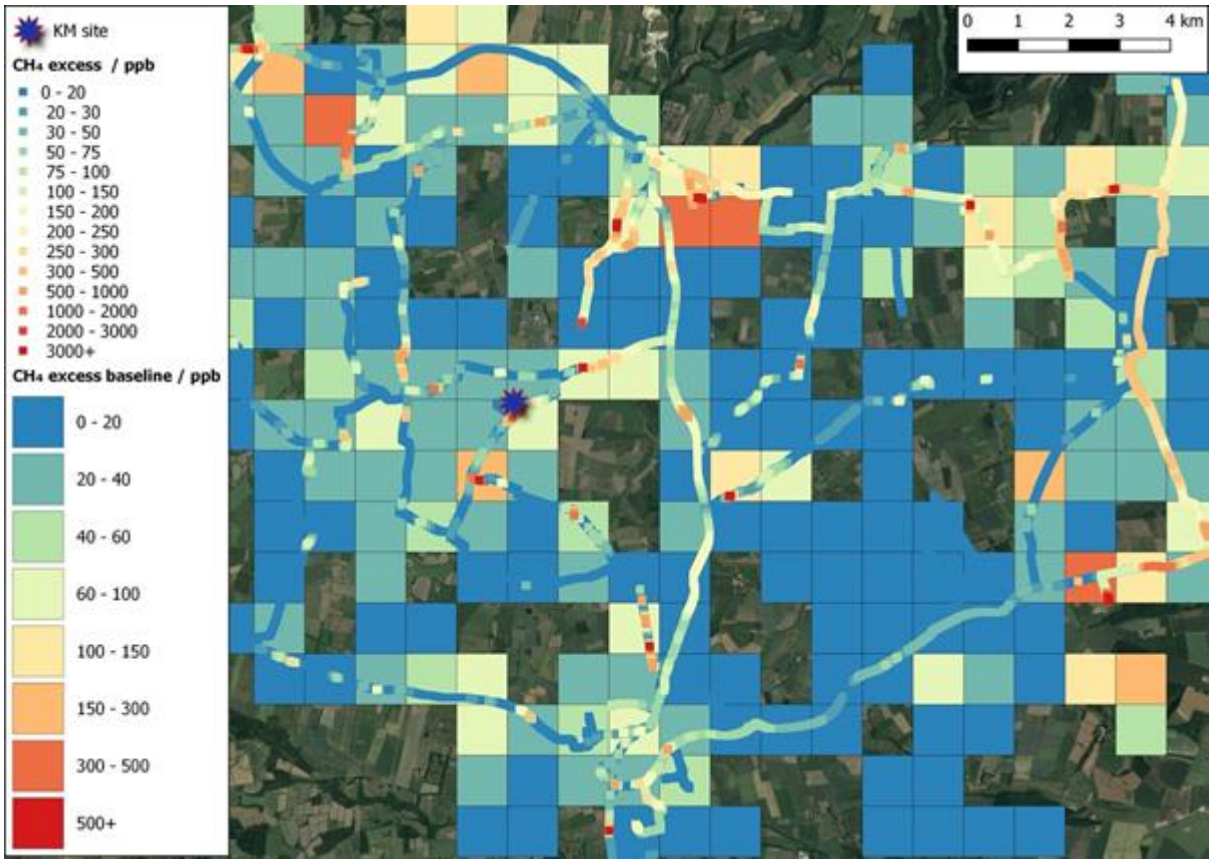


**Figure 1-25. Mapping of methane excess over background levels on the RY11 survey compared to baseline excess over background averages in 1km$^2$ for RY1-9 surveys (Lowry et al., 2020). © RHUL, 2020.**

### 1.9.7 RY10-11 C2:C1 data

As for the Fylde region the C2:C1 ratio clearly distinguishes the biogenic sources from the swathe of gas leak emission plumes seen in an arc between Pickering and Malton (Figure 1-26). As found in Phase 3 and 4 surveys the ratios for gas leaks tend to fall in the range 0.05 to 0.08. The two separate clusters of biogenic points toward the SE of the area represent the same plume from the East Knapton Quarry landfill measured at different distances from source during predominant SW-WSW winds.

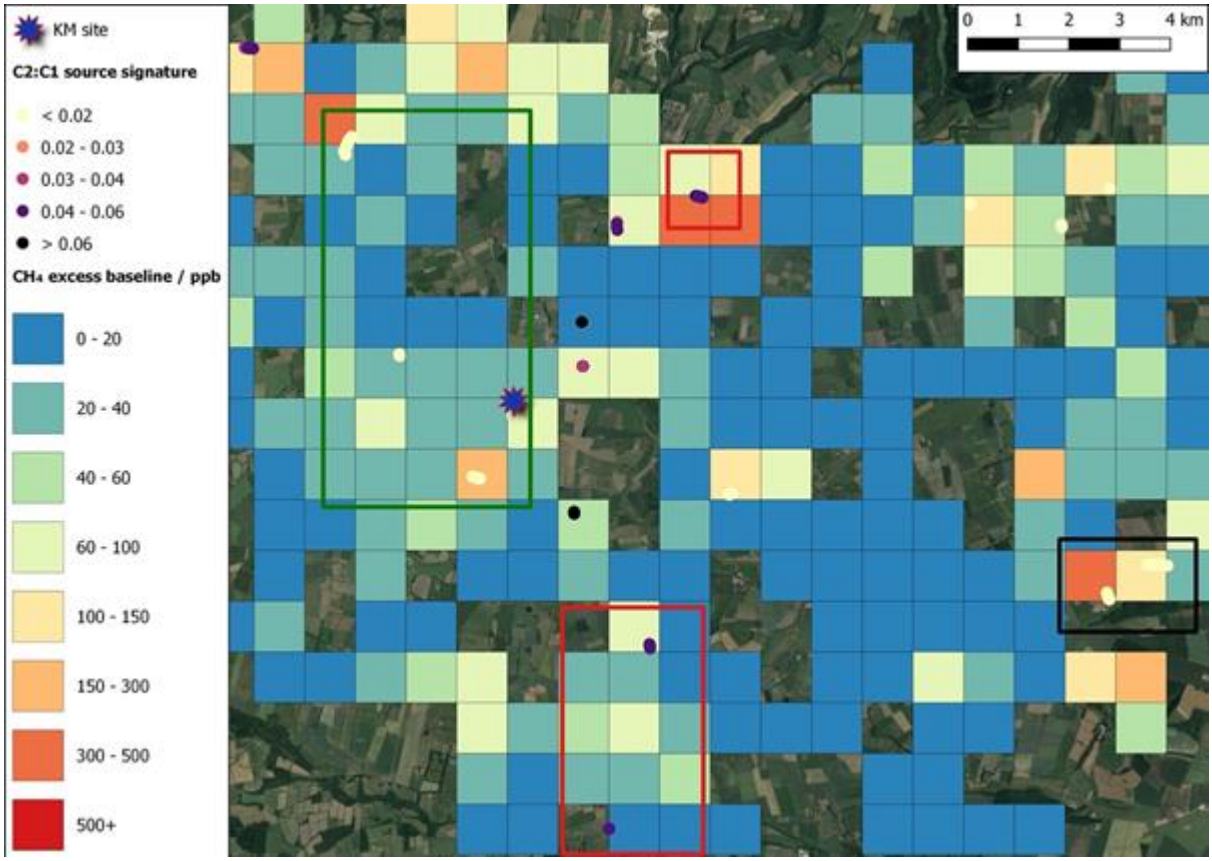


**Figure 1-26. KM11 C2:C1 data. Highlighted emission peaks are coloured as follows: Red to Black cicles - Gas leaks, Pale Yellow - Biogenic emissions from manure piles, landfill sites, dairy farms and sheep. Red boxes – gas leak areas, black boxes – restored landfills, green boxes – farm areas. © RHUL, 2020.**

### 1.9.8 RY 10-11 surveys - isotopic source signatures

Many sources have persisted throughout Phases 2 to 5, most notable being the Pickering gas offtake station, which has shown consistent $\delta^{13}C$ signatures in the range -42 to -40 ‰ (Table 1-5). Other identified and persisting gas leaks have signatures in this range also. The East Knapton Quarry landfill (black box to east side of Figure 1-27) has given signatures in the range -61 to -58 ‰ over the 2017-20 period, typical of active UK landfill sites. Manure piles are often present all year in the Ryedale region in contrast to the Fylde and as such they were sampled during a range of temperatures, and during some very wet and very dry periods. This influenced the degree of oxygenation vs anaerobic activity, resulting in a wide range of measured signatures from more oxygenated (-49 ‰) to more anaerobic (-63 ‰). Cow barns varied from -67 to -59 ‰, but overall they average more than 2 ‰ lower than in the Fylde region (-64 compared to -62 ‰). Most were identified as Friesian Holstein dairy cattle in both regions so the difference is most likely related to differing waste management practices.

### 1.9.9 Summary – Mobile surveys

The following points summarise the findings of Phase 5 mobile surveys in comparison to earlier phases and between the two regions:

1. Dairy farms are the most widespread $CH_4$ emitters in both regions, with up to 20 farms in Fylde and 10 in Vale of Pickering being regularly surveyed.
2. There has been some shift toward sheep farming in both areas, producing a more dispersed $CH_4$ source compared to the cow barn point sources. The increase in sheep

numbers was apparent in the Vale of Pickering region in Phase 4, but not until Phase 5 in the Fylde.

3. Manure piles are a more constant feature in Vale of Pickering, whereas in the Fylde they are less prevalent and mostly found emitting in summer.

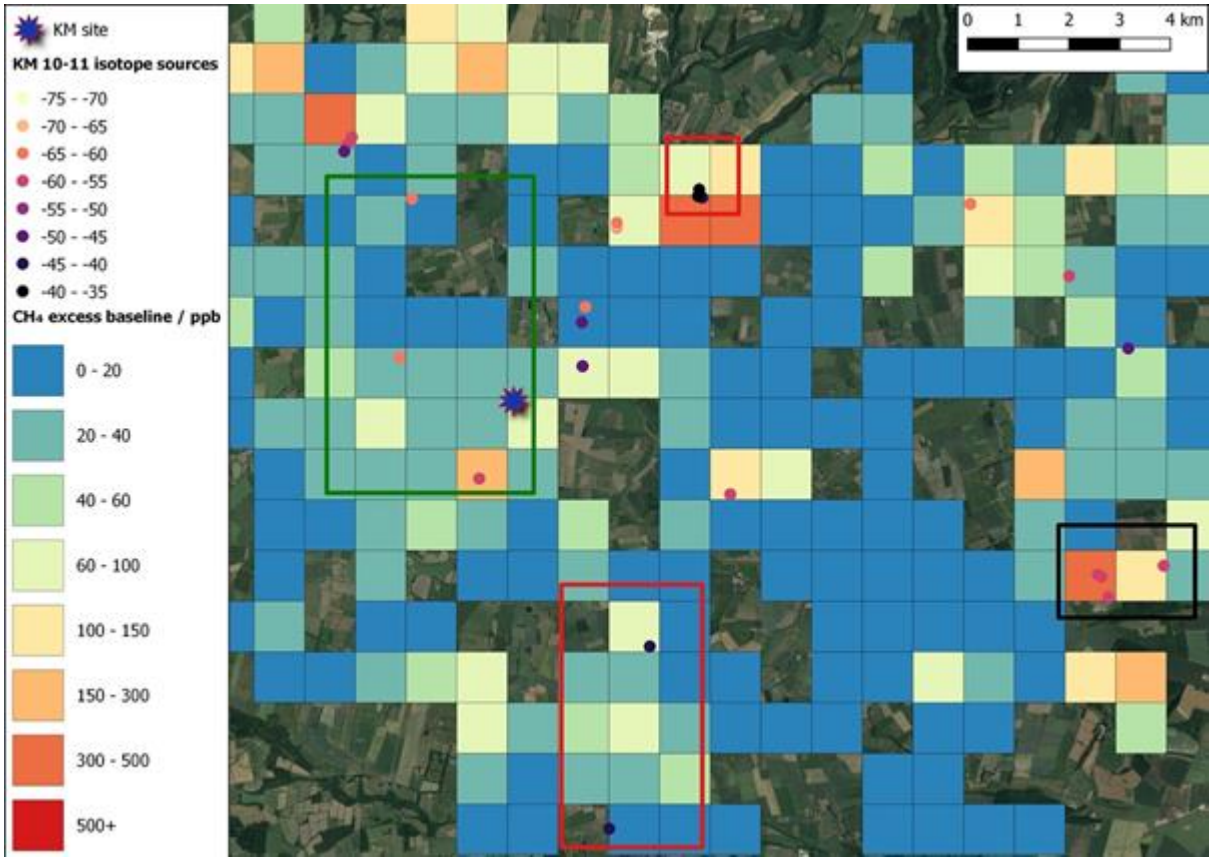


**Figure 1-27. $\delta^{13}C$ source signatures for samples taken during RY10-11 surveys. $\delta^{13}C$ determined from spot sampling and analysis through GC-IRMS at Royal Holloway university (Fisher et al., 2006). Coloured boxes are as for the C2:C1 analysis in Figure 1-26. © RHUL, 2020.**

The points below have been confirmed by the repeat surveys in the Fylde and Vale of Pickering, but are consistent with studies in other parts of the UK.

4. Older restored landfill sites without gas capture are significant emitters if they are still young enough to be in the gas generation window (filled to 1990s and 2000s) and were not well managed. Those with gas capture are not major emitters once closed and capped.
5. Most above-ground gas infrastructure emits some CH4 but is very variable. The spread of gas governors has resulted in new emission sources, but as these are low pressure relief valves they are intermittent and often not detected during surveys.
6. Pipeline leaks often change position. The larger leaks are detected and repaired and there are emissions during pipeline replacement projects, but some stretches of road with smaller leaks or away from urban population can go undetected for years and although picked-up during mobile surveys they are not possible to pinpoint accurately.

**Table 1-5. $\delta^{13}C$ signatures of the main methane sources seen on each campaign in the Vale of Pickering identified from Keeling plot analysis. The Pickering offtake station survey with two source signatures in March 2019 was because two distinctive peaks could be sampled from the installation during the unusual southerly wind direction.**

| Source | Location (Lat, Long) | $\delta^{13}C$ signatures (‰) | | | | | | | | | | |
|---|---|---|---|---|---|---|---|---|---|---|---|---|
| | | Oct 2016 | Jan 2017 | Jun 2017 | Oct 2017 | Jan 2018 | Mar 2018 | Jul 2018 | Nov 2018 | Mar 2019 | Dec 2019 | Feb 2020 |
| Pickering gas offtake station | 54.236°N 0.762°W | -41.7 | -42.4 | -40.6 | -42.9 | -42.0 | -42.0 | -41.9 | -41.2 | -41.4, -40.4 | -38.9 | -40.2 |
| Gas leak A170 | 54.264°N 0.905°W | | | | -41.4 | -41.5 | -41.6 | | | | | |
| Gas leak, Kirby Misperton | 54.207°N 0.798°W | | | -39.9 | | | -44.2 | | | | | -36.6 |
| Gas leak, Edenhouse Road | 54.157°N 0.779°W | | | | | -40.9 | -41.4 | | -40.6 | -40.8 | | -40.7 |
| Caulklands landfill (closed) | 54.242°N 0.711°W | -57.4 | -57.3 | -59.0 | | | -57.9 | | | | | |
| Knapton landfill (active) | 54.162°N 0.644°W | | | -58.5 | -58.6 | -59.6 | -61.1 | -58.7 | -61.4 | -56.2 | -59.3 | -59.6 |
| Manure piles | Many | | | -49.7 | -56.7 | | -50.1 | -63.4 | | -51.2 | -49.6 | -55.8 |
| Dairy farms | Many | -63.6 | -59.3 | -64.7 | -66.2 | -67.3 | -65.5 | -67.0 | -64.1 | -63.9 | -63.2 | -64.9 |

# 2 Air quality

## 2.1 INTRODUCTION

This section reports the Air Quality (AQ) dataset for the Kirby Misperton (KM) and Preston New Road (PNR) measurement sites (Figure 1-1 and Figure 1-2). The statistical analysis of the AQ dataset for both sites is presented and interpreted in the context of sources of emissions using meteorological data to aid analysis. The analysis provides information on the annual climatology of air pollution at both locations along with representative insight into shorter-term variability in air pollution. The baseline analysis is framed specifically with reference to the attainment of UK and European Commission (EC) Directive air quality standards at both locations. This uses a range of metrics including annual means, frequency of exceedance of 1 hour and 8 hour mean concentrations. As detailed in Table 1-2, hydraulic fracturing operations took place at the PNR during this measurement period (Phase 5). KM remained as a baseline site with no further significant industrial activity taking place on the site since 2018.

## 2.2 THE BASELINE DATASET

The dataset used in this report was collected using surface monitors located at KM and PNR and covers the observation period from 1 February 2019 until 31 January 2020. The dataset includes local meteorology (measured at 2 m above ground), nitrogen oxides (NO and $NO_2$, collectively $NO_x$), particulate matter (PM) in a number of aerodynamic size ranges (PM1, PM2.5, PM4, PM10), ozone ($O_3$), speciated non methane hydrocarbons (NMHCs) and hydrogen sulphide ($H_2S$). The data are archived and publically accessible at the NERC Centre for Environmental Data Analysis (CEDA). Measurements are available at 1 minute intervals, except NMHCs which are reported as weekly-average values, see: http://browse.ceda.ac.uk/browse/badc/envbaseline. The environment baseline is firstly examined on a site by site basis followed by comparison of the climatologies of pollution at each site.

## 2.3 RESULTS AND DISCUSSION

Managing and improving air quality in the UK is driven by European (EU) legislation on ambient air quality standards and also commitments to limit transboundary emissions, through the National Emissions Ceiling Directive and the Gothenburg protocol. The 2008 ambient air quality directive (2008/50/EC) sets legally binding limits for outdoor air pollutants that impact on human health and includes $NO_2$, $O_3$, benzene, $PM_{10}$ and $PM_{2.5}$. The UK also has air quality strategy targets for 1,3-butadiene.

All these parameters have been measured as part of the environmental monitoring project. Within the UK, ambient air quality is controlled with the aspiration that all locations meet either the prescribed Limit Values or Target Values depending on the species. EU Limit values are legally binding concentrations that must not be exceeded. There are prescribed averaging times associated with each pollutant, and for some pollutants a number of exceedances for particular averaging times are allowed in each year. Target values are meant to be attained where possible by taking all necessary measures not entailing disproportionate costs.. All EU directive standards are listed here: http://ec.europa.eu/environment/air/quality/standards.htm. The UK air quality objectives for data parameters measured as part of the air quality baseline are shown in Table 2-1.

### 2.3.1 Summary of annual means of air pollutants at KM and PNR

Table 2-2 shows a summary of the Phase 5 annual mean concentrations of various air pollutants at both KM and PNR and a restatement of the annual directive limit value. The average of pollutants at both sites is similar. The main difference is the $NO_x$ at PNR, which is twice as high as KM. This is likely due to a nearby main road that runs to the south east of the PNR monitoring station.

**Table 2-1. UK National and EC air quality objectives.**

| Pollutant | Concentration ($\mu g/m^3$) | Averaging period | Legal nature | Permitted exceedances | Approx concentration (ppb) |
|---|---|---|---|---|---|
| Fine particles ($PM_{2.5}$) | 25 | 1 year | Limit value | none | n/a |
| Nitrogen dioxide ($NO_2$) | 200 | 1 hour | Limit value | 18 per year | 104.7 |
| | 40 | 1 year | Limit value | none | 20.9 |
| Coarse particles ($PM_{10}$) | 50 | 24 hours | Limit value | 35 per year | n/a |
| | 40 | 1 year | Limit value | none | n/a |
| Benzene | 5 | 1 year | Limit value | none | 1.88 |
| Ozone ($O_3$) | 120 | Maximum daily 8-hour mean | Target value | 25 days averaged over 3 years | 60.1 |

**Table 2-2. Summary of annual statistics for KM and PNR locations for various air pollutants and comparison against annual mean limit values.**

| Pollutant | Annual Mean at KM Feb 2019 - Jan 2020 | Annual mean at PNR Feb 2019 - Jan 2020 | Annual mean Limit value |
|---|---|---|---|
| $O_3$ | 22.7 ppb | 22.4 ppb | 60.1 ppb |
| $PM_{2.5}$ | 7.4 $\mu g/m^3$ | 7.7 $\mu g/m^3$ | 25 $\mu g/m^3$ |
| $PM_{10}$ | 11.1 $\mu g/m^3$ | 11.5 $\mu g/m3$ | 40 $\mu g/m^3$ |
| NO | 0.4 ppb | 0. 9 ppb | No limit value |
| $NO_2$ | 2.0 ppb | 4.7 ppb | 20.9 ppb |
| $NO_x$ | 2.4 ppb | 5.6 ppb | No limit value |
| Benzene | 0.3 ppb | 0.4 ppb | 1.88 ppb |
| $H_2S$ | 0.7 ppb | 0.3 ppb | - |
| $SO_2$ | 0.4 ppb | 0.9 ppb | - |

**Table 2-3. Measured exceedances of air quality standards. See Table 2-1 for details of UK National and EC air quality objectives**

| Pollutant | KM | PNR | Limit |
|---|---|---|---|
| $O_3$ | 3 x 8-hour exceedances | 0 x 8-hour exceedances | 60.1 ppb |
| $PM_{10}$ | 0 x 24-hour exceedances | 0 x 24-hour exceedances | 50 $\mu g/m^3$ |
| $NO_2$ | 0 x 1-hour exceedances | 0 x 1-hour exceedances | 200 $\mu g/m^3$ |

Within the measurement period there were no $NO_2$ or $PM_{10}$ exceedances of UK air quality limits at either site. However, $O_3$ at KM exceeded the 8 hour average of 60.1 pbb on three occasions between 24/08/19 and 27/08/19, reaching a maximum of 88 ppb. This was due to the UK experiencing a heat wave during this period and anticyclonic weather conditions which resulted in a build-up in pollution and increased $O_3$ production. Although the instrument at PNR did not measure any exceedances, the $O_3$ concentration was also elevated (up to 58 ppb).

### 2.3.2 Spatially resolved air pollution climatologies

The annual mean values for air pollution allow for comparison against national targets. $NO_x$, $O_3$, PM (PM1, PM2.5, PM4 and PM10) and meteorological data have all been collected at 1-minute time resolution and this is advantageous for data analysis as a more detailed climatology of air pollution can be constructed at the local scale.

The daily averages for the Phase 5 period are shown in Figure 2-1 and Figure 2-2.

The $O_3$ at KM is highest in August; as mentioned earlier this coincides with a heat wave experienced across the UK. These anticyclonic conditions also resulted in a build-up of particulate matter. Any gaps in the data are due to instrument maintenance and failures.

### 2.3.3 Kirby Misperton (KM) detailed analysis

There has been no additional shale gas operational activity at the KM site during this project period and it remained in a baseline state for the whole of the measurement period, having retuned to this in 2018 after on-site preparations for hydraulic fracturing of the shale gas well (equipment mobilisation/de-mobilisation) ceased (Ward et al., 2019). The site continues to operate as a conventional gas well site as it has since the beginning of the project. As mentioned previously there were some instrument failures at the monitoring site which resulted in data loss at certain periods.

To enable a full baseline climatology of air pollution to be established it is important to examine the influence of wind direction. Table 2-2 reports the annual means for pollutants measured under the Air Quality Directive whereas Table 2-4 reports those metrics by individual 45-degree wind sector. In the UK it is most common for air from the East (E) and Southeast (SE) to be most polluted as winds from these directions often bring air from the SE of England and from continental Europe. The lowest concentrations of air pollution are typically observed during periods of high wind speed Atlantic westerly airflow. The measurements at KM continue to be similar to those observed throughout the initial baseline with the highest concentrations of $NO_x$ to the S and SE of the site with no influence from activity on the site itself (W).

(a)

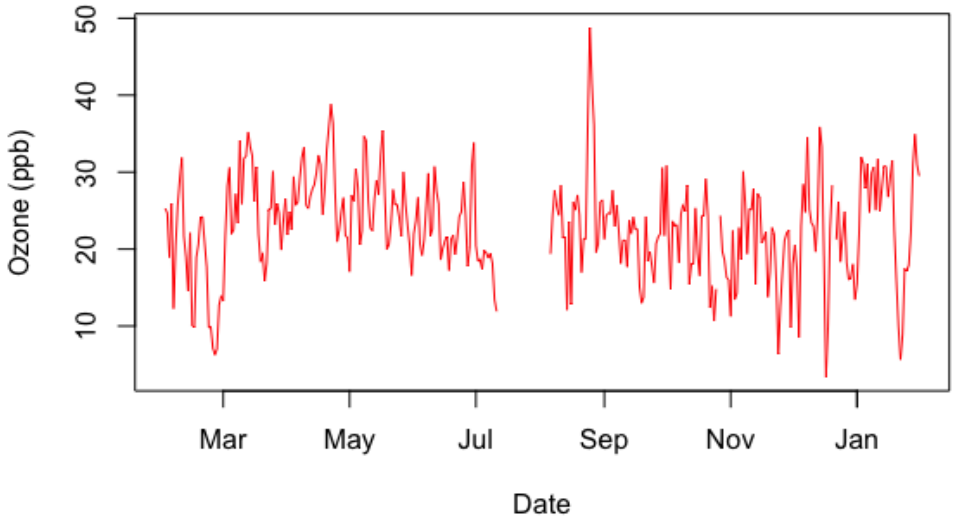


(b)

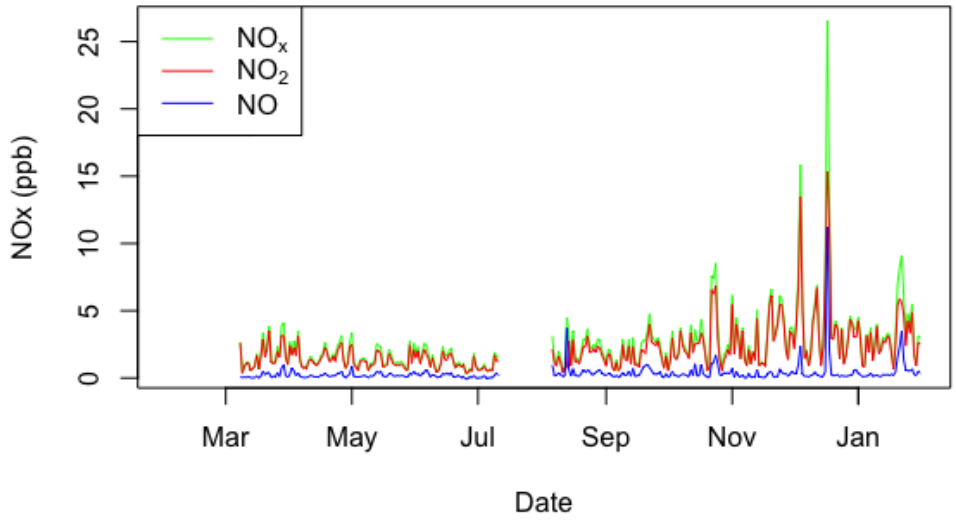


(c)

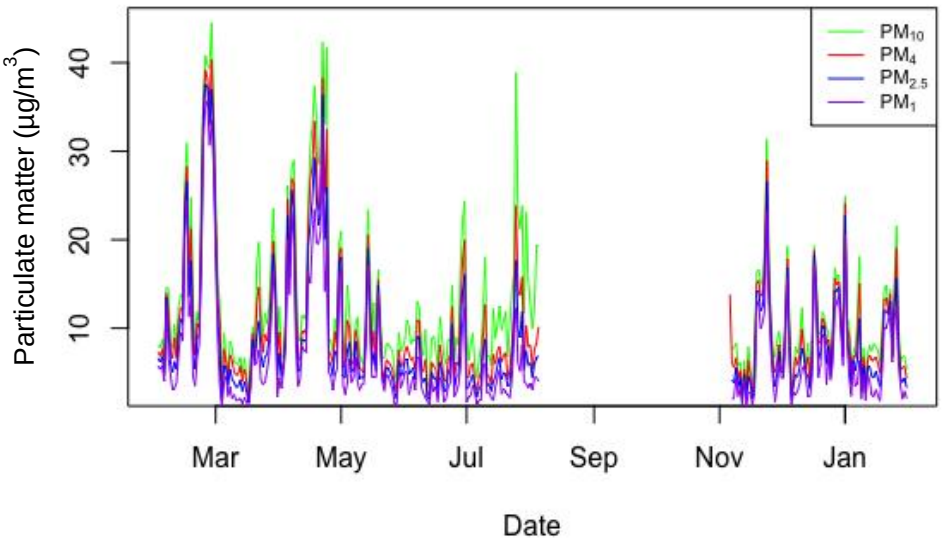


**Figure 2-1. Phase 5 daily time series at the KM site for (a) $O_3$, (b) NO, $NO_2$, $NO_x$ (c) $PM_1$, $PM_{2.5}$, $PM_4$, $PM_{10}$ over the period February 2019 - January 2020. Gaps in time series indicate missing data. © University of York, 2020.**

(a)

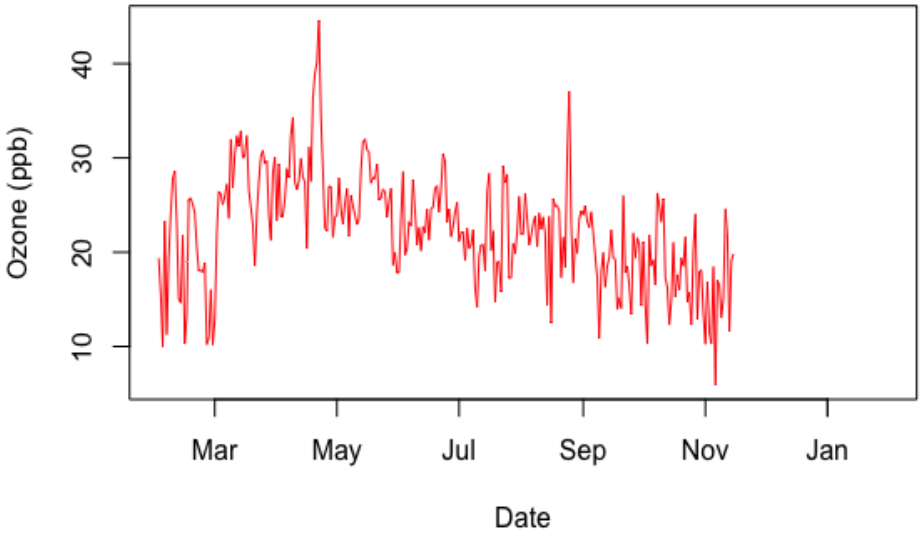


(b)

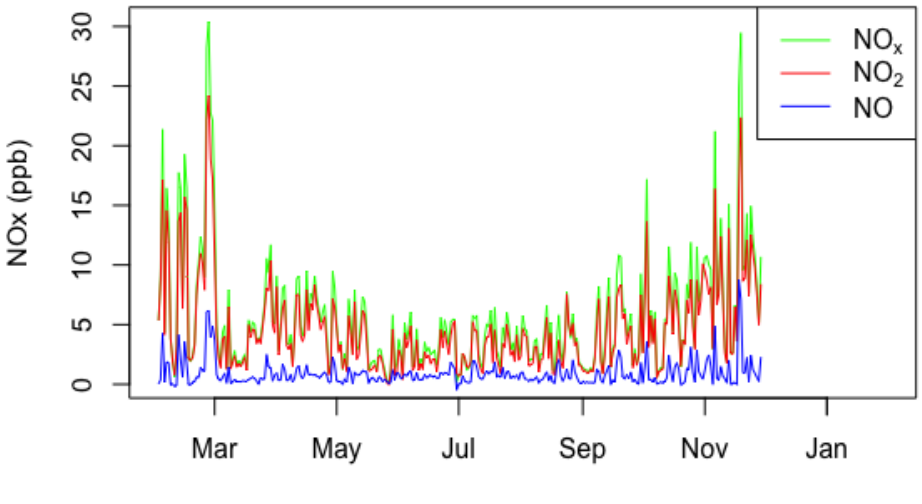


(c)

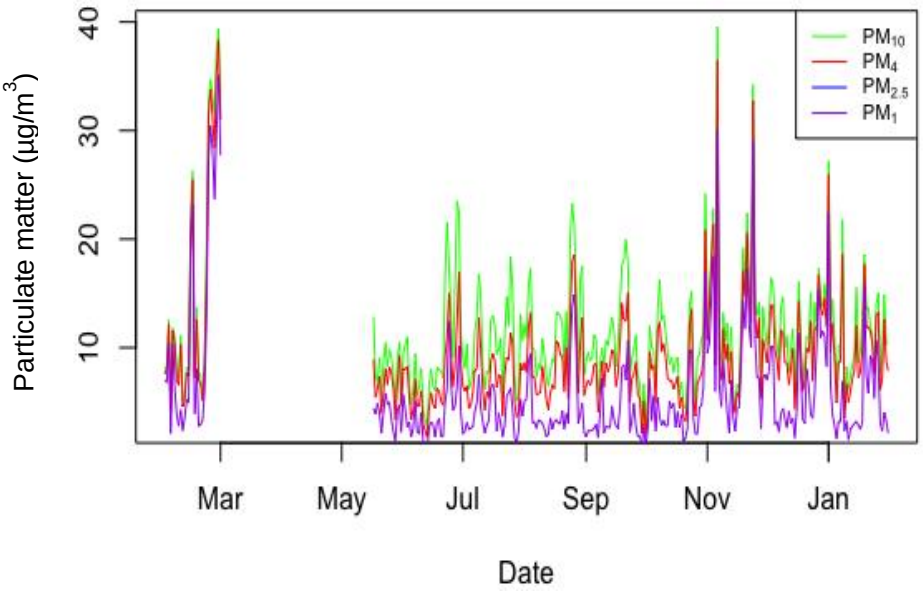


**Figure 2-2. Phase 5 daily time series at the LP site for (a) $O_3$, (b) NO, $NO_2$, $NO_x$ (c) $PM_1$, $PM_{2.5}$, $PM_4$, $PM_{10}$. over the period February 2019 - January 2020. Gaps in time series indicate missing data. © University of York, 2020.**

**Table 2-4. Phase 4 wind sector averages at KM.**

| | 45-degree wind sector | | | | | | | |
|---|---|---|---|---|---|---|---|---|
| | **N** | **NE** | **E** | **SE** | **S** | **SW** | **W†** | **NW** |
| **$O_3$ (ppb)** | 21.9 | 23.9 | 26.2 | 23.7 | 22.9 | 24.9 | 26.9 | 26.8 |
| **NO (ppb)** | 0.4 | 0.2 | 0.1 | 0.4 | 0.4 | 0.4 | 0.2 | 0.1 |
| **$NO_2$ (ppb)** | 1.9 | 1.9 | 2.2 | 2.6 | 2.8 | 2.1 | 1.2 | 1.2 |
| **$NO_x$ (ppb)** | 2.2 | 2.2 | 2.4 | 2.9 | 3.2 | 2.5 | 1.5 | 1.6 |
| **$PM_{2.5}$ (µg/m$^3$)** | 8.5 | 12.1 | 12.3 | 9.3 | 8.7 | 6.7 | 5.6 | 5.9 |
| **$PM_{10}$ (µg/m$^3$)** | 12.4 | 16.7 | 17.6 | 13.4 | 12.4 | 10.1 | 9.2 | 9.4 |
| **$H_2S$ (ppb)** | No data | 0.7 | 0.6 | 0.6 | 0.5 | 0.4 | 0.8 | 0.5 |
| **$SO_2$ (ppb)** | 0.4 | 0.3 | 0.3 | 0.4 | 0.4 | 0.4 | 0.2 | 0.1 |

† Sector within which the shale gas well lies.

#### 2.3.3.1 DIURNAL VARIATION OF AIR POLLUTION AT KM

The diurnal variation of $O_3$, $NO_x$ and PM at KM are shown in Figure 2-3. $O_3$ shows a typical diurnal profile with a peak just after midday, similar to those shown in previous reports. $O_3$ is lowest at night and peaks just after midday, as expected in the general context of UK oxidative air chemistry. This is due to a combination of factors: boundary-layer height, daytime photochemical production, and night-time surface depletion..

The $NO_2$ profile increases in the morning and late afternoon as described in previous reports. However, there does appear to be a peak mid-morning in the NO measurements. The ratio of NO to $NO_2$ is biased towards $NO_2$ indicating that very close-by combustion sources are not dominating the local $NO_x$. This is similar to Phase 4 (Ward et al., 2019) but the opposite to the Phase 3 monitoring period (Ward et al, 2018) where it was balanced towards NO due to emissions on the shale gas site associated with mobilisation/de-mobilisation of diesel-powered equipment for hydraulic fracturing operations. PM was similar to concentration observed in previous years.

#### 2.3.3.2 HEBDOMADAL CYCLES AT KM

Higher air pollution concentrations during the working week (Mon - Fri) are again clear from the $NO_x$ measurements with $NO_x$ being highest during weekdays and decreasing at the weekend (Figure 2-4). $O_3$ and PM have a less pronounced weekly cycle.

High NO observed on a Tuesday has been investigated further. It is influenced by mixing ratios of > 30ppb (100 times normal) observed on Tuesday 17$^{th}$ December. During this 24 hour period, the relative distribution of NO to $NO_2$ was balanced towards NO indicating that very close-by source of combustion impacted local air quality. However, it should be noted that generally the $NO_x$ mixing ratios are lower than observed in previous years.

(a)

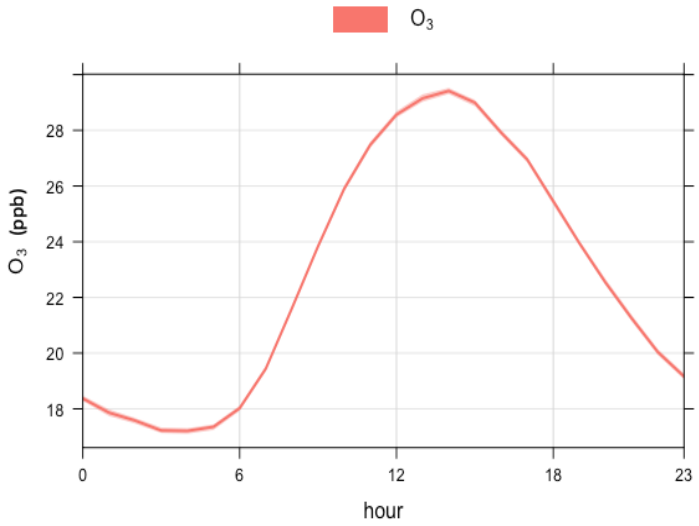


(b)

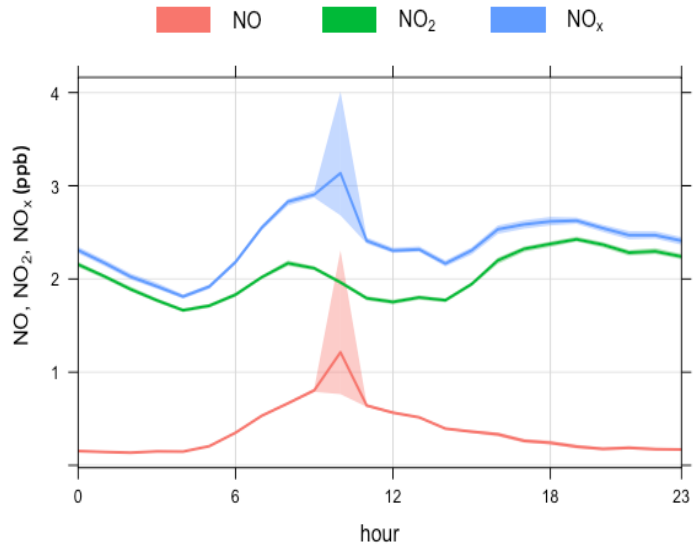


(c)

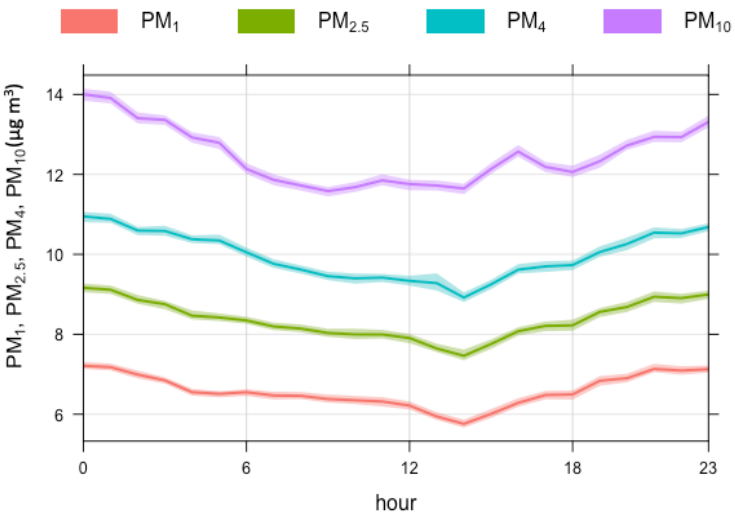


**Figure 2-3. Diurnal variation of $O_3$, $NO_x$ and PM at the KM measurement station meaured over the period February 2019 - January 2020. Shaded areas indicate the 95% confidence inteval. © University of York (2020).**

(a)

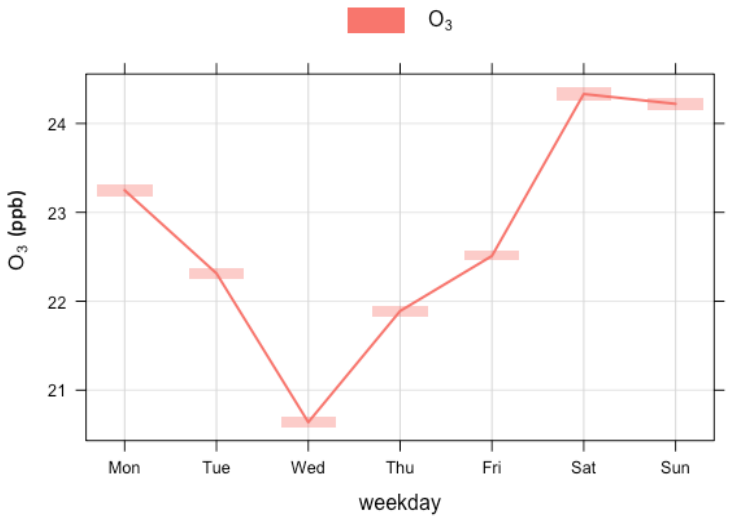


(b)

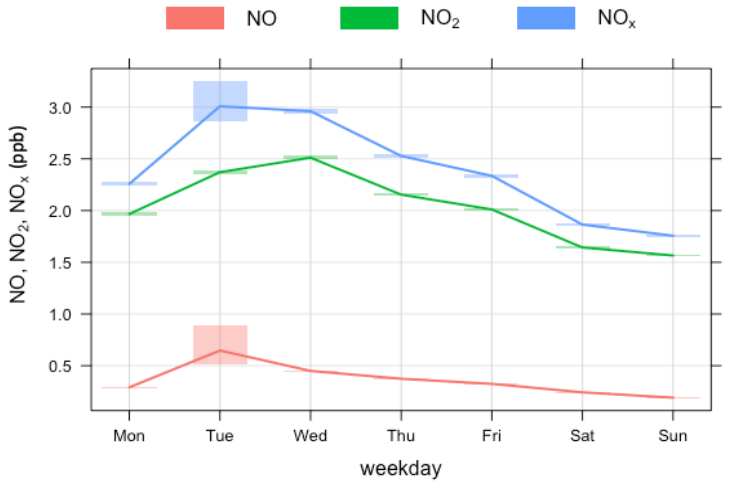


(c)

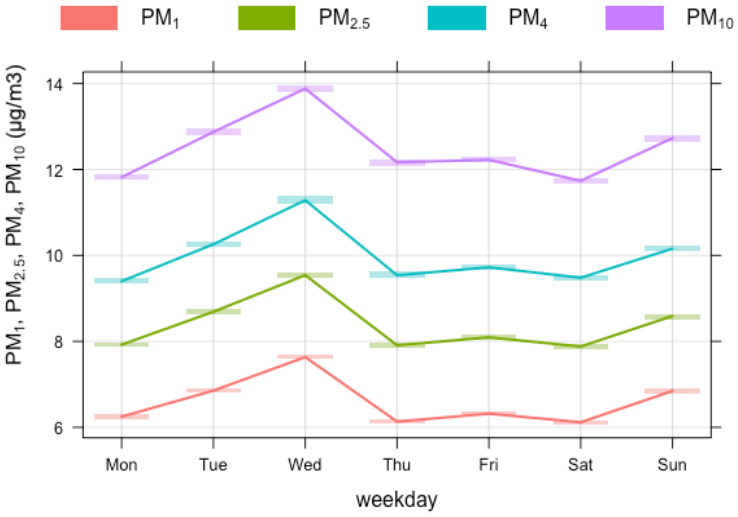


**Figure 2-4. Hebdomadal variation at KM for (a) NOx and (b) PM measured over the period February 2019 - January 2020. Shaded areas indicate the 95% confidence inteval. © University of York (2020).**

(a)

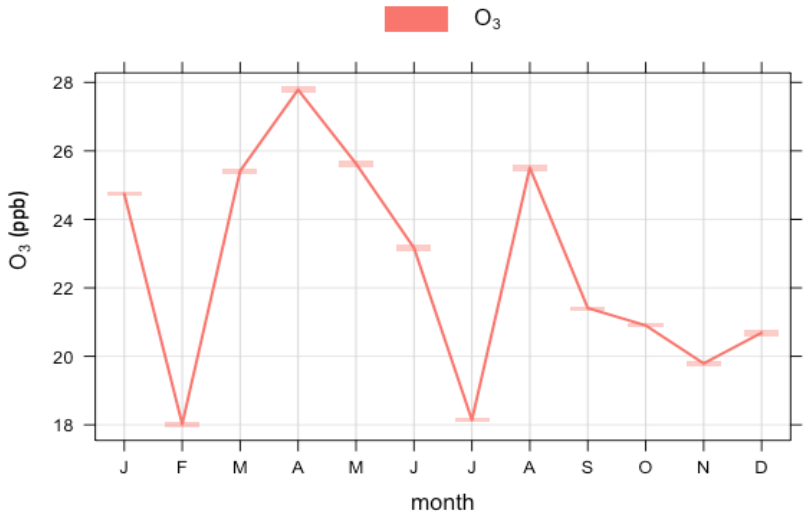


(b)

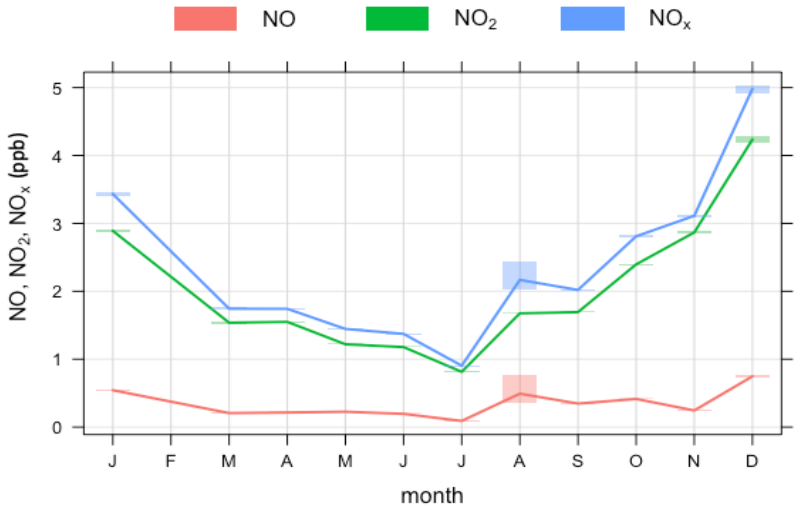


(c)

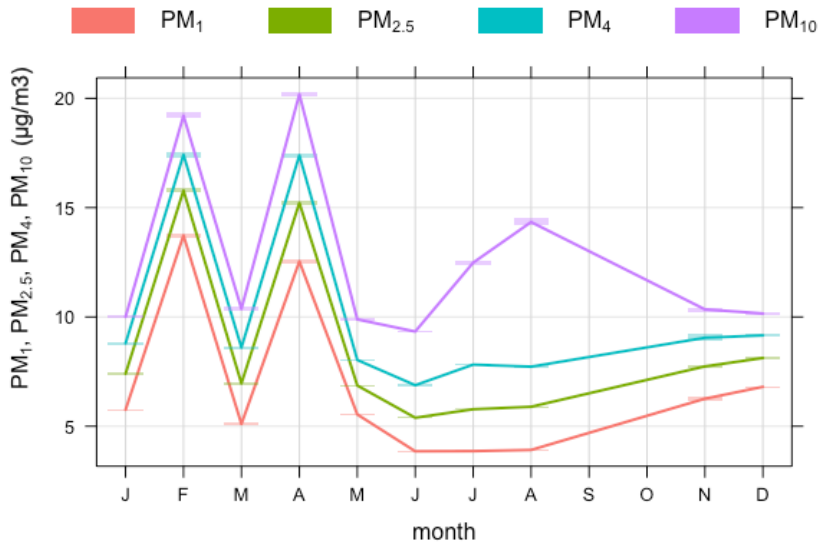


**Figure 2-5. Annual variation at KM for (a) NOx and (b) PM measured over the period February 2019 - January 2020. Shaded areas indicate the 95% confidence inteval. © University of York (2020).**

#### 2.3.3.3 ANNUAL CYCLES AT KM

KM has previously shown annual typical cycles that would be expected for UK air quality, and this is again the case (Figure 2-5). $NO_x$ shows highest concentrations during the winter months and minima in the summer. PM shows maximas in February and April, this is typical for the measurements observed previously at KM and is likely due to agriculture as it is known to be a significant contributor of PM in spring months. The site is surrounded by farmed land.

The $O_3$ measurements for July should be discarded due to low data coverage (<50%) in that month because of an instrument failure. $O_3$ concentrations peak in the spring, as observed previously, and also there is a further peak in August, due to the heat wave described earlier.

#### 2.3.3.4 SOURCE APPORTIONMENT FOR KM

Figure 2-6 shows polar plots for the same pollutants, with concentrations (colour scale), wind direction (radial scale) and wind speed. For many situations concentrations would be expected to decrease with increasing wind speed due to increased dilution but there are some instances where this process can lead to increases, for example due to plume grounding or the transport of air over long distances. Combining the two types of data analysis gives some indication of source regions of pollutants.

As in Phase 2 (Ward et al., 2017), $O_3$ concentrations were highest in the spring from all wind directions except those to the direct south and at the KMA site itself (centre of the polar plot). In the winter months the highest $O_3$ comes from the east and is highest when wind speeds are higher; this is likely due to the impact of efficient long range transport of this pollutant to the site.

By breaking the plots down into season it can be seen that the peaks in PM are in the spring ($PM_{2.5}$ and $PM_{10}$). $NO_x$ does not show the same behaviour so it can be inferred that the sources of the high PM concentrations are not due to road traffic. As particle suspension can increase with increasing wind speed, this could be due to sea spray from the east coast or particles from spoil heaps, wind-blown dust or similar. It may also reflect an agricultural source to the east of the site, and this would coincide with times when ammonia emissions are generally at their highest from muck spreading. There seems to be a constant source of PM all year round from the east close to the site; there is a milking shed and farm close by so these emissions are likely to be related to farming activities.

The $NO_2$ event in December 2019, mentioned previously, appears to have a source to the south of the site at higher wind speeds as well as locally with low wind speeds. This has not been present in previous reports and there does not seem to be an obvious source and so may be due to a local short-lived event.

### 2.3.4 **Preston New Road (PNR) detailed analysis**

To enable a full baseline climatology of air pollution to be established it is important to examine the influence of wind direction. Table 2-2 reports the annual means for pollutants measured under the Air Quality Directive whereas Table 2-5 reports those metrics by individual wind sector. In the UK it is most common for air from the East (E) and Southeast (SE) to be most polluted as this often bring air from the SE of England and from continental Europe.

The lowest concentrations of air pollution are typically observed during periods of westerly airflow. The PNR site also has the influence of the main road (A583) to the South of the site and its influence has been clearly seen in the $NO_x$ and PM measurements in previous reports, with the SE having the highest $NO_x$ and PM measurements. However in the Phase 4 period this changed and the highest $NO_x$ measurements were from the Southwest (SW) and particulates from the West (W). This was attributed to the increased activity at the shale gas site to the west of the monitoring station. Table 2-5 shows that the measurements during Phase 5 have returned to the values seen during the earlier baseline period with the E and SE showing highest averages of PM and $NO_x$ due to vehicle movement on the road. This pattern is believed to reflect the suspension of hydraulic

fracturing operations early in Phase 5 and the subsequent moratorium leading to very little vehicle movement and/or power generations activity on the shale gas site since then.

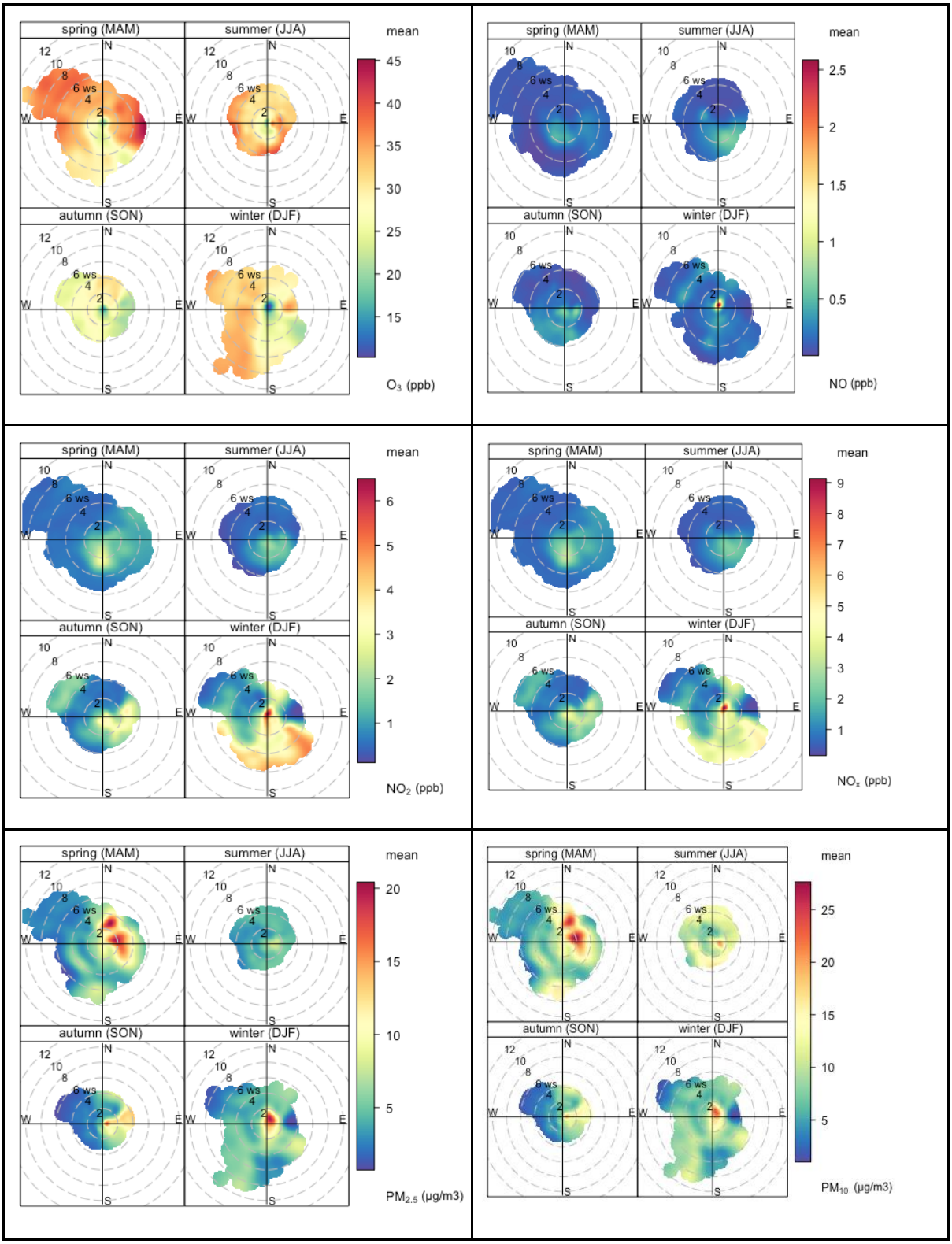


**Figure 2-6. Polar plots for KM (a) $O_3$ (b) NO (c) $NO_2$, (d) NOx, (e) $PM_{2.5}$, (f) $PM_{10}$ measured over the period February 2019 - January 2020. © University of York, 2020.**

**Table 2-5. Phase 5 monitoring period wind sector averages at PNR.**

| | 45-degree directional wind sector | | | | | | | |
|---|---|---|---|---|---|---|---|---|
| | **N** | **NE** | **E** | **SE** | **S*** | **SW** | **W†** | **NW** |
| $O_3$ (ppb) | 20.3 | 22.2 | 20.8 | 17.4 | 21.0 | 24.6 | 26.4 | 24.9 |
| NO (ppb) | 0.4 | 0.8 | 1.5 | 1.7 | 1.2 | 0.5 | 0.5 | 0.3 |
| $NO_2$ (ppb) | 3.7 | 5.5 | 7.9 | 8.5 | 4.8 | 1.9 | 2.2 | 2.2 |
| $NO_x$ (ppb) | 4.0 | 6.2 | 9.4 | 10.1 | 6.1 | 2.3 | 2.7 | 2.4 |
| $PM_{2.5}$ ($\mu g/m^3$) | 5.1 | 8.7 | 12.0 | 11.0 | 5.1 | 6.0 | 5.5 | 5.4 |
| $PM_{10}$ ($\mu g/m^3$) | 7.6 | 12.7 | 16.4 | 14.2 | 8.3 | 10.6 | 9.5 | 9.1 |
| $H_2S$ (ppb) | No data | 0.6 | 0.5 | 0.5 | 0.3 | 0.2 | 0.1 | 0.2 |
| $SO_2$ (ppb) | 0.3 | 0.8 | 1.5 | 1.5 | 1.6 | 1.5 | 0.5 | 0.3 |

† Sector within which the shale gas well lies

* Sector within which the A583 (Preston New Road) lies

#### 2.3.4.1 DIURNAL VARIATION OF AIR POLLUTION AT PNR

The $O_3$ and $NO_x$ diurnal plots (Figure 2-7) are similar to those observed in Phase 4 (Ward et al, 2019), the $O_3$ diurnal is almost identical to the KM data (Figure 2-3). The $NO_x$ diurnal plot for PNR is heavily influenced by road traffic, with $NO_x$ increasing in the morning, due to the boundary layer and local traffic sources. The early evening peak is again due to the evening rush hour. The PM2.5 and PM10 values are slightly higher than the previous year but in line with the Phase 3 data (Ward et al, 2019). The plot of PM (Figure 2-7) shows a slight diurnal, again linked to rush hour traffic, with the smoothing of the peaks in the PM diurnal possibly indicating a further more constant source of PM.

#### 2.3.4.2 HEBDOMADAL VARIATION OF AIR POLLUTION AT PNR

The pattern of higher traffic-related NOx emissions during the working week can clearly be seen in Figure 2-8, with them highest during the week and decreasing at the weekend, i.e. reflecting traffic volumes. $O_3$ is highest at the weekend, coinciding with the lowest $NO_x$. There is still a small decrease midweek in $NO_x$ which is a pattern consistently seen at PNR, it is still unclear why this difference should occur as there are no immediate reasons why traffic volumes might be lower at certain times of the week. PM is constant throughout the week and shows a similar profile and concentrations to previous years.

#### 2.3.4.3 ANNUAL VARIATION OF AIR POLLUTION AT PNR

The instrument used to measure Particulate Matter (FIDAS) was unserviceable for almost 3 months in the spring so a full annual cycle of measurements was not possible. However, Figure 2-9 shows annual cycle for $O_3$ and $NO_x$. These show typical cycles in the context of UK air quality and have already been partially discussed.

(a)

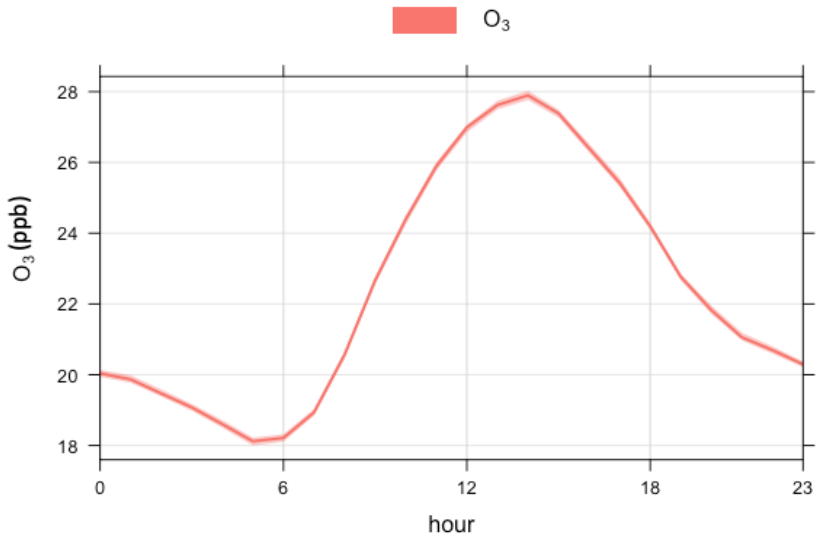


(b)

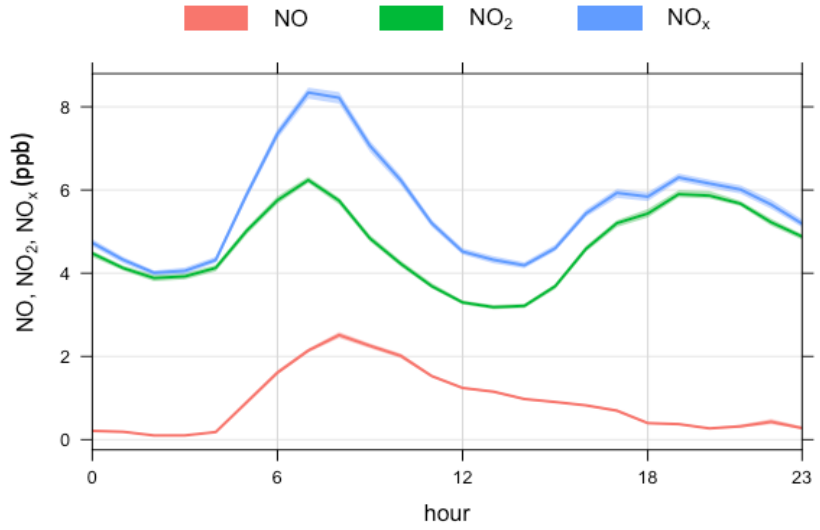


(c)

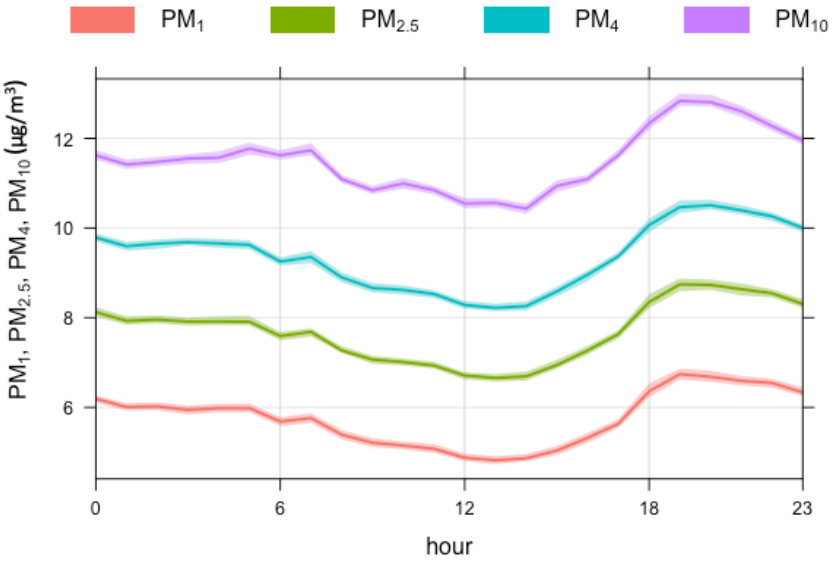


**Figure 2-7. Diurnal variations a PNR for (a) $O_3$ (b) $NO_x$ and (c) PM measured over the period February 2019 - January 2020. © University of York, 2020.**

(a)

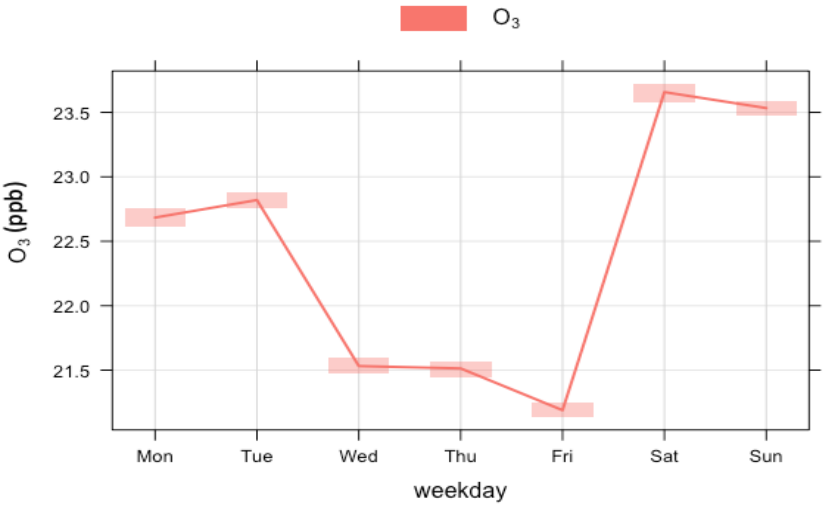


(b)

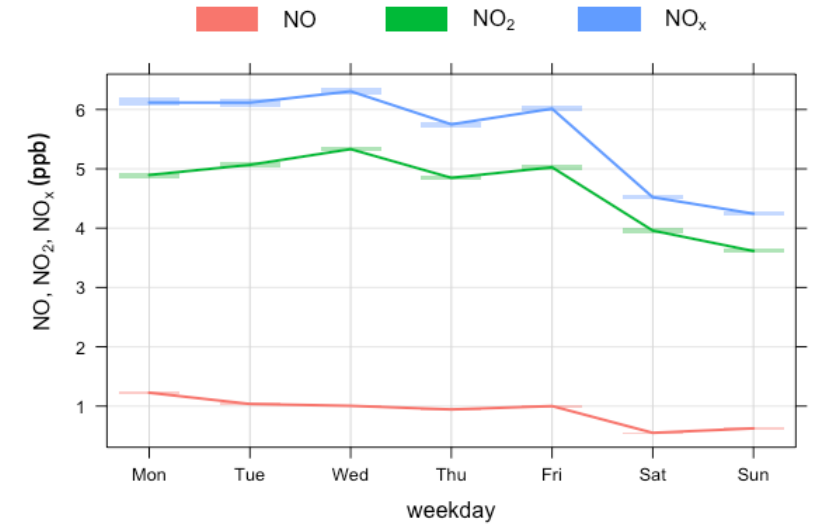


(c)

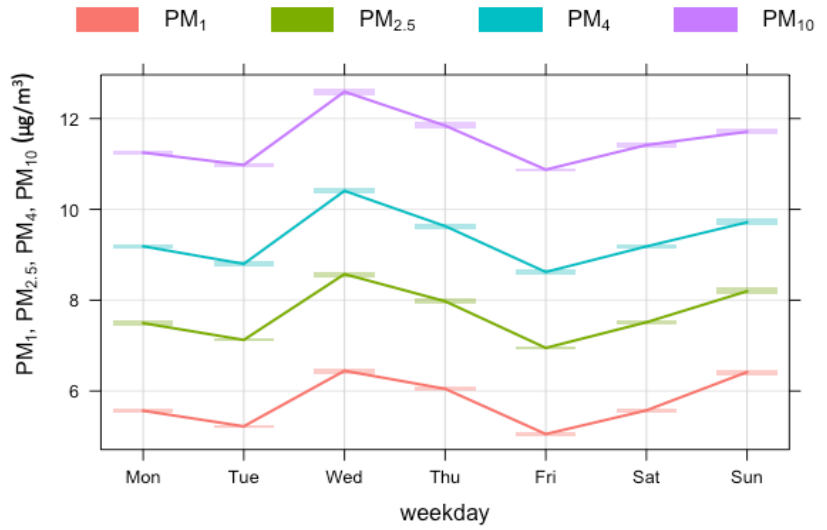


**Figure 2-8. Hebdomadal cycles at PNR for (a) $O_3$ (b) $NO_x$ and (c) PM measured over the period February 2019 - January 2020. © University of York, 2020.**

(a)

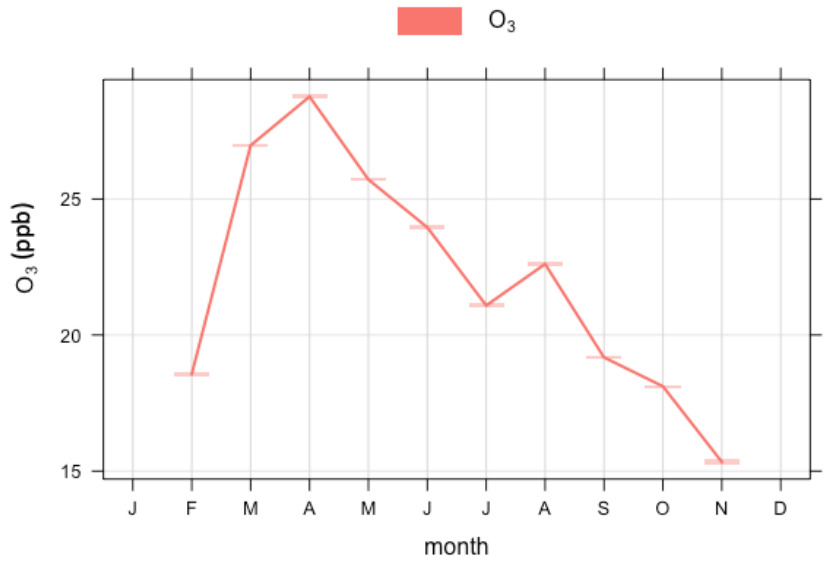


(b)

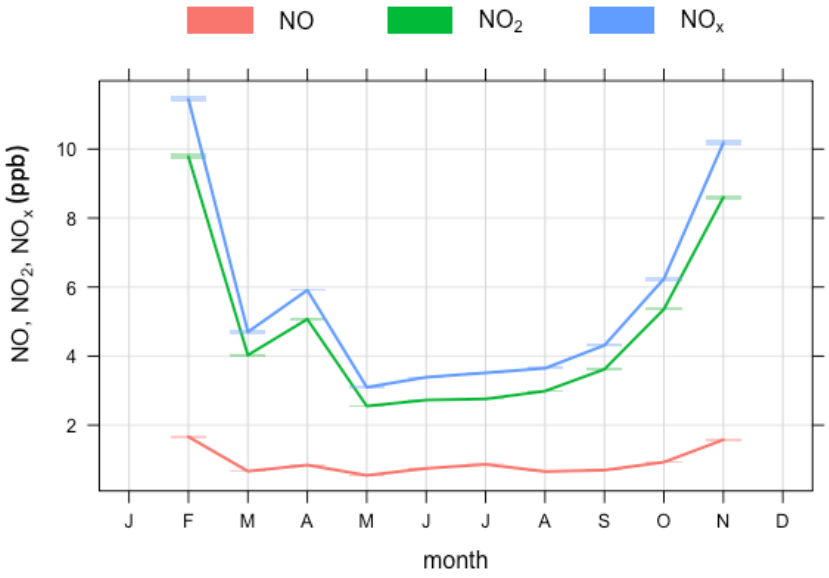


**Figure 2-9. Annual cycles at PNR for (a) $O_3$ and (b) $NO_x$ measured over the period February 2019 - January 2020. © University of York, 2020.**

### 2.3.4.4 Source apportionment for PNR

As in the previous years, $O_3$ concentrations are highest in the spring when the wind speed is at its highest and from the west (Figure 2-10). This corresponds with the peak in the northern hemispheric and North Atlantic $O_3$, and the impact of efficient long-range transport of this pollutant to the monitoring site. Elevated $O_3$ is indicative of an aged air mass as it is not a primary emission but produced through chemical reactions in the air mass. It is observed easily at the PNR site due to its position on the west of England and clean background air observed from the west. The influence of the Atlantic air is also shown in the PM measurements, which are all enhanced in the higher wind speed westerly air masses, particularly in the coarser fraction arising from maritime aerosols.

The large $NO_x$ source visible in the Phase 4 data to the south east of the site (Ward et al, 2019) is not as high in concentration (maximum in previous years of 40ppb). It is more pronounced in the winter and is more likely to be local and road sources as all the industrial activity at the site had ceased by December when winter measurements start.

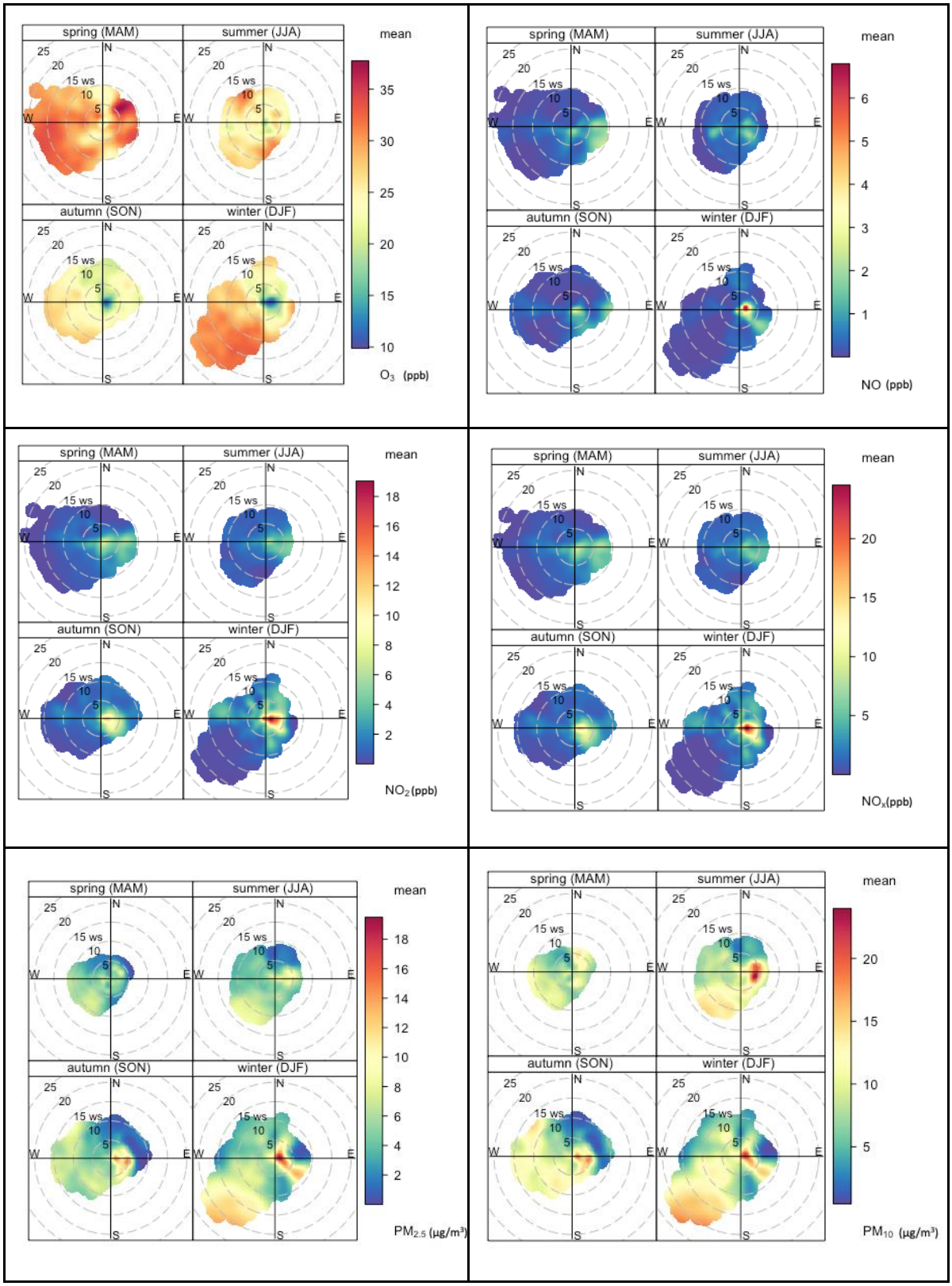


**Figure 2-10. Polar plots for PNR (a) $O_3$, (b) NO (c) $NO_2$, (d) $NO_x$, (e) $PM_{2.5}$, (f) $PM_{10}$ measured over the period February 2019 - January 2020. © University of York, 2020.**

The enhanced concentrations of PM to the south east of the site has been visible in previous data, and represents a local influence as well as the enhanced regional PM sources in easterly air masses. The higher concentrations of PM at highest SW wind speeds may be due to the influence of the Atlantic air masses, especially in the coarser fraction.

### 2.3.5 Non-methane hydrocarbons at KM and PNR during Phase 5

Non-methane hydrocarbon (NMHC) samples have been taken weekly at both monitoring sites, with samples collected on a Monday between 9:30 am – 11:30 am. A summary of NMHC concentrations for KM and PNR is shown in Figure 2-11. They are also summarised in Table 2-6 and Table 2-7. NMHCs are able to give an indication of air mass origin; in areas of oil and gas production higher lighter alkanes such as ethane and propane may indicate fugitive emissions. Alkanes are saturated hydrocarbons including methane, ethane, propane, and higher alkane members. In cases where the observed value was below the minimum detection limit, half this value was used in averaging, i.e. 0.005 ppb.

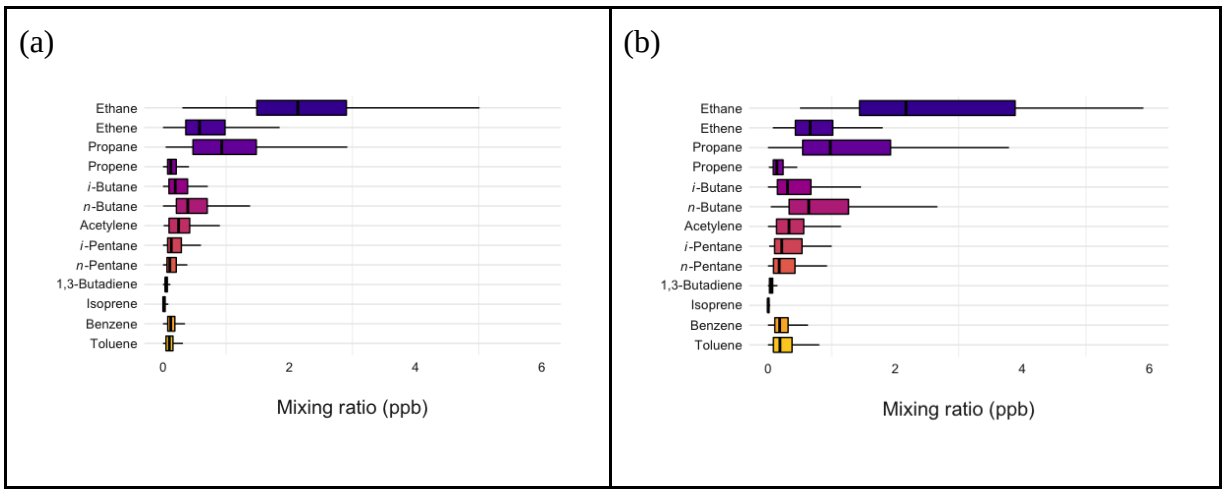


**Figure 2-11. Selected hydrocarbon boxplot of annual hydrocarbon mixing ratios measured at KM (a) and PNR (b) during the period February 2019 - January 2020. Vertical bars are median values. The left and right edges of the box correspond to the 25th and 75th percentiles respectively. The horizontal whiskers show the largest or smallest values no further than 1.5 times the interquartile range respectively. Data beyond the end of the whiskers are not included here. © University of York, 2020.**

Figure 2-12 and Figure 2-13 highlight the seasonal cycle in hydrocarbon mixing ratios at each site. The highest values are generally observed in the winter months when the boundary layer is shallow and oxidation is slowest, and decreases in the summer months when the boundary layer is deeper and oxidation rates are faster. This cycle is much more obvious in the KM data where values are also much lower than at PNR. Higher mixing ratios at PNR were observed in October - December. As highlighted in Table 1-2, flow testing procedures were being carried at the PNR shale gas site during this period and the observed higher mixing ratios maybe due to work on the site, but as all hydrocarbon ratios increase in this period it could also be another local source. Whilst this type of sampling is enough to identify changes in mixing ratios as a response to changes in broad atmospheric conditions throughout the year, it is unlikely to be of a sufficient time resolution to pick up enhancements due to short-term events happening on the shale gas site itself. In addition to this, although the monitoring station is positioned downwind of the predominant wind direction of the gas well site, any specific events will only be possible to identify provided the wind direction transports air from the shale gas site to the monitoring station.

**Table 2-6. Summary of NMHC measurements for the Phase 5 period at KM, N = 35. All NMHC have an uncertainty of < 10%.**

| Hydrocarbon | Mean concentration (ppb) | Minimum concentration (ppb) | Maximum concentration (ppb) |
|---|---|---|---|
| Ethane | 2.6 | 0.3 | 5.3 |
| Ethene | 0.8 | <0.1 | 3.3 |
| Propane | 1.2 | <0.1 | 3.0 |
| Propene | 0.3 | <0.1 | 3.7 |
| Isobutane | 0.4 | <0.1 | 1.9 |
| N-butane | 0.7 | <0.1 | 2.7 |
| Isopentane | 0.5 | <0.1 | 3.0 |
| N-pentane | 0.2 | <0.1 | 1.1 |
| Benzene | 0.2 | <0.1 | 0.4 |
| Toluene | 0.1 | <0.1 | 0.3 |

**Table 2-7. Summary of NMHC measurements for the Phase 5 period at PNR, N = 46. All NMHC have an uncertainty of < 10%.**

| Hydrocarbon | Mean concentration (ppb) | Minimum concentration (ppb) | Maximum concentration (ppb) |
|---|---|---|---|
| Ethane | 5.2 | 0.5 | 60.7 |
| Ethene | 1.3 | 0.1 | 8.6 |
| Propane | 1.7 | 0.1 | 125.6 |
| Propene | 0.3 | <0.1 | 1.9 |
| Isobutane | 7.1 | <0.1 | 118.3 |
| N-butane | 9.7 | <0.1 | 186.0 |
| Isopentane | 4.0 | <0.1 | 70.3 |
| N-pentane | 2.4 | <0.1 | 48.4 |
| Benzene | 0.3 | <0.1 | 3.8 |
| Toluene | 0.2 | <0.1 | 1.5 |

As in previous years the mean hydrocarbon mixing ratios at KM are generally lower than PNR. At both sites alkanes have the highest means and maximum values. Although PNR values are slightly higher with more variability, the pattern of the distribution of speciated hydrocarbons is similar.

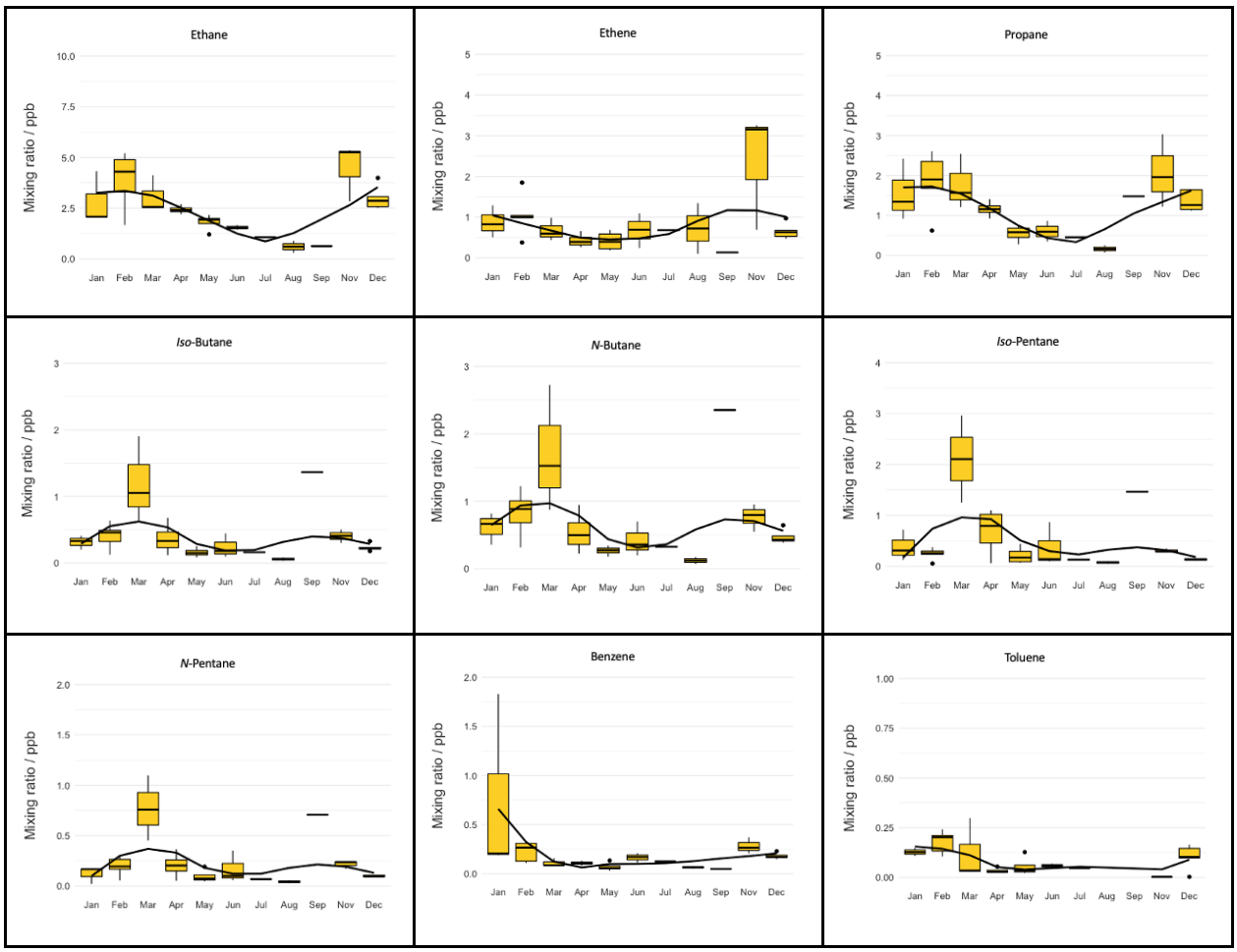


**Figure 2-12. Monthly variation in selected hydrocarbons at KM measured over the Phase period. The left and right edges of the box correspond to the 25th and 75th percentiles respectively. The black dots indicate outliers and not all are included due to scale. © University of York, 2020.**

### 2.3.6 Emissions to air during nitrogen lift (January 2019) at PNR

Between December 2018 and February 2019 increased $CH_4$ mixing ratios were observed at the PNR monitoring station as detailed earlier. This was found to be due to a nitrogen lift procedure being carried out at the hydraulic fracturing site which resulted in a cold methane venting event. Nothing immediately stood out when looking at the time series of the air quality data so further data mining was carried out to see if any signatures could be identified.

Small enhancements in NO and $NO_2$ over the background were measured during the $CH_4$ emissions period in January 2019, shown in Figure 2-14. These enhancements were correlated with the enhancements in $CH_4$. Mixing ratios of $NO_2$ reached approximately 60 ppb during the largest $CH_4$ enhancements over background (during westerly winds). However, larger $NO_x$ mixing ratios, of over 100 ppb, were observed when the wind was from the south east. The large mixing ratios under south-easterly winds were likely representative of vehicle emissions from the nearby main road (A583). Regardless, the observed correlation in $CH_4$ and $NO_x$ during the January enhancement period is indicative of a $NO_x$ source that was not measured during baseline observations. This source was likely associated with operations conducted at the shale gas extraction facility, possibly

due to incomplete combustion of methane in the flare stacks, the operation of generators or increased vehicular activity.

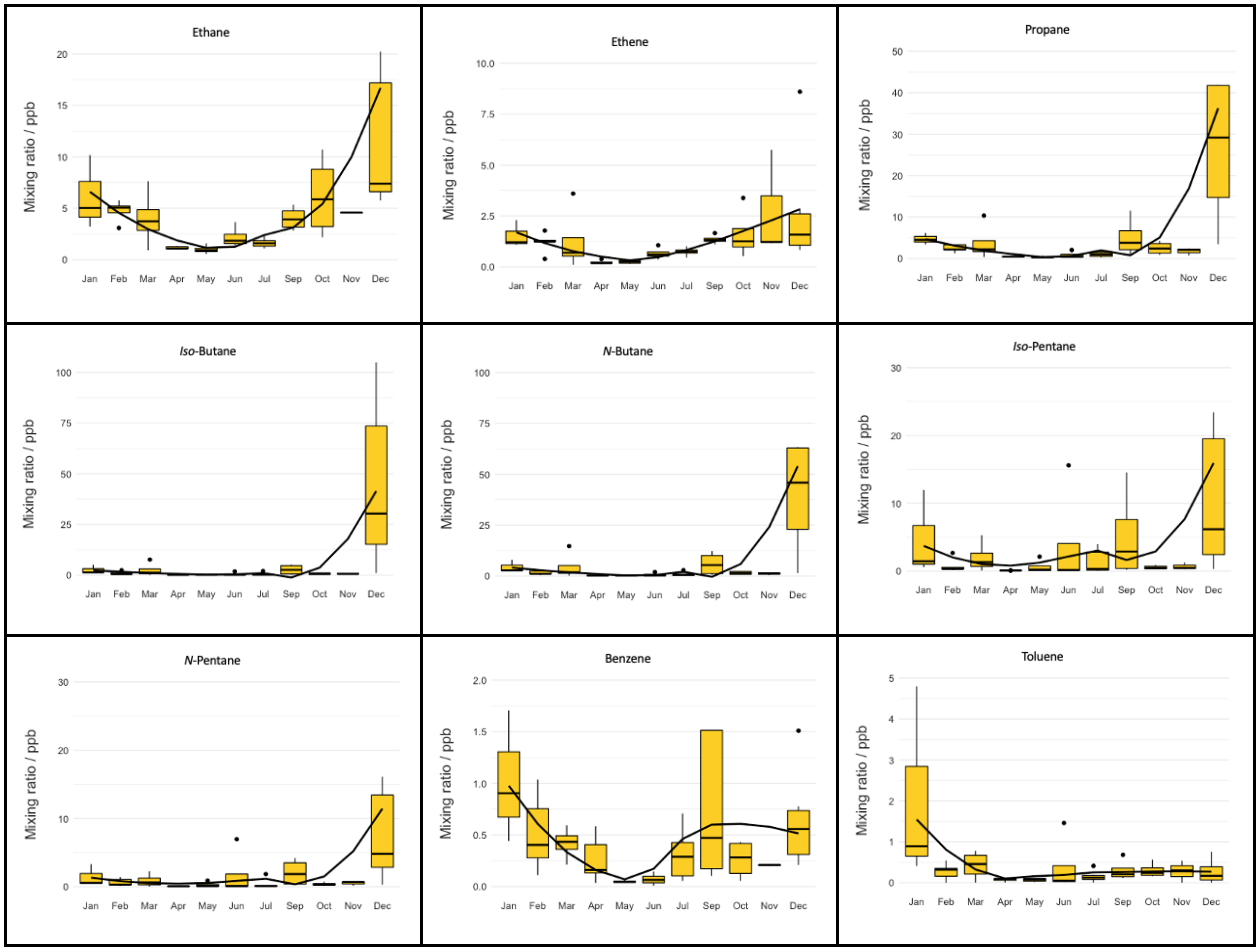


**Figure 2-13. Monthly variation in selected hydrocarbons at PNR measured over the period February 2019 - January 2020. The left and right edges of the box correspond to the 25th and 75th percentiles respectively. The black dots indicate outliers and not all are included due to scale. © University of York, 2020.**

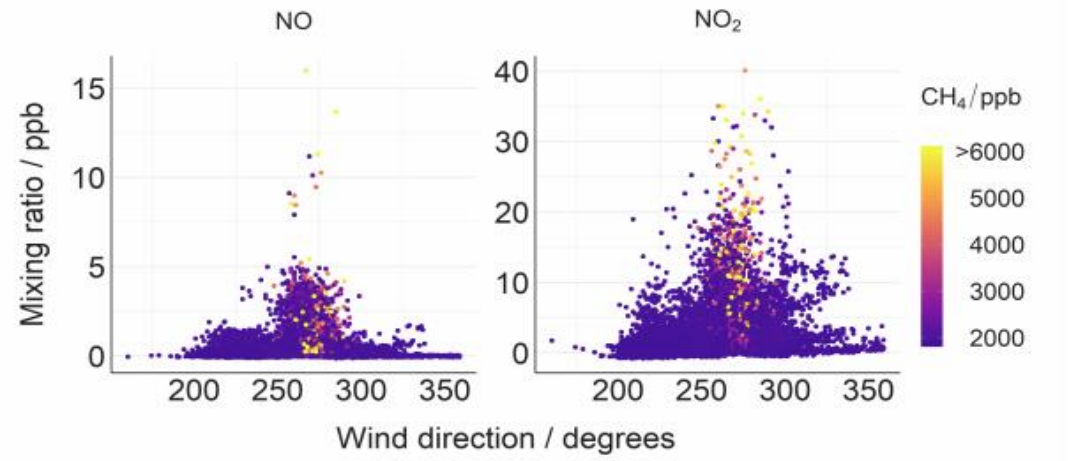


**Figure 2-14. NO and $NO_2$ mixing ratios, as function of wind direction, measured between 11/1 - 17/1/19. Data are coloured by $CH_4$ mixing ratios with higher mixing ratios of NO and $NO_2$ correlated with greater enhancements in $CH_4$ mixing ratios. © University of York, 2020.**

The average NO and $NO_2$ concentrations throughout the period before the nitrogen lift until immediately after (1st February 2016 - 1st February 2019) were 2.10 ppb and 5.58 ppb respectively, with maximum 1-minute average mixing ratios of 642.2 ppb and 287.8 ppb recorded on 24th May 2017 under easterly wind conditions. The average NO and $NO_2$ mixing ratios during the period of enhanced $CH_4$ were 3.09 ppb and 9.94 ppb respectively, which are elevated above the overall measurement period average. The EU limit value for $NO_2$ is 200 µg $m^{-3}$ measured as a 1-hour mean, which is not to be exceeded more than 18 times in a year. Figure 2-15 shows that $NO_2$ concentrations at the PNR monitoring station were well below the limit value with no exceedances occurring throughout the whole measurement period. Interestingly, the maximum hourly averaged $NO_2$ of 51.1 ppb was measured on 23rd January 2019 during south-easterly wind conditions, suggesting this is independent of increased emissions during the nitrogen lift and flow testing operations at the shale gas site.

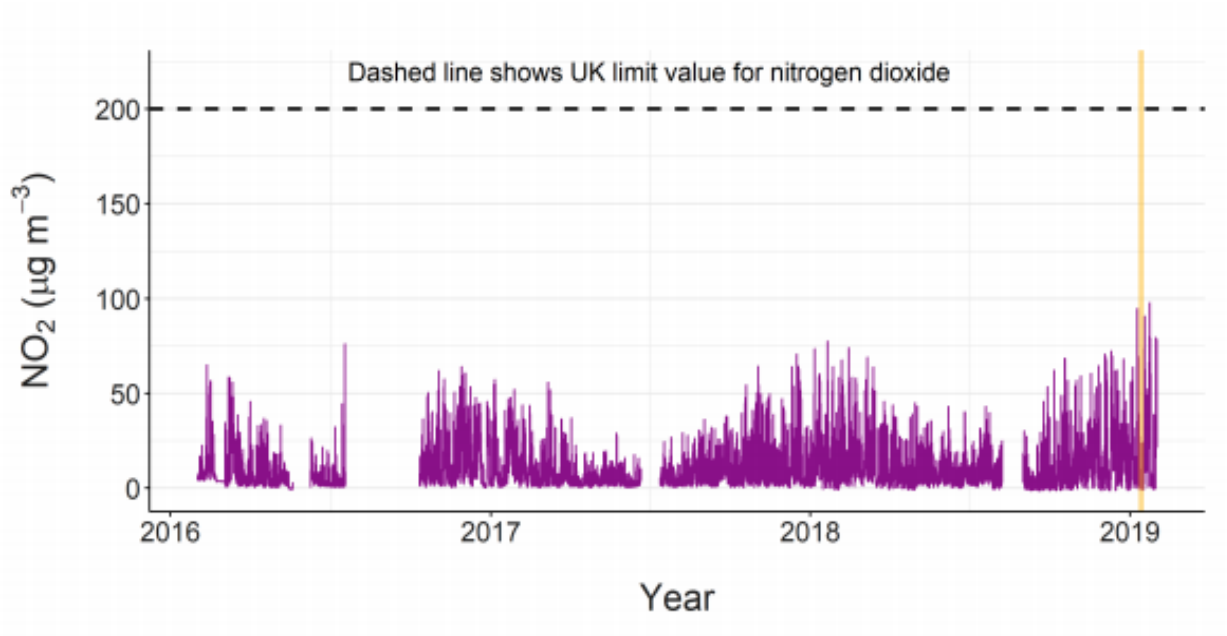


**Figure 2-15. Hourly average $NO_2$ time series at PNR for the measurement period up to 1st February 2019. The dashed line shows the 1-hour UK limit value which must not be exceeded more than 18 times a year. The yellow shaded area highlights the $N_2$ lift period when enhanced $CH_4$ was detected. © University of York, 2020.**

No measureable enhancements in $H_2S$ were measured during the period when the nitrogen lift operations took place. This is consistent with the measured composition of the extracted shale gas, which was reported to not contain $H_2S$ (Cuadrilla Resources Ltd, 2019).

Figure 2-16 shows that measured mixing ratios of other volatile organic compounds (sampled 14th January 2019 between 09:30 and 11:30) were also elevated above the baseline mean, when accounting for seasonal variance and wind direction. Table 2-8provides a list of the 21 VOCs measured, with their mean baseline mixing ratio compared to their mixing ratio as measured on 14th January 2019. The mixing ratios of heptane and iso-pentane in January 2019 were almost 10 times greater than their mean baseline value. Substantial enhancements were also observed for many other alkanes including ethane, propane, n-butane and n-pentane. Enhancements in benzene (4.4 times greater than the baseline mean) and toluene (5.8 times greater than the baseline mean) were also measured. The ratios of iso-pentane to n-pentane, and propane to acetylene, have previously been used as signatures of oil and gas operations (Gilman et al., 2013; Swarthout et al., 2013). The ratio of iso-pentane to n-pentane measured on 14th January was greater than any ratio recorded during almost three years of baseline measurements. The ratio of propane to acetylene recorded on 14th January was over twice as large as the ratios recorded during winter months in

the prior measurement period, suggesting a greater influence from shale gas operations-related emissions. These large deviations in the VOC ratios measured during the emissions period confirms the influence of a previously unmeasured source with a characteristic natural gas, i.e. shale gas, signature.

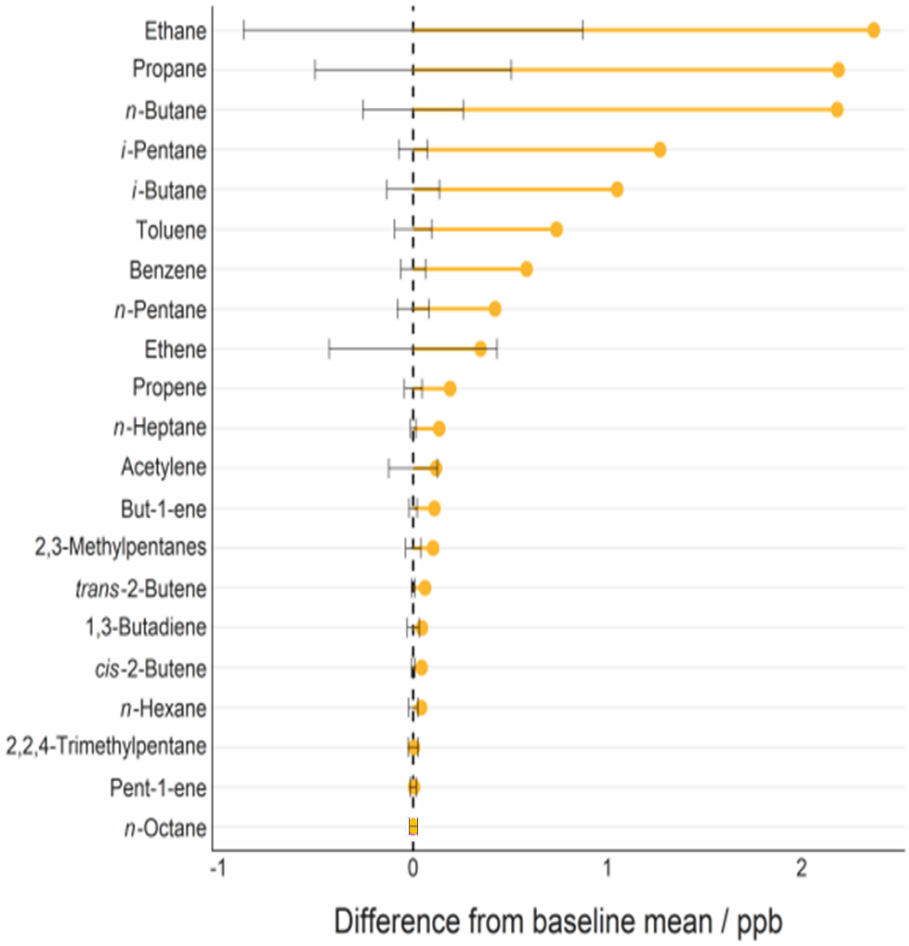


**Figure 2-16. Difference between the measured hydrocarbon mixing ratios on 14th January 2019 and the mean hydrocarbon mixing ratios measured under westerly winds between 1st December and 1st February throughout the previous two baseline years (orange dots). The error bars show one standard deviation from the mean. The mixing ratios of many alkane hydrocarbons were much greater than the baseline mean. © University of York, 2020.**

Figure 2-17 shows hydrocarbon measurements in the UK from three sites currently operating as part of the Automatic Urban Rural Network (AURN). London Marylebone Road is an Urban Traffic site, London Eltham is a Suburban Background site and Chilbolton Observatory is a Rural Background site. The concentrations observed at PNR on the 14th January 2019 are most similar to London Eltham and between 27% and 76% lower than London Marylebone Road. Concentrations of all the hydrocarbons shown are elevated above the background levels measured at Chilbolton Observatory except for propene which was 21% lower. The largest differences were iso-pentane and n-butane which were 230% and 252% higher at PNR compared to Chilbolton. However, the hydrocarbon concentrations observed at PNR are still within what is generally observed at urban and suburban sites across the UK.

**Table 2-8. Mean baseline concentrations and concentrations measured on 14th January 2019 (during emissions period) of 21 volatile organic hydrocarbons (VOCs). The absolute change in concentration and the percentage increase is concentration is also provided.**

| Compound | Mean baseline concentration* / ppb | 14th January 2019 concentration / ppb | Concentration change / ppb | Ratio Jan2019: baseline / % |
|---|---|---|---|---|
| ethane | 2.66 ± 0.87 | 5.03 | + 2.37 | 1.9 |
| propane | 1.21 ± 0.50 | 3.40 | + 2.19 | 2.8 |
| *n*-butane | 0.59 ± 0.26 | 2.77 | + 2.18 | 4.7 |
| iso-pentane | 0.17 ± 0.07 | 1.44 | + 1.27 | 8.6 |
| iso-butane | 0.31 ± 0.14 | 1.36 | + 1.05 | 4.4 |
| toluene | 0.15 ± 0.09 | 0.89 | + 0.74 | 5.8 |
| benzene | 0.17 ± 0.06 | 0.75 | + 0.58 | 4.4 |
| *n*-pentane | 0.14 ± 0.08 | 0.57 | + 0.42 | 3.9 |
| ethene | 0.74 ± 0.43 | 1.08 | + 0.35 | 1.5 |
| propene | 0.08 ± 0.05 | 0.27 | + 0.19 | 3.4 |
| heptane | 0.02 ± 0.01 | 0.15 | + 0.13 | 9.8 |
| acetylene | 0.46 ± 0.13 | 0.57 | + 0.12 | 1.3 |
| but-1-ene | 0.03 ± 0.02 | 0.13 | + 0.11 | 5.2 |
| methylpentane | 0.04 ± 0.04 | 0.14 | + 0.10 | 3.5 |
| trans-2-butene | 0.009 ± 0.008 | 0.07 | + 0.06 | 7.4 |
| 1,3-butadiene | 0.04 ± 0.03 | 0.08 | + 0.04 | 2.1 |
| cis-2-butene | 0.010 ± 0.010 | 0.05 | + 0.04 | 5.3 |
| hexane | 0.03 ± 0.02 | 0.07 | + 0.04 | 2.5 |
| 2,2,4-trimethylpentane | 0.02 ± 0.03 | 0.02 | 0.00 | 1.2 |
| pent-1-ene | 0.011 ± 0.016 | 0.01 | 0.00 | 1.3 |
| *n*-octane | 0.02 ± 0.03 | 0.01 | 0.00 | 0.9 |

* Baseline refers to hydrocarbon measurements made during December-January-February in 2017 and 2018. The mean was calculated as the mean of all measurements during this period made under westerly wind conditions (number of samples = 9). The quoted uncertainty is equivalent to 1σ (one standard deviation) from the mean.

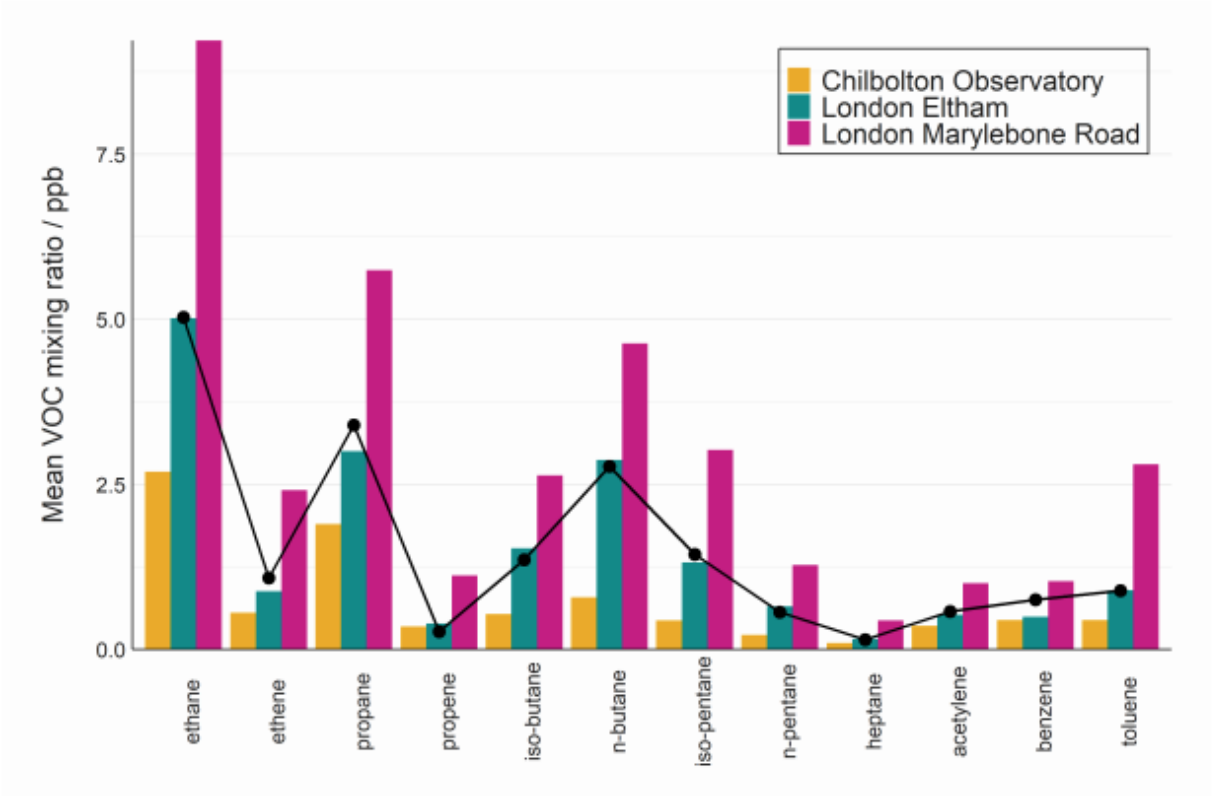


**Figure 2-17. Mean hydrocarbon mixing ratios between 2016 and 2019 at selected AURN sites. The black line shows the measured hydrocarbon concentrations on 14th Jan 2019 during the nitrogen lift. © University of York, 2020.**

#### 2.3.6.1 VEHICLE SURVEY AT PNR

One survey was conducted by the University of York using their mobile monitoring laboratory on 19th October 2019. This was part of a series of intensive surveys involving York University, University of Manchester and Royal Holloway University to coincide with hydraulic fracturing and flow testing operations at the shale gas site.

The flare stacks were operational at the time of surveying (although the heat haze varied significantly in intensity) and the winds were generally westerly (as measured by the fixed-site monitoring station). Methane mole fraction, measured during three laps around the shale gas site, is shown in Figure 2-18 (a-c) and Figure 2-18 (d) shows the methane:ethane ratio.

Enhancements in both methane ($CH_4$) and ethane ($C_2H_6$) were measured downwind (to the east) of both the shale gas site and the dairy farm. As the dairy farm is adjacent to the shale gas site and is a known source of methane emissions, it was not possible to determine whether the enhancement detected was due to emissions from the shale gas site or the dairy farm. The area to the east of the farm also contains a known natural gas supply pipe leak, as identified during baseline mobile monitoring conducted by RHUL, and also observed during the RHUL survey (mobile survey A) on 24th November 2019.

The ethane:methane ratio for natural gas sources of thermogenic origin in the Fylde region is expected to range from 0.05 to 0.06. Figure 2-18(d) shows that the ratio was less than this for the majority of the survey, indicating sources of biogenic origin, except for the area of methane enhancement downwind of the shale gas site, farm and leaking gas pipe.

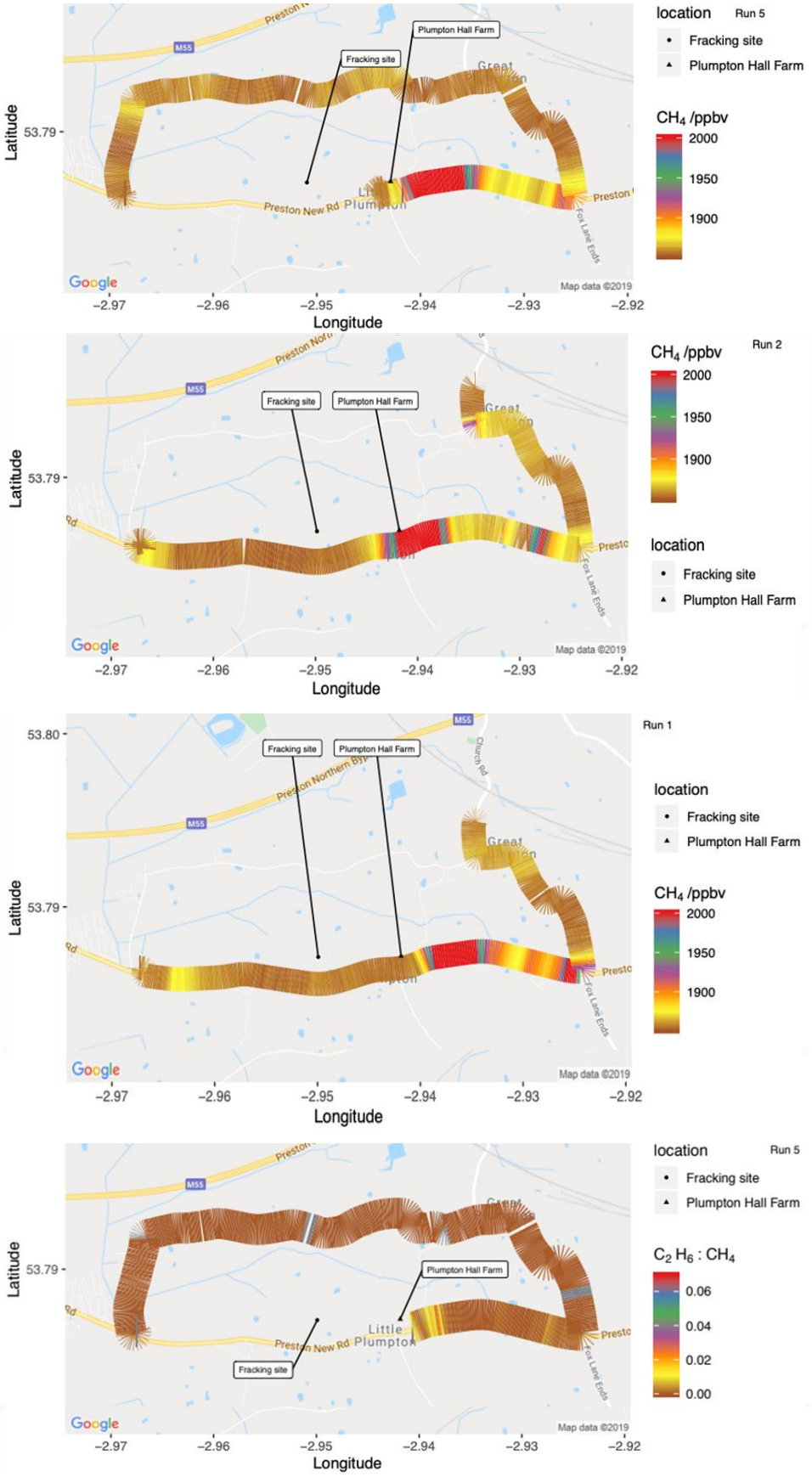


**Figure 2-18. $CH_4$ mole fraction (a-c) of the three different lap around the PNR shale gas site in the mobile laboratory. Panel (d) shows the measured ethane:methane ratios for one of these runs. © University of York, 2020.**

It is therefore not possible to determine whether the elevated ratios was a result of detected emissions from the shale gas site. A whole air sample was taken in this area which showed enhancements in both ethane and propane but not in other hydrocarbons, such as acetylene, benzene and toluene, usually associated with roadside emissions. The background mixing ratios of hydrocarbons, alongside mixing ratios measured close to the enhancement of methane and ethane, are shown in Figure 2-19.

No detectable enhancements in $H_2S$ were observed during the measurement period.

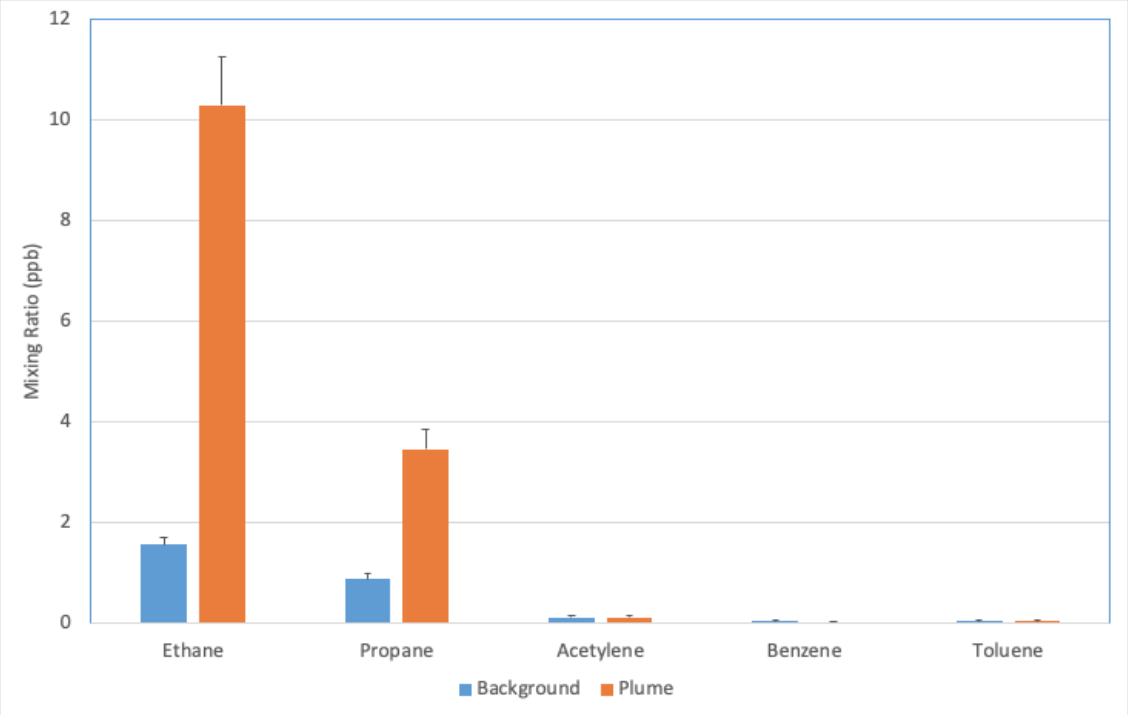


**Figure 2-19. Selected hydrocarbons measured in background location in the Fylde, in an area of no methane / ethane enhancement and within the plume detected on 19/10/19. © University of York, 2020.**

## 2.4 REFERENCES


Allen, G., Shaw, J., Shah, A., Pitt, J., Ricketts, H., Williams, P., Ward, R. 2019. Environmental baseline monitoring project: Methane enhancements detected at Little Plumpton air monitoring site. Nottingham, UK, British Geological Survey. https://www.bgs.ac.uk/news/item.cfm?id=9410.

Cuadrilla Resources Ltd, Preston New Road-1z HFP Report. https://www.ogauthority.co.uk/media/5845/pnr-1z-hfp-report.pdf, accessed 05/08/2019, 2019a.

Cuadrilla Resources Ltd, https://cuadrillaresources.com/media-resources/press-releases/cuadrilla-shale-gas-initial-flow-test-results/, accessed 24/06/2019, 2019b.

Environment Agency, Environment Agency: EPR Compliance Assessment Report for Preston New Road Exploration Site EPR/AB3101MW, issued 28/03/2019, 2019.

EPA, Oil and Natural Gas Sector Liquids Unloading Processes, U.S. EPA Office of Air Quality Planning and Standards, 2014.

France, J. L et al. : Facility level measurement of off-shore oil & gas installations from a small airborne platform: Method development for quantification and source identification of methane emissions. Atmospheric Measurement and Techniques, submitted.

Fisher, R., Lowry, D., Wilkin, O., Sriskantharajah, S. and Nisbet, E. G.: High-precision, automated stable isotope analysis of atmospheric methane and carbon dioxide using continuous-flow isotope-ratio mass spectrometry, Rapid Communications in Mass Spectrometry, 20, 200-208, 2006.

Gu, H.: Transient aspects of unloading oil and gas wells with coiled tubing, Soc. Petrol. Eng. J., SPE-29541-MS, https://doi.org/10.2118/29541-MS, 1995.

Keeling, C. D.: The concentration and isotopic abundances of carbon dioxide in rural and marine air, Geochimica et Cosmochimica Acta, 24, 277-298, 1961.

Lowry, D. L., Fisher, R. E., France, J. L., Coleman, M., Lanoisellé, M., Zazzeri, G., Nisbet, E. G., Shaw, J. T., Allen, G., Pitt, J. and Ward, R. S.: Environmental baseline monitoring for shale gas development in the UK: Identification and geochemical characterisation of local source emissions of methane to atmosphere, Sci. Tot. Env., 708, 134600, https://doi.org/10.1016/j.scitotenv.2019.134600, 2020.

Pasquill, F.: The estimation of the dispersion of wind-borne material, The Meteorological Magazine, 90, 1063, 33-49, 1961.

Purvis, R. M., Lewis, A. C., Hopkins, J. R., Wilde, S. E., Dunmore, R. E., Allen, G., Pitt, J. and Ward, R. S.: Effects of 'pre-fracking' operations on ambient air quality at a shale gas exploration site in rural North Yorkshire, England, Sci. Tot. Env, 673, 445-454. https://doi.org/10.1016/j.scitotenv.2019.04.077, 2019.

Shah, A., Pitt, J. R., Ricketts, H., Leen, J. B., Williams, P. I., Kabbabe, K., Gallagher, M. W. and Allen, G.: Testing the near-field Gaussian plume inversion flux quantification technique using unmanned aerial vehicle sampling, Atmos. Meas. Tech. Discuss., https://doi.org/10.5194/amt-2019-289, 2019.

Shah, A., Ricketts, H., Pitt, J. R., Shaw, J. T., Kabbabe, K., Leen, J. B. and Allen, G.: Unmanned aerial vehicle observations of cold venting from exploratory hydraulic fracturing in the United Kingdom, Env. Res. Commun., 2, 021003, https://doi.org/10.1088/2515-7620/ab716d, 2020.

Shaw, J. T., Allen, G., Pitt, J., Mead, M. I., Purvis, R. M., Dunmore, R., Wilde, S., Barker, P., Bateson, P., Bacak, A., Lewis, A. C., Lowry, D., Fisher, R., Lanoisellé, M., and Ward, R. S.: A baseline of atmospheric greenhouse gases for prospective UK shale gas sites, Sci. Tot. Env., 684, 1-13, https://doi.org/10.1016/j.scitotenv.2019.05.266, 2019.

Shaw, J. T., Allen, G., Pitt, J., Shah, A., Wilde, S., Laurence, S., Fan, Z., Ricketts, H., Williams, P. I., Bateson, P., Barker, P., Purvis, R., Lowry, D., Fisher, R., France, J., Coleman, M., Lewis, A. C., Risk, D. A. and Ward, R. S.: Methane flux from flowback operations at a shale gas site, *in review*.

Ward, R. S., Smedley, P. L., Allen, G., Baptie, B. J., Daraktchieva, Z., Horleston, A., Jones, D. G., Jordan, C. J., Lewis, A., Lowry, D., Purvis, R. M., Rivett, M. O.: Environmental baseline monitoring project: Phase II final report, British Geological Survey, Nottingham, UK, OR/17/049 (Unpublished), 2017.

Ward, R. S., Smedley, P. L., Allen, G., Baptie, B. J., Cave, M. R., Daraktchieva, Z., Fisher, R., Hawthorn, D., Jones, D. G., Lewis, A., Lowry, D., Luckett, R., Marchant, B. P., Purvis, R. M., Wilde, S.: Environmental baseline monitoring project: Phase III final report, British Geological Survey, Nottingham, UK, OR/18/026 (Unpublished), 2018.

Ward, R.S., Smedley, P. L., Allen, G., Baptie, B. J., Barkwith, A. K. A. P., Bateson, L., Bell, R. A., Bowes, M., Coleman, M., Cremen, G., Daraktchieva, Z., Gong, M., Howarth, C. H., Fisher, R., Hawthorn, D., Jones, D. G., Jordan, C., Lanoisellé, M., Lewis, A. C., Lister, T. R., Lowry, D., Luckett, R., Mallin-Martin, D., Marchant, B. P., Milne, C. J., Novellino, A., Pitt, J., Purvis, R. M., Rivett, M. O., Shaw, J., Taylor-Curran, H., Wasikiewicz, J. M., Werner, M. and Wilde, S.: Environmental Monitoring Phase 4 Final Report (April 2018-March 2019), British Geological Survey Open Report, OR/19/044, 2020.

Whiticar, M. and Schaefer, H.: Constraining past global tropospheric methane budgets with carbon and hydrogen isotope ratios in ice. Phil. Trans. R. Soc. A, 365, 1793–1828, 2007.

# 3 Radon

## 3.1 INTRODUCTION

Radon, $^{222}Rn$, a radioactive, colourless and odourless gas with a half-life of 3.82 days is the largest source of radiation exposure for most of the UK population and is the second highest cause of lung cancer after smoking (Darby et al., 2005).

In 2014, Public Health England (PHE) reviewed the potential public health impact of possible chemical and radiological pollutants resulting from shale gas activities (Kibble et al., 2014). The PHE review recognised that radon would be released to air but expected this to be at a low concentration. PHE could not envisage a plausible mechanism by which shale gas extraction processes could significantly change the amount of radon entering properties from the ground. PHE also recognised, however, that people might measure radon in their home after such activities start and misattribute any high levels to the shale gas activities rather than from existing natural sources. Radon measurements were recommended in outdoor air and in homes, in order to assess the baseline and provide evidence on radon distributions before shale gas extraction commenced.

The Vale of Pickering is an area which has been selected for shale gas extraction. Whilst the majority of the area of the Vale does not have naturally elevated radon potential, there are areas of naturally elevated radon potential, called radon Affected Areas, at around 5 to 8 km north and south of the KM8 shale gas site (Figure 3-1). In radon Affected Areas at least 1% of homes are expected to have radon levels at or above the UK Action Level of 200 Bq $m^{-3}$ as an annual mean (Miles et al., 2007). To determine the effect of shale gas extraction on levels of radon, should it take place, baseline monitoring of radon levels within these radon Affected Areas is required prior to commencement of shale gas extraction for comparison with results at the same locations after shale gas extraction has begun.

PHE has been monitoring indoor and outdoor radon levels at various locations in the Vale of Pickering since October 2015. Four areas were selected for indoor radon monitoring in the Vale of Pickering: Kirby Misperton and Little Barugh, Yedingham, Pickering and Malton. Pickering and Malton are both areas of established elevated radon potential.

Indoor radon concentrations exhibit diurnal, monthly and seasonal variations (Miles and Algar, 1988), thus long-term testing gives a better estimate of the annual average radon concentration. PHE recruited 153 householders in 2015/2016 who agreed to receive standard packs of passive detectors by post for several consecutive periods of 3 months. In addition, each home was issued a further two passive detectors for householders to carry out monitoring over a longer period of up to a year.

Four locations (areas) were selected in the Vale of Pickering for outdoor radon monitoring: Kirby Misperton (15 monitoring points), Yedingham (7 points), Pickering (8 points) and Malton (6 points). The Vale of White Horse (a non-Affected Area) in Oxfordshire was selected as an additional control (8 points).

Outdoor radon levels have been measured in the Vale of Pickering as part of the baseline monitoring programme using a specifically developed outdoor kit (Wasikiewicz et al., 2019). The plastic pots were positioned in discreet open-air locations. The initial locations of the monitoring points in the Vale of Pickering are shown in Figure 3-1. However, the number and location of monitoring points in Pickering and Malton had to be changed several times as some of the monitoring kits were removed or vandalised, requiring the relocation of some monitoring points or the installation of new detectors.

An active radon monitor (AlphaGUARD) and passive detectors were placed in the enclosure at the KM8 shale gas site, alongside the greenhouse gas and air quality monitoring instrumentation, to assess the short-term variation and long-term average radon concentrations at the site.

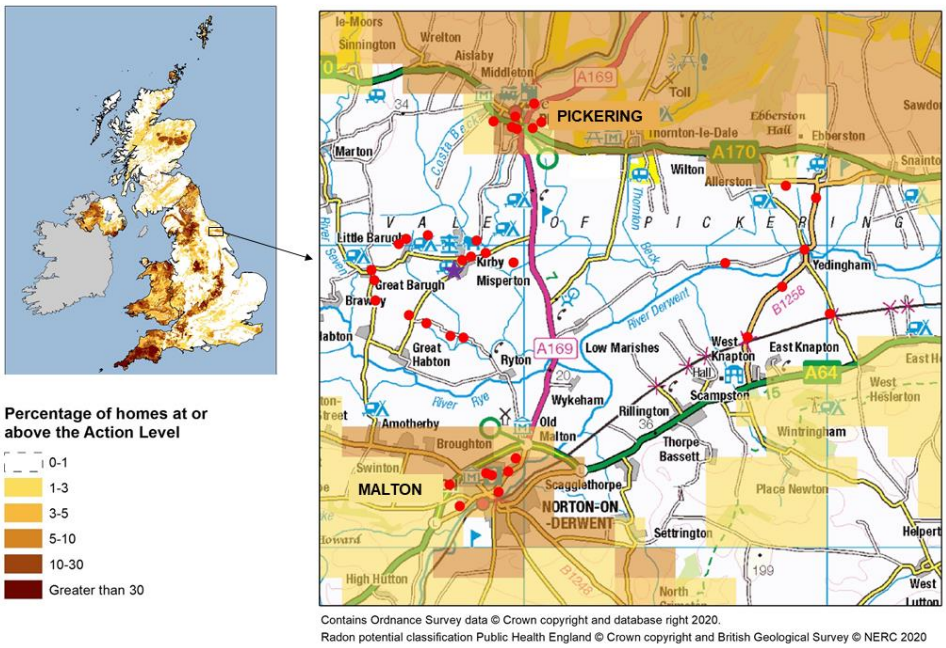


**Figure 3-1. Radon potential in the Vale of Pickering. The location of KM8 is shown with a purple star. The outdoor monitoring points are given with red dots. Contains Ordnance Survey data © Crown Copyright and database rights 2020. © PHE, 2020.**

## 3.2 INDOOR RADON MONITORING

### 3.2.1 Results for indoor monitoring

Some 94 properties in the Vale of Pickering were included in the fifth phase of the monitoring from April 2019 to March 2020. Measurements in this study follow the PHE Validation scheme (Daraktchieva et al., 2018) for handling, placement and reporting of results for homes. Results from the four consecutive 3-month tests covering the period from December 2018 to December 2019 are presented in Table 3-1. The annual average radon concentrations were calculated employing seasonal correction factors as outlined in the PHE Validation scheme (Daraktchieva et al., 2018).

Annual average radon concentrations were estimated from each 3-month result using UK seasonal correction factors (Daraktchieva, 2017) and occupancy factors (Daraktchieva, 2018). The outdoor radon concentration, 4 Bq $m^{-3}$ (Wrixon et al., 1988), was subtracted from each result since it is an additive component (Gunby et al., 1993); only positive values were selected, i.e. values that were negative or zero due to subtraction of the outdoor radon were disregarded.

For consistency, a cut-off date of two weeks beyond the 3-month monitoring period is used. This means that the number of results recorded per period varies because some participants returned their detectors too late for inclusion in the analysis and report. Moreover, the number of monitored houses decreased because some participants withdrew from the study for various reasons, including moving home.

The indoor radon concentrations were found to be log-normally distributed (Cohen, 1986; Nero et al., 1986; Miles, 1998; Daraktchieva et al., 2014). The range, geometric mean and geometric standard deviation were calculated for each data set and these are presented in Table 3-1. It was confirmed that homes in Kirby Misperton and Little Barugh are situated in an area with low radon potential.

The monitoring during the 15th period (June 2019 - September 2019) identified that one house in Yedingham (an area identified as having low radon potential) had a result which was above the UK radon Action Level of 200 Bq $m^{-3}$. The results for the same house in the same periods for 2017 and 2018 were similar. The results for all the other periods were below the Action Level. This house was also confirmed to have quite low radon concentrations in the winter periods of 2017, 2018 and 2019 and showed a reverse seasonality pattern, i.e. high radon results in the summer and low radon results in the winter. It has been estimated that 4% of houses in the UK have a reverse seasonality pattern, i.e. summer high and winter low (Miles at al., 2012).

Pickering and Malton are situated in areas with higher radon potential (Miles et al., 2007) as is evident from Figure 3-1. Pickering has been confirmed as a radon Affected Area. Malton is also a radon Affected Area but for the third and fifth phases of the project there was an insufficient number of properties to provide good statistics. However the results from the first, second and fourth phases of the project indicated that Malton is situated in an area with elevated radon potential (Ward et al, 2019).

**Table 3-1. Range and distribution of estimated annual average indoor radon measurements from December 2018 to December 2019.**

| Area (number of homes) | Thirteenth 3-month reported results (Dec 18-Mar 19), Bq $m^{-3}$ | | | Fourteenth 3-month reported results (Mar 19-Jun 19), Bq $m^{-3}$ | | | Fifteenth 3-month reported results (Jun 19-Sep 19), Bq $m^{-3}$ | | | Sixteenth 3-month reported results (Sep 19-Dec 19), Bq $m^{-3}$ | | |
|---|---|---|---|---|---|---|---|---|---|---|---|---|
| | Range | GM | GSD | Range | GM | GSD | Range | GM | GSD | Range | GM | GSD |
| Kirby Misperton and Little Barugh (20/21/18/17) | 11 - 60 | 20 | 1.7 | 11 - 66 | 22 | 1.6 | 17 - 78 | 31 | 1.6 | 13 - 74 | 31 | 1.8 |
| Yedingham (22/18/15/15) | 10 - 79 | 28 | 2.1 | 15 - 108 | 29 | 2.1 | 17 - 233 | 39 | 2.7 | 14 - 129 | 29 | 2.5 |
| Pickering (27/25/22/23) | 7 - 172 | 31 | 3.0 | 9 - 220 | 38 | 2.8 | 12 - 294 | 45 | 3.0 | 7 - 608 | 44 | 4.0 |
| Malton (22/15/15/14) | 21 - 98 | 39 | 1.7 | 17 - 89 | 34 | 1.7 | 15 - 146 | 34 | 2.1 | 17 - 91 | 44 | 1.8 |

GM = geometric mean GSD = geometric standard deviation

This report includes the analysis of the aggregated results of four years of continuous measurements (December 2015 - December 2019). It consists of four 3-month results per year (16 monitoring periods) where all detectors were returned within two weeks of the end of each monitoring period. Annual average radon concentrations were estimated from each 3-month result using factors as specified in the UK Validation scheme.

**Table 3-2. Geometric mean (GM), geometric standard deviation (GSD) and Shapiro-Wilk p-values for 4 years of measurements from December 2015 to December 2019.**

| Area (number of aggregated results 1st/2nd/3rd/ 4th year) | First year (Dec 2015 - Dec 2016) | | | Second year (Dec 2016 - Dec 2017) | | | Third year (Dec 2017 - Dec 2018) | | | Fourth year (Dec 2018 - Dec 2019) | | |
|---|---|---|---|---|---|---|---|---|---|---|---|---|
| | GM Bq $m^{-3}$ | GSD | p-value | GM Bq $m^{-3}$ | GSD | p-value | GM Bq $m^{-3}$ | GSD | p-value | GM Bq $m^{-3}$ | GSD | p-value |
| Kirby Misperton and Little Barugh (110/103/94/76) | 21 | 1.8 | 0.48 | 24 | 1.9 | 0.52 | 23 | 1.7 | 0.42 | 25 | 1.7 | 0.28 |
| Yedingham (112/109/93/70) | 27 | 2.2 | 0.37 | 26 | 2.3 | 0.33 | 24 | 2.1 | 0.94 | 30 | 2.4 | 0.11 |
| Pickering (161/154/126/97) | 45 | 3.0 | 0.79 | 40 | 3.2 | 0.07 | 35 | 2.6 | 0.26 | 39 | 3.2 | 0.57 |
| Malton (70/48/78/66) | 33 | 2.3 | 0.92 | 23 | 1.9 | 0.16 | 32 | 1.8 | 0.07 | 37 | 1.8 | 0.10 |

The aggregated results for each area were converted to logarithmic values. The normality of the logarithm-transformed data was studied using the Shapiro-Wilk normality test, (Shapiro and Wilk,

1965) with the R statistical package (R Core Team, 2014). The data is normally distributed if $p > 0.05$. The p-values of log-transformed data, calculated and given in Table 3-2, for areas of Kirby Misperton and Little Barugh, Yedingham, Pickering and Malton are greater than 0.05, so we could conclude that all the log-transformed sample data are normally distributed. The geometric mean (GM) and geometric standard deviation (GSD) for each distribution were also calculated and are given in Table 3-2.

### 3.2.2 **Seasonality of indoor radon**

Seasonality of indoor radon was studied using the 16 periods of 3-month consecutive measurements in each home, without seasonal correction. Data were only included from the 42 homes in the Vale of Pickering where results were available for all the measurement periods (November/December 2015 to December 2019) - Kirby Misperton and Little Barugh (13 homes), Yedingham (12 homes), Pickering (15 homes) and Malton (2 homes).

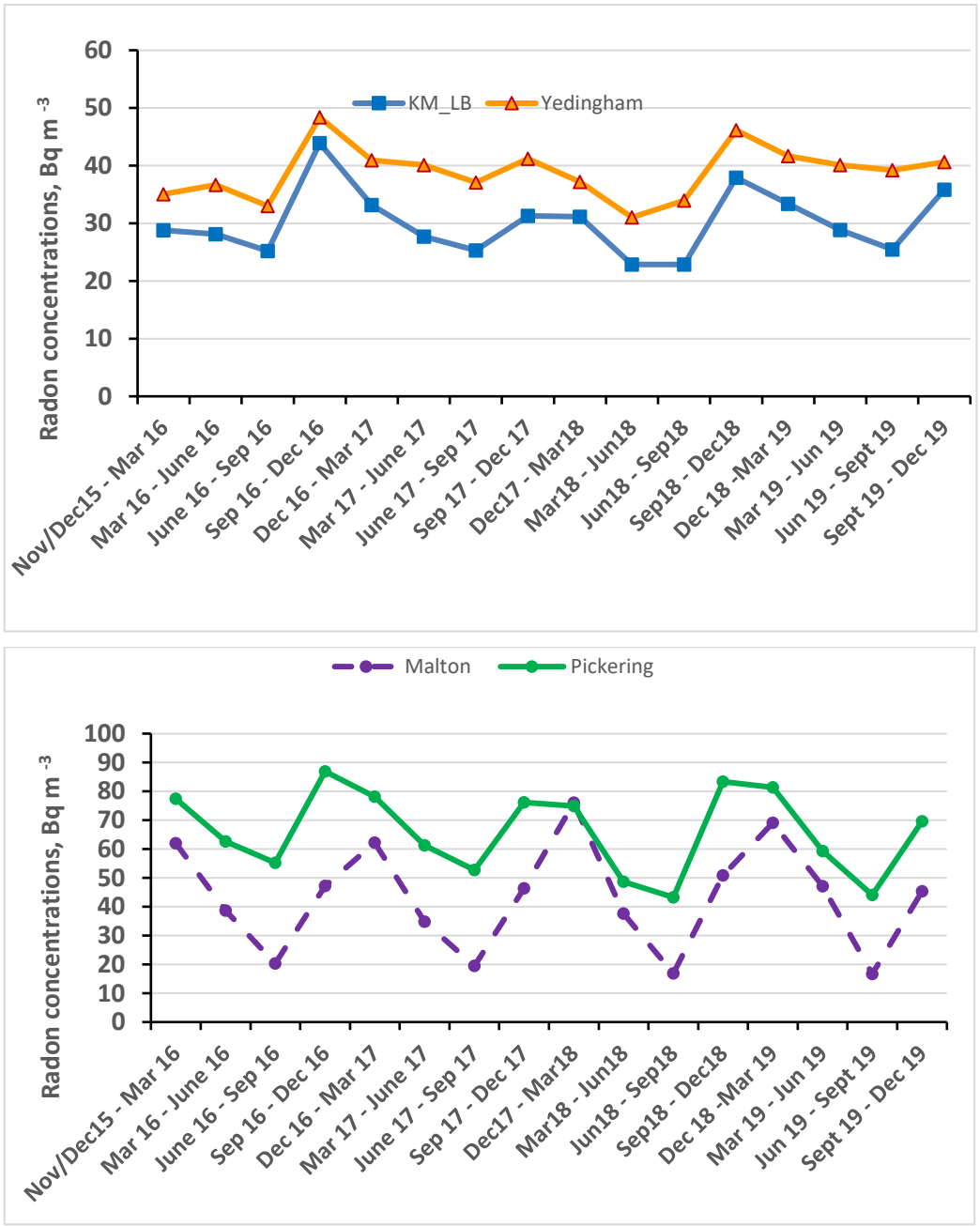


**Figure 3-2. Seasonal variation of average indoor radon concentrations in the area of Kirby Misperton and Little Barugh (KM_LB), Yedingham, Pickering and Malton. © PHE, 2020.**

The average radon concentrations were calculated by aggregating the results for homes in each of the areas of Kirby Misperton and Little Barugh (KM-LB), Yedingham, Pickering and Malton for each of the measurement periods. The results are presented in Figure 3-2. The monitored homes follow the normal UK seasonal pattern with a more pronounced minimum in summer (June to September) and maximum in winter (December to March). These findings are in very good agreement with results from an earlier study in which 84% of houses in the UK were identified as following the normal seasonality pattern (Miles et al., 2012).

## 3.3 OUTDOOR RADON MONITORING

### 3.3.1 Results for outdoor measurements

Aggregated results from October 2015 to October 2019 for the areas around Kirby Misperton, Yedingham, Pickering and Malton are given in Table 3. Outdoor results are approximately normally distributed, so the parameters reported in the table are the arithmetic mean and the standard deviation for each area.

**Table 3-3. Arithmetic mean and standard deviation of aggregated outdoor radon results (October 2015 to October 2019) using 1-year, 6-month and 3-month detectors.**

| Monitoring period / Area | 1-year October 2015 - October 2016 | 3-month October 2016 – January 2017 | 3-month January 2017 - April 2017 | 1-year April 2017 – April 2018 | 1 year April 2018 - April 2019 | 6-month April 2019- October 2019 |
|---|---|---|---|---|---|---|
| | Arithmetic mean, Bq $m^{-3}$ | Arithmetic mean, Bq $m^{-3}$ | Arithmetic mean, Bq $m^{-3}$ | Arithmetic mean, Bq $m^{-3}$ | Arithmetic mean, Bq $m^{-3}$ | Arithmetic mean, Bq $m^{-3}$ |
| **Kirby Misperton** | 8±1 | 4±1 | 5±3 | 3±1 | 9±3 | 7±3 |
| **Yedingham** | 9±2 | 4±1 | 5±1 | 3±1 | 7±2 | 4±1 |
| **Pickering** | 8±1 | 4±1 | 6±2 | 3±1 | 8±4 | 4±1 |
| **Malton** | - | 5±1 | 5±2 | 3±1 | 8±5 | 3±1 |

In April 2017 the monitoring was changed from 3-monthly to 6-monthly monitoring. The results for each location for each period were averaged. It was not possible to obtain results for all sites as some of the detectors had been removed or vandalised during the measurement period. Pickering and Malton were the most difficult sites for monitoring. Some sites where this damage occurred were relocated; for these monitoring points the 1-year monitoring results were not available. The change of location had some disruptive effect on the monitoring in these areas. It did not, however, have an impact on the overall results which confirmed that the outdoor radon levels in both Pickering and Malton were similar to those in Kirby Misperton and Yedingham.

The results from the control area in Oxfordshire are shown in Figure 3-3. The points were located in private gardens. Monitoring was carried out from October 2015 to January 2020. The number of participants varied during the monitoring.

## 3.4 MONITORING AT THE KMA SITE

The data from the AlphaGUARD continual radon monitoring instrument, placed in the outdoor air quality monitoring cabinet on the KMA site between April 2016 and February 2020 were analysed. The inherent background of the instrument resulting from the longer half-life alpha-emitting radionuclides (from environmental exposure and materials within the instrument), was taken into account when data were processed. The radon data, taken at 1 hour intervals, are log-normally distributed. The distribution parameters for several 3-month periods and two 6-month periods are given in Table 3-4. The average of the radon concentrations measured was 5 Bq $m^{-3}$. In order for a comparison to be made between the outdoor radon concentrations measured with the instrument

and the other outdoor results which use passive detectors, passive detectors were also placed in the enclosure at the KM8 site.

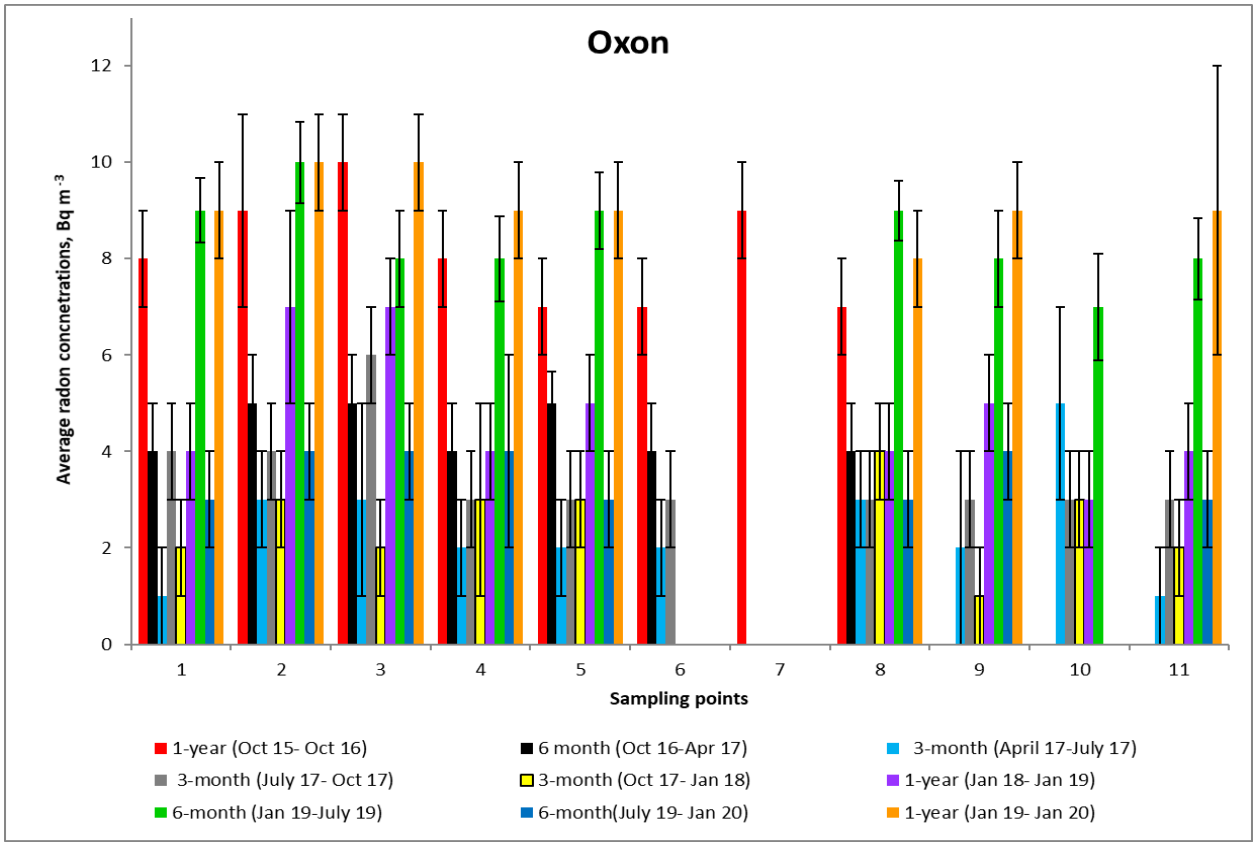


**Figure 3-3. Average radon concentrations at the outdoor sampling points in Oxfordshire.**

**Table 3-4. Range and distribution of outdoor radon measurements made with the AlphaGUARD instrument and passive detectors at the KMA site.**

| Period of monitoring | AlphaGUARD | | | | Passive detectors | |
|---|---|---|---|---|---|---|
| | Bq m$^{-3}$ | | | | Bq m$^{-3}$ | |
| | Range | Arithmetic Mean (AM) | Geometric Mean (GM) | Geometric Standard Deviation (GSD) | Arithmetic Mean (AM) | Standard Deviation (SD) |
| April 2016 - July 2016 | 1 - 46 | 5 | 5 | 2.0 | 4 | 1 |
| July 2016 - October 2016 | 1 - 81 | 6 | 4 | 2.4 | 8 | 1 |
| October 2016 - January 2017 | 1 - 50 | 6 | 4 | 2.5 | 7 | 1 |
| January 2017 - April 2017 | 1 - 29 | 4 | 3 | 2.3 | 5 | 1 |
| April 2017 - July 2017 | 1- 47 | 5 | 3 | 2.4 | 7 | 1 |
| July 2017 - October 2017 | 1 - 38 | 5 | 3 | 2.4 | 7 | 1 |
| October 2017 - July 2018 | 1 - 62 | 5 | 3 | 2.1 | - | - |
| October 2018 - April 2019 | 1 - 41 | 5 | 4 | 2.6 | 5 | 1 |
| April 2019 - July 2019 | 1 - 57 | 7 | 4 | 2.8 | 3 | 1 |
| July 2019 - November 2019 | 1 - 62 | 6 | 4 | 2.6 | 5 | 1 |
| November 2019 - February 2020 | 1 - 18 | 4 | 3 | 2.2 | | |

The radon concentrations measured using 10 passive detectors were compared with the concentrations measured with the AlphaGUARD for the various periods as shown in Table 3-4. It was found that the arithmetic means measured with the AlphaGUARD were similar to the arithmetic means measured with passive detectors for the same monitoring periods. This demonstrates a good agreement between the two different measurement techniques.

A graph showing the raw data obtained from the AlphaGUARD, without background correction for the monitoring period between April 2019 and February 2020, is given in Figure 3-4.

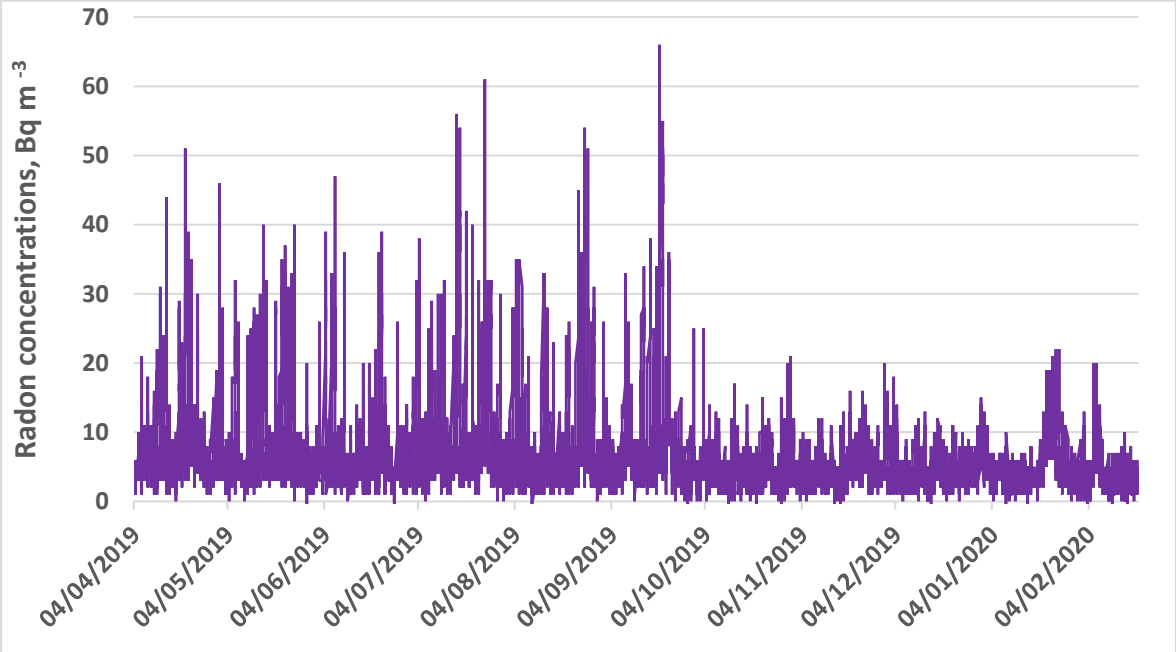


**Figure 3-4. Time series of radon concentrations recorded by the AlphaGUARD instrument at the KMA site between April 2019 and February 2020. © PHE (2020).**

## 3.5 COMPARISON OF YEAR 1, YEAR 2, YEARS 3 AND YEAR 4 RESULTS

Year to year variation of indoor radon was studied with measurements from 42 homes where results were available for all 16 measurement periods. The indoor radon levels did not show any obvious difference between the four years of monitoring (Table 3-2 and Figure 3-2).

There is an indication of year to year variability of outdoor radon. The results from the first year and fourth year of monitoring were about twice as high as the radon concentrations measured during the second year and third year (Table 3-3).

## 3.6 SUMMARY - RADON

### 3.6.1 Indoor radon

The analysis of the results for homes measured in the Vale of Pickering showed distributions of indoor radon concentrations consistent with the usual log-normal distribution for indoor radon.

The results for the Kirby Misperton and Little Barugh area are consistent with the status of not being a radon Affected Area.

The results from the control site at Yedingham were consistent with its status as an area with low radon potential. Only one property, which exhibited reverse seasonality, was found to have a radon level above the Action Level, however, due to the reverse seasonality the annual average radon concentration cannot be estimated correctly using seasonal correction factors.

The results for Pickering confirmed the prior status as a radon Affected Area (1-10% of homes predicted to exceed the Action Level of 200 Bq $m^{-3}$), with radon concentrations spread over a wide range from about 10 to 650 Bq $m^{-3}$ and several homes (3-8% of houses monitored) being found to have results exceeding the Action Level. Each householder was given standard advice on any action required; those with high radon levels were given additional information on reducing their radon concentrations.

Radon levels above 200 Bq $m^{-3}$ were measured in some homes in Malton at the beginning of this study that confirmed our classification as a radon Affected Area; standard advice to reduce radon levels was issued to the occupiers of these homes.

The seasonal variation of indoor radon was also studied for all areas. It was found that all except one of the monitored houses followed the normal seasonal pattern in the UK with the highest radon concentrations in winter and lowest radon concentrations in summer. It should be noted that the number of results for Malton is rather small compared to the other areas where results were assessed.

### 3.6.2 Outdoor radon

The results from the first and fourth year of monitoring of outdoor air are about twice as high as the radon concentrations observed previously in the UK of 4 Bq $m^{-3}$ (Wrixon et al., 1988). The results from the second and third year of the monitoring indicated levels closer to those previously measured. There is no indication of elevated outdoor radon concentrations in the Pickering or Malton radon Affected Areas. The analysis of results for another control site in Oxfordshire showed similar concentrations.

### 3.6.3 Monitoring at the KM8 site

Results from the AlphaGUARD active monitor and passive detectors both placed in the KM8 enclosure are in good agreement with the average outdoor radon concentrations within the area of Kirby Misperton. The active monitoring showed significant variations over time, however the annual average measured at the KM8 site was consistent using both measurement techniques.

## 3.7 REFERENCES


Cohen, B. L., 1986. A national survey of $^{222}Rn$ in US homes and correlating factors. Health Physics 51 (2), 175-183.

Daraktchieva, Z., Miles, J. H. C., McColl, N., 2014. Radon, the lognormal distribution and deviation from it. J. Radiol. Prot. 34(1):183-190.

Daraktchieva, Z., 2017. New correction factors based on seasonal variability of outdoor temperature for estimating annual radon concentrations in UK, Rad. Prot. Dosimetry 175-1: (65-74).

Daraktchieva Z., 2018. Review and Update of Occupancy Factors for UK homes. © Crown copyright 2018 Chilton, PHE-CRCE-044.

Daraktchieva Z, Howarth C B., Gooding T D., Bradley E J and Hutt N., 2018. Validation Scheme for Organisations Making Measurements of Radon in UK Buildings: 2018 Revision, © Crown Copyright 2018, Chilton, PHE-CRCE-040.

Darby S., Hill D., Auvinen A., Barros-Dios J M., Baysson H., Bochicchio F. *et al*., 2005. Radon in homes and risk of lung cancer: collaborative analysis of individual data from 13 European case-control studies. BMJ, 330 :223.

Gunby, J. A., Darby, S. C., Miles, J. C. H., Green, B. M. R., Cox, D. R., 1993. Factors affecting indoor radon concentrations in the United Kingdom. Health Physics 64 (1), 2-12.

Hunter N., Howarth C B., Miles J C H., Muirhead C R., (2005) Year-to-year variations in radon levels in a sample of UK houses with the same occupants. Seventh International Symposium on the Natural Radiation Environment (NRE-VII). In: Radioactivity in the Environment Book Series, vol. 7. Elsevier, 438-447.

Kibble A., Cabianca T., Daraktchieva Z., Gooding T., Smithard J., Kowalczyk G., McColl N P., Singh M., Mitchem L., Lamb P., Vardoulakis S., and Kamanyire R., 2014. Review of the Potential Public Health Impacts of Exposures to Chemical and Radioactive Pollutants as a Result of the Shale Gas Extraction Process, © Crown Copyright 2014, Chilton, PHE-CRCE-009.

Miles J. C. H., and Algar R. A., 1988. Variations in radon-222 concentrations. J Radiol. Prot 8 (2), 103-106.

Miles, J. C. H. Mapping radon- prone areas by lognormal modelling of house radon data. Health Physics 74(3), 370-378 (1998).

Miles J. C. H., Appleton J. D., Rees D. M., Green B. M. R., Adam K. A. M., Myers A. H., 2007. Indicative Atlas of Radon in England and Wales (Chilton), HPA-RPD-033.

Miles, J. C. H., Howarth, C. B., and Hunter, N., (2012) Seasonal variation of radon concentrations in UK homes. J. Radiol. Prot. 32, 275-287 (2012) and 2014 corrigendum J. Radiol. Prot. 34, 493. http://dx.doi.org/10.1088/0952-4746/34/2/493.

Nero, A. V., Schwehr, M. B., Nazaroff, W. W., Revzan, K. L., 1986. Distribution of airborne Radon-222 concentrations in U.S. homes. Science 234(4779), 992-997.

R Core Team (2014). R: A language and environment for statistical computing. R Foundation for Statistical Computing, Vienna, Austria. URL http://www.R-project.org/

Shapiro, S. S. & Wilk, M. B., 1965. An analysis of variance test for normality (complete samples). Biometrika, 52(3–4), pp.591–611. Available at: https://doi.org/10.1093/biomet/52.3-4.591.

Wasikiewicz, J. M., Daraktchieva, Z., Howarth, C. B., 2019. Passive etched track detectors application in outdoor radon monitoring. Perspectives in Science, 12, 100416, 1-5.

Wrixon A. D., Green B. M. R., Lomas P. R., Miles J. C. H., Cliff K. D., Francis E. A., Driscoll C. M. H., James A. C., and O'Riordan M. C. 1988. Natural Radiation Exposure in UK Dwellings. Report NRPB-R190 (London: Her Majesty's Stationery Office).

# 4 Water monitoring

## 4.1 INTRODUCTION

Monitoring of groundwater and streamwater chemistry has continued over the project period in both the Vale of Pickering (Figure 4-1) and Fylde (Figure 4-2) investigation areas. As no shale-gas activities have been undertaken by the operator at the Kirby Misperton site during the reporting period, monitoring there has been conducted on a quarterly schedule, during May 2019, August 2019, November 2019 and February 2020. Sites sampled included the regular monitoring network of third-party boreholes and streams, BGS-installed boreholes into the Superficial (Quaternary and/or Kimmeridge formations) and Corallian aquifers, and Third Energy boreholes located on the KMA site. In addition, depth samples from the multilevel samplers were collected twice: in August 2019 and February 2020.

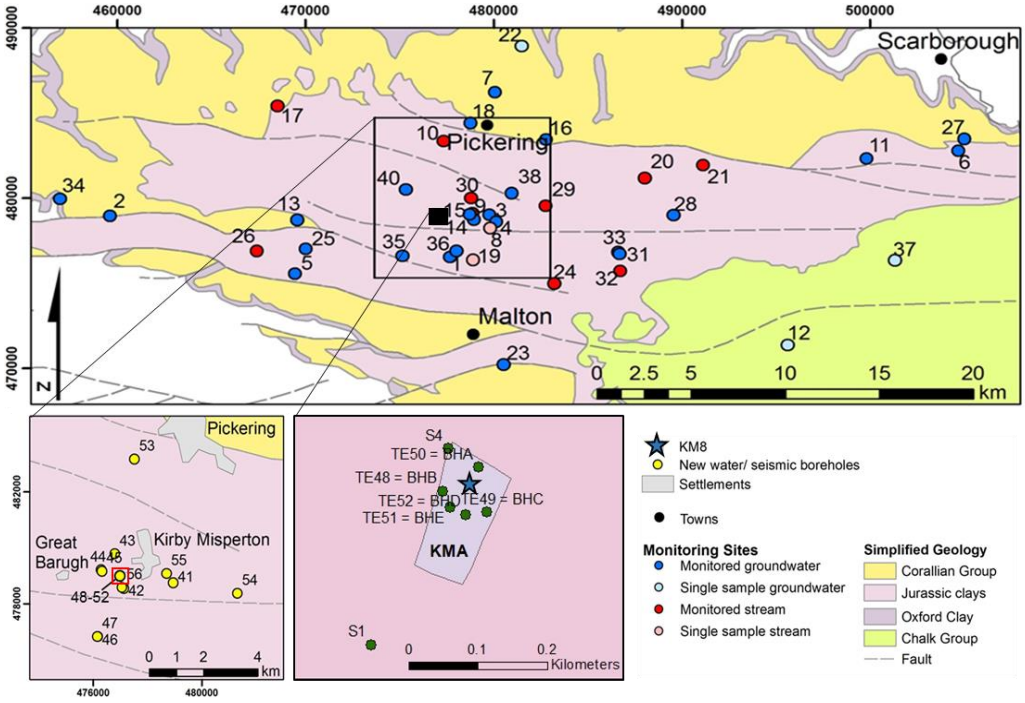


**Figure 4-1. Geological map of the Vale of Pickering showing sampling locations used in this report. Insets shows boreholes close to Kirby Misperton and the shale gas well site (KMA).**

In the Fylde, 10 rounds of water sampling were carried out over the project period, the increased frequency in response to the plan for hydraulic fracturing of PNR borehole 2 by Cuadrilla. Hydraulic fracturing took place during August 2019 but was halted shortly afterwards because of the induced seismicity response. Following the moratorium on shale-gas activity in England, announced in November 2019, sampling returned to a quarterly schedule. Sampling of PNR boreholes was undertaken in April, June, July (early and late), November, December 2019 and March 2020. Sampling of some or all third-party boreholes, BGS boreholes and streams in the monitoring network took place in the same months plus September and October 2019.

Sampling has been conducted following standard recognised procedures with QA for chemical analysis according to good laboratory practice. UKAS-accredited methods have been used where available for the analytes measured. Real-time hourly monitoring of the BGS boreholes has continued throughout the project period in both investigation areas, with outputs reported in near real-time to the BGS website.

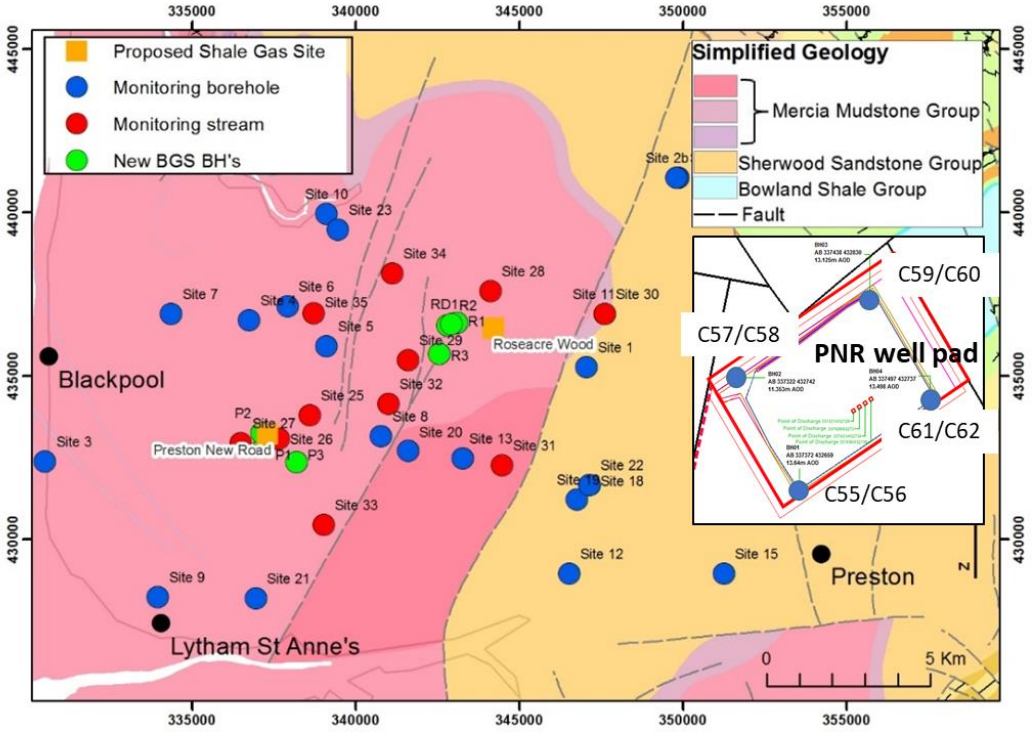


**Figure 4-2. Geological map of The Fylde showing sampling locations used in this report. Inset shows boreholes close to the shale gas well site (PNR).**

## 4.2 WATER MONITORING NETWORK

### 4.2.1 Vale of Pickering

A substantial body of baseline water-chemistry data has been built up for the Vale of Pickering investigation area and shows many consistencies over the time since the network monitoring was initiated. Results for calcium (Ca), sodium (Na), chloride (Cl) and dissolved methane ($CH_4$) are shown as an illustration for individual sites in the Superficial aquifer, BGS-installed boreholes in the Superficial aquifer, Corallian aquifer and streams in Figure 4-3, Figure 4-4, Figure 4-5, Figure 4-6 respectively.

Results show the Na(-$HCO_3$) dominance of groundwater from the Superficial aquifer (reflecting clay influence), Ca(-$HCO_3$) dominance of groundwater from the marginal (exploited) areas of the Corallian aquifer (reflecting limestone influence), and the diverse compositions of the streamwaters (reflecting runoff from diverse lithologies). Some sites show greater temporal variability than others. Groundwater from the Superficial aquifer shows a large range of concentrations of dissolved $CH_4$, but with high concentrations being reproducibly high. Variability in $CH_4$ concentration is matched by variability in solute concentration and much of the variation appears to be related to differing input horizons in the Superficial deposits (Quaternary sands/clays, weathered Kimmeridge) in relation to pumping regimes and groundwater levels.

As all samples were collected in the absence of shale-gas exploration activity in the Vale of Pickering, the whole dataset can be regarded as baseline. A subset of data acquired are illustrated here, but the dataset serves to illustrate the large variation in compositions, both spatial and temporal, that the baseline encompasses. The spatial variation is associated with variations in lithology, landuse and hydrogeology, with additional temporal variability associated with recharge, water use and management, and modern anthropogenic contamination.

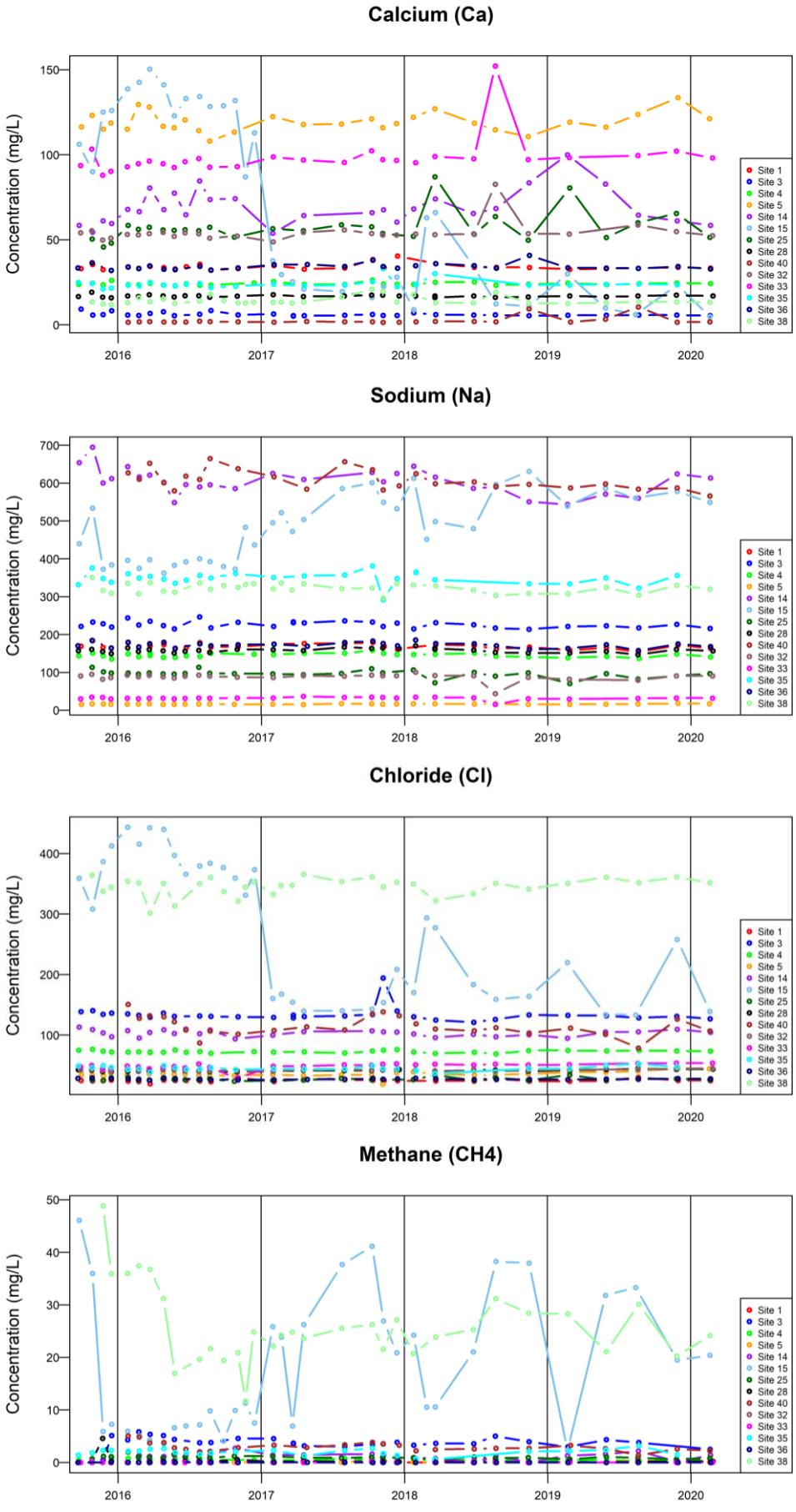


**Figure 4-3. Monitoring data for calcium, sodium, chloride and methane in groundwater from the Superficial aquifer, Vale of Pickering.**

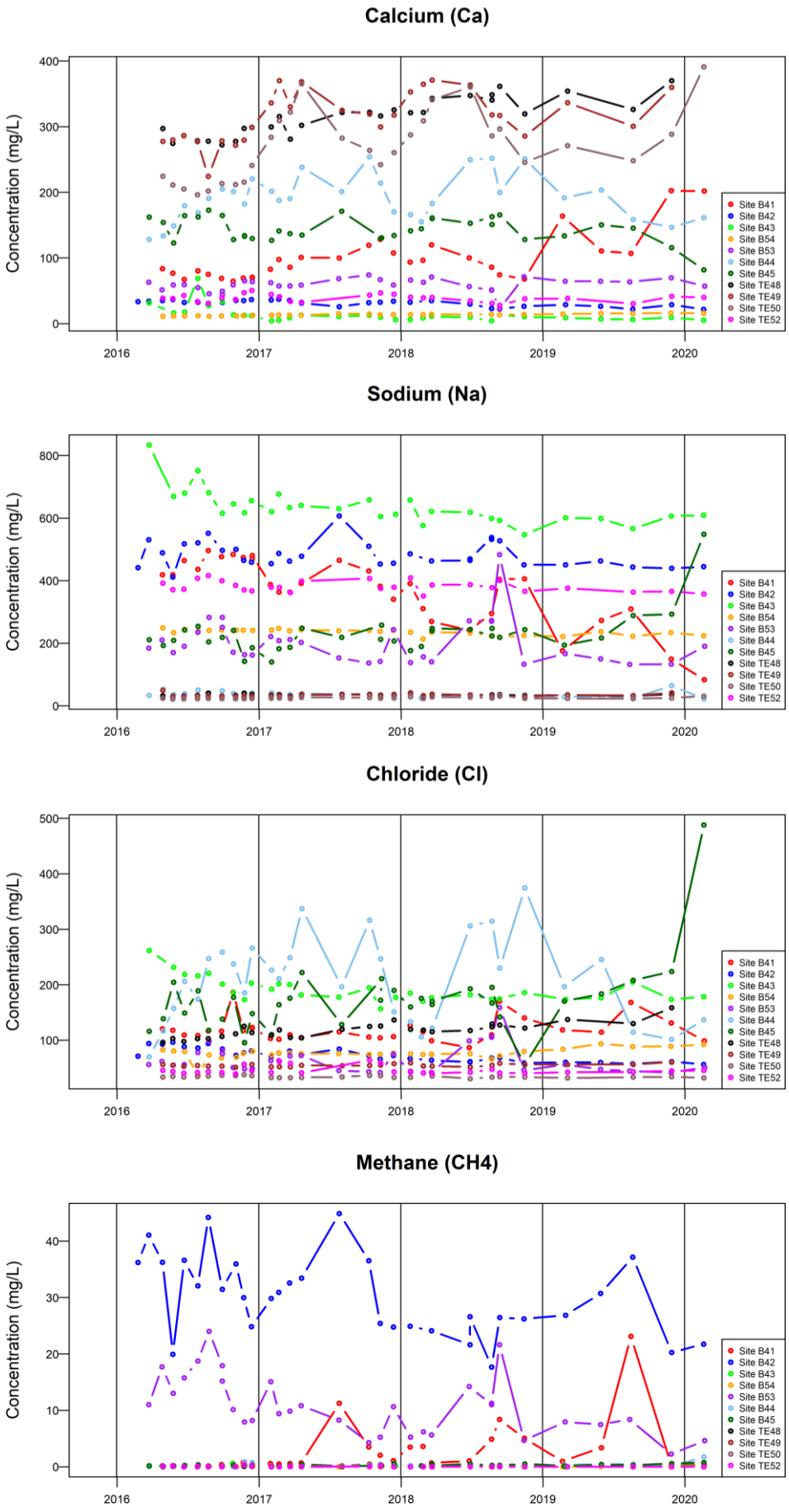


**Figure 4-4. Monitoring data for calcium, sodium, chloride and methane in groundwater from the BGS and Third Energy boreholes in the Superficial aquifer, Vale of Pickering.**

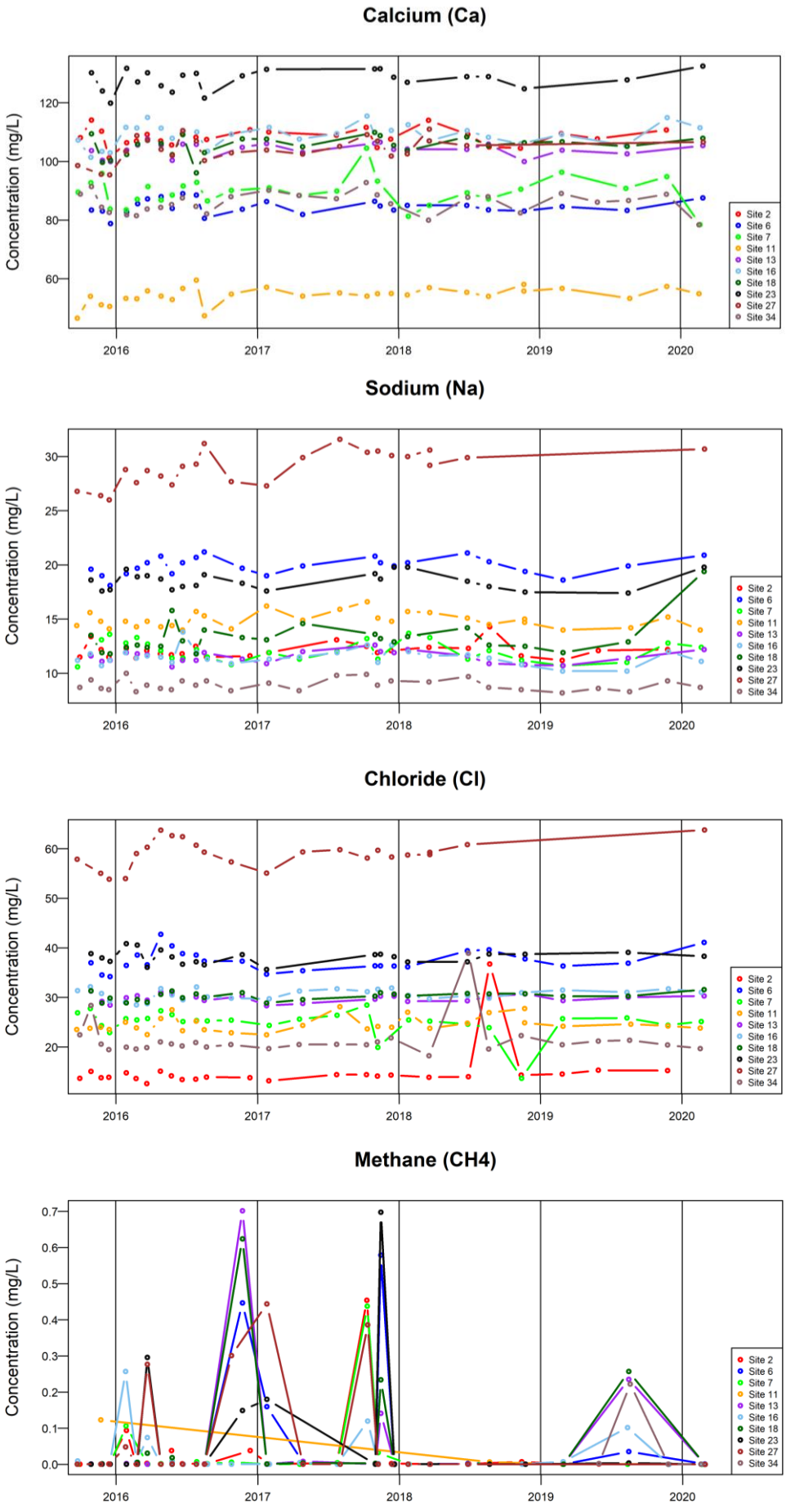


**Figure 4-5. Monitoring data for calcium, sodium, chloride and methane in groundwater from the Corallian aquifer, Vale of Pickering.**

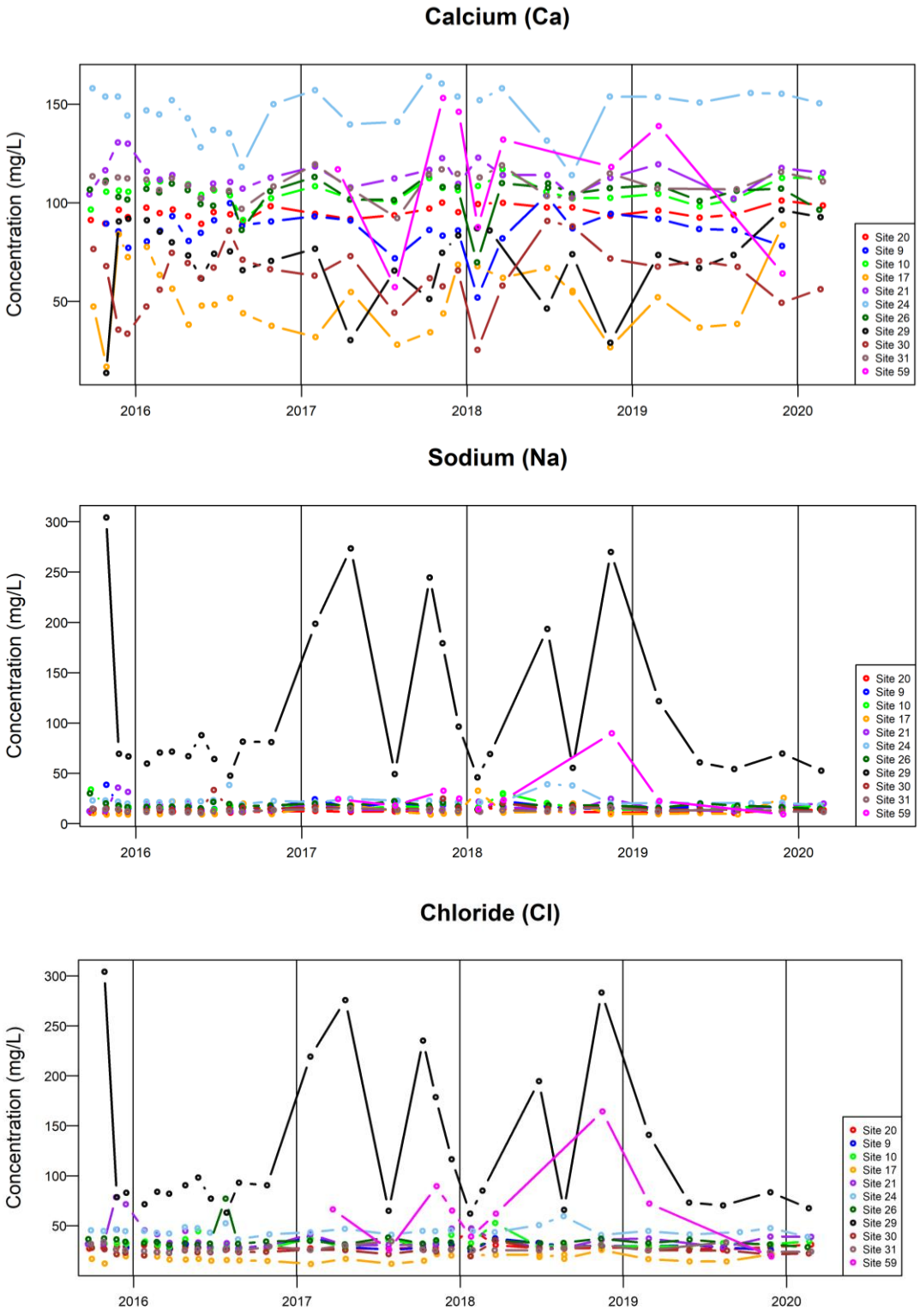


**Figure 4-6. Monitoring data for calcium, sodium and chloride in streamwater from the Vale of Pickering.**

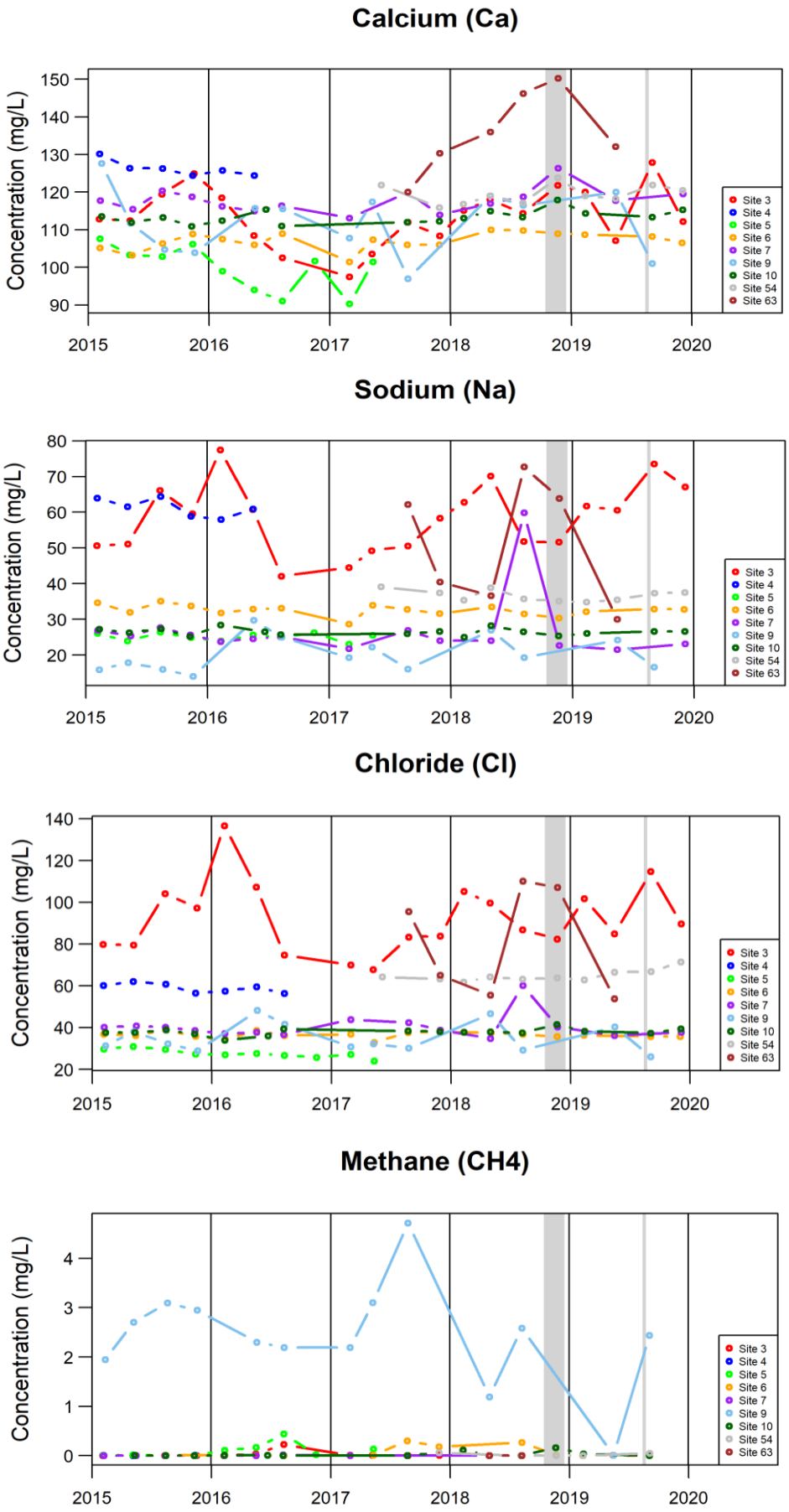


**Figure 4-7. Monitoring data for calcium, sodium, chloride and methane in groundwater from the Superficial (Quaternary) aquifer of the Fylde, Lancashire (intervals of hydraulic fracturing at PNR are shown in grey).**

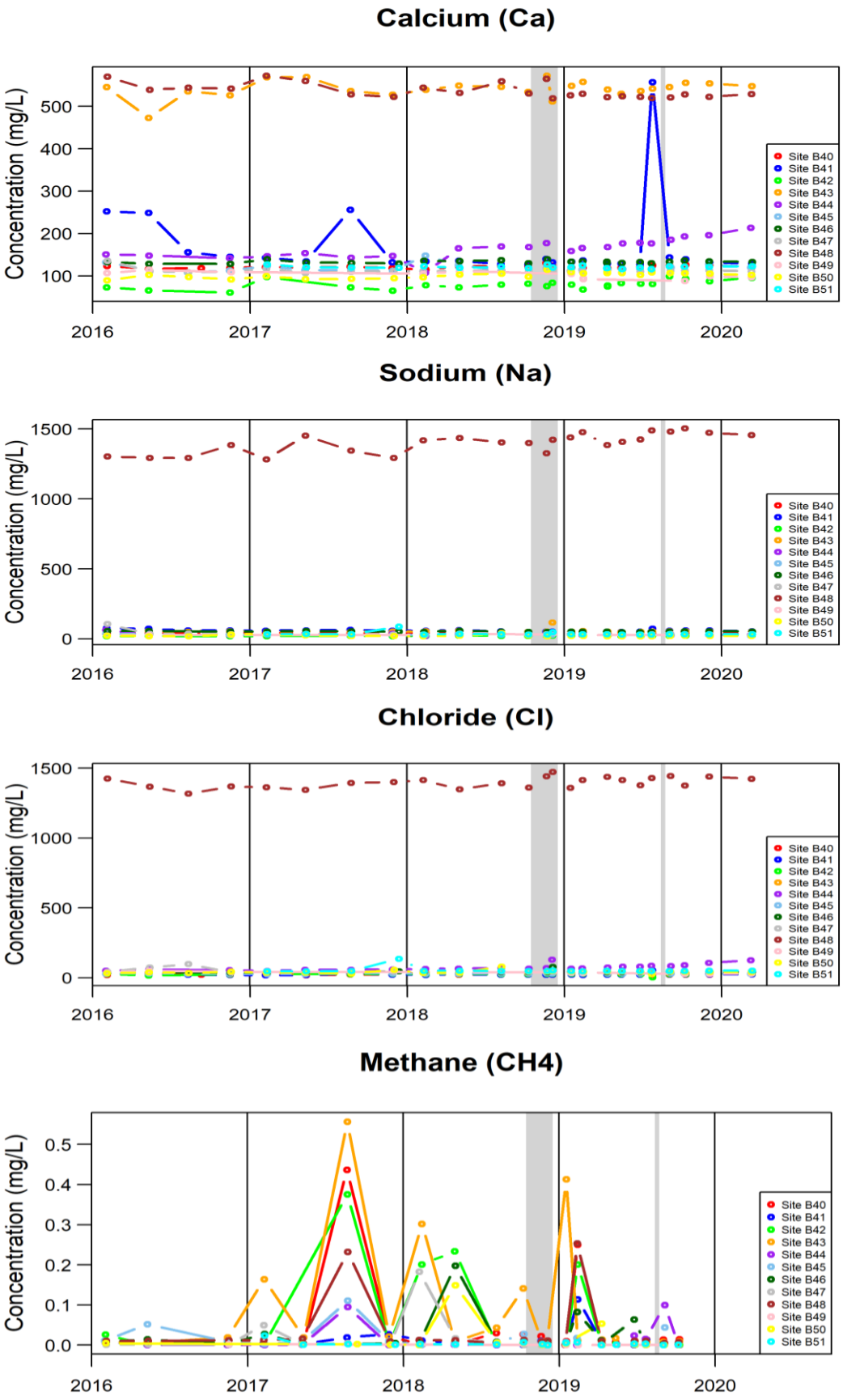


**Figure 4-8. Monitoring data for calcium, sodium, chloride and methane in groundwater from the BGS boreholes in the Superficial aquifer, Fylde, Lancashire.**

### 4.2.2 The Fylde, Lancashire

Temporal variations in concentrations of the same subset of analytes: Ca, Na, Cl and $CH_4$, are shown for groundwater from the Superficial (Quaternary) aquifer from third-party boreholes in the

regular monitoring network and from BGS-installed boreholes in Figure 4-7 and Figure 4-8 respectively. Compositions are also related to reaction of groundwater with host aquifer minerals and the groundwaters in the Superficial aquifer are dominantly reducing. Methane is present in some of the groundwaters but in much lower concentrations than observed in Superficial aquifers of the Vale of Pickering. Temporal variability is evident from the plots but no major trends were observed over the project reporting period. No responses linked to hydraulic fracturing and subsequent operations were observed from the chemical data.

Comparisons of data from BGS and Cuadrilla (shale gas site operator) laboratories for selected analytes in groundwater from the PNR site are also given in Figure 4-9. Some difficulties arise in comparisons, as that Cuadrilla data are often provided/reported without specifying the units of measurement on the Environment Agency's website. Some $CH_4$ data for the first quarter of 2019 are also given as zeros, despite samples in the same batch having defined detection limits. The zero entries are therefore indistinguishable between non-detects and missing values. In addition, nitrate data appear to be inconsistently given as $NO_3$ or N in different reporting periods. Despite these uncertainties, comparisons with the BGS analytical results have been made using best judgement.

Figure 4-9 shows the intervals of hydraulic fracturing (HF) in the boreholes 1z and 2 at PNR shale gas site. Results for Ca, Na and Cl show temporal variation within boreholes. Results for Ca show some increase (around 8%) from BGS data in the first sample at some sites during HF of 1z, but not in data from Cuadrilla and not in post HF 1z activity. Na and Cl, as indicators of salinity, show but no evidence of perturbations relative to the baseline either during or after hydraulic fracturing. Results for BH01B show the largest increase post HF 1z but this borehole has the largest variability in chemical compositions of all the sites. Likewise, $CH_4$ data reveal variability (especially for BH01B) but no evidence of departure from the baseline range following hydraulic fracturing. Data for $CH_4$ in BGS samples from March 2020 are not yet available to report due to closure of the laboratory as a result of the Covid-19 restrictions. A more thorough statistical evaluation of the chemical variations will be carried out once all quality-assured data have been reported.

## 4.3 DEPTH PROFILES

Depth profiles of selected analytes in groundwater from our multi-level samplers in the Vale of Pickering to the east of Kirby Misperton are shown (with the extra two sets of samples from 2019–2020) in Figure 4-10. The CMT and Waterloo multi-level sampler systems have been described in earlier reports (Ward et al., 2018, 2019). The profiles show distinct compositions of samples derived from the CMT and Waterloo samplers, the CMT ports taking water from a combination of Quaternary and shallow Kimmeridge horizons, while the Waterloo ports derive almost entirely from the Kimmeridge. The profiles demonstrate the overall consistency of analyses over time, albeit with $CH_4$ concentrations being relatively low in the last round of sampling (February 2020) and with one anomalously low $CH_4$ analysis from the deepest sampling port (Figure 4-10).

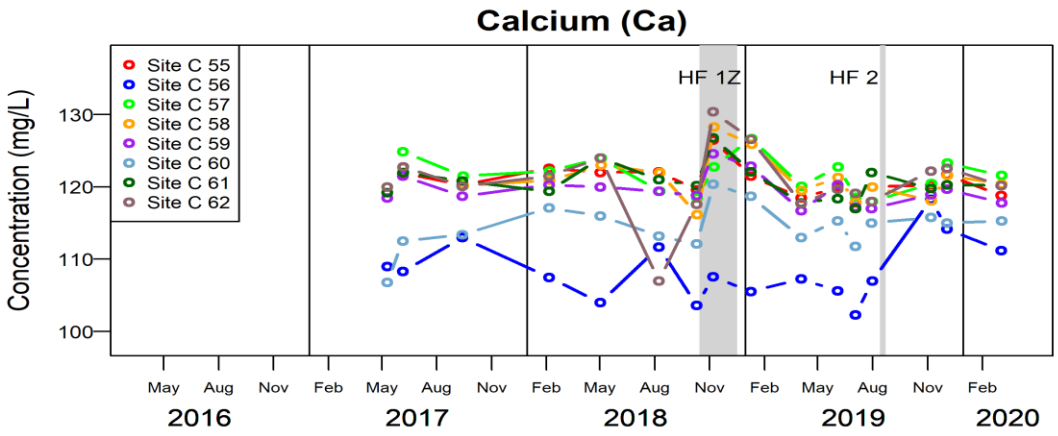
Calcium (Ca)
Concentration (mg/L)
Site C 55
Site C 56
Site C 57
Site C 58
Site C 59
Site C 60
Site C 61
Site C 62
HF 1Z
HF 2
100
110
120
130
May
Aug
Nov
Feb
2016
2017
2018
2019
2020

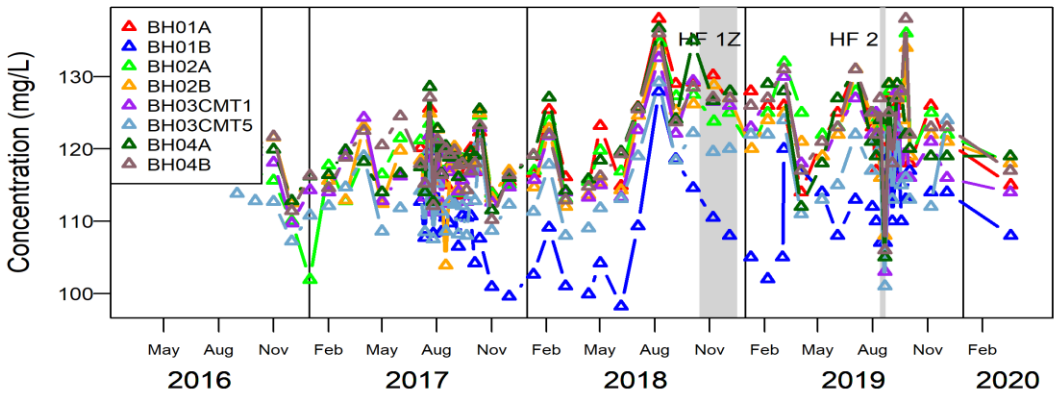
Concentration (mg/L)
BH01A
BH01B
BH02A
BH02B
BH03CMT1
BH03CMT5
BH04A
BH04B
HF 1Z
HF 2
100
110
120
130
May
Aug
Nov
Feb
2016
2017
2018
2019
2020

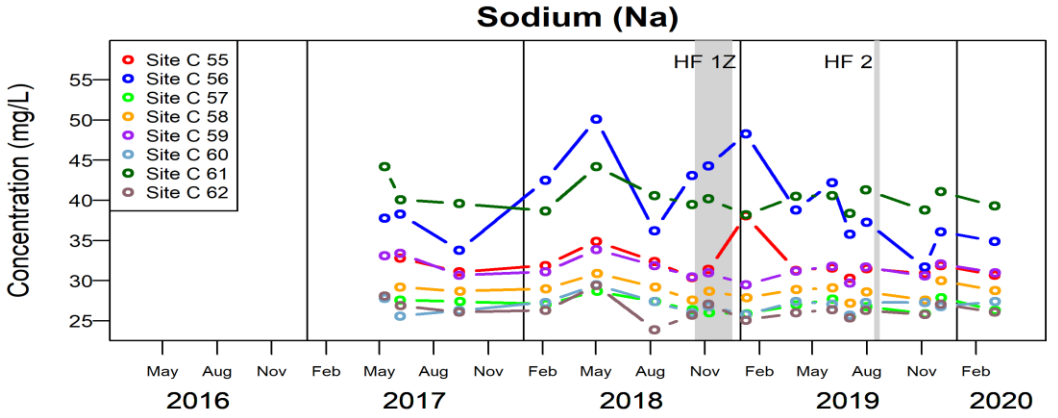
Sodium (Na)
Concentration (mg/L)
Site C 55
Site C 56
Site C 57
Site C 58
Site C 59
Site C 60
Site C 61
Site C 62
HF 1Z
HF 2
25
30
35
40
45
50
55
May
Aug
Nov
Feb
2016
2017
2018
2019
2020

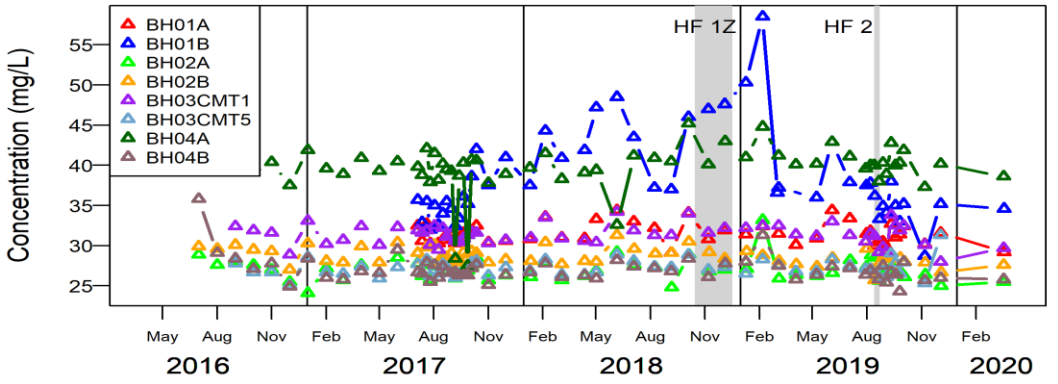
Concentration (mg/L)
BH01A
BH01B
BH02A
BH02B
BH03CMT1
BH03CMT5
BH04A
BH04B
HF 1Z
HF 2
25
30
35
40
45
50
55
May
Aug
Nov
Feb
2016
2017
2018
2019
2020

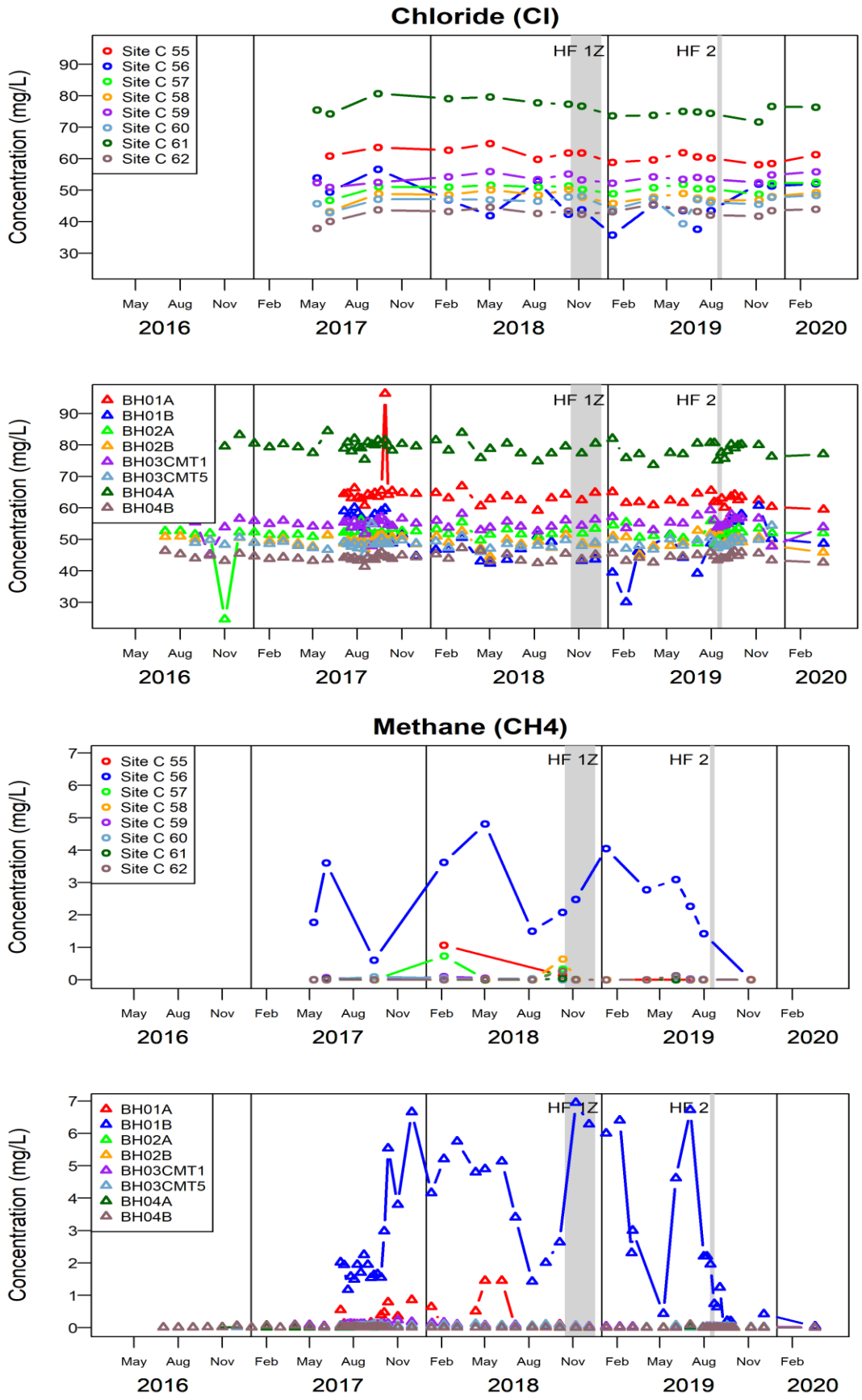


**Figure 4-9. Monitoring data for selected analytes in the PNR boreholes from BGS data (circles) and Cuadrilla data (triangles). Site colours correspond.**

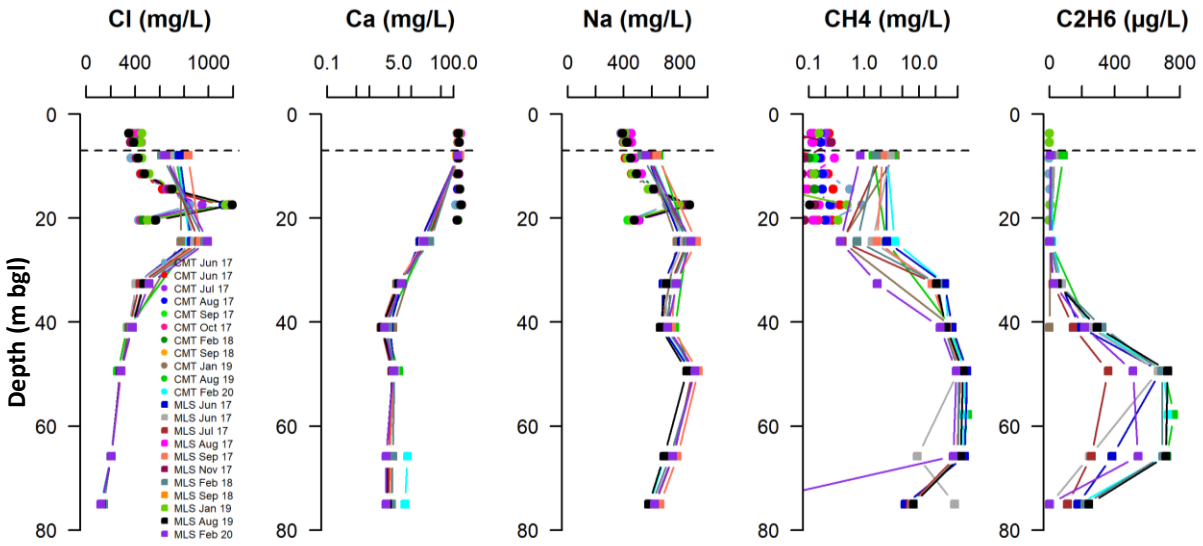


**Figure 4-10. Profiles of groundwater chemistry in the CMT and MLS sampler systems, Vale of Pickering (note log scale on $CH_4$).**

## 4.4 REAL-TIME MONITORING

Real-time monitoring data for groundwater pH, specific electrical conductance (SEC), temperature and groundwater level are shown for sensors installed in BGS monitoring boreholes (EBM 1–5, 12) in the shallow Superficial aquifer of The Fylde, Lancashire are shown in Figure 4-11. Perturbations due to maintenance and calibration are visible from vertical spikes in the time series. Results over the reporting period are comparable with the longer-term trends: temporal variability in pH measurements is largely an artefact of instrument drift, resulting in the characteristic saw-tooth pattern with sharp adjustment following calibration. The other analytes are less prone to instrument drift. Seasonal variability is observed in the temperature data. SEC and water level show less variability. None of the traces demonstrates any clear groundwater response to the hydraulic fracturing operations at PNR during 2019 (or 2018).

Real-time data for groundwater pH, specific electrical conductance, temperature and groundwater level from sensors installed in the BGS boreholes in the shallow Superficial aquifer of the Vale of Pickering (EBM 7–10, 13) are shown in Figure 4-12. Compositions measured over the project period have been consistent with earlier measurements. Groundwater pH shows some variability due to instrument drift although some of the variation also corresponds with other chemical changes (e.g. SEC in EBM 8). Specific electrical conductance is particularly variable in two of the boreholes: the variation reflects influence of different lithological horizons (Quaternary, Kimmeridge) with recharge and pumping regimes and is broadly consistent with variations observed from the groundwater sampling data.

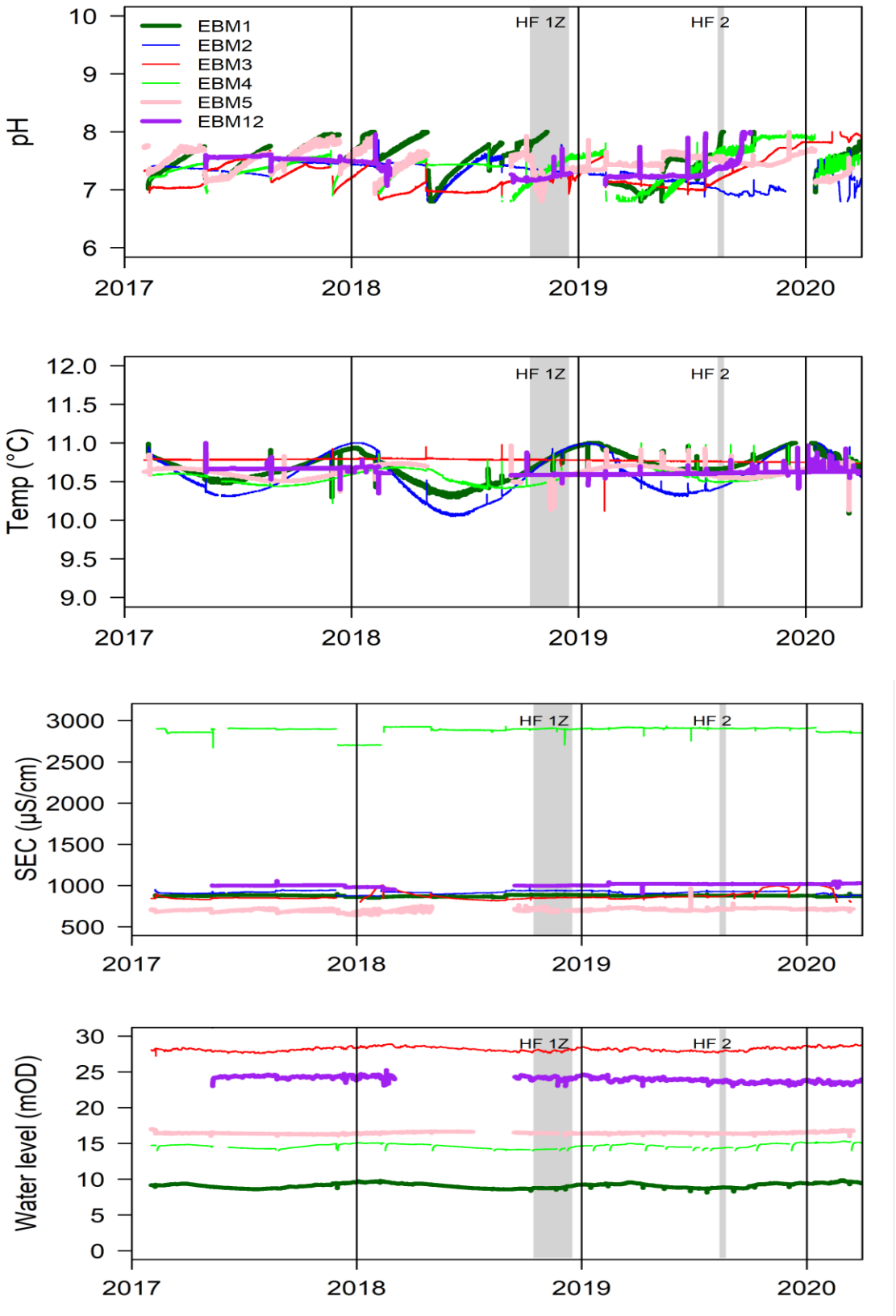


**Figure 4-11. Real-time data for groundwater pH, specific electrical conductance, temperature and groundwater level (above ordnance datum) from downhole sensors in the BGS monitoring network, Fylde, Lancashire; thick lines are for sensors in boreholes clustered around the PNR site, thin lines are for sensors around Roseacre.**

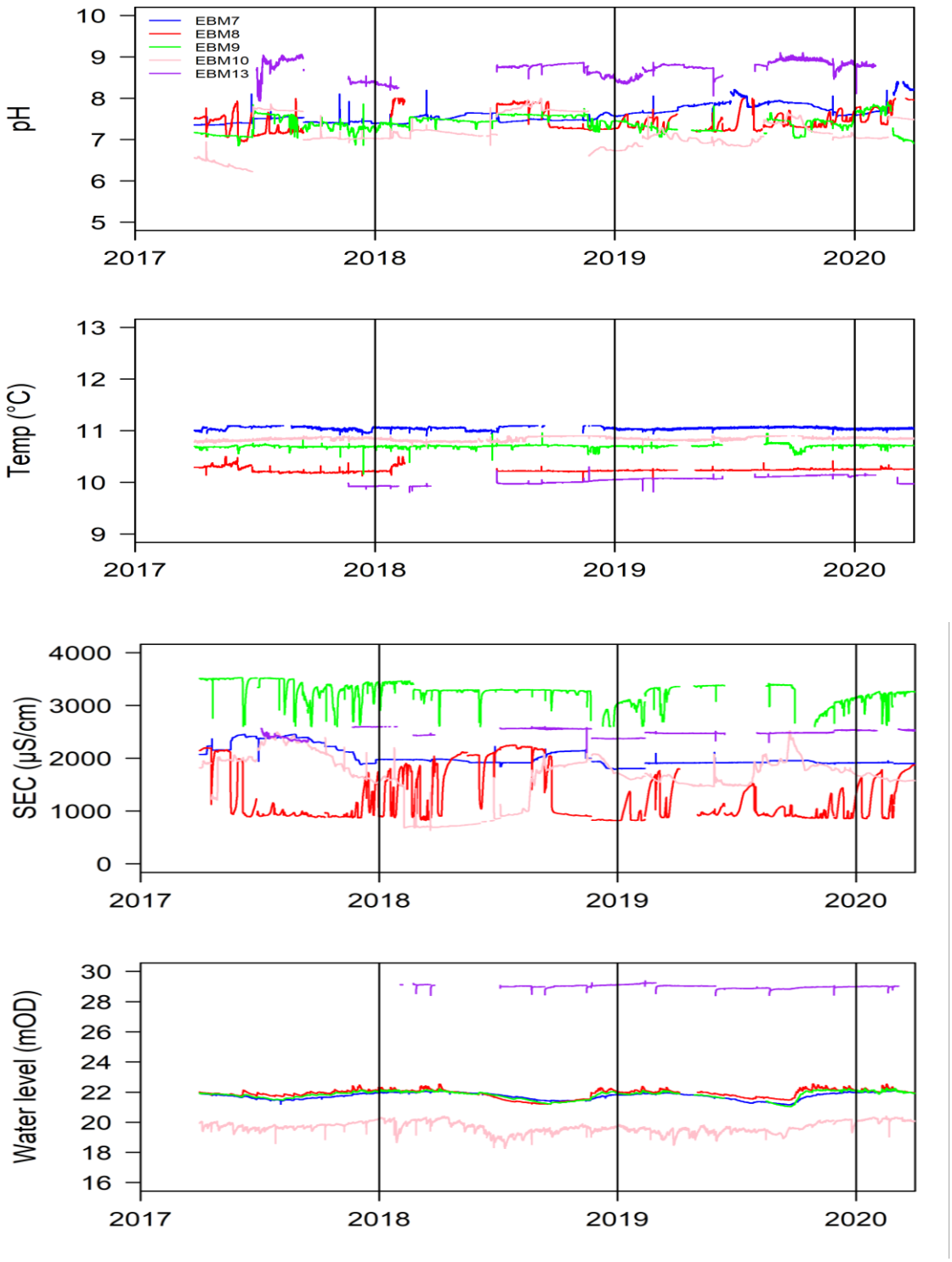


**Figure 4-12. Real-time data for groundwater pH, specific electrical conductance, temperature and groundwater level (above ordnance datum) from downhole sensors in the BGS monitoring network, Vale of Pickering.**

## 4.5 DISSOLVED GAS ANALYSIS

An investigation to compare analyses of dissolved gases in groundwater by two independent laboratories was carried out for selected samples collected during March 2020. This was initiated as a response to the discrepancies observed between previous dissolved methane analyses from different laboratories, as reported in Ward et al. (2019). 50 sites were sampled in duplicate for analysis by each laboratory; neither method is UKAS-accredited.

Samples for analysis in the BGS laboratory were collected inline from pumped boreholes using flexible tubing from the wellhead, with collection at pump pressure into valved steel cylinders of known volume. Gas was separated by extraction into a headspace of known volume, with analysis by GC-FID at the BGS Wallingford laboratory. Analyses include results for methane, carbon dioxide, and where detectable, for ethane. Detection limits for methane were typically 0.05 mg/L. Precision on methane analysis is approximately 5% RSD (cf. Darling and Milne, 1995).

Samples for analysis by an independent laboratory were collected during the same site visit using the same inline sampling system. Aliquots were collected into filled sealed glass vials of known volume, following the agreed laboratory sampling protocol. Sample preparation involved degassing into a headspace, with analysis by GC-FID. Analytical detection limit for methane was typically 0.01 mg/L. Laboratory documentation for the method quotes an expanded uncertainty for methane analysis of 14% (95% confidence).

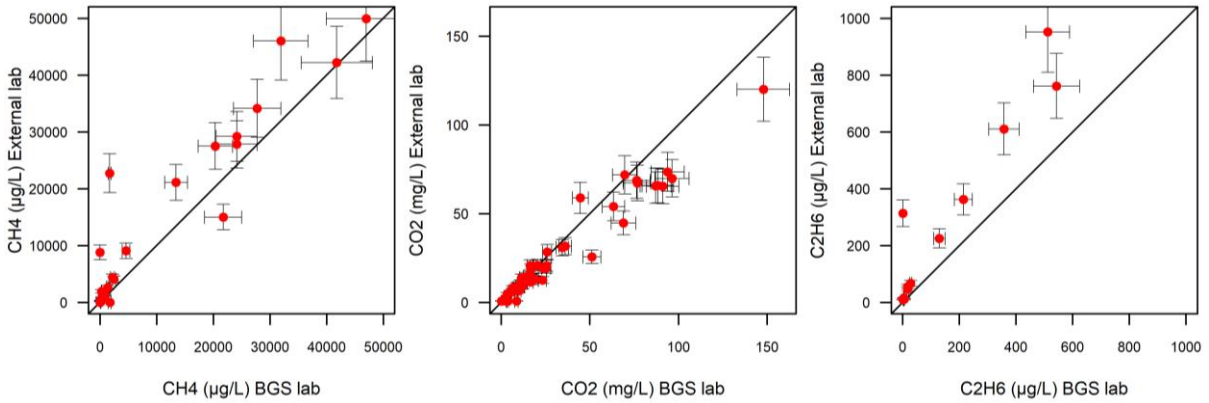


**Figure 4-13. Comparison of analytical data for methane ($CH_4$), carbon dioxide ($CO_2$) and ethane ($C_2H_6$) from two independent laboratories. Error bars represent approximate expanded uncertainty of 15%.**

The results (Figure 4-13) show some biases towards lower concentrations for $CH_4$ and $C_2H_6$ from the BGS laboratory relative to the external laboratory. For methane, the discrepancies are largest at relatively low $CH_4$ concentrations (up to 200% differences at <10 mg/L), ranging between ±40% at concentrations >10 mg/L. Average differences are 15% lower in the BGS analyses than the external laboratory at concentrations >10 mg/L; values agree within error at the highest observed concentrations. For $CO_2$, BGS analyses were on average 20% higher than the external laboratory data at concentrations >20 mg/L. For ethane, BGS analyses were on average 50% lower where ethane concentrations were >100 µg/L (Figure 4-13). The discrepancies warrant further investigation into sampling and analytical protocols and further replicate analysis, preferably with a round-robin laboratory process.

The discrepancies have implications for determination of C1/C2 ratios in the groundwater samples. Ethane was not detectable in all samples and so C1/C2 ratios could not be estimated for all samples. Results from the laboratory comparison are shown in Figure 4-14. Results are comparable at $C1/C2_M$ ratios <2000, but one sample had a much greater discrepancy and requires checking by repeat sampling and inter-laboratory analysis. This site has the highest and most variable $C1/C2_M$ ratio (BGS data) of all sites in our monitoring network (11,000–160,000, n=31).

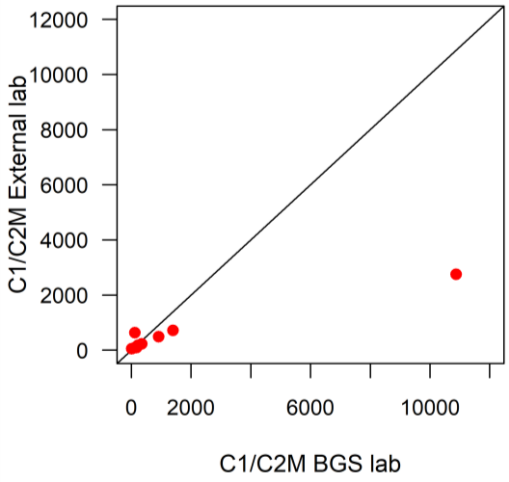


**Figure 4-14. C1/C2 (methane/ethane) ratios for groundwater samples from the BGS laboratory compared to the External laboratory.**

## 4.6 WATER MONITORING SOFTWARE FOR BASELINE EVALUATION

Ward et al. (2019) developed a statistical algorithm to compare post-baseline sets of measurements of a groundwater analyte with the available baseline data. The approach required a number of rounds of sampling to be conducted during the baseline period. In each round, the analyte would be measured at each borehole. The data were then used to quantify the degree of variation in the average of the measured values in each baseline sampling round. Similar rounds of sampling would then be conducted in the post-baseline (operational) period and the average values for each would be compared to the baseline period. The algorithm identified rounds of post-baseline sampling where the average of the measured values appeared to be inconsistent with the baseline period.

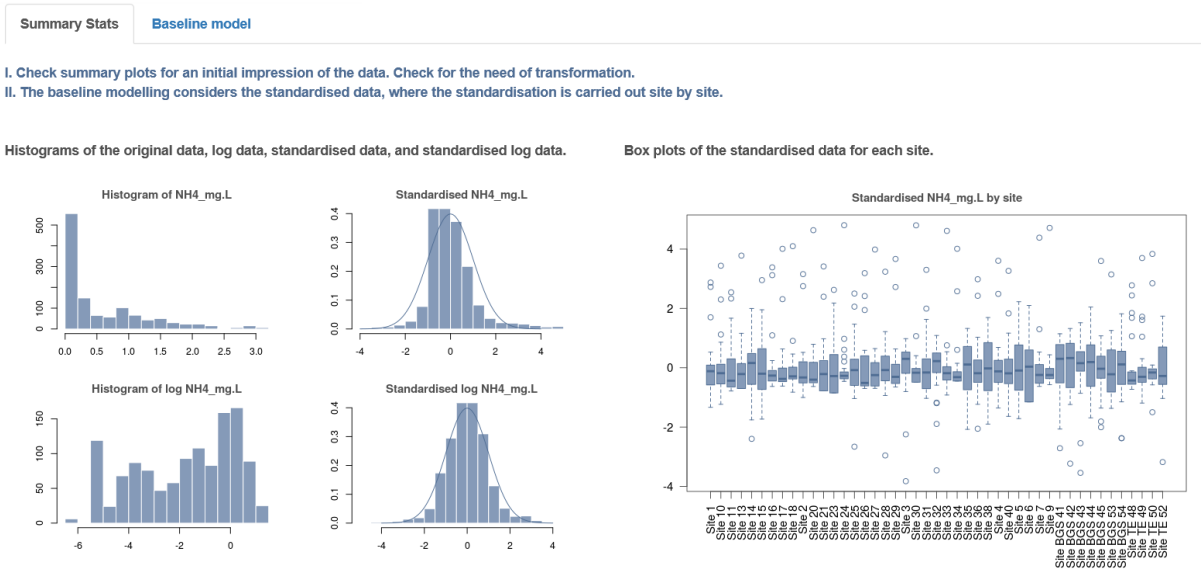


**Figure 4-15. Summary plots and statistics for baseline NH4 measurements from 45 locations produced in the R-Shiny app.**

The full details and a demonstration of the algorithm were provided previously (Ward et al., 2019). The measurements differed greatly from location to location so it was necessary to scale the measurements from each borehole by their mean and standard deviation. This scaling meant that any missing measurements from a round of sampling only had a small influence on the results.

Simulation tests demonstrated that based on available data from the monitoring of the Vale of Pickering, 30 rounds of baseline sampling would be required to assess the expected degree of variation in groundwater measurements.

A user-friendly version of the algorithm has been implemented in the R-Shiny programming language. This prototype app could be made available to end-users to install to a PC or from a website. The application reads in a .csv file of the groundwater chemistry measurements provided by the user. The user defines when the baseline period ended. The app can be used to plot summary statistics of the analyte (Figure 4-15) or to run the statistical algorithm described above (Figure 4-16). Additionally, the app can be used to consider each borehole individually and identify post-baseline measurements that are large relative to the baseline measurements (Figure 4-17). Descriptions of the various outputs are included in the app.

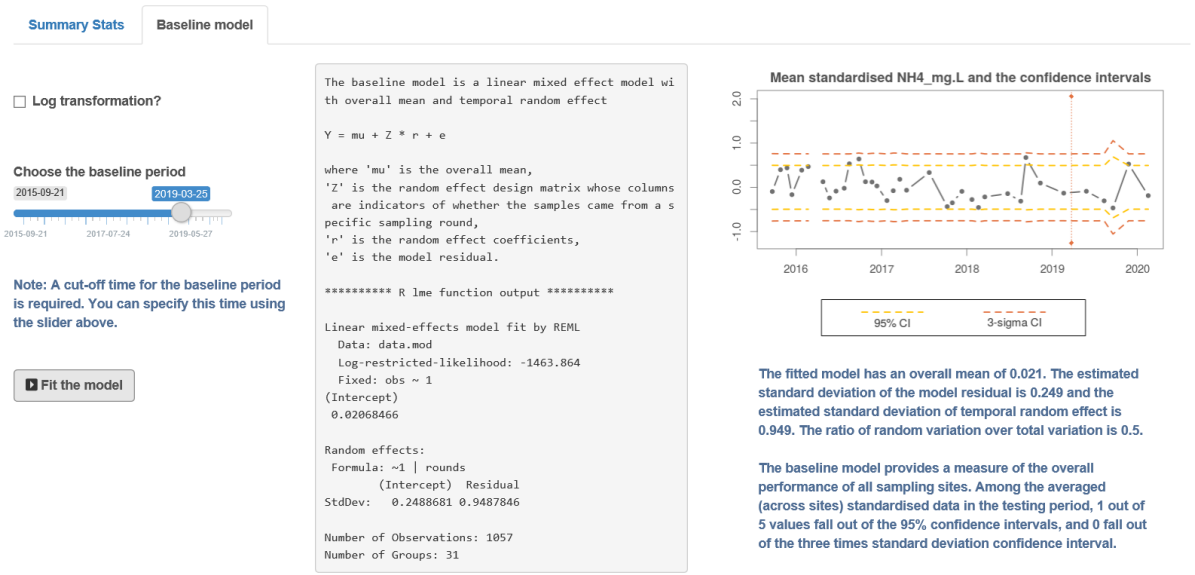


**Figure 4-16. Output from the statistical model run I the R-Shiny app. In the left hand panel the user defines the end of the baseline sampling period. Note that a notional date has been selected to demonstrate the app. The middle panel provides technical details.**

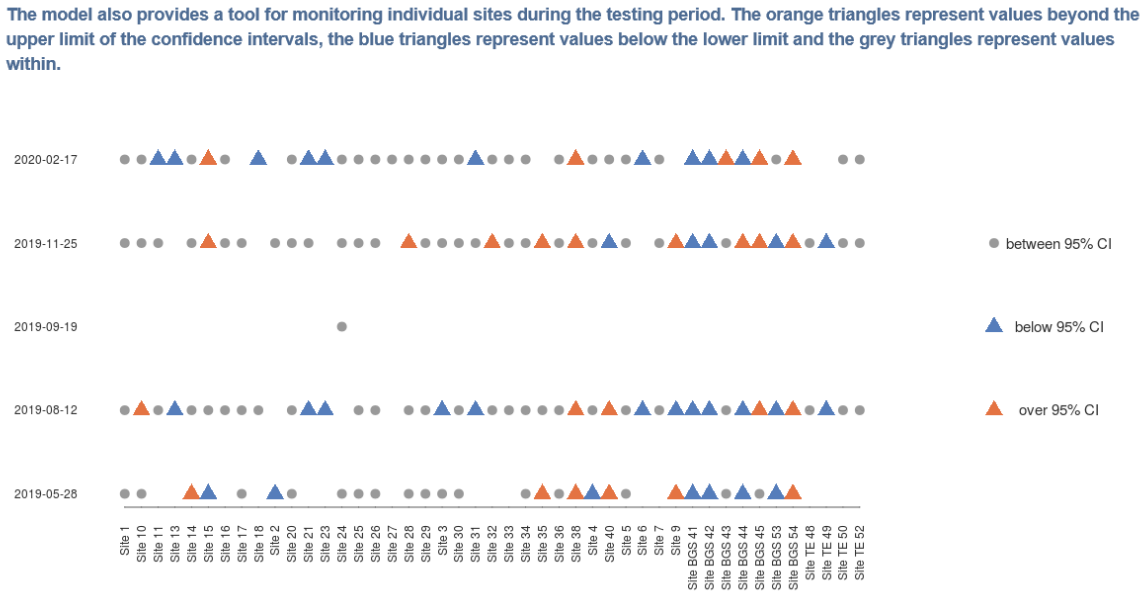


**Figure 4-17. Graphical summary of post-baseline measurements from the R-Shiny app. Orange triangles indicate measurements that are large relative to the baseline. Blue triangles indicate measurements that are small relative to the baseline**

## 4.7 SUMMARY

For the Vale of Pickering, the water-chemistry data from both collected samples and real-time monitoring highlight the large spatial and temporal variability in baseline compositions of groundwater and surface water and the large differences according to aquifer lithology, hydrogeology, landuse and anthropogenic activity. Earlier reports have also highlighted temporal variability in groundwater chemistry related to artefacts resulting from new borehole installations. The datasets produced and the assessments presented (Ward et al., 2019, 2018) have indicated the many issues involved in monitoring design for acquisition of a robust groundwater and surface-water baseline.

For Lancashire, collected monitoring samples and real-time monitoring also highlight the spatial and temporal variability in baseline compositions but monitoring here also covers periods of hydraulic fracturing. The data acquired do not show evidence for contamination of groundwater or surface water from shale-gas exploration, either during periods of hydraulic fracturing or subsequently.

In both Lancashire and the Vale of Pickering, the shallow (Superficial) aquifers closest to the proposed or actual shale-gas exploration sites are strongly influenced by reactions with aquifer minerals and, due to the prevalence of clay deposits and organic matter, are naturally reducing to strongly reducing. In Lancashire, concentrations of $CH_4$ are seen up to around 7 mg/L in a small number of boreholes but concentrations are otherwise low (µg/L range). In the Vale of Pickering, high concentrations of $CH_4$ (>10–80 mg/L) are a feature of some shallow groundwaters from the Superficial (Kimmeridge ± Quaternary) aquifer, and $C_2H_6$ is detected at some sites.

Observed discrepancies in $CH_4$ and $C_2H_6$ in Vale of Pickering analyses between two independent laboratories echo the discrepancies in data identified earlier (Ward et al., 2019) between different analytical laboratories. The discrepancies have implications for interpretation of processes and dissolved-gas provenance. Further work on sampling protocols and analysis of dissolved gases is necessary and will be carried in future investigations within ongoing BGS projects in order to explore this issue further.

## 4.8 REFERENCES

Darling, W.G., Milne, C.J., 1995. Quantitative analysis of dissolved gases: preparation and calculations. British Geological Survey Report (WD/95/10).

Ward, R.S., Smedley, P.L., Allen, G., Baptie, B.J., Cave, M.R., Daraktchieva, Z., Fisher, R., Hawthorn, D., Jones, D.G., Lewis, A., Lowry, D., Luckett, R., Marchant, B.P., Purvis, R.M., Wilde, S. 2018. *Environmental baseline monitoring: Phase III final report (2017-2018).* Nottingham, UK, British Geological Survey, 143pp. OR/18/026.

Ward, R.S., Smedley, P.L., Allen, G., Baptie, B.J., Barkwith, A.K.A.P., Bateson, L., Bell, R.A., Bowes, M., Coleman, M., Cremen, G., Daraktchieva, Z., Gong, M., Howarth, C.H., Fisher, R., Hawthorn, D., Jones, D.G., Jordan, C., Lanoiselle, M., Lewis, A.C., Lister, T.R., Lowry, D., Luckett, R., Mallin-Martin, D., Marchant, B.P., Miller, C.A., Milne, C.J., Novellino, A., Pitt, J., Purvis, R.M., Rivett, M.O., Shaw, J., Taylor-Curran, H., Wasikiewicz, J.M., Werner, M., Wilde, S. 2019. Environmental Monitoring – Phase 4 Final Report. OR/19/044.

# 5 Seismicity

## 5.1 INTRODUCTION

We have continued to operate the networks of seismometers installed to monitor background seismicity in the Vale of Pickering, Yorkshire, and The Fylde, Lancashire, throughout the reporting period. All but five of the twenty stations show levels of data completeness that are over 95%. There was no significant change in recorded noise levels at any of the stations during the reporting period and the networks remained capable of events with magnitudes of 0.5 ML or less. The monitoring networks successfully detected a number of small local seismic events at distances of 100 km away or greater. The proximity of many of the events in the Vale of Pickering to quarries where blasting is known to take place, along with recorded waveforms that are characteristic of a shallow source, suggests that all these events are quarry blasts. All the suspected blasts occurred during the daytime, which adds further evidence to an anthropogenic origin. The magnitudes of these events range from 1.0 ML to 2.0 ML.

We used the dense array of surface seismometers on the Fylde Peninsula to study the seismicity associated with hydraulic fracturing of the Carboniferous Bowland Shale at the Preston New Road (PNR) shale gas site in August 2019. We used a conventional energy transient algorithm to detect seismic events with magnitudes as low as -1.7 ML during operations and find that the magnitude of completeness, $M_c$, for events detected using only surface sensors is -0.5 ML. We use this value of $M_c$ to estimate a *b*-value of 1.0, similar to the *b*-value observed for seismicity during operations in 2018. The detected seismicity is strongly clustered at the start of operations, presumably closely associated with periods of injection, with only small numbers of events outside these times. However, after 21 August, we observe more scattered behaviour with a number of larger trailing events that occur outside the periods of operation (hydraulic fracturing) during the evening or night. The largest of these trailing events had a magnitude of 2.9 ML and occurred on 26 August at 07:30 UTC, almost 72 hours after a hydraulic fracture stage on 23 August. This is the largest fracking related earthquake recorded in the UK to date and we received over 2000 reports from members of the public who felt the earthquake. Around 200 reports stated that damage had been observed, mainly minor cracks in plaster,

We compared the catalogue of seismicity detected using only surface sensors during operations in October to December 2019 with the catalogue of over 38,000 events detected using a down-hole geophone array, allowing us to assess the suitability of surface arrays in high noise environments for the reliable characterisation of induced seismicity during operations. Event locations calculated using the surface data are generally comparable to those located using the downhole sensors but show considerably more scatter, making it harder to interpret the results in terms of possible fault reactivation. However, we find that the magnitude of completeness for events detected using only surface sensors in near real-time without template matching is close to the 0.0 ML amber light threshold, which highlights the problem of reliable characterisation of induced seismicity during operations using surface monitoring networks.

Processed event data (comprising automatically determined and manually revised event parameters) are available from our FTP site at ftp://seiswav.bgs.ac.uk/events/.

## 5.2 BACKGROUND

The primary aim of the seismicity work package was to deploy a network of seismic sensors to monitor background seismic activity in the vicinity of proposed shale gas exploration and production near Kirby Misperton, North Yorkshire and Blackpool, Lancashire. The data collected would then be used to allow reliable characterisation of baseline levels of natural seismic activity in the region. This will facilitate discrimination between any natural seismicity and induced seismicity related to shale gas exploration and production operations. A further aim was to make recommendations for a suitable traffic-light system to mitigate earthquake risk. The initial design

requirement for the seismic monitoring network was reliable detection and location of earthquakes with magnitudes of 0.5 and above within a 20 km by 20 km area around the Kirby Misperton site.

## 5.3 NETWORK PERFORMANCE

The seismic monitoring network around Kirby Misperton consists of seven near-surface sensors (red squares in Figure 5-1a) and four sensors installed in boreholes (orange squares in Figure 5-1(a)). The latter comprise of three down-hole geophones and a down-hole broadband seismometer. The borehole sensors are situated at a depth of approximately 30 m below the surface and are all close to the Kirby Misperton drill site. Installing instruments in boreholes is intended to improve the signal-to-noise ratio of the recorded data and allow smaller events to be detected and located.

The seismic monitoring network in The Fylde consists of eight near-surface sensors (red squares in squares in Figure 5-1a). We also receive real-time data from four stations installed and operated by Liverpool University (Figure 5-1b). The latter were installed independent of this project and data from these is not guaranteed. During periods of hydraulic fracturing we also received data from stations installed by Cuadrilla Resources Ltd. (Figure 5-1b) to meet regulatory requirements for mitigating the risk of induced seismicity. Data from all sites were used in the analysis below.

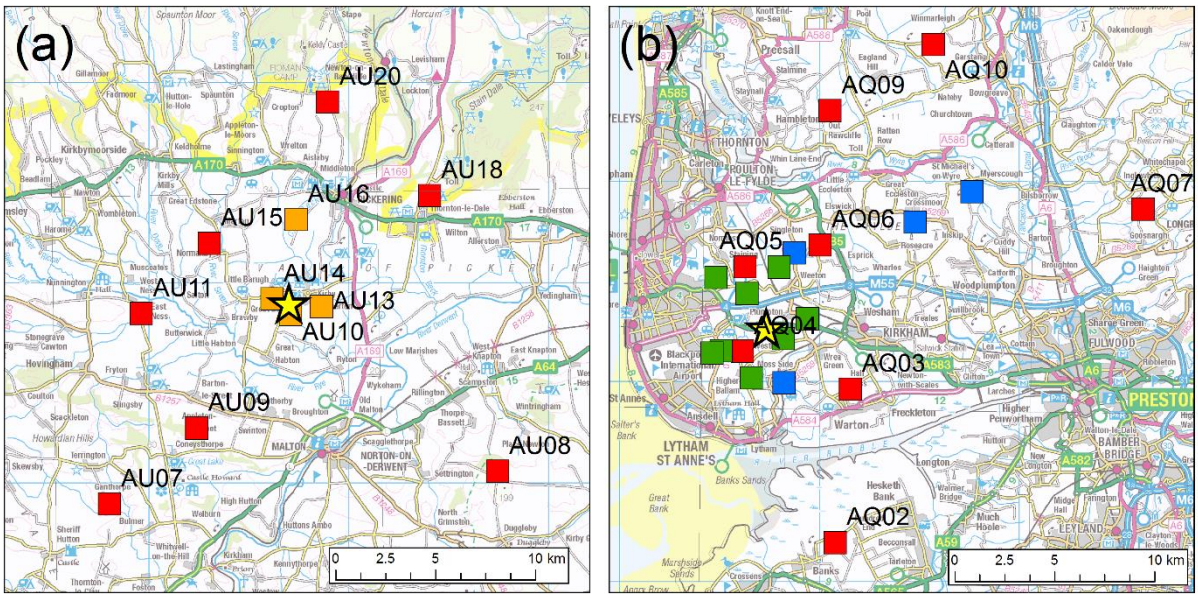


**Figure 5-1. Ordnance Survey maps of the Vale of Pickering (a) and of the Fylde peninsula (b). Red squares show the surface sensors and the orange squares in (a) show the locations of the borehole sensors. There are also surface sensors co-located with some of the borehole sensors. Green and blue squares in (b) show the locations of sensors installed by Cuadrilla Resource Ltd. and Liverpool University respectively. The yellow stars shows the locations of the Kirby Misperton and Preston New Road drill sites. Contains Ordnance Survey data © Crown Copyright and database rights 2020**

Continuous data from all stations are transmitted in near real-time to the BGS office in Edinburgh, where the data are processed and archived. The completeness of these data can be easily checked to gain an accurate picture of network performance. The completeness levels are shown in Figure 5-2. All stations in the Vale of Pickering except AU10 and AU16 show data completeness of greater than 95% for the time period 1/4/2019 to 31/03/2020. AU10 and AU16, which were 91% and 85% complete, respectively. Three stations in Lancashire had data completeness of less than 95%: AQ02 was 93% complete; AQ04 was 91% complete and AQ12 was 94% complete. This means that the detection capability of both networks was good over this time period and loss of data was minimal. The level of data completeness is similar to the values for previous years.

A value of over 95% is extremely good for data transmitted in near real-time using mobile phone networks and is better than many of the BGS permanent monitoring stations that use similar technology. Data losses result from failure of outstation hardware, communications problems, or failure of central data processing. The data acquisition is able to recover from short breaks in communications links to outstations by re-requesting missing packets of data from local data buffers, but failure of outstation hardware requires intervention by local operators or maintenance visits.

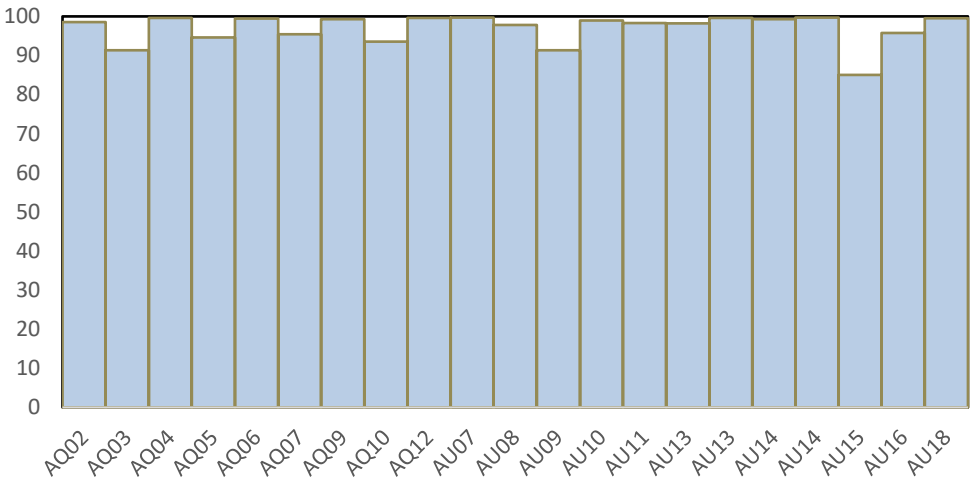


**Figure 5-2. Data completeness for the period 1/4/2019 to 31 /03/2020 for monitoring stations in the Vale of Pickering (AU07-AU20) and Blackpool (AQ02-AQ12).**

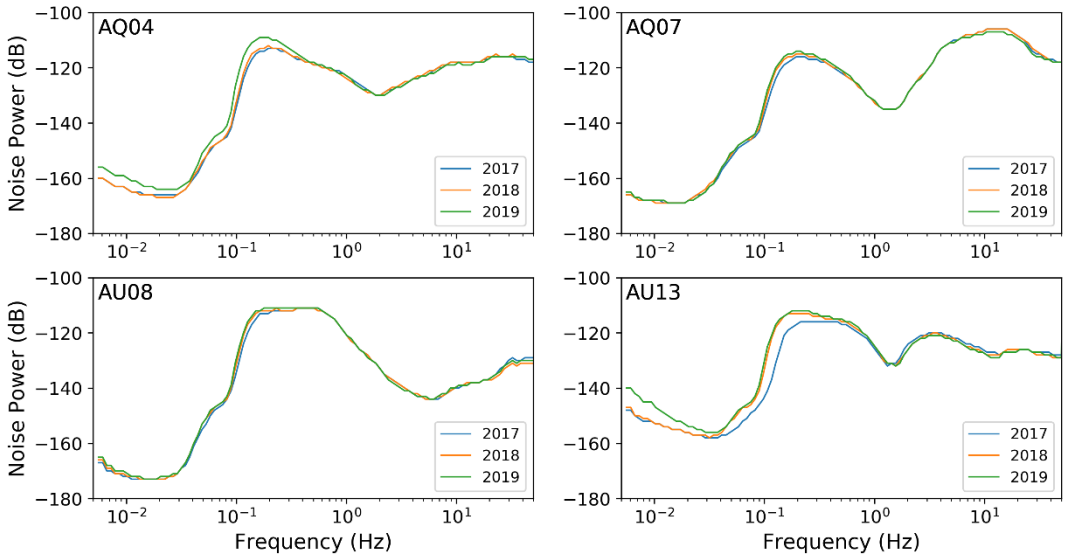


**Figure 5-3. Median noise levels as a function of frequency at four selected stations in the Vale of Pickering and Lancashire networks for 2017, 2018 and 2019. AQ04, AQ07 and AU08 are at the surface. AU13 is in a shallow borehole.**

## 5.4 STATION NOISE AND PERFORMANCE

We use power spectral density (PSD), calculated from one-hour segments of continuous data, to characterize noise levels at a range of frequencies at each of the installed stations. A statistical analysis of the PSDs yields probability density functions (PDFs) of the noise power for each of the frequency bands at each station and component. Figure 5-3 compares the median noise levels

calculated at two stations in the Vale of Pickering network (AU08 and AU13) and two stations in the Lancashire network and (AQ04 and AQ07) in the time periods, 1/1/2017 to 31/12/2017 (blue lines), 1/1/2018 to 31/12/2018 (orange lines) and 1/1/2019 to 31/12/2019 (green lines). Although there are clear differences in noise levels at different stations, the noise levels at each station do not change significantly in different time periods, demonstrating that there is no significant degradation in performance. This is also the case for the other stations in the network.

Comparing the median noise levels at the selected stations in the Vale of Pickering and Blackpool networks shows that the Blackpool stations are noisier than those in the Vale of Pickering and most other stations in the BGS permanent network. This is because the Fylde Peninsula is densely populated, with many sources of cultural noise.

## 5.5 DATA PROCESSING AND ANALYSIS

Continuous data from all installed stations are transmitted in real-time to the BGS offices in Edinburgh and have been incorporated in the data acquisition and processing work-flows used for the permanent UK network of real-time seismic stations operated by BGS. A simple detection algorithm is applied to the data from the Vale of Pickering and the Fylde peninsula, including data from permanent BGS monitoring stations in the region, to detect possible events (see https://earthquakes.bgs.ac.uk/data/home). An experienced analyst has reviewed all detections.

Figure 5-4 shows earthquake activity from the BGS earthquake catalogue in 100 km squares centred on the Kirby Misperton and Preston New Road sites. Yellow circles show earthquakes in the time period from 1/4/2019 to 31/03/2020. Apart from a magnitude 0.7 ML earthquake close to Kirby Misperton on 22 September 2015 at the very start of the monitoring project, no other earthquakes have been detected in the immediate locality of the Vale of Pickering, however, a number of other earthquakes from the surrounding region, along with quarry blasts have been detected.

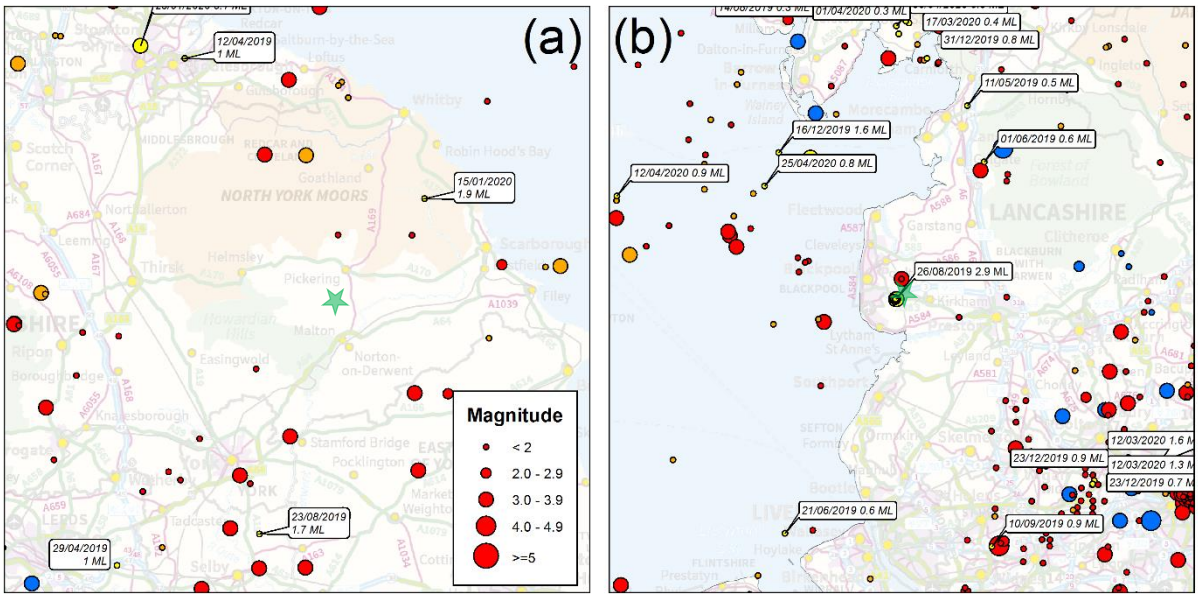


**Figure 5-4. Earthquake activity in 100 km squares centred on Kirby Misperton (a) and Preston New Road (b). Earthquakes in the time period from 1/4/2019 to 31/03/2020 are marked by yellow circles. Circles are scaled by magnitude. The locations of the shale gas wells are marked by green stars. Contains Ordnance Survey data © Crown Copyright and database rights 2020**

In the time period from 1/4/2019 to 31/03/2020, the closest earthquake to the network was a magnitude 1.9 ML earthquake near Fylingdales in North Yorkshire on 15 January 2020. The

epicentre was approximately 23 km northeast of Kirby Misperton. A magnitude 1.7 ML earthquake was detected near Ricall in North Yorkshire on 23 August 2019, approximately 52 km to the south. A magnitude 3.1 earthquake was detected near Stockon-on-Tees on 23 January 2020, approximately 48 km northwest. BGS received reports from over 800 people who felt the earthquake.

Apart from the seismicity associated with hydraulic fracturing operations at the Preston New Road shale gas site, a number of earthquakes were detected in The Fylde Peninsula region in the period from 1/1/2019 to 31/03/2020. The closest of these to the shale gas site was a magnitude 2.4 ML event in the Irish Sea on 11 July 2019, 28 km to the northwest and just south of Barrow-in-Furness. A smaller event with a magnitude of 0.6 ML was also detected in the Irish Sea, 45 km to the southwest. Onshore, a magnitude 0.9 ML earthquake was detected on 10 September near St Helens, 44 km to the southeast. Magnitude 0.5 ML and 0.6 ML events were detected near Halton, Lancashire on 11 May 2019 and near Ellel, Lancashire on 1 June 2019, approximately 35 km and 28 km northeast of Preston New Road site.

A number of other events were detected in the Vale of Pickering. The proximity of the calculated locations to quarries where blasting is known to take place, along with the recorded waveforms that are characteristic of a shallow source, suggests that all these events are of an explosive origin, i.e. quarry blasts. All of the suspected blasts occurred during the working week during the day, which provides further evidence of the man-made origin of these events, since we might expect natural seismicity to be more evenly distributed throughout the day. Twelve events were detected in the time period from 1/4/2019 to 31/03/2020 that were located just north of Pickering in close proximity to the Newbridge quarry, where a number of other quarry blasts have been detected in the past three years. The magnitudes of these events range from 1.0 ML to 1.6 ML. Five blasts were detected close to a quarry south of Malton. The magnitudes for these events ranged from 1.4 to 2.0 ML.

## 5.6 SEISMICITY INDUCED BY HYDRAULIC FRACTURING OPERATIONS AT PRESTON NEW ROAD, LANCASHIRE, 2019

Hydraulic fracturing operations in the PNR-2 well at Preston New Road, Lancashire, started on 15 August 2019. This well is offset by approximately 200 m from the PNR-1Z well that was hydraulically fractured in October and December 2018. We used the dense array of surface seismic stations installed by BGS for baseline monitoring as well as stations installed by the operator, Cuadrilla Resources Ltd, to determine locations and magnitudes for the detected microseismicity. We found that seismicity occurred during periods of injection for individual hydraulic fracturing stages, however, a number of larger "trailing" events were observed well outside the periods of operations. The largest of these had a magnitude of 2.9 ML and occurred on 26 August at 07:30 UTC, almost 72 hours after a hydraulic fracture stage on 23 August. This is the largest fracking related earthquake recorded in the UK to date. An event with a magnitude of 2.1 ML was recorded on 24 August at 22:01 UTC. Seismicity was observed to move from west to east corresponding to the west to east progression of hydraulic fracturing in the lateral well. The largest events occurred towards the east end of the horizontal well. The seismicity led to a premature end to operations in the PNR-2 well with only eight of the possible 47 hydraulic fracture stages completed. No further hydraulic fracturing took place during the reporting period and a moratorium is currently in place.

### 5.6.1 Event Detection and Location

Events were initially detected using the Carltrig STA/LTA (short-term average/long-term average) algorithm (Johnson et al., 1995). We used the NonLinLoc (NLLoc) non-linear earthquake location algorithm (Lomax et al., 2009) to calculate hypocenters for the detected events. This algorithm provides robust constraints on location uncertainties compared with traditional single-event location codes. A total of 125 microseismic events were detected in near real-time using the Carltrig STA/LTA algorithm. 17 of these had magnitudes greater than 0.0 ML, the amber TLS

(Traffic Light System) threshold, and 7 had magnitudes greater than the TLS limit of 0.5 ML. The largest event had a magnitude of 2.9 ML and was felt by at least 2000 people. The smallest event detected in near real-time had a magnitude of -1.7 ML.

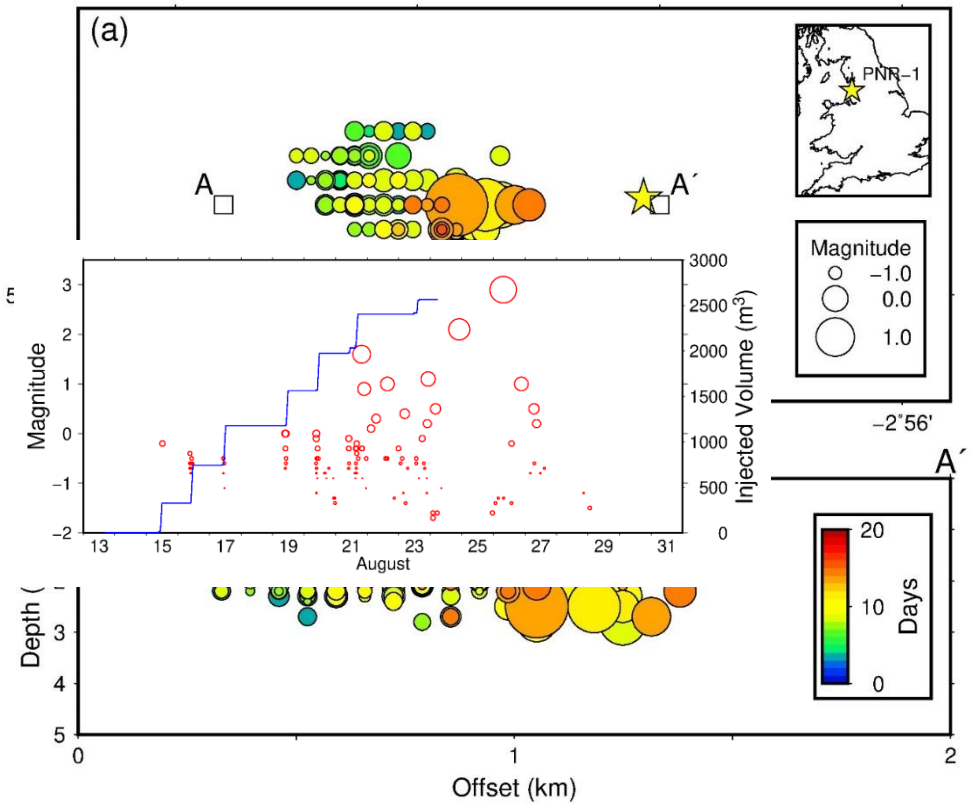


**Figure 5-5. (a) Map of events detected by the surface monitoring network during operations. Events are coloured by time and scaled by magnitude. The yellow star shows the surface position of the PNR-2 well. Map inset shows the location of the site. (b) Depth cross-section showing event depths along an east-west profile from A to A´.**

Locations for all detected events and calculated using NLLoc are shown in Figure 5-5. Events are coloured by time and move from west to east corresponding to the direction of hydraulic fracturing in the horizontal well PNR-2. Event depths are around 2 km, but increase slightly from around 2.0 km at the toe of the well to approximately 2.5 km closer to the heel. Horizontal errors varied from around 400 to 750 m, with events better constrained in latitude than longitude. Depth errors varied from 500 m to 1 km.

Figure 5-6 shows detected seismicity as a function of time during operations (red circles). No operational data was available at the time of writing. Operations started on 15 August 2019 and only seven of these stages were completed as operations were suspended following a magnitude of 2.9 ML earthquake on 26 August at 07:30 UTC, almost 72 hours after a hydraulic fracture stage on 23 August, and that was strongly felt locally at distances of up to a few kilometres from the epicenter. The events initially show quite strong clustering that is associated with periods of injection and there are relatively few events outside these periods, suggesting that activity decays rapidly with time after injection stops. However, after 21 August, we observe more scattered behavior with a number of larger trailing events outside of periods of operation during the evening or night. Some of these trailing events appear to have their own dependent events.

**Figure 5-6. Seismicity as a function of time during operations (red circles). Circles are scaled by magnitude (-1 to 2.9 ML). Blue line show cumulative volume of fluid injected during operations.**

### 5.6.2 **Activity rates and magnitude of completeness**

To assess the completeness of the catalogue we calculated magnitude of completeness, $M_c$, using the *b*-value stability method of Cao and Gao (2002). This model is based on the assumption that *b*−value estimates ascend for cut-off magnitudes less than $M_c$ and remains constant for cut-off magnitudes greater than or equal to $M_c$. This gives $M_c$ = -0.5± 0.2 ML, comparable to the magnitude of completeness for the surface catalogue collected during operations in October-December 2018. Errors were calculated using bootstrapping. We then calculate the *b*-value for the catalogue using maximum likelihood method of Aki (1965), finding a *b*-value of 1.000 ± 0.163, with an activity rate, *a*, of 1.172. Figure 5-7 shows the frequency magnitude distributions for both the events recorded in August 2019 (left) and events recorded in October-December 2018 (right), along with the calculated *b*-values and activity rates. The *b*-values from both data sets are comparable, though it is notable that the frequency magnitude distribution for 2019 has a much longer tail that contains the larger trailing events. This is not inconsistent with random sampling of an exponential distribution.

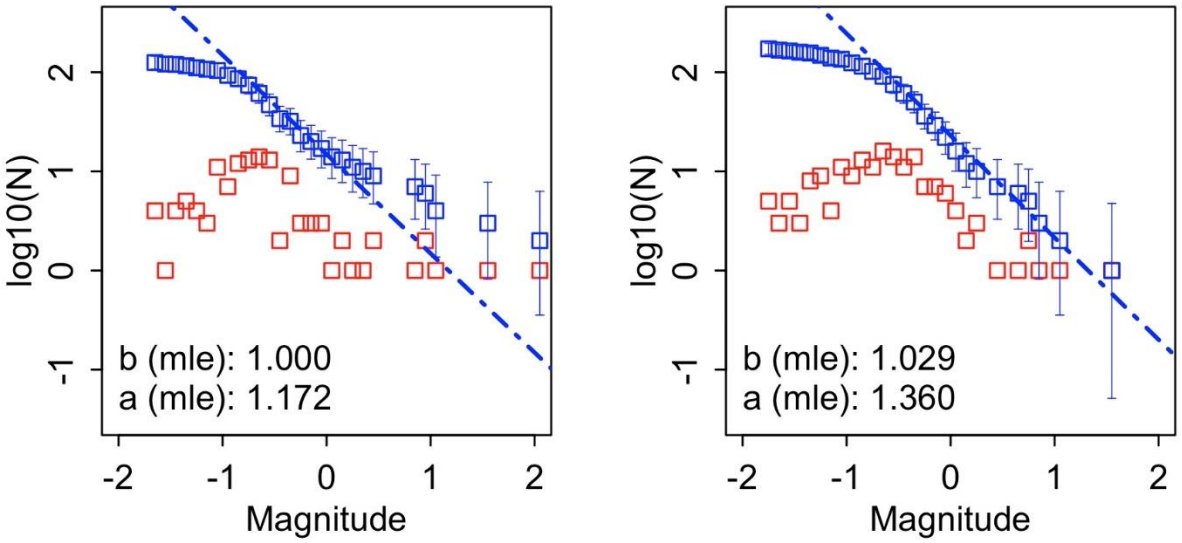


**Figure 5-7. Frequency magnitude distributions for events in 2019 (left) and events October-December 2018 (right). Red squares show incremental data and blue squares show incremental data. The blue dashed lines show the maximum likelihood estimate of the *b*-value and rate parameter.**

### 5.6.3 Intensity of ground shaking

Earthquake intensity is a qualitative measure of the strength of shaking of an earthquake determined from the observed effects on people, objects and buildings. A number of intensity scales have been developed including the Modified Mercalli (MM) scale and the European Macroseismic Scale (EMS). These consist of increasing degrees of intensity, each designated by Roman numerals or integers. For a given earthquake, intensity is normally greatest at the epicentre and decreases with distance from this point.

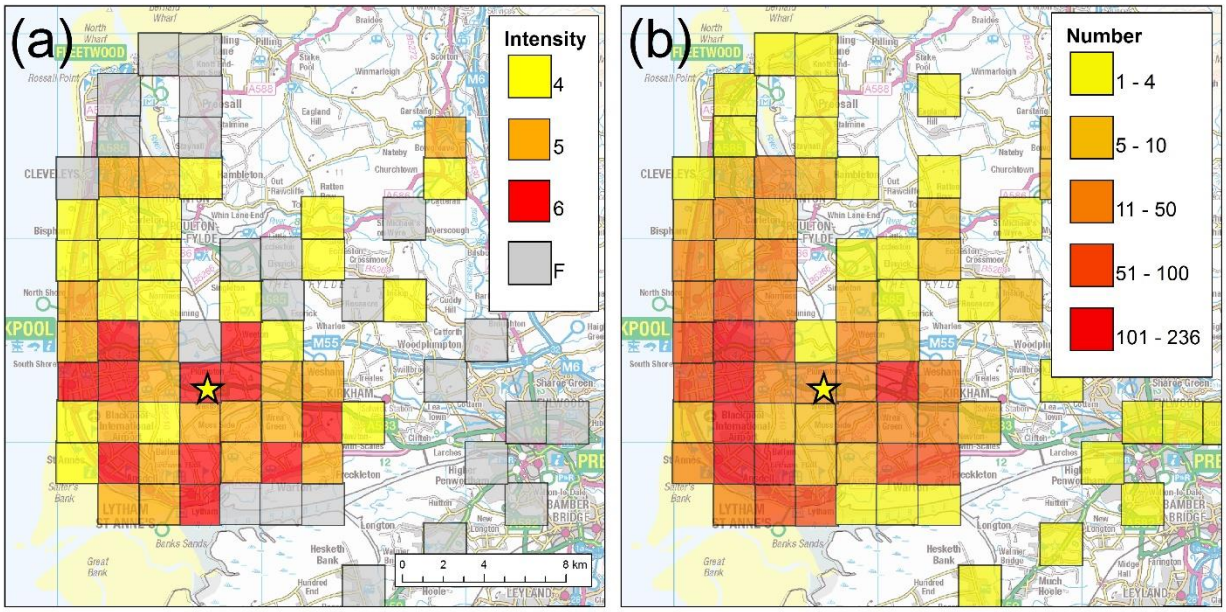


**Figure 5-8. Macroseismic intensities for the magnitude 2.9 ML earthquake at Preston New Road on 26 August 2019 (a). Intensities are calculated in 2 km grid squares from over 2000 reports from people who felt the earthquake. (b) shows the number of observations in each grid square. A minimum of five observations is needed in any grid square to calculate a value of intensity, otherwise the value is recorded as "Felt", but no intensity is calculated (grey squares). Contains Ordnance Survey data © Crown Copyright and database rights 2020**

We received over 2000 reports from members of the public who felt the magnitude 2.9 ML earthquake on 26 August and these data were used to determine macroseismic intensities at different locations in 2 km grid squares. The results are shown in Figure 5-8. The event was widely felt at distances of up to a few kilometres from the epicenter. Almost 200 reports stated that damage had been observed, mainly minor cracks in plaster, which resulted in intensities of 6 EMS in a number of locations. However, an intensity of 6 EMS or greater should not be taken as evidence that a given earthquake actually caused specific damage, as we have made no effort to validate individual reports of damage and these need to be checked by a suitably qualified person.

## 5.7 ASSESSING THE PERFORMANCE OF THE SURFACE SEISMIC MONITORING NETWORK AT PRESTON NEW ROAD

Hydraulic fracturing of the Carboniferous Bowland Shale was carried out at Preston New Road, Lancashire in October-December 2018. Operations in the PNR-1 well were accompanied by microseismicity (Clarke *et al*., 2019) that was recorded by both a dense network of surface sensors and by a downhole geophone array in the adjacent PNR-2 well. Baptie and Luckett (2019) used a combination of conventional, energy transient detection algorithms along with template matching to detect 169 events with magnitudes as low as -1.8 ML using only the data recorded on the surface sensors. The largest event had a magnitude of 1.6 ML. By contrast, over 38,000 microseismic

events were detected using the data from the downhole geophone array over the same period of time by Cuadrilla Resources geophysical processing contractor.

Locations for all events in both the surface and downhole catalogues are shown in Figure 5-9. Events are coloured by time and scaled by magnitude. The locations of the events in the downhole catalogue (Figure 5-9b) clearly move from west to east corresponding to different stages of

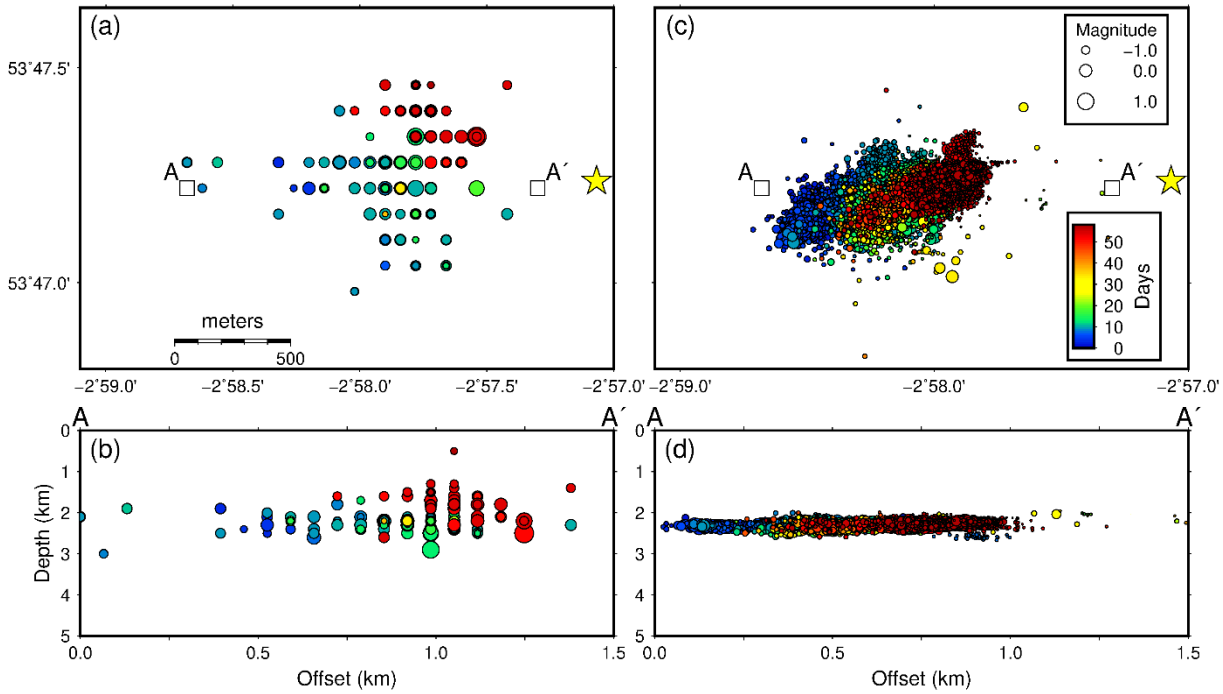


**Figure 5-9. Maps of event locations for the surface (a) and the downhole catalogues (c). Events are coloured by time and scaled by magnitude. (b) and (d) show depth cross sections for the surface and the downhole catalogues respectively.**

hydraulic fracturing in the horizontal well PNR-1z. The locations calculated using only the surface data (Figure 5-9a) are more scatted but also show the same sense of movement from west to east, although the locations appear to be shifted slightly to the east in comparison with the downhole locations. Event depths calculated using the downhole data are around 2280 m, but decrease slightly from around 2300 m at the toe of the well to approximately 2250 m closer to the heel. Event depths calculated using the surface data are again comparable but again show more scatter.

Horizontal errors for the surface locations varied from around 400 to 750 m, with events better constrained in latitude than longitude. Depth errors varied from 500 m to 1 km. Location uncertainties for the downhole data were not provided but typical location uncertainties for downhole microseismic data are around 10-20 m in depth and slightly larger uncertainties in horizontal location.

Figure 5-10 shows the frequency magnitude distributions calculated for the downhole (left) and surface catalogues (right), together with the maximum likelihood estimates of the b-values and activity rates. The observed roll-off in the magnitude-frequency relationship at low magnitudes leads to the concept of a completeness magnitude, $M_c$, which can be defined as the lowest magnitude at which (approximately) 100% of the earthquakes in a space-time volume are detected (Rydelek and Sacks, 1989). A correct estimate of $M_c$ is crucial since a value too high leads to under-sampling, by discarding usable data, while a value too low leads to erroneous seismicity parameter values and thus to a biased analysis, by using incomplete data.

We calculated a magnitude of completeness, $M_c$, for each catalogue using the b-value stability method of Cao and Gao (2002), which gives $M_c$ = -1.5 for the downhole catalogue and $M_c$ = -0.5 for the surface catalogue. Using only events detected in near real-time increases the magnitude of completeness of the surface catalogue to around 0.0 ML. We then calculate *b*-values for each catalogue using maximum likelihood method of Aki (1965). Using a completeness magnitudes of -1.0 gives a *b*-value of 1.207 and an activity rate of 1.904 for the downhole catalogue. The high *b*-value for the entire catalogue seems to agree with high b-values calculated for other examples of induced seismicity. We obtain a *b*-value of 1.029 and an activity rate of 1.360 for the surface catalogue.

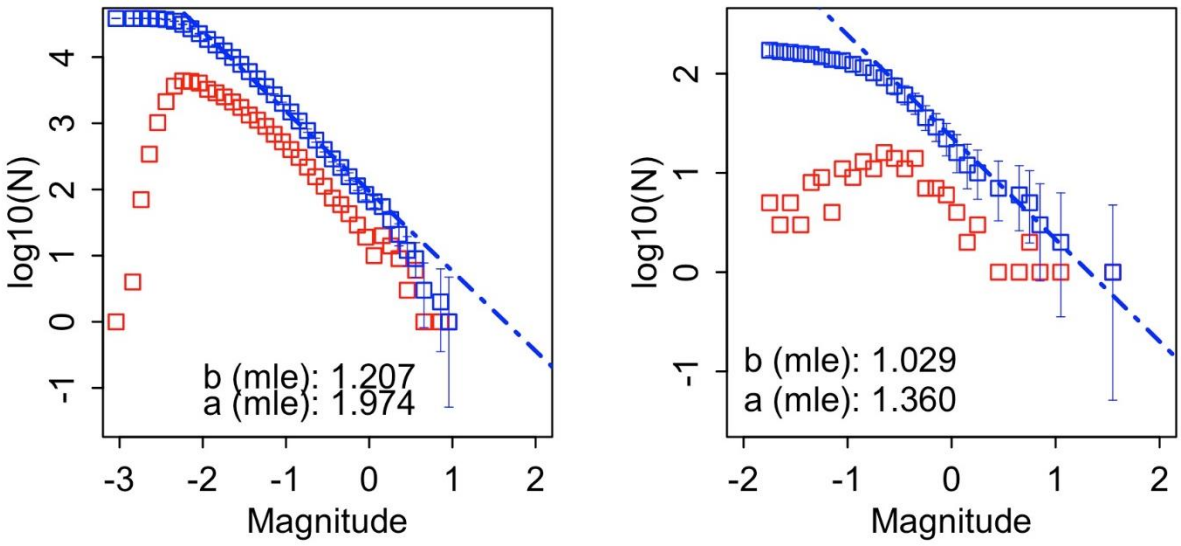


**Figure 5-10. Frequency magnitude distributions calculated for the downhole (left) and surface catalogues (right). Red and blue squares show incremental and cumulative data respectively. The blue dashed lines show the maximum likelihood estimates of the b-value and activity rate estimated using for completeness magnitudes of -1.0 and -0.5 for the downhole and surface catalogues respectively.**

A comparison of the events detected in near real-time using the energy transient algorithm and those detected using template matching shows that all events with a magnitude of 0.0 ML or above were detected in near real-time, although it is possible that events with completely different waveforms to the templates used may not have been detected.. Further evidence for the detection capability of the network is provided by the measurements of the magnitude of completeness, Mc, which suggests a value of at least 0.0 ML for the real-time catalogue. This value is reduced to -0.5 ML for the template matching catalogue.

## 5.8 DATA AVAILABILITY

Helicorder plots showing 24 hours of data from each station are available online and can be found on our web site and at http://www.earthquakes.bgs.ac.uk/research/BaselineMonitoring.html. The web pages also contain background information on the baseline monitoring project as well as educational material to explain the scientific context. Processed event data (automatically determined and manually revised event parameters) are also available from our FTP site at ftp://seiswav.bgs.ac.uk/events/. Continuous recordings of ground motions from all stations are stored in a public open-data archive. These data are available in the standard data format developed in the international seismological community for data exchange.

## 5.9 CONCLUSIONS

The networks of seismometers installed to monitor background seismicity in both the Vale of Pickering and the Blackpool areas have been successfully operated throughout the reporting period. All but five of the twenty stations show levels of data completeness that are over 95%. There was no significant change in recorded noise levels at any of the stations in the network.

The monitoring networks have successfully detected a number of small local seismic events at distances of 100 km away or greater. The proximity of many of the events in the Vale of Pickering to quarries where blasting is known to take place, along with recorded waveforms that are characteristic of a shallow source, suggest that all these events are quarry blasts. All the suspected blasts occurred during the daytime, which adds further evidence to an anthropogenic origin. The magnitudes of these events range from 1.0 ML to 2.0 ML.

We used a conventional, energy transient detection algorithm to detect seismic events with magnitudes as low as -1.7 ML during hydraulic fracturing operations at Preston New Road in August 2019 using only surface sensors. We find that the magnitude of completeness for the catalogue of events detected during operations is -0.5 ML and we use this value to estimate a *b*-value of 1.0 for this catalogue, similar to the *b*-value observed for seismicity during operations in 2018.

The detected seismicity is strongly clustered at the start of operations, presumably closely associated with periods of injection, with only small numbers of events outside these times. However, after 21 August, we observe more scattered behavior with a number of larger trailing events that occur outside the periods of operation during the evening or night. The largest of these trailing events had a magnitude of 2.9 ML and occurred on 26 August at 07:30 UTC, almost 72 hours after a hydraulic fracture stage on 23 August. This is the largest fracking-related earthquake recorded in the UK to date.

We compared the catalogue of seismicity detected using only surface sensors during operations in October to December 2019 with the catalogue of over 36,000 events detected using a down-hole geophone array, allowing us to assess the suitability of surface arrays in high noise environments for the reliable characterisation of induced seismicity during operations. Event locations calculated using the surface data are generally comparable to those located using the downhole sensors but show considerably more scatter, making it harder to interpret the results in terms of possible fault reactivation.

Finally, we find that the magnitude of completeness for events detected using only surface sensors in near real-time without template matching is close to the 0.0 ML amber light threshold, which further highlights the problem of reliable characterisation of induced seismicity during operations using surface monitoring networks.

## 5.10 REFERENCES

Aki, K. (1965), Maximum Likelihood Estimate of b in the Formula logN = a - bM and its confidence limits, Bulletin of the Earthquake Research Institute, 43: 237-239.

Baptie, B. and Luckett, R. (2019), Seismicity induced by hydraulic fracturing operations at Preston New Road, Lancashire, 2018, Proceedings of the Society for Earthquake and Civil Engineering Dynamics Conference 2019.

Cao, A.M. and Gao, S.S. (2002). Temporal variations of seismic b-values beneath northeastern japan island arc, Geophysical Research Letters, 29, doi:10.1029/2001GL013775.

Clarke, H., Verdon, J.P., Kettlety, T., Baird, A.F. and Kendall J.-M. (2019). Real-Time Imaging, Forecasting, and Management of Human-Induced Seismicity at Preston New Road, Lancashire, England, Seismological Research Letters, 90 (5): 1902–1915.

Johnson C., Bittenbinder A., Bogaert B., Dietz L. and Kohler, W. (1995), Earthworm: A Flexible Approach to Seismic Network Processing, IRIS Newsletter, 14(2): 1-4

Lomax A., Michelini A. and Curtis, A. (2009), Earthquake Location, Direct, Global-Search Methods, in Encyclopedia of Complexity and System Science, Part 5, Springer, New York, 2449-2473

Schaff, D.P. and Richards, P.G. (2004), Repeating seismic events in China, Science, 303: 1176–1178

Peterson, J. (1993), Observation and modelling of seismic background noise, U.S. Geological Survey Tech. Rept., 93-322, 1-95.

# 6 Ground Motion

## 6.1 INTRODUCTION

Responding to concern and speculation as to whether shale gas operations at depth could cause long-term surface ground deformation is a primary motive to include ground motion monitoring in this environmental monitoring programme. At public outreach events during the project, the authors have encountered genuine concern that induced seismicity may be accompanied by surface ground motion. Furthermore, we have received results from a community project that used drones to monitor land in the immediate vicinity of the Preston New Road (PNR) shale gas site. Their (unpublished) study concluded that the land moved 20 m horizontally and up to 5 m vertically due to hydraulic fracturing. Whilst there is no substantiated evidence for a change of this magnitude, it is important to investigate impartially whether the operations at PNR have altered the baseline of ground surface motion.

The Oil and Gas Authority (OGA) requires hydraulic fracturing operators to adhere to controls and protocols, including "to measure levels of ground motion close to nearby dwellings and other structures" to understand the risk of disturbance to people and damage to buildings and other vulnerable structures arising from induced seismicity. They also expect a "decision tree to describe what action would be taken in response to the detection of induced seismicity and measured ground motion" (OGA, 2018). This type of ground motion measurement is not the same as monitoring longer term ground deformation (subsidence/uplift). In this case satellite monitoring is an effective tool whereas the low frequency of measurement makes it generally unsuitable for measuring the short-term impacts of induced seismicity required by the OGA.

Conventional oil and gas operations have on rare occasions been shown to result in subsidence above compacting oil and gas reserves (Geertsma and Opstal, 1973) and a recent study suggests that surface uplift in eastern Texas was due to fluid injection, which was distinguished using satellite remote sensing (Shirzaei et al., 2016). These studies do not imply that shale gas operations at depth will cause ground motion, but recent research shows that Interferometric Synthetic Aperture Radar (InSAR) complements seismic data by providing insight into earthquake precursors from pre-seismic ground deformation (Moro et al., 2017).

The Final Report of the Phase 4 Environmental Monitoring Project (Ward et al., 2019) and a peer reviewed paper (Jordan et al., 2019) detailed the InSAR ground motion monitoring undertaken at PNR and the Vale of Pickering, North Yorkshire up to the end of March 2019. The ground motion analysis covered the pre-hydraulic fracturing baseline and the first phase of hydraulic fracturing and testing at PNR (well PNR-1z) from October 2018 to January 2019. This report describes the InSAR data that covers the period between January 2019 and January 2020 when another period of hydraulic fracturing operations took place at PNR (well PNR-2)

Two InSAR techniques were utilised to detect and monitor ground motion (i) RapidSAR (Spaans and Hooper, 2016) from SatSense Ltd and (ii) ISBAS (Sowter et al., 2013; Bateson et al., 2015) from Terra Motion Ltd. Interpretation of all the InSAR data was undertaken by BGS.

RapidSAR provides two results (i) 'RapidSAR urban' where the full Sentinel-1 resolution and point density is retained, and (ii) the lower resolution 'RapidSAR rural' where the detected motions are averaged for each cell in the radar image. The latter has the advantage that the effects of multiple weaker signals (which would not normally become a measurement point) are combined to create a signal that is sufficient to be a measurement point. The results are measurements within rural areas, which do not exist in the RapidSAR urban result. ISBAS provides more measurement points than RapidSAR rural over vegetated areas, but with a lower accuracy. Therefore, the combination of these multiple techniques can reduce or eliminate the inherent limitations of a single method, play a complementary role, and greatly improve the capability to detect ground displacements across different UK landcover types (Cigna and Sowter, 2017).

## 6.2 PHASE 5 INSAR DATA

Five InSAR datasets were analysed for the 2019 to 2020 time period (Table 6-1) encompassing a total of ~14.8 million measured points: over the PNR site. RapidSAR urban has a density of ~1,000 targets/km$^2$ (Figure 6-1a, c), RapidSAR rural has a density ~100 targets/km$^2$ (Figure 6-1b, d) and ISBAS has a density of ~2,000 targets/km$^2$ (Figure 6-1e).

**Table 6-1. Sentinel-1 image metadata analysed for Phase V at the PNR site. 'Asc' refers to the ascending geometry and 'Desc' refers to the descending geometry.**

| Satellite | Time period | No. of scenes in the stack | Processing mode | Processed by |
|---|---|---|---|---|
| Sentinel-1 (Asc) | 2019-2020 | 59 | RapidSAR -Urban | SatSense |
| Sentinel-1 (Asc) | 2019-2020 | 59 | RapidSAR -Rural | SatSense |
| Sentinel-1 (Desc) | 2019-2020 | 64 | RapidSAR - Urban | SatSense |
| Sentinel-1 (Desc) | 2019-2020 | 64 | RapidSAR -Rural | SatSense |
| Sentinel-1 (Asc) | 2019-2020 | 59 | ISBAS | Terra Motion |

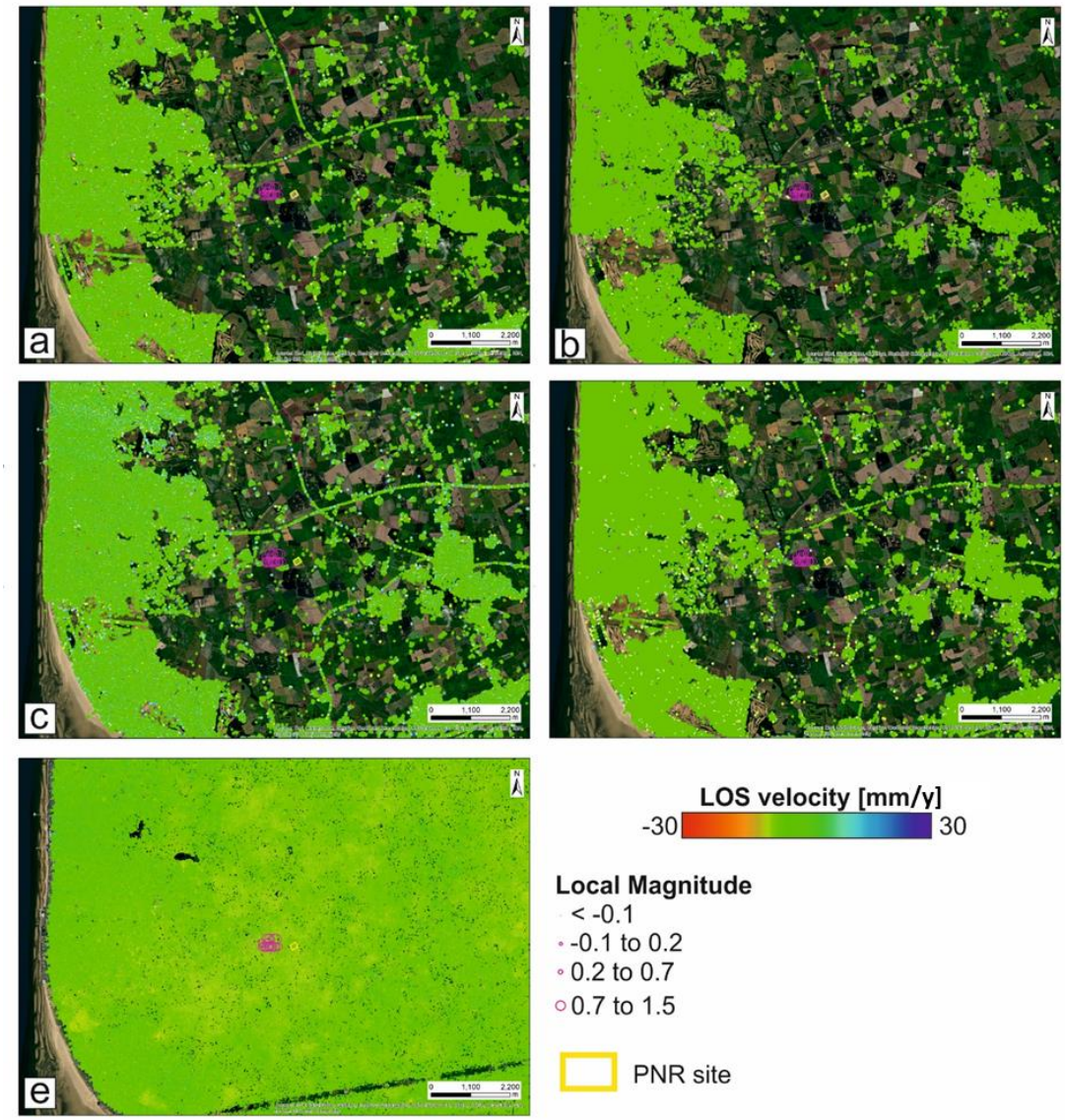


**Figure 6-1. Average Line of Sight (LOS) velocities for the PNR site: RapidSAR – Urban ascending (a), RapidSAR – Rural ascending (b), RapidSAR – Urban descending (c), RapidSAR – Rural descending (d) and ISBAS ascending (e). Positive values mean movement towards the satellite along the LOS, negative values mean movement away from the satellite along the LOS.**

### 6.2.1 **Lancashire Ground Motion Baseline**

During Phase 4 of the project (Ward et al, 2019) two temporal baselines were produced for Lancashire; one from 1992-2000 (Figure 6-2a) and the second from May 2015 to January 2019 (Figure 6-2b). The Phase IV InSAR data also included InSAR results for the period from October 2018 to January 2019 when hydraulic fracturing started at PNR. Phase V InSAR data extends this analysis and covers the period January 2019 to January 2020.

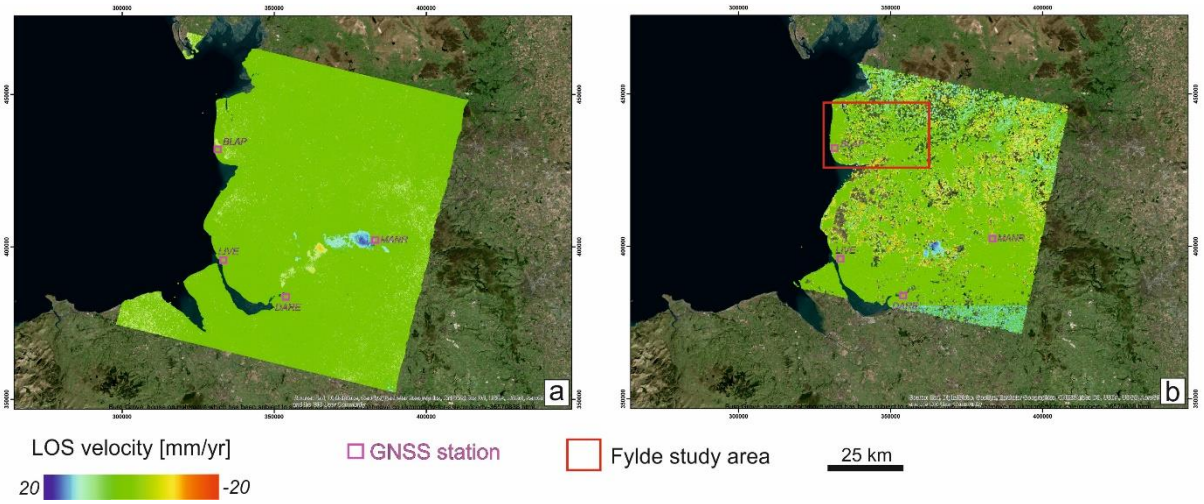


**Figure 6-2. ISBAS ERS average annual velocities for 1992–2000 copyright BGS © UKRI (a). SatSense RapidSAR Rural Sentinel-1 descending average velocity for 2015–2019 (b). Red box indicates Fylde study area (see Figure 6). Background imagery: ESRI - World Imagery basemap. Modified from Jordan et al. (2019).**

The Lancashire data show a range of ground motions including a discrete area of uplift northwest of Salford due to the rise in groundwater levels following cessation of water pumping in abandoned coalmines (Cigna and Sowter, 2017). There is also an area of subsidence in the Bickershaw-Goldborne-Leigh region, likely due to mining activity in the Bickershaw-Goldborne-Leigh collieries including water abstraction (Arrick et al., 1995). This subsidence, which resulted in the formation of the Pennington Flash is discussed in detail in Ward et al. (2018). Two areas of subsidence in The Fylde area (south of Blackpool) correspond to 'peat and blown sand' on the published geological maps. Boreholes from the area indicate the presence of 'sand and peat' at the top of the stratigraphy, suggesting that the subsidence is most likely caused by the existence of compressible ground.

Sentinel-1 data for the 2015-2019 period reveal similar patterns of baseline motion to the 1990's data. However the discrete area of uplift at the Pennington Flash was subsiding in the 1990's. Similar patterns of ground motion (subsidence following by uplift) are commonly observed over areas of coal mining in the UK (e.g. the Durham coalfield, Gee at al., 2017) and elsewhere in Europe (Przyłucka et al., 2015). They represent the transition from subsidence linked to active groundwater pumping, to surface uplift that is related to the influx of groundwater and an increase in pore pressure after pumping ceases when coal mines are abandoned.

A closer examination of the PNR area for the full time span of 2015 to 2020 (see Figure 6-2) indicates that this area is stable; the average annual velocities in the region of the PNR site for the Sentinel-1 data indicate that the area has remained largely stable since 2015.

## 6.3 GROUND MOTIONS DURING THE PERIOD OF HYDRAULIC FRACTURING

### 6.3.1 Hydraulic Fracturing Activity

Two periods of hydraulic fracturing have occurred at PNR:

1. Well PNR-1z: 15th October 2018 – 17th December 2018
2. Well PNR-2: 15th August 2019 – 21st August 2019

| Day | Date | Stage | Fluid ($m^3$) | Proppant (tonnes) | TLS Seismicity | | Comments |
|---|---|---|---|---|---|---|---|
| | | | | | During | Trailing | |
| Tuesday | 15-Oct | 1 | 2 | 0 | | | mini-frac |
| Tuesday | 16-Oct | 1 | 162 | 0 | | | mini-frac and main-frac |
| Wednesday | 17-Oct | 2 | 317 | 22 | | | mini-frac and main-frac |
| Thursday | 18-Oct | 3 | 394 | 51 | | | mini-frac and main-frac |
| Friday | 19-Oct | 12 | 34 | 0 | 0.3 ML | | mini-frac cut short |
| Saturday | 20-Oct | 12 | 222 | 7 | | | main-frac cut short due to downhole data delay |
| Sunday | 21-Oct | | 0 | | | | |
| Monday | 22-Oct | 13 | 385 | 37 | | | mini-frac then main-frac cut short operational issue |
| Tuesday | 23-Oct | 14 | 129 | 2 | 0.4 ML | | mini-frac, then main-frac cut short amber |
| Wednesday | 24-Oct | 18 | 11 | 0 | | 0.48 ML | main-frac cut after minifrac due to trailing amber 0.48 |
| Thursday | 25-Oct | 22 | 351 | 17 | 0.37 ML | | main-frac cut short after amber pumping |
| Friday | 26-Oct | 30 | 142 | 4 | 0.76 ML | | continued after 0.26 amber, but cut short after red |
| Saturday | 27-Oct | 31 | 112 | 2 | | 0.78 ML | cut short due to downhole data delay, before trailing |
| Sunday | 28-Oct | | 0 | 0 | | | |
| Monday | 29-Oct | 32 | 119 | 5 | 1.0 ML | | mini-frac, then main-frac cut short after red |
| Tuesday | 30-Oct | 41, 39 | 31 | 0 | | | two mini-fracs only |
| Wednesday | 31-Oct | 37, 40 | 26 | 0 | | | two mini-fracs only |
| Thursday | 01-Nov | | 0 | 0 | | | flowed back, no injection |
| Friday | 02-Nov | 35, 38 | 29 | 0 | | | two mini-fracs only |
| Saturday | 03-Nov | | 0 | 0 | | | |
| Sunday | 04-Nov | | 0 | 0 | | 0.66 ML | |
| Monday | 05-Nov | | 0 | 0 | | | flowed back, no injection |
| ------ FLOWED BACK; HIATUS IN OPERATIONS ------ | | | | | | | |
| Friday | 07-Dec | | 0 | 0 | | | flowed back, no injection |
| Saturday | 08-Dec | 37 | 78 | 4 | | | main-frac |
| Sunday | 09-Dec | | 0 | 0 | | | |
| Monday | 10-Dec | 37 | 107 | 3 | | | main-frac |
| Tuesday | 11-Dec | 38 | 268 | 28 | | 1.5 ML | main-frac, 0.1 and 0.0 amber trailing |
| Wednesday | 12-Dec | | 0 | 0 | | | |
| Thursday | 13-Dec | 39 | 261 | 27 | | | main-frac |
| Friday | 14-Dec | 40 | 251 | 20 | 0.86 ML | | main-frac cut short after 0.1 amber, 0.86 red |
| Saturday | 15-Dec | 41 | 18 | 0 | | | mini-frac |
| Sunday | 16-Dec | | 0 | 0 | | | |
| Monday | 17-Dec | 41 | 431 | 50 | | | main-frac |
| | TOTALS | | 3877 | 278 | | | |

**Table 6-2. Summary of hydraulically fractured stages and Traffic Light Events recorded during 2018 operations on Preston New Road well PNR-1z (OGA 2019).**

Hydraulic fracturing of the PNR-1z well at the PMR site started in October 2018 and was completed by mid-December (Environment Agency, 2019) and Table 6-2. Flow testing of the well occurred during January 2019.

Hydraulic fracturing of the PNR-2 well commenced on the 15th August 2019. On the 21st August, three trailing red light events (1.55 ML, 0.87 ML, 1.0 ML) were detected, and operations were paused for a total period of 48 hours. Hydraulic fracturing resumed on 23rd August, and a series of

trailing red traffic light events (1.1 ML, 0.5 ML, 2.1 ML, 2.9 ML, 0.5 ML) were detected over the following five days, during which all operations were suspended. The largest event occurred on 26th August at 08.30 BST, and was recorded as a magnitude 2.9 ML event. Ground velocities from the event were measured between 5 to 8 mm/second, and it was widely felt across the region, with reports to regulators and the operator of potential superficial damage to buildings (see Section 5). This event is believed to be the largest recorded induced seismic event from hydraulic fracturing in the United Kingdom. Operations were suspended from Friday 23rd August 2019, and on 2nd September 2019 the OGA announced that hydraulic fracturing would remain suspended whilst investigations were conducted into these events (OGA, 2019).

### 6.3.2 InSAR ground motions

The InSAR time series for points at or near to the PNR site were examined in detail to establish if hydraulic fracturing activities produced detectable ground motion. In particular, the Sentinel-1 time-series motion patterns for the period October 2018 – February 2019 and January 2019 – January 2020 were compared to the Sentinel-1 time-series baseline of May 2015 – September 2018.

Although the average annual velocities in the region of the PNR site for the ISBAS Sentinel-1 data indicate that it is stable over the 2015-2019 period, variations are evident in the ISBAS time series, acquired from an average of the InSAR points directly over the site (Figure 6-3). The variations represent natural fluctuations and measurement noise, which are part of the baseline for this area. Therefore, any motion caused by the hydraulic fracturing would need to either exceed this variation or represent a change in the established style of the baseline variation for it to be attributed to shale gas activities. For the PNR site, the baseline variation observed in phase IV (orange line, Figure 6-3) in motion is approximately 15 mm, whilst the standard deviation is 5 mm (Figure 6-3). During the hydraulic fracturing operations, the variation from the baseline mean is approximately 10 mm, which is greater than one standard deviation (4 mm for this collection of points) but still within the baseline variation observed in the baseline period; the pattern of ground motions have therefore not changed during the hydraulic fracturing.

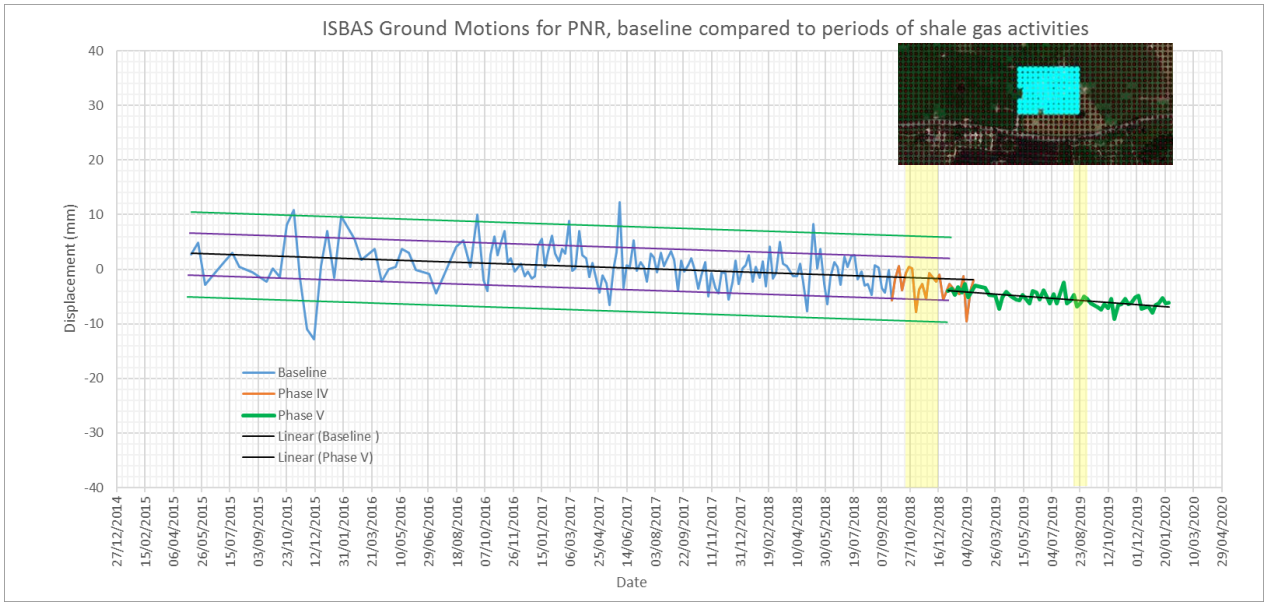


**Figure 6-3. ISBAS time series for the average of the measurement points over the PNR site (as indicated in inset). The time series for the pre-fracturing baseline (blue line) and the continuation for the phase IV period of interest (orange) are shown, along with the time series for the phase V period of activity (green). The black trendline shows the average motion whilst the green trendlines mark the maximum and minimum deviations from the mean, the purple trendlines indicate one standard deviation from the average trend line. Yellow highlights the periods of hydraulic fracturing.**

The green time series in Figure 6-3, covering 2019 and the start of 2020, represents the Phase V project period. Two observations are notable here; one is that the variability within the green time series is much smaller than the variability in the baseline. This is a result of the continued refinement of the processing algorithms and/or different filtering applied to the results. The other notable observation is that the Phase V time series does not show any significant differences to the ground motion characteristics observed in the baseline or phase IV motions.

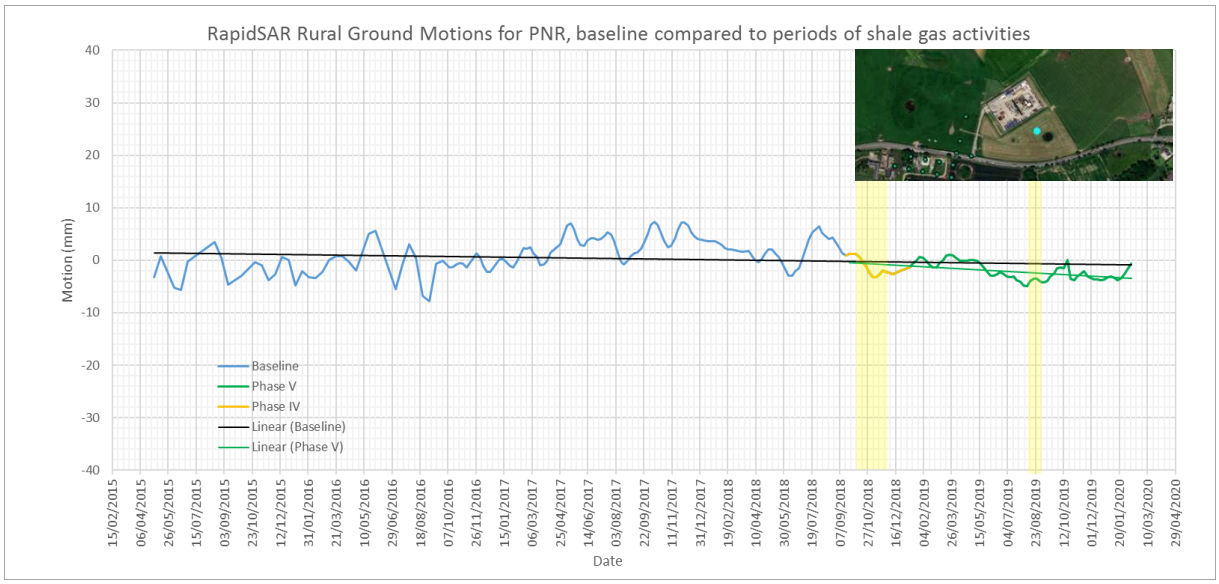


**Figure 6-4. RapidSAR Rural time series for a selected point over the PNR site. Blue – baseline time series, orange – phase IV time series (active hydraulic fracturing), green – phase V time series (active hydraulic fracturing). The black line is the linear trend line for the baseline and phase V, the green line is the linear trend for the period of hydraulic fracturing. Inset shows location of points selected over PNR site. Yellow highlights the periods of hydraulic fracturing.**

RapidSAR results (Figure 6-4) are in line with the ISBAS results and also indicate that over the last five years the PNR site has remained stable, with average displacement rates of less than 0.5 mm/yr. Furthermore, the periods of active shale gas activities (indicated in orange and green) do not show a marked change from the baseline period (blue). The average linear rate of motion for the entire time period (black line) and the linear rate of motions for the period when shale gas activities were occurring (straight green line) are plotted on each time series graph. There appears to be a slight increase in the linear rate of motion during the period of activity, however there are other periods within the time series when similar rates can be observed. Without a longer time series, it is difficult to conclude if this increase in rate is significant.

Periods of hydraulic fracturing (yellow stripes in Figure 6-3 and Figure 6-4) do not exhibit ground motions that are significantly different to other periods of the established baseline.

## 6.4 SEISMIC ACTIVITY AND GROUND MOTION

According to the BGS earthquake database[4], around 180 seismic events between October 2018 and September 2019 have been detected in a radius of ~1.5 km from the site along the horizontal length of the PNR-1z well.. This was during hydraulic fracturing operations at Preston New Road in 2018 and 2019, (Figure 6-5).

[4] http://www.earthquakes.bgs.ac.uk/earthquakes/dataSearch.html

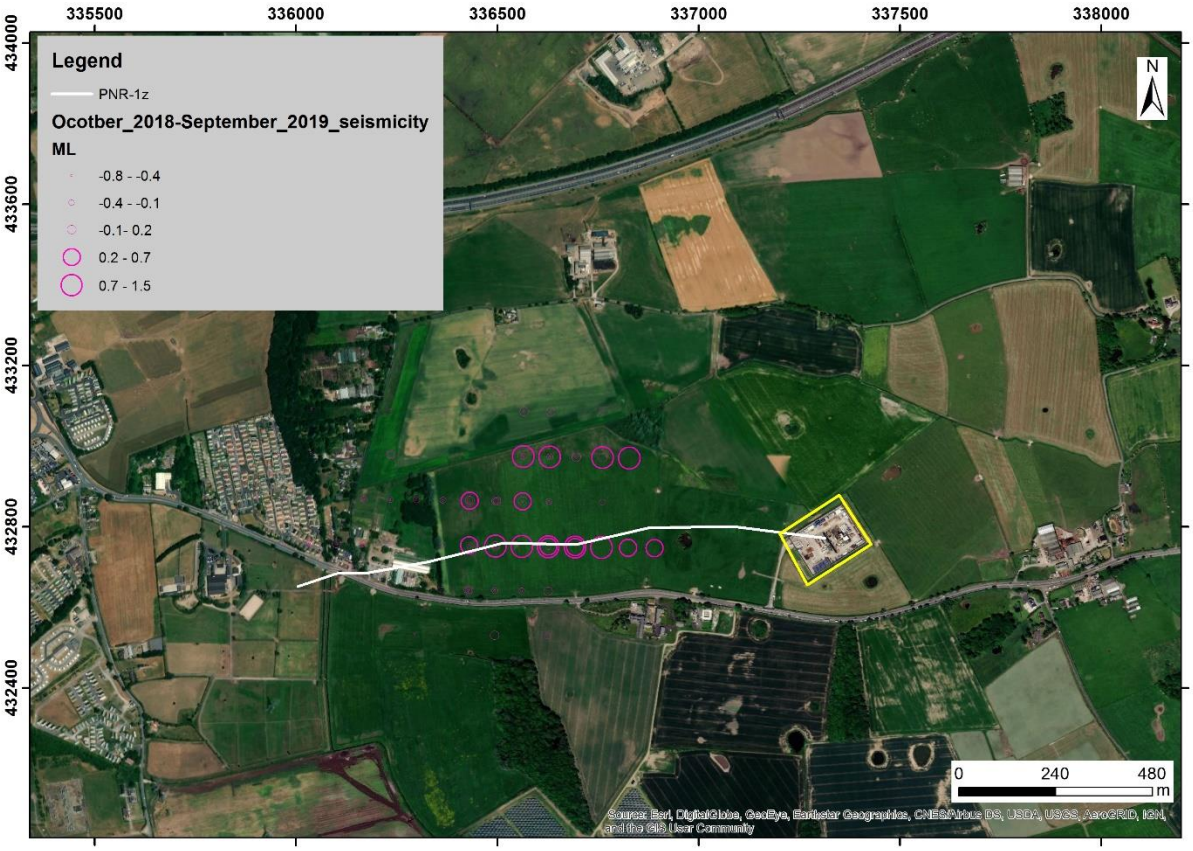


**Figure 6-5. PNR site location (yellow rectangle) with epicentres of the seismic events that occurred between October 2018 and September 2019. Preston New Road-1z lateral extension from Cuadrilla (2018). Coordinate system: British National Grid. Data: Google DigitalGlobe**

### 6.4.1 Analysis of InSAR points closest to seismic events

During Phase IV, the largest seismic event took place 11th on December 2018 with a magnitude of 1.5 ML at a depth of 1.6 km. The second largest event, 1.1 ML, took place on 29th of October 2018 at a depth of 2.9 km. Both of these events occurred at approximately the same location (largest purple circle on Figure 6-6). The largest seismic events occur under arable fields; the closest RapidSAR points are approximately 500 m to the south (green square on Figure 6-6).

The RapidSAR time series show no evidence of a change in ground motion at the time of the seismic activity compared to the preceding period. Figure 6-7 shows the time series for the pre hydraulic fracturing baseline (blue line) and the period when hydraulic fracturing took place (orange line). The black trend line shows the average motion whilst the green lines mark the maximum and minimum deviations from the mean. The yellow areas mark the dates of the strongest seismic event that took place in Phase IV and Phase V. InSAR continues to detect ground motion during the hydraulic fracturing period, and at the time of the seismic events, but the motion is no larger than the variation observed during the baseline period, and the trend of the average motion (i.e. slight subsidence) is relatively unchanged (Figure 6-7).

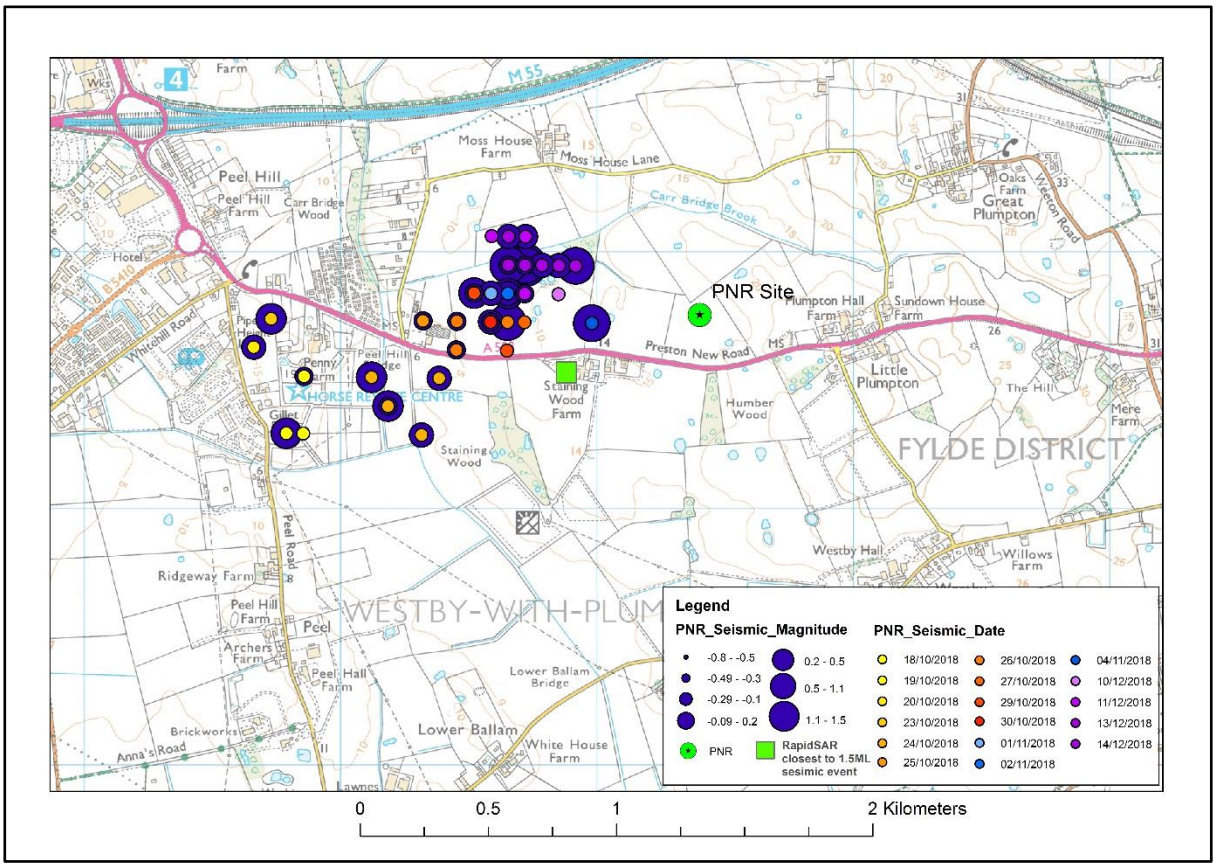


**Figure 6-6. PNR site showing location, date and magnitude of seismic events and location of the InSAR time series shown in Figure 6-7. Contains Ordnance Survey data © Crown Copyright and database rights 2020. Seismic data © BEIS.**

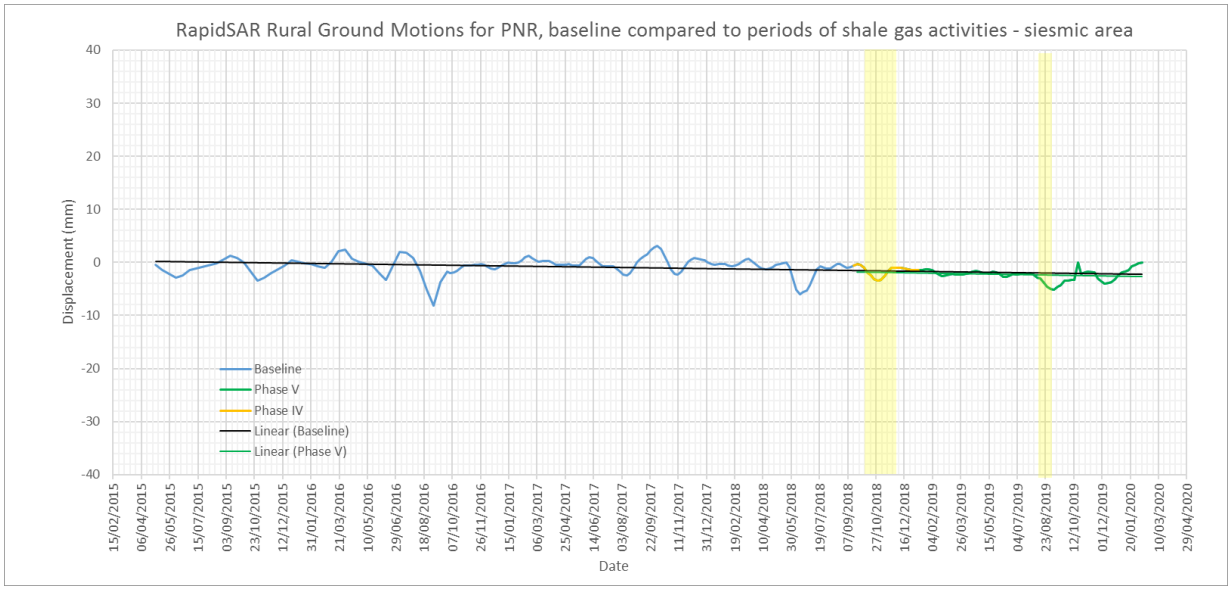


**Figure 6-7. Filtered InSAR time series for RapidSAR Sentinel-1 point closest to the largest magnitude earthquake on Figure 6-6. Yellow highlights on graph indicate dates of seismicity.**

During Phase V several seismic events took place as the PNR-2 well was fractured; on the 21st August, three events (1.55 ML, 0.87 ML, 1.0 ML) were detected. Between the 23rd and 28th August, a series of seismic events (1.1 ML, 0.5 ML, 2.1 ML, 2.9 ML, 0.5 ML) were detected. The

largest event occurred on 26th August at 08.30 BST, and was recorded as a magnitude 2.9 ML event.

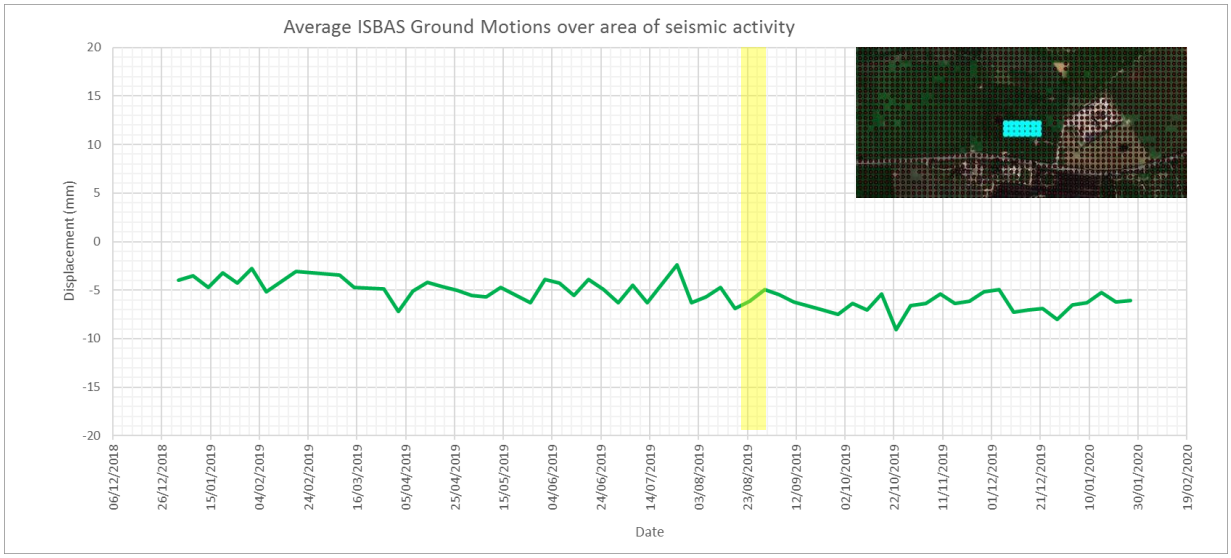


**Figure 6-8. Average ISBAS Sentinel-1 time series for area of greatest seismicity. Vertical yellow area on graph indicates date of seismicity. Inset shows location of ISBAS points used.**

Plotting the average ISBAS time series for a selection of points directly above the area with the highest magnitude seismic events, as shown on Figure 6-5, reveals no change in ground motion behaviour during late August 2019, the period when the highest magnitude seismic event took place (Figure 6-8).

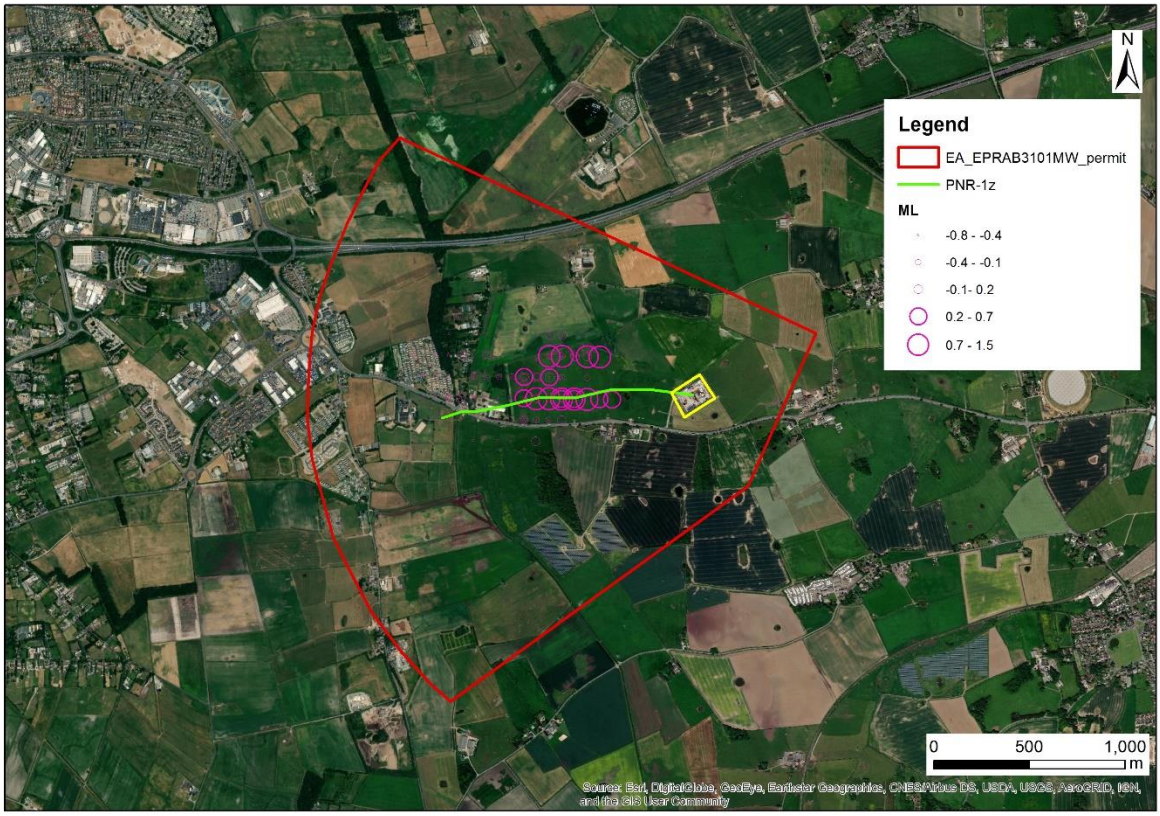


**Figure 6-9. Red line area associated with Environmenta Permit EPRAB3101MW, location of the PNR-1z well and epicentres of seismic events occurred between October 2018 and September 2019. Data: Google DigitalGlobe**

### 6.4.2 **Analysis of local InSAR response**

To understand if there was a regional ground motion response to the seismic events the displacements for all the InSAR points within the permit area were examined (Figure 6-9).

The time series-analysis has considered the targets within the red line boundary associated to Environmental Permit EPRAB3101MW (Environment Agency, 2019b) for the PNR site. This is underlain by the two shale gas wells and is where most of the Cuadrilla seismometers arrays are concentrated, and where the October 2018 and September 2019 seismic events occurred (Figure 6-9).

The permit area covers ~4.7 km$^2$ within this area sit the following InSAR observations :

- 1,646 points for RapidSAR urban ascending
- 160 points for RapidSAR rural ascending
- 2,385 points for RapidSAR urban descending
- 249 points for RapidSAR rural descending
- 11,583 points for ISBAS ascending

For each dataset the points and their time series were extracted from the database and an average time series derived for the permit area. The interquantile range (IQR) for each of the time series was examined to identify and remove outliers. Outliers are defined as observations that fall below the first quartile - 1.5×IQR or above the third quartile + 1.5×IQR (Figure 6-10).

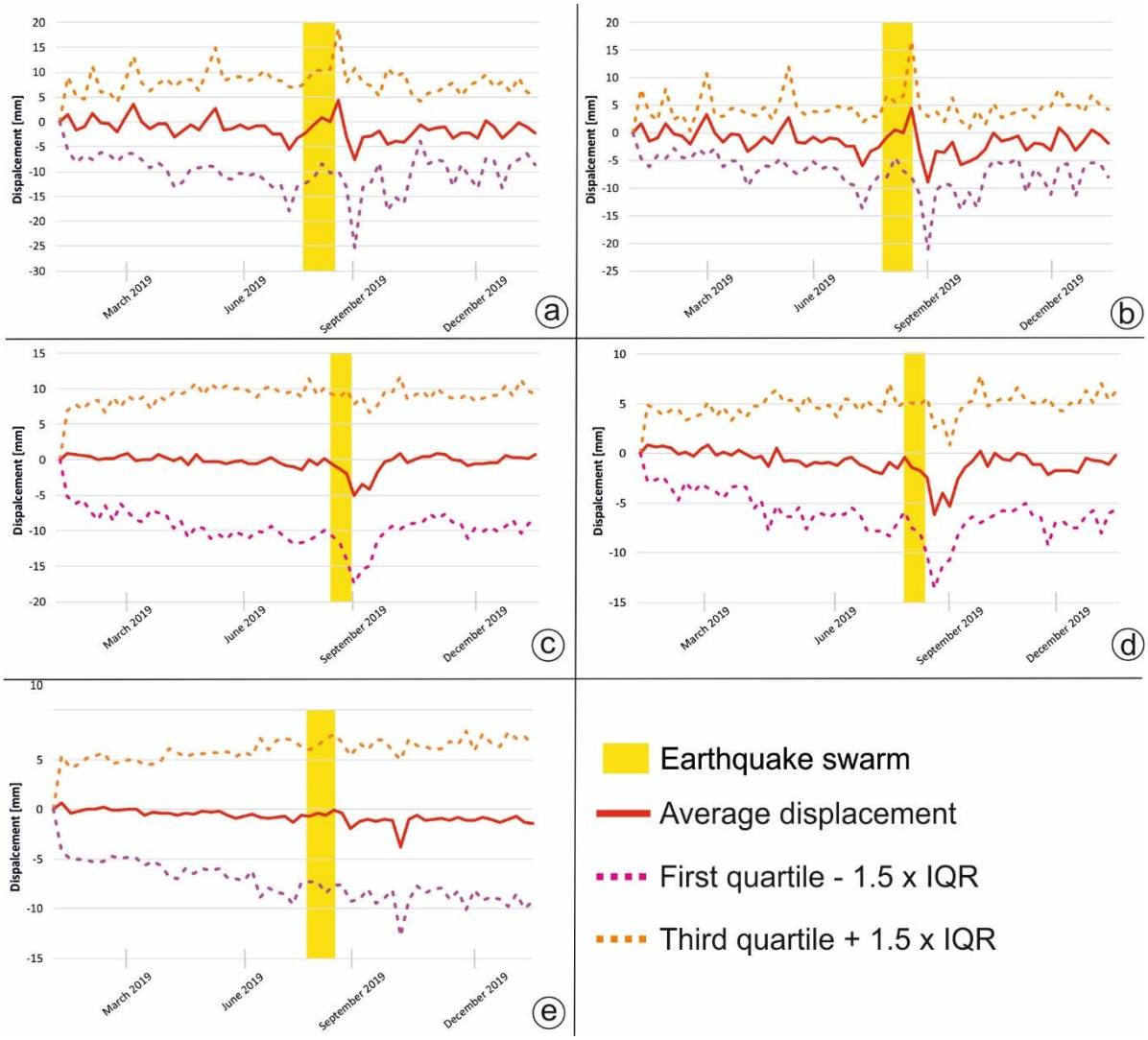


**Figure 6-10. Time series for the period January 2019 – January 2020 from RapidSAR ascending urban (a), from RapidSAR ascending rural (b), from RapidSAR descending urban (c), from RapidSAR descending rural (d) and ISBAS ascending (e).**

The interquartile analysis highlights that each processing methodology produces a similar ground motion pattern for the area of interest; namely a slightly subsiding signal. It is also evident that the RapidSAR results have a slightly higher dispersion than the ISBAS results (~2.5 mm/yr vs 2.2 mm/yr) but overall both sets of InSAR data indicate that this area is roughly stable and continues to follow the patterns observed in the baseline.

The average time series were also examined to assess any impact of the shallow seismic events (≤ 2.9 km of depth) on the ground motion. The period of highest magnitude seismicity (August 2019) highlighted in yellow in Figure 6-10.

The ISBAS results (Figure 6-10e) show no change in this region at the time of the seismicity. However, the RapidSAR results (Figure 6-10a-d) show a sharp acceleration during the August 2019 earthquake swarm in the area of interest. Although this motion has a magnitude of approximately 5mm, it is within the variability observed both within the 2015-2018 InSAR dataset (see Figure 6-4) and the natural fluctuations and measurement noise established within the baseline for the area.

## 6.5 PNR GROUND MOTION SUMMARY

The Fylde InSAR ground motion baseline analysis utilised ERS-1/2 and Sentinel-1 data. The stack of ERS-1/2 data (covering the period from 1992 to 2000) was processed using SBAS and ISBAS techniques (i.e. two levels of analysis in total). The assessment indicates that the majority of the full region covered by the satellite image stack was stable, however discrete zones were affected by ground motion. The uplift and subsidence in the Manchester area relates to coal mining (Cigna and Sowter, 2017), while the subsidence in the west of the Fylde is related to compressible ground. These examples, corroborated by GNSS in this research covering the baseline period, provide validation of the ground motion determined by InSAR in the region.

Analysis of Sentinel-1 InSAR data for the pre-hydraulic fracturing period (2015-2018) reveals that the motion patterns observed in the 1990's data are still evident, although their locations have shifted slightly (compressible ground to the west of the Fylde) or the signal pattern has switched from subsidence to uplift (Leigh) due to changes in groundwater pumping related to past mining activities. Phase IV examination of the time series for the hydraulic fracturing period (October 2018- December 2018) shows no evidence of change compared to the baselines established in both the Sentinel-1 or ERS baseline time series. Examination of the Sentinel-1 time series for points closest to seismic events also showed no evidence of change at the time of those events.

The ERS and Sentinel-1 time series reveal a variability about the mean trend of the ground motion. Any meaningful syn- or post-hydraulic fracturing ground motion signals would therefore need to exceed this variability or change the pattern of motion recorded. No such variance from the baseline was revealed in this research. It should be noted that the research was undertaken at one site where hydraulic fracturing occurred, and that (i) extending the study for a longer period would help to rule out delayed ground motion responses at the surface and (ii) this ground motion may not represent the situation at other sites where the geology and operations differ.

In Phase V two sources of InSAR ground motion data for the period from January 2019- January 2020 were processed and interpreted for the PNR site and wider area i.e. Sentinel-1 ascending and descending. Two InSAR processing techniques (i.e., ISBAS and RapidSAR) were used to ensure that the best coverage of measurements was obtained both spatially and temporally. This approach was designed to provide the best chance of capturing motion that could be related to hydraulic fracturing.

In line with the results from Phase IV, the ground motions in the 2019 to 2020 period did not significantly deviate from the variability and patterns observed in the baselines. This was true for both points directly over the area of hydraulic fracturing and the region defined in the planning application.

## 6.6 ACKNOWLEDGEMENTS

ERS-1 data were obtained via a Category-1 ESA project ID:13543 'Enhancing landslide research and monitoring capability in Great Britain using C-band satellite SAR imagery and change detection, InSAR and Persistent Scatterers techniques'. Sentinel-1 data have been obtained via the ESA Copernicus Program. The authors would like to acknowledge ©Terra Motion Ltd and SatSense Ltd. who processed the ISBAS and RapidSAR data, respectively.

## 6.7 REFERENCES

Arrick, A., Forster, A., Clark, D., Stewart., M.,Lawrence, D., 1995. A geological background for planning and development in Wigan. Volume 2: A user's guide to Wigan's ground cnditions. British Geological Survey Technical Report, No. WN/95/3.

Bateson, L., Cigna, F., Boon, D.,Sowter, A., 2015. The application of the ISBAS InSAR method to the South Wales Coalfield. International Journal of Applied Earth Obseration and Geoinformation, 34, 249-257. https://doi.org/10.1016/j.jag.2014.08.018

Cigna, F. and Sowter, A., 2017 The relationship between intermittent coherence and precision of ISBAS InSAR ground motion velocities: ERS-1/2 case studies in the UK. Remote Sensing of Environment, 202, 177-198. https://doi.org/10.1016/j.rse.2017.05.016

Cuadrilla, 2018. Hydraulic Fracture Plan PNR 1/1Z. Available at: https://cuadrillaresources.uk/wp-content/uploads/simple-file-list/Hydraulic-Fracturing/Hydraulic-Fracture-Plan-PNR-11Z.pdf [accessed on 17/3/2020]

Environment Agency, 2019a. Preston New Road – Background Air Quality Monitoring March 2019. Available at https://consult.environment-agency.gov.uk/onshoreoil-and-gas/information-on-cuadrillas-preston-new-roadsite/supporting_documents/Preston%20New%20Road%20Air%20Quality%20Report%20%20March%202019.pdf

Environment Agency, 2019b. Variation and consolidation notice: Cuadrilla Bowland Limited. Available at: https://www.gov.uk/government/publications/pr4-3pj-cuadrilla-bowland-limited-eprab3101mwv005-environmental-permit-issued [accessed on 18/3/2020]

Gee, D., Bateson, L., Sowter, A., Grebby, S., Novellino, A., Cigna, F., Marsh, S., Banton, C., Wyatt, L., 2017. Ground Motion in Areas of Abandoned Mining: Application of the Intermittent SBAS (ISBAS) to the Northumberland and Durham Coalfield, UK. Geosciences , 7, 85. https://doi.org/10.3390/geosciences7030085

Geertsma, J. and Opstal, V., 1973. A numerical technique for predicting subsidence above compacting reservoirs, based on the nucleus of strain concept. Verhandelingen Kon Ned. Geol. Mijnbouwk, 28 (1973), 63-78

Jordan C. J., Bateson L., Novellino, A., 2019. Environmental baseline monitoring for shale-gas development: Insights for monitoring ground motion using InSAR analysis. Science of the Total Environment, 696, 134075. https://doi.org/10.1016/j.scitotenv.2019.134075

Moro, M., Saroli, M., Stramondo, S. et al., 2017. New insights into earthquake precursors from InSAR. Sci Rep 7, 12035. https://doi.org/10.1038/s41598-017-12058-3

OGA, 2019. Interim report of the scientific analysis of data gathered from Cuadrilla's operations at Preston New Road. Available at https://www.ogauthority.co.uk/media/6149/summary-of-pnr1z-interim-reports.pdf

OGA, 2018. Consolidated Onshore Guidance, version 2.2. – June 2018. Available at https://www.ogauthority.co.uk/media/4959/29112017_consolidated-onshore-guidance-compendium_vfinal-002.pdf

Przyłucka, M., Herrera, G., Graniczny, M., Colombo, D., Béjar-Pizarro, M. (2015). Combination of conventional and advanced DInSAR to monitor very fast mining subsidence with TerraSAR-X data: Bytom City (Poland). Remote Sensing, 7(5), 5300-5328. https://doi.org/10.3390/rs70505300

Shirzaei, M., Ellsworth, W.L., Tiampo, K.F., Gonzalez, P.J., Manga, M., 2016. Surface uplift and time-dependent seismic hazard due to fluid injection in eastern Texas. Science 353, 1416–1419. https://doi.org/10.1126/science.aag0262

Sowter, A., Bateson, L., Strange, P., Ambrose, K., Syafiudin, M.F., 2013. DInSAR estimation of land motion using intermittent coherence with application to the South Derbyshire and Leicestershire coalfields. Remote Sens. Lett., 4(10), 979–987. https://doi.org/10.1080/2150704X.2013.823673

Spaans, K.; Hooper, A., 2016. InSAR processing for volcano monitoring and other near-real time applications. Journal of Geophysical Research: Solid Earth 121 (4), 2947–2960. https://doi.org/10.1002/2015JB012752

Ward, R.S., Allen, G., Baptie, B.J., Bateson, L., Bell, R.A., Butcher, A.S., Daraktchieva, Z., Dunmore, R., Fisher, R.E., Horleston, A., Howarth, C.H., Jones, D.G., Jordan, C.J., Kendall, M., Lewis, A., Lowry, D., Miller, C.A., Milne, C.J., Novellino, A., Pitt, J., Purvis, R.M., Smedley, P.L., Wasikiewicz, J.M., 2018. Preliminary assessment of the environmental baseline in the Fylde, Lancashire. Nottingham, UK, British Geological Survey, 104pp. (OR/18/020) (Unpublished).

Ward, R.S., Smedley, P.L., Allen, G., Baptie, B.J., Daraktchieva, Z., Horleston, A., Jones, D.G., Jordan, C.J., Lewis, A., Lowry, D., Purvis, R.M., Rivett, M.O., 2017 Environmental Baseline Monitoring Project. Phase II, final report. British Geological Survey, 163pp. (OR/17/049) (Unpublished)

Ward, R.S., Smedley, P.L., Allen, G., Baptie, B.J., Barkwith, A, Bateson, L., Bell, R.A., Bowes, M, Coleman, M, Cremen, G, Daraktchieva, Z., M, Fisher, R.E., Gong, M., Howarth, C.H., Jones, D.G., Jordan, C.J., Lanoiselle, M, M., Lewis, A., Lister, T,R, Lowry, D., Luckett, R, Mallin-Mertin, D, Marchant, B, Miller, C.A., Milne, C.J., Novellino, A., Pitt, J., Purvis, R.M., Rivett, M, Shaw, R, Wasikiewicz, J.M., Werner, M., = Wilde S., 2020. Environmental Monitoring – Phase 4 Final Report (April 2018-March 2019). Nottingham, UK, British Geological Survey, 197pp. (OR/19/044) (Unpublished)

# 7 Soil gas

## 7.1 INTRODUCTION

The soil gas element of the project seeks to establish baseline conditions for the concentrations of gases in the soil, flux of key gases from the soil to the atmosphere, and near-ground ambient levels of gases. There is therefore some overlap with the greenhouse gas monitoring (Section 1). Since radon was measured at a subset of the surveyed locations there is also some linkage to the radon work (Section 3).

Baseline soil gas measurements, like those for other elements of the project, provide a basis against which to assess any future changes that might result from shale gas activities. Although of low probability, there is the potential for gas to escape from depth along geological pathways (faults, fractures and other higher permeability zones) or man-made features, especially wells (either pre-existing or drilled for shale gas exploration, evaluation or development). Whilst large faults may be known from existing geological maps and/or data acquired during hydrocarbon exploration (e.g. 3-D seismic data), or become apparent from seismicity or ground motion studies, smaller faults and fractures may be present but unknown. The completion (suspension, plugging, decommissioning and abandonment) of existing deep boreholes can be of variable quality depending on the age of the well and these can provide potential conduits for upward migration of gases; there are a number of hydrocarbon wells in the Vale of Pickering that are more than 50 years old. New wells also represent a potential migration pathway if not properly constructed.

It is very difficult to predict where fluid migration from depth might reach the surface whether it follows natural or man-made pathways. Natural seepage of gas along faults tends to occur at limited sites, metres to tens of metres across, along only a very small proportion of the fault length (e.g. Annunziatellis et al., 2008; Johnson et al., In press; Ziogou et al., 2013). Borehole leaks can occur at the wellhead or, if fluid escapes from the annulus of the well, can migrate laterally and reach the surface up to several kilometres away (e.g. Allison, 2001).

Although soil gas monitoring is not a statutory requirement for shale gas activities, it is necessary at landfill sites (Environment Agency, 2010) and is often used to satisfy regulatory requirements for monitoring at geological $CO_2$ storage sites (European Union, 2009a, b). The activity is included in this study because of public concern about gas leakage from shale gas sites and to contribute to a comprehensive environmental baseline in two area of shale ags development.

## 7.2 SITE SELECTION

Site selection was based on a mixture of scientific and pragmatic considerations and the general principles are described in Smedley et al., 2015. At the Kirby Misperton site (KMA) and Preston New Road (PNR) site the continuous monitoring equipment has been located close to air quality and greenhouse gas atmospheric monitoring systems. Thus equipment was sited at, or very close to, the shale gas sites. A further site in the Vale of Pickering is located 1km to the east of the shale gas site close to BGS groundwater monitoring wells with naturally high methane concentrations. In addition three locations in the Vale of Pickering, and two locations in Lancashire (Roseacre and Preston New Road), formed the basis of the repeat baseline surveys, these locations were adapted as specific plans for shale gas development changed over the course of the project.

## 7.3 MONITORING ACTIVITIES

Soil gas monitoring in this phase of the project was limited to survey work in the Vale of Pickering and The Fylde, Lancashire. Two surveys at each location were planned in spring through autumn. One survey was planned to run concurrently with atmospheric and radon monitoring survey but waterlogged ground conditions meant that soil gas monitoring could not take place. This, and all

other UK autumn soil gas surveys, were postponed until ground conditions could improve in early spring 2020, and ultimately had to be abandoned as COVID-19 restrictions were imposed.

Therefore, we report new data from two soil gas surveys carried out in the spring and early summer 2019. We also report processed eddy covariance (EC) data from the PNR monitoring station which was not available during the previous reporting period; all new EC data up to March 2020 is appended in this report and the complete set of eddy covariance data is also distinguished into pre- and post-fracking data for the first time. For clarity, the term 'post-fracking' or 'post-hydraulic fracking' refers to soil gas data collected after hydraulic fracking commenced at Preston New Road.

## 7.4 RESULTS AND DISCUSSION

### 7.4.1 Eddy covariance (EC) monitoring - PNR

The Eddy Covariance (EC) system collects meteorological information and $CO_2$ observations at high temporal resolution (10 Hz). Post-processing allows $CO_2$ flux to be determined and the covariance of vertical and horizontal wind statistics and $CO_2$ flux to be calculated (see Ward et al 2018*)* using EddyPro® standard methods. Flux of $CO_2$ determined by EC is net vertical, driven in part by turbulent horizontal flow, and is measured at a height of 2.5 m above ground level. EC measurements provide a continuous context that complements direct measurements of soil to atmosphere $CO_2$ flux taken during discrete soil gas surveys in Lancashire.

EC data are presented at 30 minute averaged intervals between 19th January 2016 and 22nd January 2020. There are several periods of no data collection related to file corruption, sensor failure or the system being serviced. Periods of downtime across the entire deployment are detailed in Table 7-2.

**Table 7-1 Periods of no EC data for the PNR site between 19/01/2016 and 22/01/2020**

| EC down periods (Date UTC) | Days |
|---|---|
| 04/05/2016 13:00 – 19/05/2016 22:30 | 15 |
| 28/01/2017 16:30 – 10/03/2017 14:00 | 41 |
| 21/06/2017 12:00 – 13/07/2017 12:30 | 22 |
| 09/10/2017 15:00 – 31/10/2017 17:00 | 22 |
| 02/03/2018 13:30 – 22/03/2018 10:00 | 20 |
| 17/05/2018 12:30 – 20/09/2018 12:00 | 126 |
| 26/09/2018 12:30 – 17/10/2018 15:30 | 21 |
| 02/11/2018 13:30 – 19/12/2018 11:30 | 47 |
| 10/03/2019 18:30 – 17/04/2019 15:00 | 38 |

A plot of $CO_2$ vs wind speed is used to derive background gas concentration, which is similar to the global average background. In Figure 7-1 we see the data for baseline monitoring period (black circles) and during/after hydraulic fracturing operations at the PNR site - from 15th October 2018 - (orange circles). In general, the post hydraulic fracturing results match well with the background. There are some higher than average values at higher wind speeds observed during both period suggesting that $CO_2$ is being added to the atmosphere from a reasonably close source. The values measured during/after hydraulic fracturing are well within the background range indicating that no enhancements in $CO_2$ were observed in the EC dataset as a result of shale gas operations.

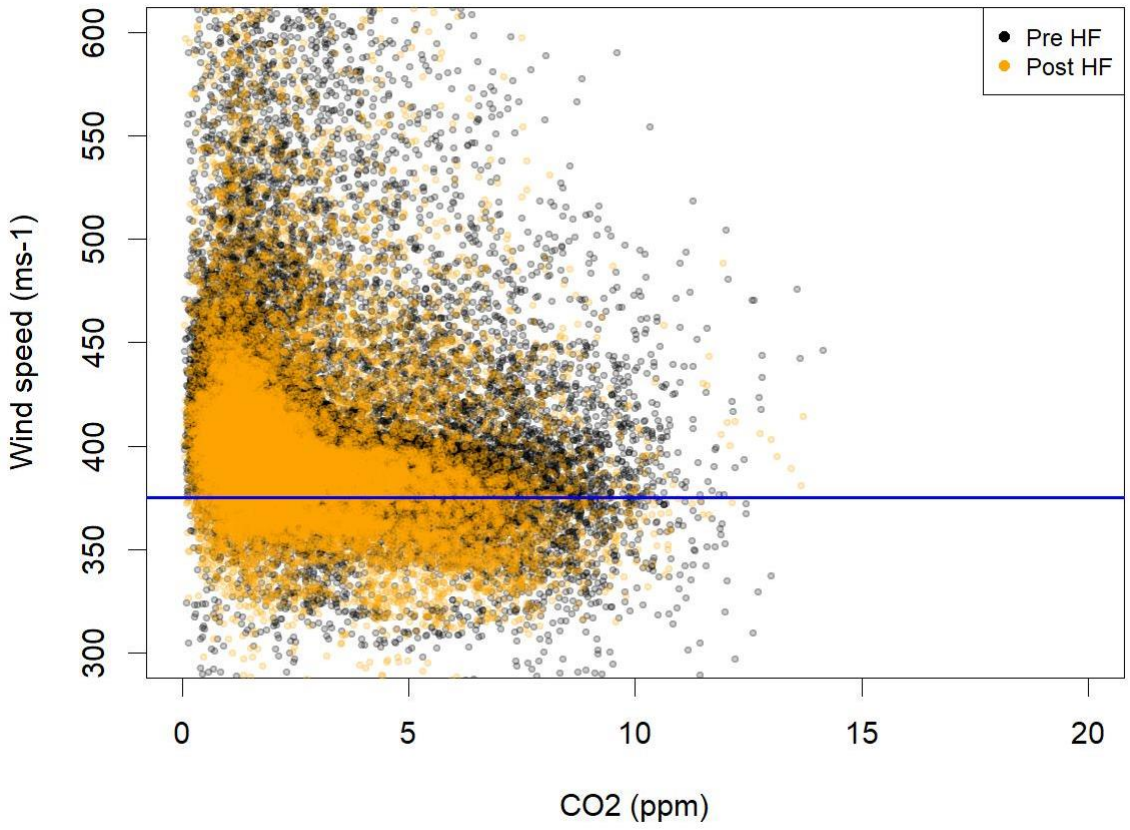


**Figure 7-1 - $CO_2$ concentration vs wind speed pre- (black) and post- (orange) hydraulic fracturing at the PNR site.**

Carbon dioxide concentration vs wind direction can be useful in attributing the direction of $CO_2$ sources or sinks. Figure 7-2 shows $CO_2$ concentration against wind direction again with a division of data into pre- and post- hydraulic fracturing. The area between the red lines in Figure 7-2 (250$^o$ to 290$^o$) acts as a guide to highlight any potential impacts from the direction of the Cuadrilla site given the potential for atmospheric dispersion.

Dispersion is dependent on multiple factors (wind speed, temperature, gas release rate, etc) and therefore dependent on conditions at a particular time. Between the red lines there are episodes post hydraulic fracturing where CO2 is below the average background and other episodes where it is greater than the average background. Again, these are well within the range of concentrations seen over the background observation period. To better quantify hydraulic fracturing impacts on atmospheric CO2, Figure 7-3 shows the mean (central bar), 25th and 75th percentiles (shoulders of the boxes), the 1.5IQR (tails) and outliers (points) pre (grey) and post (orange) hydraulic fracturing for wind directions between 250 and 290. The post hydraulic fracturing data shows slightly reduced mean CO2 and near identical range between at the 1.5IQR (interquartile range). Differences in windspeed between the pre- and post-hydraulic fracking periods may have resulted reduced $CO_2$ concentrations during the post-hydraulic fracturing period. The differences are minimal, however, and are unlikely to have a significant impact on dilution of $CO_2$. Post hydraulic fracturing atmospheric CO2 is well within the pre-hydraulic fracturing or baseline range.

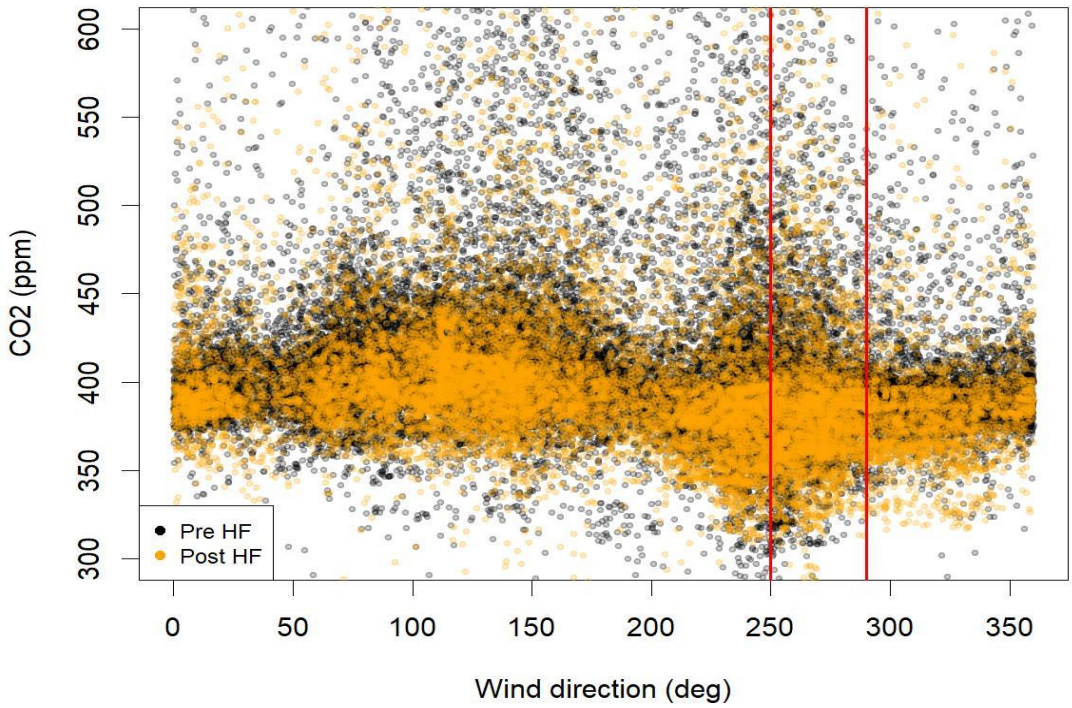


**Figure 7-2. $CO_2$ concentration vs wind direction. The area between the red lines acts as a guide for identifying potential impact from the direction of the hydraulic fracturing site relative to the position of the EC.**

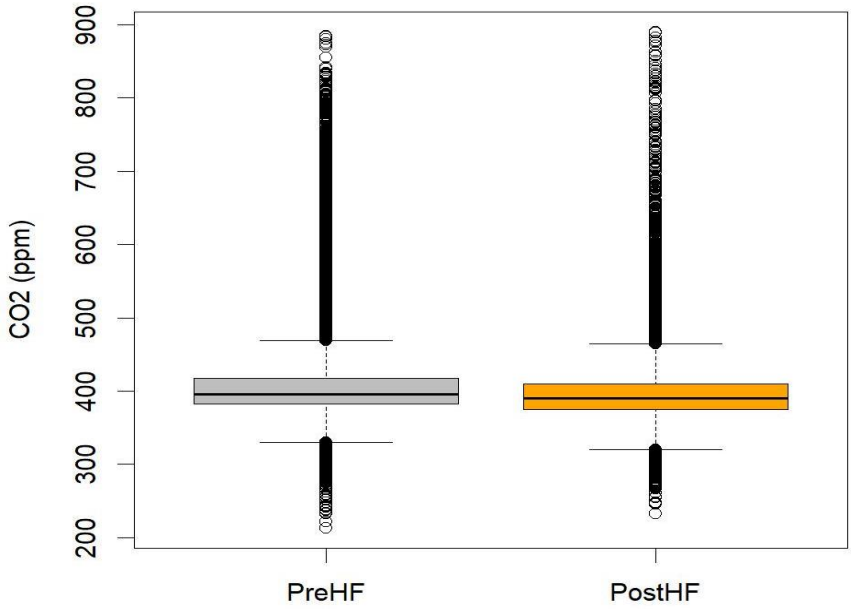


**Figure 7-3 - Atmospheric $CO_2$ concentrations pre- (grey) and post- (orange) hydraulic fracturing at PNR for wind directions between 250º and 290º. Mean (central bar), 25th and 75th percentiles (shoulders of the boxes), the 1.5IQR (tails) and outliers (points) are shown.**

Averages (48h) of temperature (Figure 7-4), net vertical $CO_2$ flux (Figure 7-5) and $CO_2$ concentration (Figure 7-6) show data pre and post hydraulic fracturing. Temperature post hydraulic fracturing has been a little lower than previous years, while net vertical $CO_2$ flux and concentration are similar to background values from the same periods in previous years.

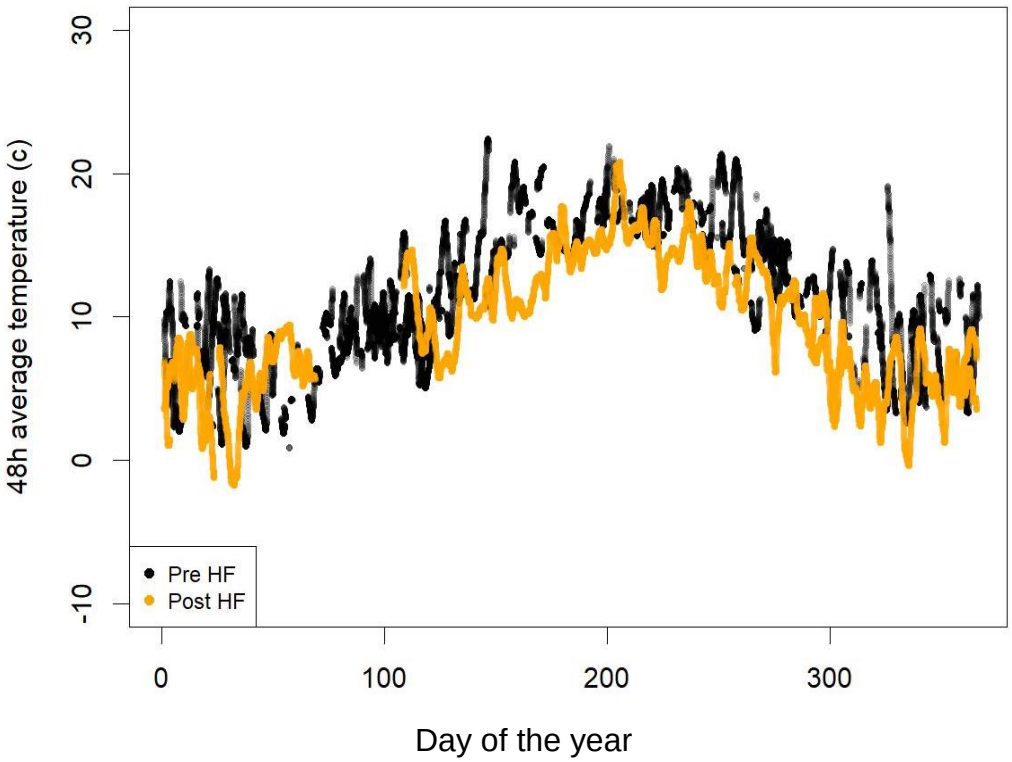


**Figure 7-4. Temperature for pre (black) and post (orange) hydraulic fracturing.**

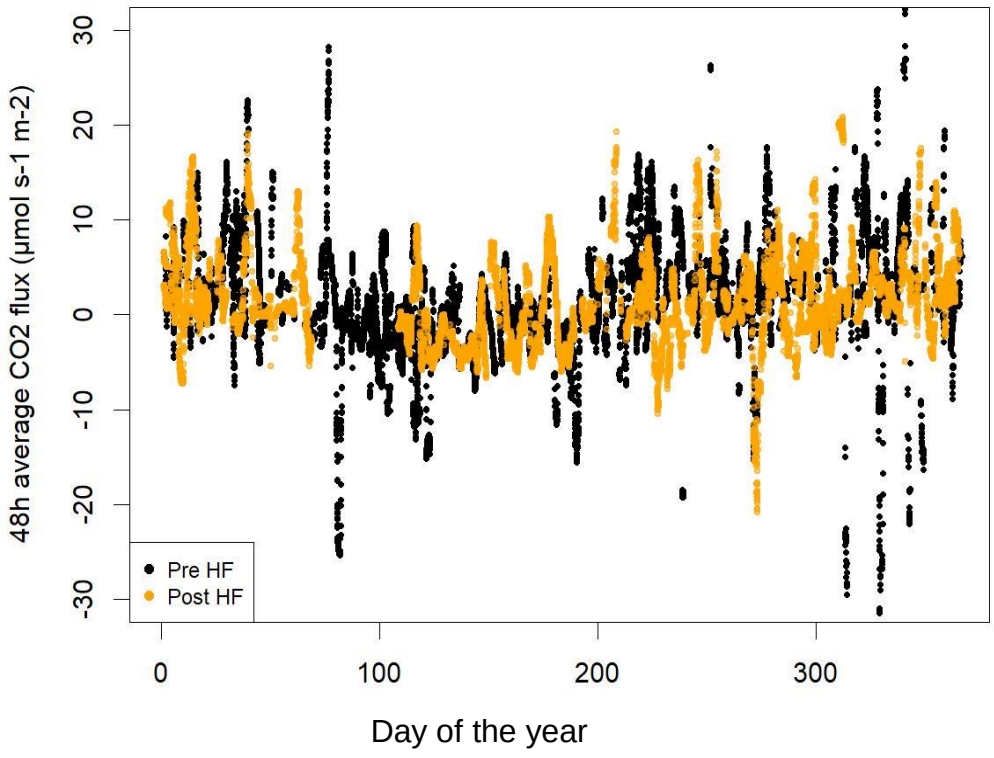


**Figure 7-5. Net vertical $CO_2$ flux for pre (black) and post (orange) hydraulic fracturing.**

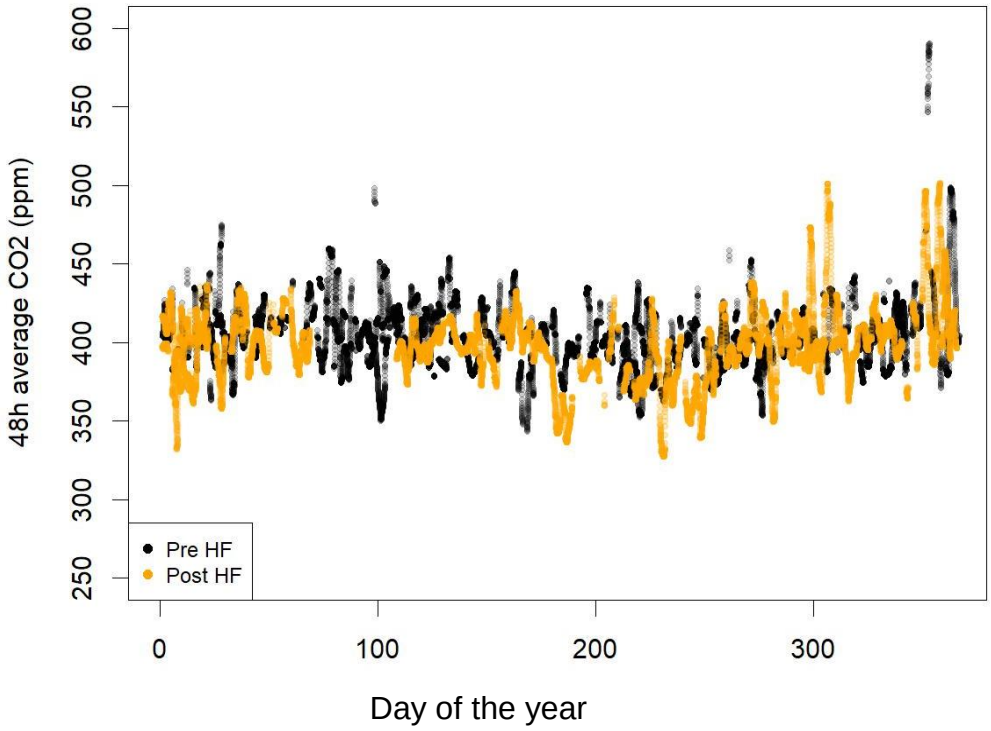


**Figure 7-6. $CO_2$ concentration (ppm) pre (black) and post (orange) hydraulic fracturing.**

### 7.4.2 Soil gas surveys

Soil gas baseline monitoring in survey mode consisted of repeated broad scale grids of $CO_2$ flux and soil gas point measurements, along with mobile laser surveys. The latter is a rapid screening exercise conducted over wide areas; the facility typically uses this method to identify anomalies that can be followed up with more detailed point measurements, but it was also used specifically in an attempt to detect near-surface manifestations of the impacts of shale gas activities.

#### 7.4.2.1 Soil gas survey – Preston New Road, April 2019.

A spatial survey of 71 $CO_2$ and $CH_4$ flux measurements, along with corresponding point measurements of soil gas at depth up to 80 cm where possible, and wide area mobile laser measurements, was completed between 9th and 12th April 2019 in fields adjacent to Preston New Road and above the lateral extensions to the shale gas wells.

$CO_2$ flux data are mapped in Figure 7-7. They compare well with data from earlier surveys undertaken in September 2018 and 2016, and August 2015 (i.e. ranging up to 60 $g/m^2/day$), although the absolute $CO_2$ fluxes are marginally lower overall than previous surveys. This could be due to the relatively wet ground conditions encountered across the Preston New Road survey area impeding surface to air flux of $CO_2$. No $CH_4$ flux was detected above the instrument limit of detection (0.08 $g/m^2/day/day$) at any of the sample points.

Soil gas measurements of $CO_2$ and $CH_4$ were obtained at 47 of the 71 sample points. $CO_2$ in soil gas measurements were repeated at the same Preston New Road sample site locations as previously visited during baseline monitoring surveys, including the further six sample sites that were added to the existing grid during the 2018 surveys.

Soil gas $CO_2$ measurements were made using two portable gas analysers; a Geotechnical GA5000 and a Draeger X–am 7000. This provides a lower limit detection of 0.01% $CO_2$ by volume in soil gas. Waterlogging meant no gas could be obtained from 22 sample points, predominantly in the west and north of the survey area. In addition, two sample points on the northern edge of the survey area were fenced off and inaccessible. $CO_2$ concentrations in soil gas ranged from 0.03%

– 10.6% (volume %) and compare well with previous surveys, albeit with $CO_2$ concentrations slightly lower overall (Figure 7-8).

Soil gas concentrations of $CH_4$ ranged from 0 to 9 ppm, although generally the soil gas $CH_4$ data are within the range seen during the baseline observation period. The outlying sample at 9 ppm coincides with high $CO_2$ (10.1%) and depleted oxygen (4.5%), and a $CO_2$ stable carbon isotope ratio ($\delta^{13}$CV-PDB) of -28.23‰, which is indicative of the biological oxidation of methane.

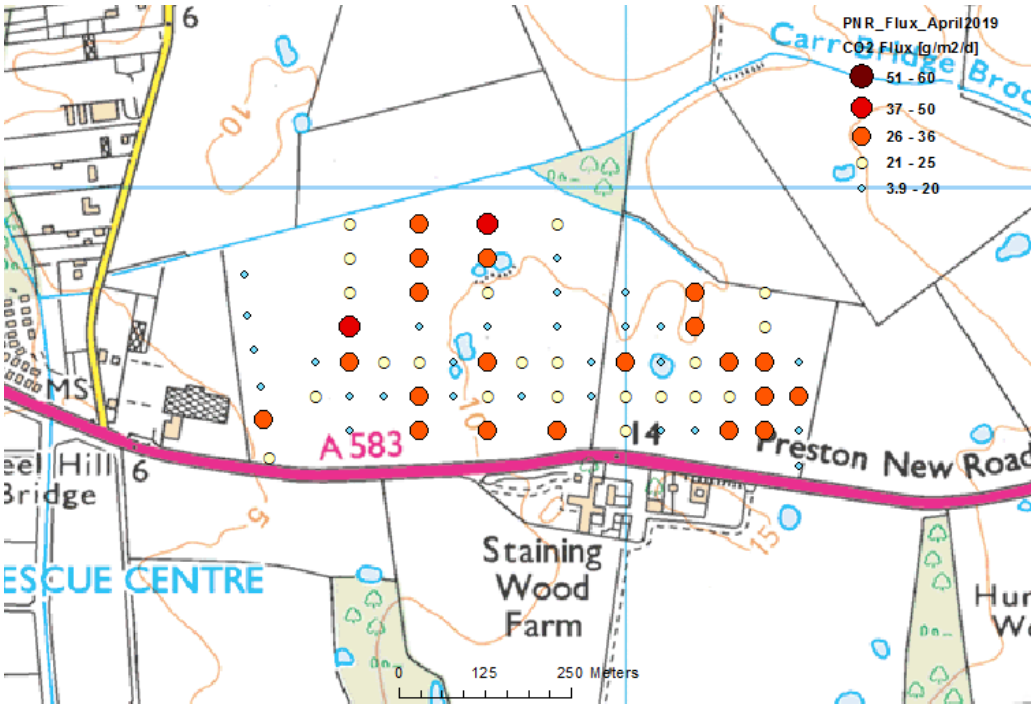


**Figure 7-7. $CO_2$ flux at PNR April 2019 (measurement units - g/m$^2$/day). Contains Ordnance Survey data © Crown Copyright and database rights 2020**

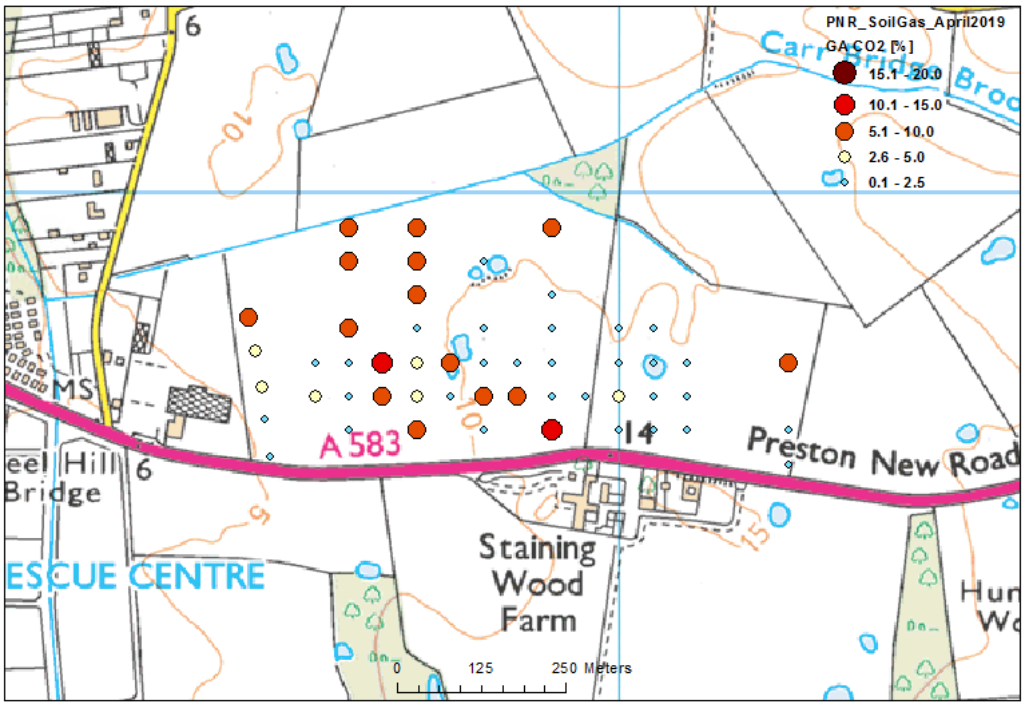


**Figure 7-8. $CO_2$ in soil gas at PNR April 2019 (measurement units - volume %). Contains Ordnance Survey data © Crown Copyright and database rights 2020**

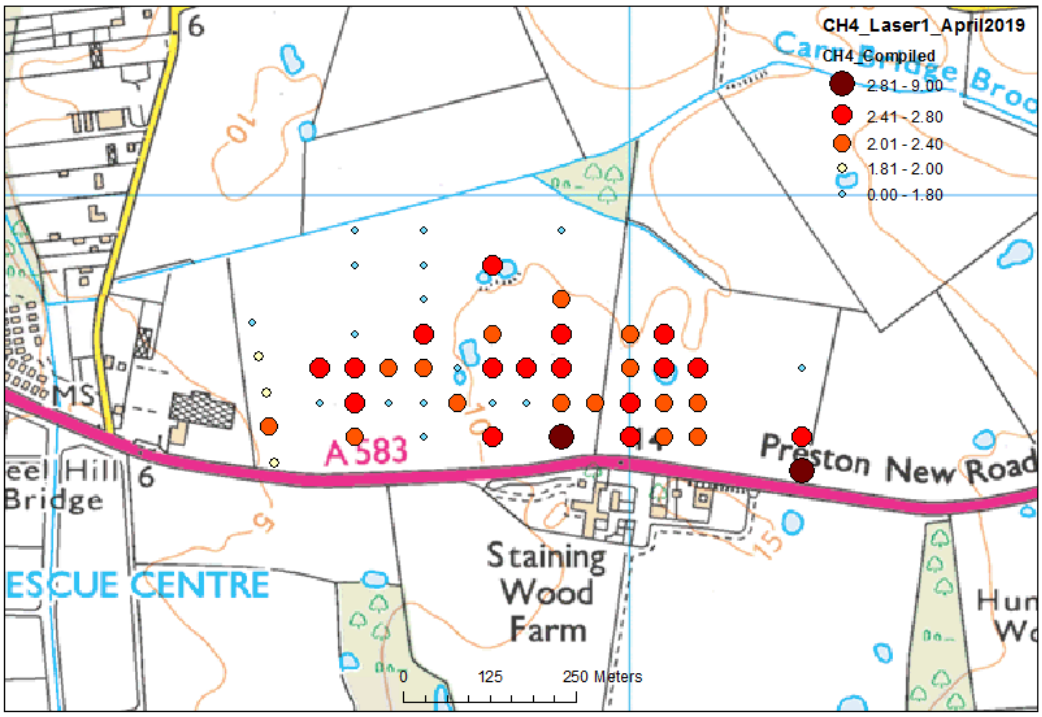


**Figure 7-9. $CH_4$ in soil gas at PNR April, 2019 (measurement units – ppm). Contains Ordnance Survey data © Crown Copyright and database rights 2020**

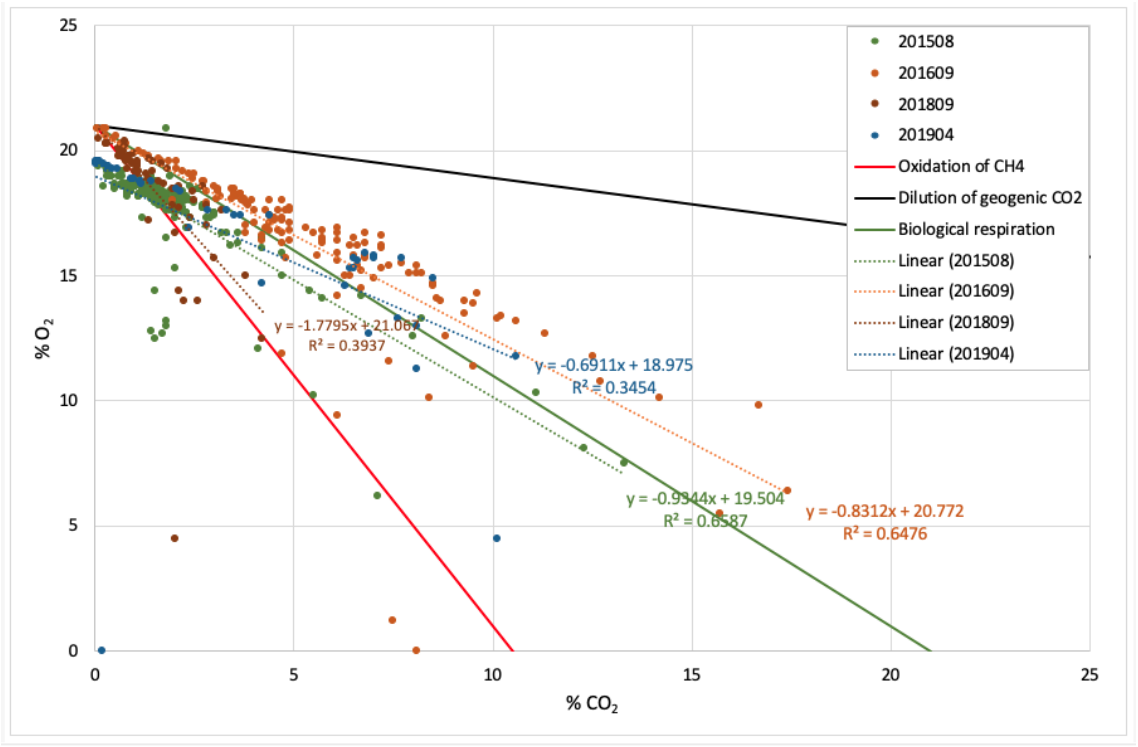


**Figure 7-10. Binary plot of soil gas compositions, Lancashire, by survey**

A process based approach (Romanak et al., 2012) has been applied to the PNR data in an attempt to apportion the source of observed soil gas $CO_2$. Figure 7-10 suggests that much of the $CO_2$ measured during the PNR surveys originates from biogenic sources in the shallow subsurface, as its relationship with soil gas oxygen lies mainly along the biological respiration line with some mixing towards the $CH_4$ oxidation line. Given the spread of $CO_2$ concentrations measured, the biogenic relationship is more obvious in data from the September 2016 survey. We would again

expect the relationship to vary between seasons, and the relationship is stronger in spring and summer than in autumn, but more data would be needed to demonstrate this. There is no indication of a deep geogenic input of $CO_2$ to near-surface soil gas.

From the available data obtained during the PNR soil gas surveys, along with ongoing eddy covariance monitoring at Little Plumpton, we have so far observed no significant changes in ground gas concentrations, and data from after hydraulic fracturing are consistent with parameter ranges observed during the baseline observation period.

#### 7.4.2.2 Soil gas survey – Vale of Pickering, June 2019.

A spatial survey of 86 $CO_2$ and $CH_4$ flux measurements, along with corresponding point measurements of soil gas at depth up to 80 cm where possible, and wide area mobile laser measurements, was completed at the Vale of Pickering between 25th and 28th June 2019. Sampling was severely restricted by ongoing agricultural activities that prevented access to entire fields, excluding around 30 of our normal sampling points.

$CO_2$ flux data are mapped in Figure 7-11. $CO_2$ flux values range between 3.5 and 41.0 g/m$^2$/day, and compare well with data from four earlier surveys conducted in November 2015, and June, August and October 2016. No $CH_4$ flux was detected at any of the Kirby Misperton sample points.

Soil gas measurements of $CO_2$ and $CH_4$ were obtained at 79 of the 86 sample points. $CO_2$ in soil gas measurements were repeated at the same sample site locations as previously visited during baseline monitoring surveys. $CO_2$ concentrations in soil gas ranged from 0.0% – 12.3% (volume %), which compares well with previous baseline surveys in this area.

Soil gas concentrations of $CH_4$ ranged from 0 to 1180 ppm. The isolated highly elevated value was coincident with extremely waterlogged conditions. Otherwise, soil gas $CH_4$ data are mostly within the range seen during previous baseline surveys. The outlying sample with 1180 ppm $CH_4$ coincided with high $CO_2$ (12.3%), depleted oxygen (2.1%), and a $CO_2$ stable carbon isotope ratio ($\delta^{13}$CV-PDB) of -27.52‰, which is, again, indicative of biological oxidation of methane.

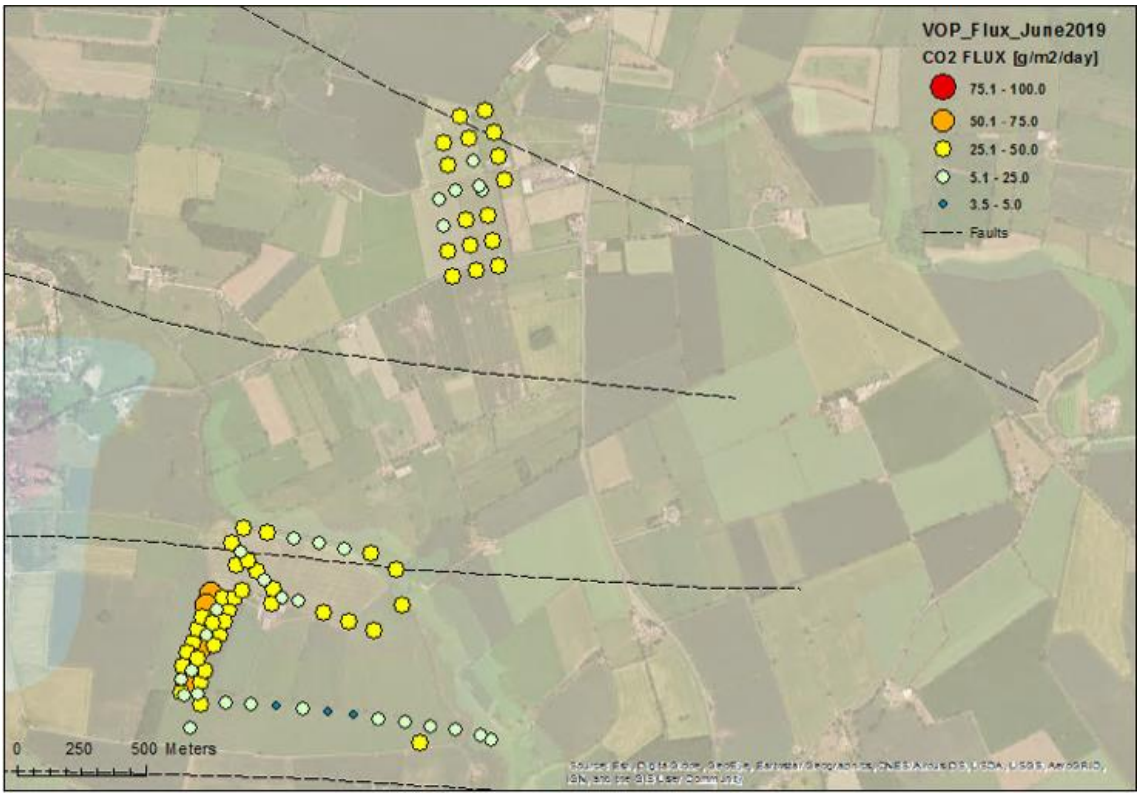


**Figure 7-11. $CO_2$ flux at PNR April 2019 (measurement units - g/m$^2$/day).**

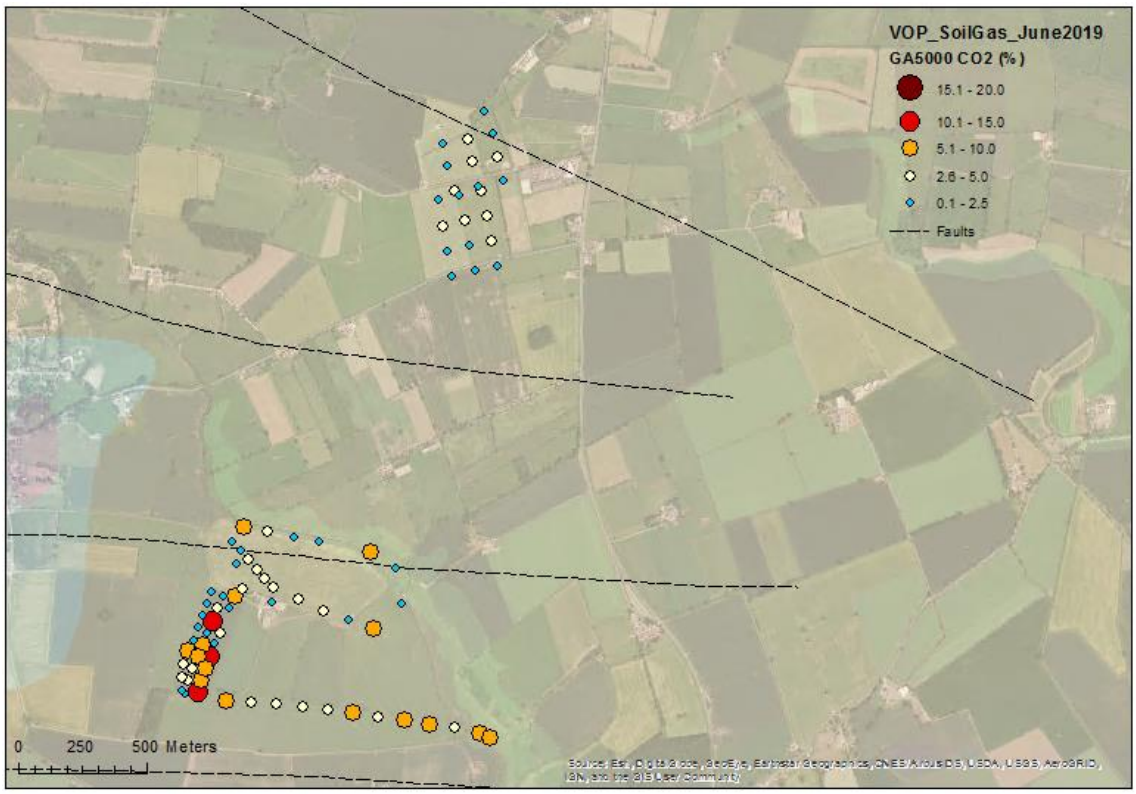


**Figure 7-12. $CO_2$ in soil gas at Kirby Misperton, June 2019 (measurement units – volume %).**


**Figure 7-13. $CH_4$ in soil gas at Kirby Misperton, April 2019 (measurement units – ppm).**

The relationship between concentrations of different soil gases, in this case $CO_2$ and $O_2$, can provide an indication of the predominant processes influencing the concentration of $CO_2$ in soil gas (Romanak et al., 2012).

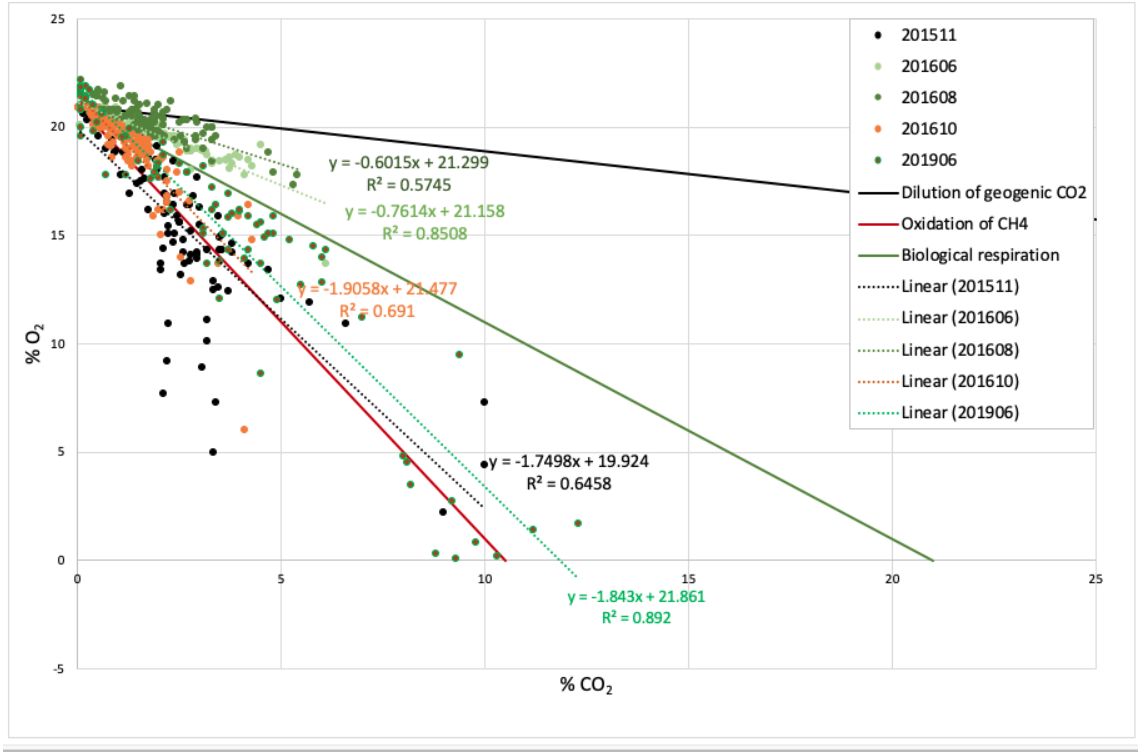


**Figure 7-14. Binary plot of soil gas compositions, Vale of Pickering, by survey**

A binary plot of soil gas oxygen and $CO_2$ (Figure 7-14) suggests that much of the $CO_2$ measured during the Vale of Pickering surveys originates from biogenic sources in the shallow subsurface, as the relationship of $CO_2$ with soil gas oxygen lies along the biological respiration line. As expected, the strength of the relationship varies between seasons; the relationship is stronger in summer than in autumn, when the relationship is more mixed towards the oxidation of methane. This agrees well with corroborative stable carbon isotope data obtained during the Vale of Pickering survey, which also indicates $CO_2$ originates from the biological oxidation of methane in the soil. There is no indication in this data of a geogenic input to soil gas $CO_2$.

## 7.5 REFERENCES


Romanak, K D, Bennett, P C, Yang, C, and Hovorka, S D. 2012. Process-based approach to $CO_2$ leakage detection by vadose zone gas monitoring at geologic $CO_2$ storage sites. *Geophysical Research Letters*, Vol. 39, L15405.

Ward, R.S., Smedley, P.L., Allen, G., Baptie, B.J., Cave, M.R., Daraktchieva, Z., Fisher, R., Hawthorn, D., Jones, D.G., Lewis, A., Lowry, D., Luckett, R., Marchant, B.P., Purvis, R.M., Wilde, S. 2018. *Environmental baseline monitoring: Phase III final report (2017-2018).* Nottingham, UK, British Geological Survey, 143pp. OR/18/026.